Thiyl Radical-Mediated ‘Click’ Strategies for Site-Selective Peptide and Protein Modification

Inés Rabadán González

2026

Trinity College Dublin

The University of Dublin

Based on research carried out under the supervision of Professor Eoin M. Scanlan

A thesis submitted to the School of Chemistry, Trinity College Dublin, The University of Dublin for the degree of Doctor of Philosophy.

I declare that this thesis has not been submitted as an exercise for a degree at this or any other university and it is entirely my own work.

I agree to deposit this thesis in the University's open access institutional repository or allow the library to do so on my behalf, subject to Irish Copyright Legislation and Trinity College Library conditions of use and acknowledgement.

I consent to the examiner retaining a copy of the thesis beyond the examining period, should they so wish (EU GDPR May 2018).

Signed: Inés Rabadán González Date: 26/09/2025

The greatest joy of life is to accomplish. It is the getting not the having. It is the giving not the keeping. I am a firm believer in the theory that you can do or be anything that you wish in this world, within reason, if you are prepared to make the sacrifices, think and work hard enough and long enough.

– Frederick Banting, 1923.

Abstract

Thiol-ene ‘click’ chemistry is a radical-chain-mediated reaction between a thiol and alkene that furnishes a robust, covalent thioether linkage. This reaction is considered a ‘click’ process due to its numerous beneficial attributes including chemoselectivity, rapid reaction times and tolerance to atmosphere conditions. Over the years, thiol-ene chemistry has been applied across diverse areas including chemical biology, polymer chemistry, materials science and for the synthesis of therapeutic agents. This thesis explores the development of thiol-ene mediated “click” reactions for peptide and protein modification, with potential applications in peptide bioconjugation methodologies relevant to drug discovery and chemical biology.

Chapter 2 presents a ‘green’ methodology for peptide bioconjugation. For the first time, peptide ligation was carried out under continuous-flow conditions using deep eutectic, bio-based solvents and aqueous conditions. The scope of this methodology was further expanded to the glycosylation of bioactive peptides demonstrating its scalable and sustainable advantages for the pharmaceutical industry.

Chapter 3 describes the use of UV-initiated thiol-yne ‘click’ reaction for peptide disulfide rebridging. The use of sodium borohydride ($NaBH_4$) as an emerging peptide disulfide reducing agent is investigated, since its use had previously been restricted to protein modifications. The strategy was extended to include a range of biomolecules and applied to an analogue of the naturally occurring hormone Somatostatin, with potential cellular bioimaging applications.

Chapter 4 outlines the application of naphthalimides as a novel type of organic photocatalyst for thiol-ene-mediated photoredox catalysis. Their aggregation-induced emission properties enabled the study of this methodology in both organic and aqueous media. Several examples of successful ligation reactions employing the novel photocatalysts are presented.

Chapter 5 focuses on the development of a covalent, site-selective thiol-ene-mediated mRNA display platform. This system consists of the incorporation of thiol-ene ‘click’ chemistry onto a standard mRNA display for more efficient discovery of peptide-based protein-protein interaction inhibitors. The efficacy of the thiol-ene mediated

process is demonstrated on a model system, highlighting potential applications for library screening methods utilising this approach.

Abbreviations

AA	Amino acid
Abz	Aminobenzamide
ACE-2	Angiotensin-Converting Enzyme 2
ADME	Absorption, Distribution, Metabolism and Excretion
Agl	Allylglycine
Aha	Azidohomoalanine
AIBN	2,2'-Azobis(isobutryonitrile)
Alloc	*N*-Allyloxycarbonyl
APCI	Atmospheric Pressure Chemical Ionization
App	Apparent
Aq.	Aqueous
Ar	Aromatic
Arg; R	Arginine
Asn; N	Asparagine
Asp; D	Aspartic Acid
ATE	Acyl Thiol-Ene
BME	β-mercaptoethanol
Boc	tert-butyloxycarbonyl
BOP	1-yloxytris(Dimethylamino)Phosphonium Hexafluorophosphate
BSA	Bovine Serum Albumin
calcd.	Calculated
Cbz	Carboxybenzyl
$CDCl_3$	Chloroform
ChCl	Choline Chloride

CLipPA	Cysteine Lipidation on a Peptide or Amino Acid
COSY	Correlation Spectroscopy
CuAAC	Copper-Catalysed Azide Alkyne Cycloaddition
Cys; C	Cysteine
d	Doublet
CH_2Cl_2	Dichloromethane
dd	Doublet of Doublets
DES	Deep Eutectic Solvent
Dha	Dehydroalanine
DIC	Diisopropylcarbodiimide
DIPEA	Diisopropylethylamine
DMAP	4-(Dimethylamino)pyridine
DMF	Dimethylformamide
DMSO	Dimethylsulfoxide
DNA	Deoxyribonucleic acid
DPAP	2,2-Dimethoxy-2-Phenylacetophenone
DTT	Dithiothreitol
EDC·HCl	1-(3-Dimethylaminopropyl)-3-ethylcarbodiimide Hydrochloride
e.g.	Exempli gratia; for example
EG	Ethylene Glycol
Equiv.	Equivalents
ESI	Electrospray Ionisation
Et	Ethyl
et al.	Et alii; and co-workers
Et_2O	Diethyl Ether

EtOAc	Ethyl Acetate
Fmoc	Fluorenylmethoxycarbonyl
g	Gram
GlucNAc	*N*-Acetyl-D-Glucosamine
Gln; **Q**	Glutamine
Glu; E	Glutamic Acid
Gly; **G**	Glycine
Glyc	Glycerol
GSH	Glutathione
h	Hour
Hag	Homo-allyl-Glycine
HAT	Hydrogen Atom Transfer
HBTU	(2-(1H-Benzotriazol-1-yl)-1,1,3,3-Tetramethyluronium Hexafluorophosphate
HCl	Hydrochloric Acid
HeLa	Human cervical cancer cell line
His; **H**	Histidine
HMBC	Heteronuclear Multiple Bond Correlation
HMPA	Hexamethylphosphoramide
HOBt	Hydroxybenzotriazole
HPLC	High-Performance Liquid Chromatography
HRMS	High Resolution Mass Spectrometry
HSQC	Heteronuclear Single Quantum Coherence
Hz	Hertz
ICT	Intramolecular charge transfer
Ile; I	Isoleucine

IR	Infrared
J	Coupling Constant
K_d	Dissociation constant
L	Litre
LC	Liquid Chromatography
LC-MS	Liquid Chromatography - Mass Spectrometry
LED	Light-Emitting Diode
Leu; L	Leucine
Lys; K	Lysine
M	Molar
m	Multiplet
m/z	Mass to Charge Ratio
MAP	4-Methoxyacetophenone
Me	Methyl
MeCN	Acetonitrile
MeOH	Methanol
Met; **M**	Methionine
min	Minutes
Mmt	Monomethoxytrityl
M.p.	Melting point
Mpa	3-merceptopropionic acid
MQ	Ultrapure
mRNA	Messenger ribonucleic acid
Mtt	Methyltrityl
Nap	1,8-Naphthalimide

NCL Native chemical ligation

NMM *N*-methylmorpholine

NMP *N*-methylpyrolidinone

NMR Nuclear Magnetic Resonance

PBS Phosphate-buffered saline

PC Photocatalyst

PCR Polymerase Chain Reaction

PEG Polyethylene glycol

pH $-\log[H_3O^+]$

PPI Protein-protein interaction

Pro; **P** Proline

PTM Post Translational Modification

Pu puromycin

PyBOP benzatriazol-1-yl-oxytripyrrolidinophosphonium hexafluorophosphate

q Quartet

RA Rink Amide

RaPID Random nonstandard peptides integrated discovery

Ref Reference

R_f Retention Factor

RP Reverse Phase

rt Room Temperature

s Singlet

SARS-Cov-2 Severe Acute Respiratory Syndrome Coronavirus 2

Ser; **S** Serine

SET Single Electron Transfer

SPAAC	Strain promoted azide alkyne cycloaddition
SPPS	Solid phase peptide synthesis
t	Triplet
tBu	tert-butyl
TCEP·HCl	Tris(2-carboxyethyl)phosphine Hydrochloride
TEA	Triethylamine
TEC	Thiol-Ene Click
TEMED	Tetramethylethylenediamine
TEMPO	2,2,6,6-Tetramethylpiperidine 1-oxyl
TEMED	Tetramethylethylenediamine
TES	Triethylsilane
TFA	Trifluoroacetic acid
THF	Tetrahydrofuran
TIPS	Triisopropylsilane
TLC	Thin Layer Chromatography
TOCSY	Total Correlation Spectroscopy
TOF	Time of Flight
Thr; T	Threonine
Trp; W	Tryptophan
Trityl	Trt Triphenylmethyl
TYC	Thiol-Yne
Tyr; **Y**	Tyrosine
Ub	Ubiquitin
UHPLC	Ultra-High Performance Liquid Chromatography
UV	Ultraviolet

UV-vis	Ultraviolet-visible
Val; V	Valine

Acknowledgements

I would first like to thank Prof. Eoin Scanlan for giving me this opportunity and allowing me to be part of his research group. Thank you, Eoin, for the guidance, trust, help and support I received during my 4 years of PhD. Thank you also for supporting me to attend conferences and support my applications which allow me to develop the network and the new opportunities I had during all these years. I am incredibly grateful to have had such a great supervisor.

Thanks to collaborators: Prof. Donald O'Shea and Sheila Fitzgerald in Royal College of Surgeons in Ireland (RSCI) and Prof. Lorenzo Guazzelli and Andrea Mezzetta in University of Pisa (Italy). As well as Science Foundation Ireland (Sfi) for funding.

My endless thanks go to Dr. John O'Brien for all the work he has done for these projects. I think, I don't know anybody with your passion, your extensive knowledge and love for what you do. I also wanted to apologise for all the 'extremely' dilute samples and all the time consumed on them to get the best NMR data. To Dr. Manuel Ruether for his knowledge and effectiveness for absolutely everything. Without you the school of chemistry would not be the same. To Dr. Brendan Twamley for the crystallography support and for the time spent in all my crystalline powder samples. I really learnt all about crystallisation methods. And finally, to Dr. Gary Hessman for his work on MS analysis, and for going through the infinite number of HPLC samples I have submitted. I am deeply grateful for all the effort you put for giving my samples in perfectly timing.

My gratitude goes to the past and current members of the Scanlan group for making these past 4 years the best time despite the stress from the PhD. Thank you for all the time together, every talk, every advice, every laugh, every conference, all the international and national trips, they became one of the most precious moments I got from this PhD and I could not be more fortunate. Thanks to Alannah who gave me such a great mentor experience. Thanks to all the past members of the Scanlan group: Harlei, Katie, Lorenzo di Simo and Mark. Thanks to Glenna for all your invaluable advices. Thanks Alby, your passion for the Irish weather made me enter in this world too. To Conor who has been the greatest colleague you can ask for. Thank you for being that attentive with me, for solving all my computer and administrative problems but specially for being such a great person. To Niki, for accompanying me in all the late hours of hard work along

with being the best partner in our third-year talk session. Thank you for all your support and deep conversations, they really meant a lot. You will surely go far. Thank you to Matthew, your arrival to our group made us 'ate that'. I am so glad to have been able to know you and to spend time together. I will never forget all our karaoke's and dances. A special thanks goes to Dr. Joshua McLean, who showed me everything I needed to know about peptide chemistry and English culture and Dr. Alejandro Prieto Castañeda for his patience, his chemistry lessons, for trusted me to finish his incredible work but mostly for his friendship. Siempre serás el mejor para mí. My deepest thanks go to Lucy McCormack. Lucy, without you, nothing of my PhD would have been the same. Thank you for all the moments together, for all the trips, for your friendship, for all the late talks, for being my partner in crime, for sharing every possible workspace with me, for showing me that the distance does not change anything, for your incalculable help…In general, for being the incredible person you are. I wish you the best in the rest of your PhD and I will come back to see your success. I will miss you, chica. Finally, and most specially, I wanted to thank my best friend Dr. Laura Ramírez Lázaro. Thank you for being an incredible friend since 2016, for bringing me to Ireland and for even at 5000 km away still being my best friend. To carry out my entire scientific career with you was one of the best things I could have asked for but share my Irish life with you has been the most wonderful experience I had. Thank you for your endless support, for being such a great flatmate and for being my family in Ireland and in any country. I will never be able to thank you for all you have given me. Now, we are separated, but we have already been once, right? This does not finish here. You are a role model, and I am immensely proud of you. What you have achieved is nothing compared with what you will. With all of this, I have no doubts I had the best group anyone could have asked for. Thank you all.

I also would like to thank Dr. Connor O'Leary for teaching me to never give up even in the hardest times and to Dr. André Campaniço for all your help in this chemical biology world along with all our 'give me 5 min and I will update you' talks. As I told you once, you are great researcher and even greater person. Thank you to all the members of the McGouran group: Valerio, Susie, Ellen, Sean, Thomas, and Jullie, and to the Connons group: Ian, Lee, Lorenzo and Iñigo for make the office the perfect place to work in. I would also thank Dr. Adam Henwood for all moments together and who I had the pleasure to work with. In addition, I wanted to thank all the Gunnlaugsson group for such fun time.

I want to extend my gratitude to Dr. Rita Petracca from Utrecht University who designed and trusted me to develop one of the best projects of my PhD thesis. I wish I could have spent more time with you, but I wish you the best in your new life. You deserve it. I would also love to thank my Utrecht girls: Amalija, Rosalba, Marinda, Lin and Julia, for welcoming me from the very first moment and for being such good friends in this new adventure.

I have no words to describe how thankful I am to Dr. Seino Jongkees from Vrije University who showed me the amazing world of chemical biology. Seino, thank you for all your 'pigeons' and your support for this project. You are an inspiration for all the scientific researchers. I am incredibly grateful to have been your first espanish-irish-italian PhD. I wanted to thank Wren, for all their help and our coffee breaks which made my writing days enjoyable. You are the cutest. To Twan (also known as Antonious) for his guidance and his 'try better' pushing that made me achieved the good results I obtained, and to the whole Jongkees group: Ryotaro, Mahaut, Feline, Roos, Julius, Sanbir and David for adopted me so kindly. Houdoe!

I would also like to thank my Spanish family in Ireland over these 4 years: Aroa, Deju, Albertillo, Davicillo, Patri, Diego, Jose Manuel, David, Oscar, Ibone, Lucia, Lorena, Vincenzo, Borlaf, Lorenzo, Sota and Toño. I wanted to thank Pilar, Claudia and Celia who accompanied me during the whole 4 years and made this experience unique. A special thanks go to Alvaro, Jorge, Kb, Ricardo, Fernando for being incredible flatmates and friends. I will never forget our birthdays and family dinners. To Samuel Velez and Alberto Penela, who were there for me in the toughest times of my PhD and always looked after me. I am very lucky to have spent all this time with you all.

I wanted to send my best wishes to my chemistry friends who are also finishing their PhDs in a different country and even on distance have shared this experience with me. Thank you, Pablo, Irene, María, Vega, Chris and Asier. Mucha suerte compañeros!

To Jaime Viciana, for his love, his empathy, his patience, his admiration to my work and to myself. Thank you for following me to every country I lived in and for support every decision I made. Estoy orgullosa de ti, del hombre en el que te estas convirtiendo y feliz de seguir creciendo a tu lado después de estos 10 años. Eres el mejor compañero de vida que se puede tener. Te quiero ñiño.

Finally, I want to thank all my family. To my uncles and cousins from my Rabadán family to my González family who has always support me.

To my parents and sister, who nothing of this would have been possible without them. Thank you for your endless support and trust on me and my work. A ti papá, por todo lo que he aprendido de ti y tu persona, pero sobre todo por enseñarme que no cuesta nada hacer las cosas bien. A ti mamá, por hacerme la mujer fuerte e independiente que soy ahora y por enseñarme a siempre seguir adelante. Y a ti Jimena, por ser la mejor hermana que se puede tener, por acompañarme todos estos años aun estando lejos, por tu sinceridad y honestidad y por, aun siendo la pequeña, enseñarme todo lo que me has enseñado.

I wanted to dedicate this thesis to my very good friend, Alejandro Padrino, who I started this journey with me and always believed in my scientific career but sadly he is no longer with us. Alex, esto va por ti. And, to my grandparents who blindly believed in me during all these years. Abueli! Por fin una doctora tendrá tu apellido!

Publications

- Prieto-Castañeda, A., Martin, H., Manna, T., Beswick, L., McLean, J. T., Pongener, **Rabadán González I**., Twamley, B., Miller, G. J. and Scanlan, Eoin M. Photoinitiated thiol–ene mediated functionalisation of 4,5-enoses, *Org. Biomol. Chem*., **2025**, 23, 5332-5338.
- **Rabadán González, I**., McLean, J. T., Ostrovitsa, N. Fitzgerald, S., Mezzetta, A., Guazzelli, L., O'Shea, D. F. and Scanlan, E. M. A thiol-ene mediated approach for peptide bioconjugation using 'green' solvents under continuous flow. *Org. Biomol. Chem.*, **2024**, 22(1), 2203-2210.

Table of contents

Abstract vii
Abbreviations ix
Acknowledgements xvi
Publications xx
Chapter 1: Introduction 1
1.1 Therapeutic Proteins and Peptides 1
1.1.1 Therapeutic Properties of Peptides 3
1.1.2 Synthetic Strategies for Peptide Modifications 3
1.2 Peptide Synthesis 6
1.2.1 Solution Phase Peptide Synthesis 6
1.2.2 Solid Phase Peptide Synthesis 9
1.2 3 Limitations of SPPS 10
1.2.4 Chemical Ligations 11
1.3 Peptide Modifications 13
1.3.1 Cysteine-selective Chemical Peptide Modification 14
1.3.2 Photochemical Peptide Modifications 16
1.4 Thiol-Ene Click reaction 18
1.4.1 Mechanistic Considerations 19
1.4.2 Thiol-yne Reaction 20
1.5 Applications of Thiol-Ene in Peptide Chemistry 21
1.5.1 Peptide Bioconjugation 22
1.5.2 Peptide Macrocyclisation and Stapling 25
1.5.3 Other Applications 29
1.6 Work Presented in this Thesis 32
Chapter 2: 'Green' thiol-ene mediated peptide bioconjugation under continous flow 34
2.1 Introduction 35
2.1.1 Continuous-Flow Chemistry 36
2.2 Previous Work Within the Scanlan group and Aims 38
2.3 Results and Discussion 38
2.3.1 Optimization of the Thiol-ene Reaction with GSH Under Batch Conditions 39
2.3.2 Optimisation of the Thiol-ene Reaction with GSH Under Continuous Flow Conditions 40
2.3.3 Scope of the Thiol-ene Reactions of GSH in Batch 42

2.3.4 Radical Mediated Thiol-ene Reactions in DESs, Bio-based and Less Harmful Solvents 45
2.3.5 Substrate Scope of the Thiol-Ene Reaction in Water Under Continuous-Flow 46
2.3.6 Thiol-Ene Mediated Glycosylation of Biologically Active Peptides in Water Under Continuous-Flow 48
2.4 Conclusions 54
Chapter 3: One-pot peptide disulfide rebridging via thiol-yne 'click' chemistry... 55
3.1 Introduction 56
3.2 Aims 58
3.3 Results and Discussion 59
3.3.1 Synthesis of disulfide peptide analogue 59
3.3.2 $NaBH_4$ reduction 60
3.3.3 TEC reaction 62
3.3.4 TYC optimization 63
3.3.5 One-pot, thiol-yne mediated disulfide rebridging reaction 66
3.3.6 Scope of one-pot thiol-yne peptide rebridging with chemically diverse alkynes 67
3.3.7 Octreotide scaffold 71
3.4 Conclusions and future work 73
Chapter 4: Naphthalimide-mediated thiol-ene photoredox catalysis 75
4.1 Introduction 76
4.1.1 Photocatalysis 77
4.1.2 Naphthalimides 77
4.2 Aims 79
4.3 Results and Discussion 81
4.3.1 Optimisation in Organic Solvents 81
4.3.2 Scope of Naphthalimides 85
4.3.3 Optimisation in Aqueous Solvents 86
4.4 Conclusion and Future Work 89
Chapter 5: Covalent site-selective screeing platform to discover protein-protein interactions inhibitors 91
5.1 Introduction 92
5.2 Aims 94
5.3 Results and discussion 95
5.3.1 Preliminary studies 96

5.3.2 Thiol-Ene Optimisation 101
5.3.3 Thiol-ene–Mediated mRNA Selection 105
5.4 Conclusions 108
Chapter 6: Conclusions 109
Chapter 7: Experimental 113
7.1 General Experimental Details 114
7.2 Experimental details for Chapter 2 117
7.2.1 General procedures 117
7.2.2 Characterisation data 120
7.2.3 Characterisation Data of Thiol-ene Products 124
7.3 Experimental details for Chapter 3 138
7.3.1 General procedures 138
7.3.2 Characterisation data 139
7.4 Characterization product of Chapter 4 153
7.4.1 Characterisation data 153
7.5 Characterization products of Chapter 5 154
7.5.1 Sequences 154
7.5.2 General Procedures 154
7.5.3 Analysis 157
7.5.4 Characterisation data 158
Chapter 8: References 162
Chapter 9: Appendix 175
9.1 Chapter 2 176
9.1.1 NMR Spectra 176
9.1.2 Analytical Calibrations 191
9.2 Chapter 3 193
9.2.1 NMR Spectra: 193
9.2.2 Analytical Calibrations 200
9.3 Chapter 4 201
9.3.1 NMR Spectra 201
9.4 Chapter 5 202
9.4.1 Urea/SDS-PAGEs reported in Chapter 5. 202

Chapter 1

Introduction

1.1 Therapeutic Proteins and Peptides

Proteins and peptides are crucial for many biological and physiological functions in living organisms. Proteins, the building blocks of life, play a crucial role in various aspects of cellular systems, including structure, binding, regulation, transport, immunity and enzymatic activities.[1] These macromolecules are present in each component of every cell, emphasising their origin from the Greek word "proteios", meaning "primary".[2] They are essential for the function of every living organism.[3] There are three categories of well-known therapeutic agents: small molecules, peptides and biologics (**Table 1.1**).[4] Peptides are a distinct category of pharmaceutical compounds, positioned in between small molecules and biologics, but possessing fundamental biochemical and therapeutical differences from their counterparts. Apart from their low stabilities and short half-lives in comparison with small molecules and biologics,[5] peptides possess sophisticated advantages such as high specificity, low immunogenicity and low-cost manufacturing.[4] Peptides intrinsically signal molecules for many physiological functions such as cellular communication, as defence molecules for the microorganism or biomarkers.[6] Peptides present an opportunity for therapeutic intervention that closely mimic natural pathways.[7]

Table 1.1: Three categories of well-established therapeutic agents and their properties.[4]

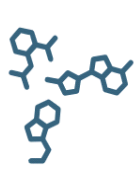

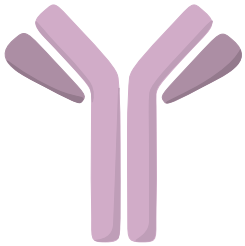

Properties	Small molecules	Peptides	Biologics
Target	Limited	Extensive	Extensive
Affinity	Low	High	High
Selectivity	Low	High	High
Toxicity	High	Low	Low
Immunogenicity	Low	Low	High
Stability	High	Low	Low
Tissue penetration	High	Low	Low
Production cost	Low	Low	High

In biology, natural peptides function as hormones and neurotransmitters for cell communication, as antibodies in the immune system to defend against pathogens and assist in transporting substances across biological membranes, amongst other activities.[8,9] They bind to cell surface receptors and trigger intracellular processes with high affinity

and specificity. Therapeutic proteins and antibodies have a similar mechanism of action to that of biologics, allowing for precise modulation of cellular responses.[10] Short peptide chains primarily serve as messengers for various endocrine signals, such as those involving G protein-coupled receptors or growth factor receptors.[11] This vital function has been leveraged to develop drugs that can act as agonists in signal transduction processes.

Exploration of therapeutic peptides began with the isolation of insulin, a 51-amino acid (AA) peptide, from animal pancreases for therapeutic use in diabetic patients during the 1920s.[12] In the following years, more than 40 peptides drug were approved worldwide.[13] In the 1950s, the nonapeptides Oxytocin[14] and Vasopressin[15] were synthesised by Vincent du Vigneau, for which he was awarded the Nobel Prize. Oxytocin (**1**, **Figure 1.1**) is a multifunctional peptide hormone, acting as a stress-coping agent, anti-inflammatory, and antioxidant.[16] Vasopressin (**2, Figure 1.1**) is a nonapeptide that serves multiple roles as a neurohormone, neuropeptide, and neuromodulator, and is integral to the homeostatic regulation of various physiological processes.[17] Both Oxytocin and Vasopressin are produced in the hypothalamus and released by pituitary glands.

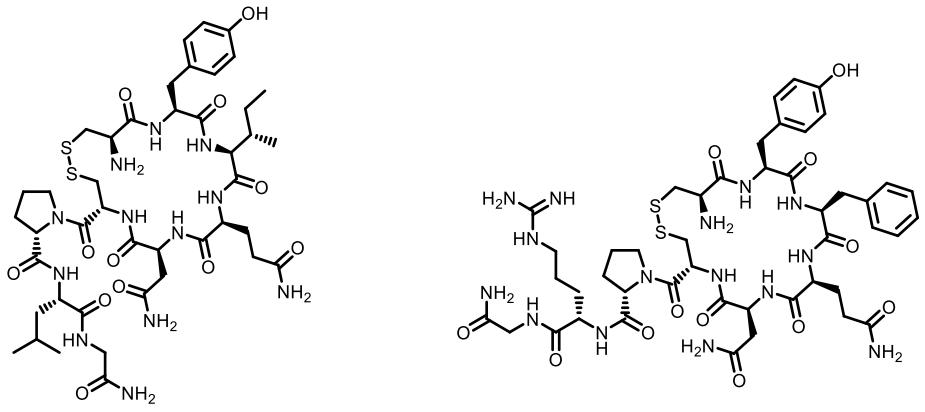

Figure 1.1: Chemical structure of Oxytocin **1** and Vasopressin **2.**

As ever more sophisticated platforms systems for peptide drug discovery and development have been established, peptide drugs have evolved beyond simple hormone mimetics and are no longer limited to natural AAs. To date, more than 170 peptides are in active clinical development, with many more in preclinical studies.[7,10]

1.1.1 Therapeutic Properties of Peptides

Therapeutic peptides are a unique class of drugs composed of specific AA sequences. They typically have molecular weights ranging from 500 to 5000 Da, which is significantly greater than those of small molecule drugs.[10] The high specificity and low toxicity of peptide drugs stem from their exceptionally tight binding to their targets, which can be attributed to the vast chemical diversity provided by the side-chain variations of native AAs.[18] Calculations based on 17 variable residues (excluding Cys, Met, and Trp, which are underrepresented in known ligands) indicate that an 83,000-membered tetrapeptide library can be generated to effectively encompass all unique protein-binding regions.[19] Peptide drugs exhibit remarkable target selectivity, which is reflected in their high success rate in clinical trials. Between 2020 and 2023, a total of 21 peptide-based drugs received regulatory approval, representing a substantial increase compared to only 10 recorded in 2012.[5,20] However, despite their promising attributes, the potential for peptides as therapeutics has been hampered by certain limitations of native peptides, including short plasma half-life, poor oral bioavailability, membrane impermeability, and limited *in vivo* stability.[7,21,22] These drawbacks of peptide therapeutics arise from the presence of numerous peptidases and excretory mechanisms which rapidly degrade and clear them *via* hydrolysis of peptidic amide bonds.[23] While this degradation plays a crucial role in regulating hormone levels and maintaining homeostasis, it possess significant challenges for therapeutic development.[24] Furthermore, the necessity for injection has made peptides a less attractive option for chronic outpatient treatments compared to oral drug delivery, which is preferred for patient compliance. In order to address these challenges, innovative chemical modification strategies have been employed to modulate pharmacokinetic properties. While appropriate formulations or drug delivery systems can help mitigate these issues,[25] chemical modification of peptides has been the primary focus of efforts to date .

1.1.2 Synthetic Strategies for Peptide Modifications

With few exceptions, most peptides exhibit oral bioavailability below 1%.[26] In order to address these limitations, various strategies has been developed to enhance the oral bioavailability and membrane permeability. These include *N*-methylation to reduce hydrogen bonding potential, cyclisation to increase structural rigidity, and the introduction of intramolecular hydrogen bonds to minimise intermolecular hydrogen

bonding and molecular flexibility.[24] Cyclosporin A **3** (**Figure 1.2**) exemplifies the successful integration of these strategies within its structure.

To overcome amide bond degradation by peptidases and proteases present in human tissues,[27] strategies such as N- and C-terminal protection, substitution of L-AA with D-AA, AA modification, cyclisation, and conjugation to macromolecules have all been employed to enhance peptide stability. Some of these approaches enhance other Absorption, Distribution, Metabolism, Excretion (ADME) properties, for example, both stability and permeability can be enhanced in cyclisation, while conjugation to macromolecules can enhance stability and reduce renal clearance. A notable example is the cyclic peptide octreotide **4** (**Figure 1.2**) an analogue of the peptide Somatostatin, which contains non-canonical AAs and has a half-life of approximately 100 minutes in humans.[28] This prolonged half-life is attributed to its binding to plasma lipoproteins, which reduces renal clearance.

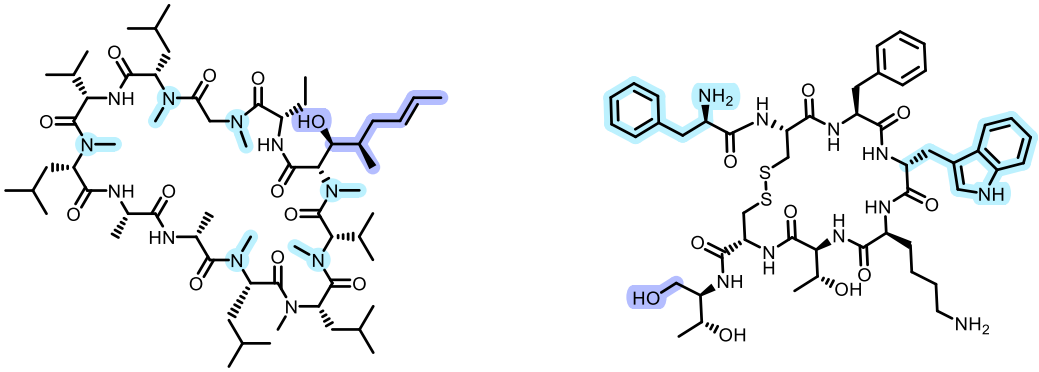

Figure 1.2: The chemical structures of cyclosporin A, **3** with *N*-methylation (in blue) and butenyl-methyl-L-threonine (Bmt) (in purple) modifications and octreotide **4**, with D-AA (in blue) and reduced terminus (in purple) modification.

Considering the therapeutic potential of cyclic peptides, cyclic peptide libraries have gained significant interest in recent years.[29-31] Advancements in biotechnology have led to the successful development of various display techniques for selecting novel peptide-based macrocyclic binders targeting previously undruggable sites.[32] In the 21st century, three primary methods have been developed for peptide library preparation: combinatorial synthetic libraries, DNA-encoded chemical libraries (DELs), phage display, and mRNA display (**Figure 1.3**).[33] The introduction of DELs has significantly expanded high-throughput screening capabilities, surpassing the conventional small molecule library size of approximately 10^6 and establishing itself as a key approach in hit

identification. Meanwhile, mRNA display effectively leverages DEL technology, further increasing the library size limit to approximately 10^{13}, thereby enhancing the discovery of novel peptide-based therapeutics.[34, 35]

In 1992, Sydney Brenner and Richard Lerner pioneered the creation of chemical libraries and individual compounds connected to DNA fragments, which serve as amplifiable identification tags or barcodes.[36] DELs are generated using a split-and-pool strategy, where each synthesised molecule is linked to a unique DNA tag. This DNA tag enables the retrospective identification of the synthetic history of the molecule.[37] Screening of DELs is conducted against an immobilised protein target, and suitable binders are identified through sequencing of the covalently attached DNA tag. (**Figure** 1.**3a**)

By contrast, phage display is an *in vivo* technique in which the translated peptide is attached to a bacteriophage cell surface protein. cDNA is added into the phage coat protein gene.[38] During infection the cDNA is translated and the library peptide becomes attached to a protein which is then displayed on the outside of the phage during phage assembly. The selected sequences can be run through several cycles of phage display to isolate binding sequences with higher affinities for the target (**Figure 1.3b**).

mRNA display involves transcribing a cDNA library into mRNA, with a puromycin molecule attached to its 3′ end. During *in vitro* translation, the ribosome reads the mRNA in the 5′ to 3′ direction, utilising the P (peptidyl) site and A (aminoacyl) site of the ribosome for tRNA binding. The P site holds the tRNA bearing the growing peptide chain, while the A site accommodates the tRNA with the next AA to be incorporated. Upon reaching the stop codon, translation ceases due to the absence of the release factor, allowing the ligated puromycin to enter the A site. Puromycin then covalently attaches to the polypeptide in the P site. The resulting polypeptide is linked to its coding mRNA tag through a DNA spacer, facilitating sequence identification. Typically, the mRNA-peptide complex undergoes reverse transcription, generating a library of cDNA-mRNA duplexes linked to their respective peptides. This is followed by the selection and isolation of binding peptides using an immobilised protein target. The cDNA sequences from the selected binders are then recovered and amplified *via* polymerase chain reaction (PCR) (**Figure 1.3c**). Successive rounds of mRNA display selection are performed until a significant enrichment of specific sequences is achieved. mRNA display has enabled the

screening of 10^{12} – 10^{14} unique library sequences, establishing it as a powerful technique for analysing vast libraries.[32] This technique has several disadvantages, such as the small scale at which peptides are synthesised. In such cases, it may be necessary to resort to synthetic organic chemistry for peptide production.

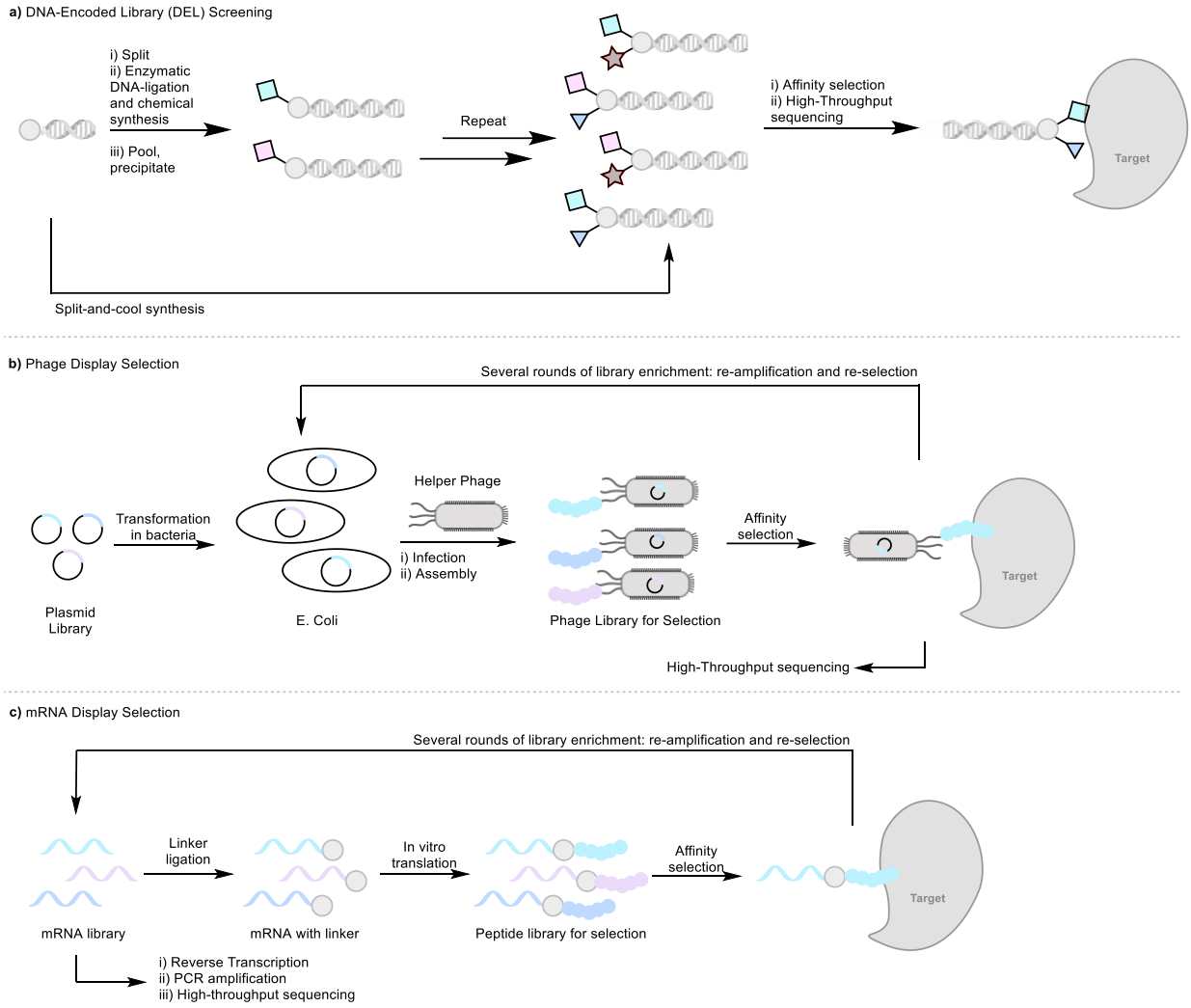

Figure 1.3: Primary methods developed for peptide library preparation in the 21st century: a) DELs, b) Phage display c) mRNA-display.[32]

1.2 Peptide Synthesis

1.2.1 Solution Phase Peptide Synthesis

The fundamental reaction of peptide synthesis is the formation of an amide or 'peptide' bond between the amino group of one AA and the carboxyl group of another. However, this reaction does not occur spontaneously under ambient conditions and requires temperatures exceeding 200 °C.[39] Usually the formation of the amide bond requires the activation of the carboxylic acid to form a reactive intermediate, followed by

the acylation of the amine and subsequent loss of the activating group. This activation of the carboxylic acid can be achieved by the conversion to highly reactive carboxylic acid derivatives such as acid chlorides or anhydrides, or by the formation of an 'active ester' *in situ* using a coupling reagent. In 1901, Emil Fischer reported the first synthesis of a dipeptide glycylglycine by hydrolysis of the diketopiperazine of glycine[40] and few years later, he developed a method of peptide coupling based on the use of acid chloride derivatives (**Scheme 1.1a**).[41] Theodor Curtius developed an azide-coupling method to synthesize *N*-protected polyglycines (**Scheme 1.1b**).[42] However, several limitations were identified with the pioneering work of Fischer and Curtius, including the explosive nature of azides and difficulties in obtaining enantiomerically pure L-AA with easily removable amino-protecting groups. Therefore, a new generation of amide coupling reagents were developed becoming commonplace in the pharmaceutical industry at that time.[43]

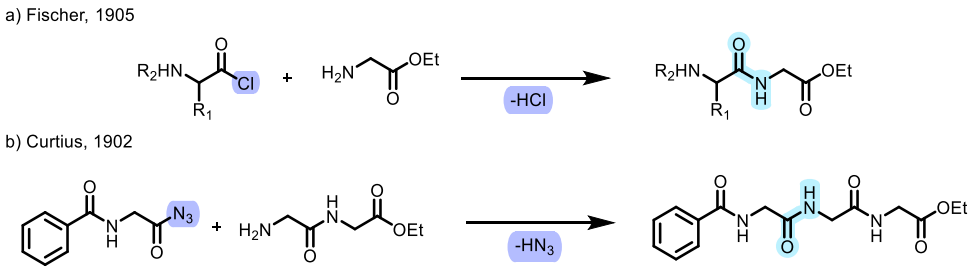

Scheme 1.1: a) Amide coupling by Fischer in 1905. b) Amide coupling by Curtius in 1902.

A key innovation in peptide chemistry lies in the introduction of the coupling reagents typically employed to synthesise the 'active ester' intermediate. The principle coupling reagents include carbodiimides such as *N,N'*-diisopropylcarbodiimide (DIC, **5**), phosphonium salts such as benzotriazol-1-yl-oxytripyrrolidinophosphonium hexafluorophosphate (PyBOP **6**) and uronium/iminium salts such as Hexafluorophosphate Azabenzotriazole Tetramethyl Uronium (HATU) **7** (**Figure 1.4a**). The high reactivity of the *O*-acylurea can undergo either direct α-hydrogen abstraction (Path A, **Figure 1.4b**), leading to formation of enolate species, or intramolecular cyclisation to the formation of an oxazolone (Path B, **Figure 1.4b**), both of which can lead to the racemised product.[44]

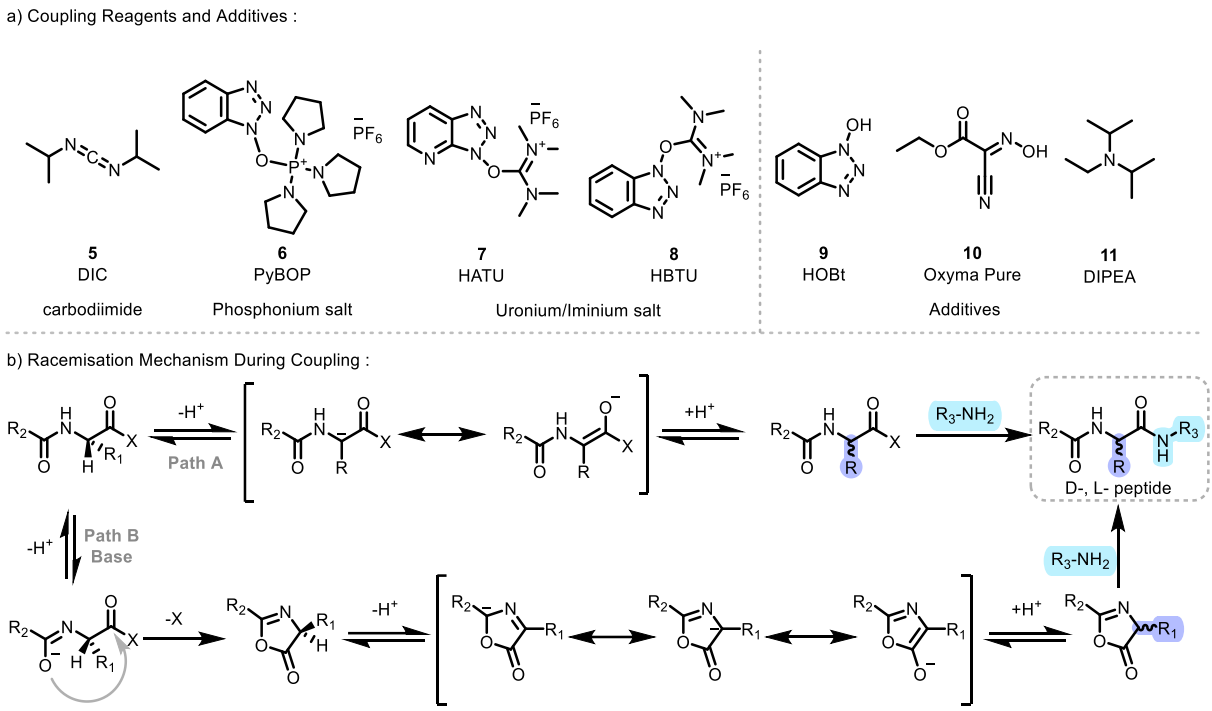

Figure 1.4: a) The chemical structures of coupling reagents and additives used for the synthesis of amide coupling. b) Racemisation mechanisms *via* enolate formation (Path A) and *via* oxazolone (Path B) occurred during amide coupling.

However, the introduction of carbamate based *N*-protecting additives such as 1-hydroxybenzotriazole (HOBt, **9**) was shown to reduce the formation of the oxazolone species.[45] This occurs due to the conversion of the *O*-acylurea ester to an *O*-benzotriazole (OBt) activated ester, stabilising the molecule and prevent *O*- to *N*-acyl transfer. HOBt was later replaced by Oxyma Pure **10**, reported by Albercio,[46] which was determined to be more favourable for industry use due to achieving superior coupling efficiencies while inhibiting racemisation and lacking the explosive character of benzotriazole additives. Tertiary amine additives such as *N,N*-Diisopropylethylamine (DIPEA, **11**) or *N*-methylmorpholine (NMM) can limit the deprotonation pathway due to their non-nucleophilic character.[47] Finally, PyBOP **6** and Hexafluorophosphate Benzotriazole Tetramethyl Uronium (HBTU) **8** (**Figure 1.4a**) have been demonstrated to be very efficient as coupling reagents due to their mild activation conditions, racemisation suppression, relative safety and low cost.[48]

Due to the multiple steps required for these deprotection/coupling methodologies, as well as the use of various coupling reagents which necessitate purification at each step, solution-phase peptide synthesis becomes ineffective and tedious. This inefficiency is further intensified by the need to repeat the process for each AA used, leading to a

significant decrease in yields and making the peptides synthesis of longer sequences nearly impossible.[49] The discovery of solid-phase peptide synthesis (SPPS) resulted in a paradigm shift which enabled modern synthetic peptide chemistry as we now know it.

1.2.2 Solid Phase Peptide Synthesis

SPPS was first developed by Merrifield in 1963 who was awarded the Nobel Prize in 1984 for the synthesis of a tetrapeptide, Leucine-Alanine-Glycine-Valine (H-Leu-Ala-Gly-Val-OH), using polystyrene resin functionalised with chloromethyl linker.[50] SPPS utilises a functionalised insoluble polymer support to facilitate the covalent attachment of the C-terminus residue of an *N*-protected AA through successive reactions and filtrations resulting in the elongation of a sequence bound to the resin (**Figure 1.5**).[51] Reactive side chains from the AA are protected by orthogonal protecting groups in order to prevent unwanted side reactions. Once the AA is attached to the resin, cycles of washings and filtration are enacted to remove any side-products and excess reagents without the need of chromatographic purification. The *N*-protecting group from the following AA is then deprotected and coupled to the existing C-terminus. The cycle is then repeated until the desired peptide sequence is complete. Finally, the AA side chains of the resin-bound peptide are globally deprotected and the peptide is cleaved from the resin. SPPS possesses several advantages over the solution-phase synthesis such as the rapid synthesis of peptides, as purification steps between coupling steps are avoided, and the ease with which more synthetically challenging couplings are achieved, due to the energy provided by microwave heating.[52] Another fundamental advantage is that the resin imparts a high level of chemical selectivity itself due to the resin serves as a temporary protecting group and also enables the specific functionalisation of the peptide C-terminus.[53]

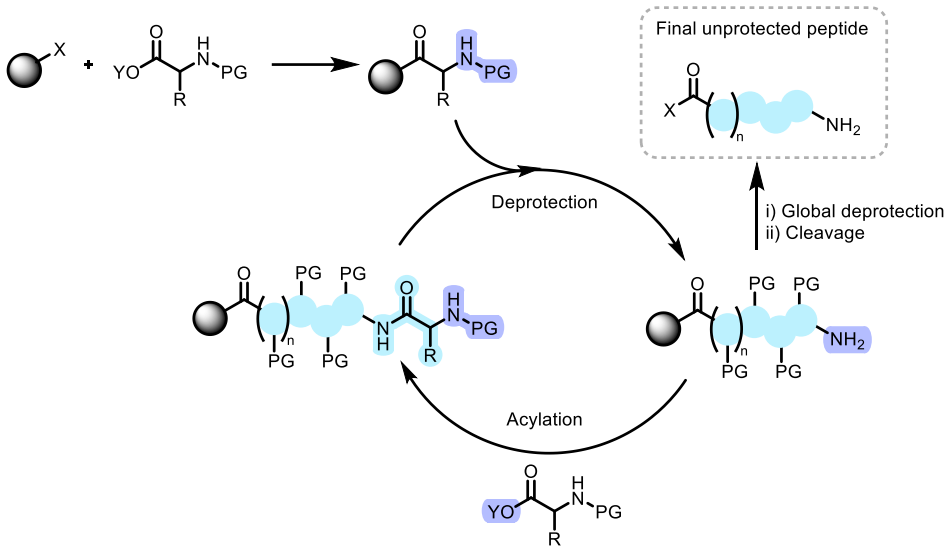

Figure 1.5: SPPS workflow. PG =Protecting Group

In 1965, Merrifield and Stewart engineered a fully automated peptide synthetiser and applied it to the synthesis of 9-AA hormone bradykinin in 32 h, allowing 4 h per AA.[54] In 1962, a 124-AA biologically active enzyme was synthesised by Gutte and Merrifield which become the largest peptide automatically synthesised at the time.[55] The application of microwave systems by Yu *et al*.[56] along with development of new supports and novel activating groups represent some of the emerging technologies that the scientific community has been focused in the recent times.[44, 57, 58] Microwave-automated solid-phase synthesisers have revolutionised both the pharmaceutical industry and academic research.[59]

1.2 3 Limitations of SPPS

Although SPPS has proven to be the most efficient methodology for peptide synthesis, it still possesses several disadvantages and ongoing challenges. For the synthesis of larger peptides (>30 AAs), it is necessary to use low-loading resins, which provide greater spacing between C-terminal attachment sites on their surface to minimise peptide aggregation. However, due to the inherently lower AA loading capacity per mmol of resin, there is a higher cost per mmol of product peptide. Kent *et al*.,[60] introduced the concept of 'difficult sequences', referring to peptide chains with a high number of AAs which tend to form intramolecular β-sheets structures, leading to increased aggregation potential (**Figure 1.6**). This aggregation arises from non-covalent hydrogen bond interactions between the hydrogen amides and the carbonyls from the core of the peptide.

Consequently, these sequences often exhibit poor deprotection and coupling efficiencies, making their handling, synthesis, and purification particularly challenging or even unfeasible.[61] Various factors contribute to the increased propensity for inter-chain interactions during peptide synthesis, including AA side chains, protecting groups, the nature of *N*-substitution on the amide backbone and the solvent system employed.[62,63]

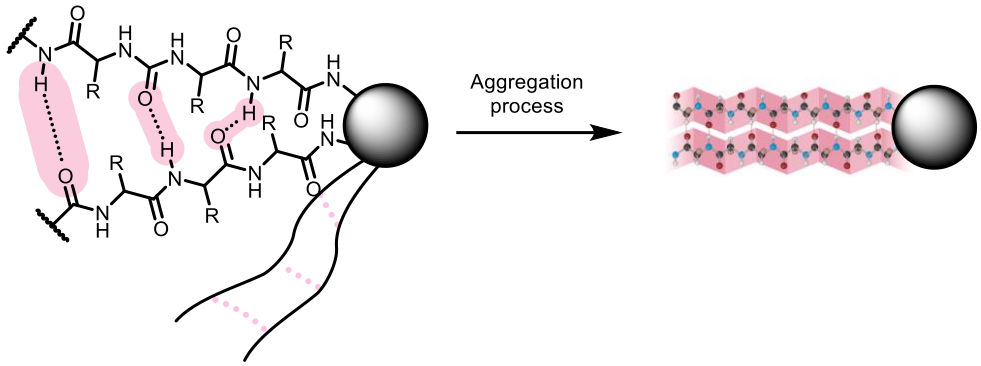

Figure 1.6: Inter-chain hydrogen bonding during on-resin peptide synthesis and aggregation into β-sheets.[61]

Additionally, large amounts of solvent and reagents are typically required, often resulting in very low overall peptide yields. In general, achieving a satisfactory yield of the final product requires at a minimum: 4 equivalents of coupling reagent/additive, 4 equivalents of AA, and 8 equivalents of base.[64] Further research is still needed to improve the synthesis of larger peptides and to develop more sustainable alternatives to the standard conditions of SPPS.

1.2.4 Chemical Ligations

Novel chemical and chemoenzymatic approaches have been developed for the synthesis of large peptides and proteins to address the limitations of SPPS. Chemical ligation has proven to be the most useful and important approach, as it enables the general coupling of unprotected peptide fragments in aqueous solution. In 1953, Wieland reported the ability to form an amide bond *via* an intramolecular acyl shift (**Figure 1.7a**).[65] They reported that valine thiophenyl ester **12** carried out amide bond formation at an accelerated rate in aqueous solution at pH >7 with unprotected Cys **13** to form Val-Cys dipeptide **14**. Following a similar principle, Kemp and Kerman[66, 67] introduced the first ligation methodology for coupling two SPPS-synthesised peptide fragments through

a "prior thiol capture strategy". In this strategy, peptide fragment 1 is protected at the C-terminus by derivatisation with an ester group. Activation of the system occurs through deprotection of a thiol group, which then reacts with the N-terminal cysteine (Cys) residue of peptide fragment 2, forming a disulfide bond. The "capture site" is defined by the thiol residue, which facilitates the attachment of the second peptide fragment. An intramolecular acyl transfer subsequently forms a new amide bond between peptide fragments 1 and 2, and the final peptide is then released from the template (**Figure 1.7b**). The kinetics of the acyl transfer process have been shown to be highly sensitive to steric effects, with reaction times ranging from 3 hours for Ala to 51 hours and 34 hours for Val and proline (Pro), respectively.[68] This methodology was applied to the synthesis of the 29-residue C-terminus of the protein basic trypsin inhibitor.[69]

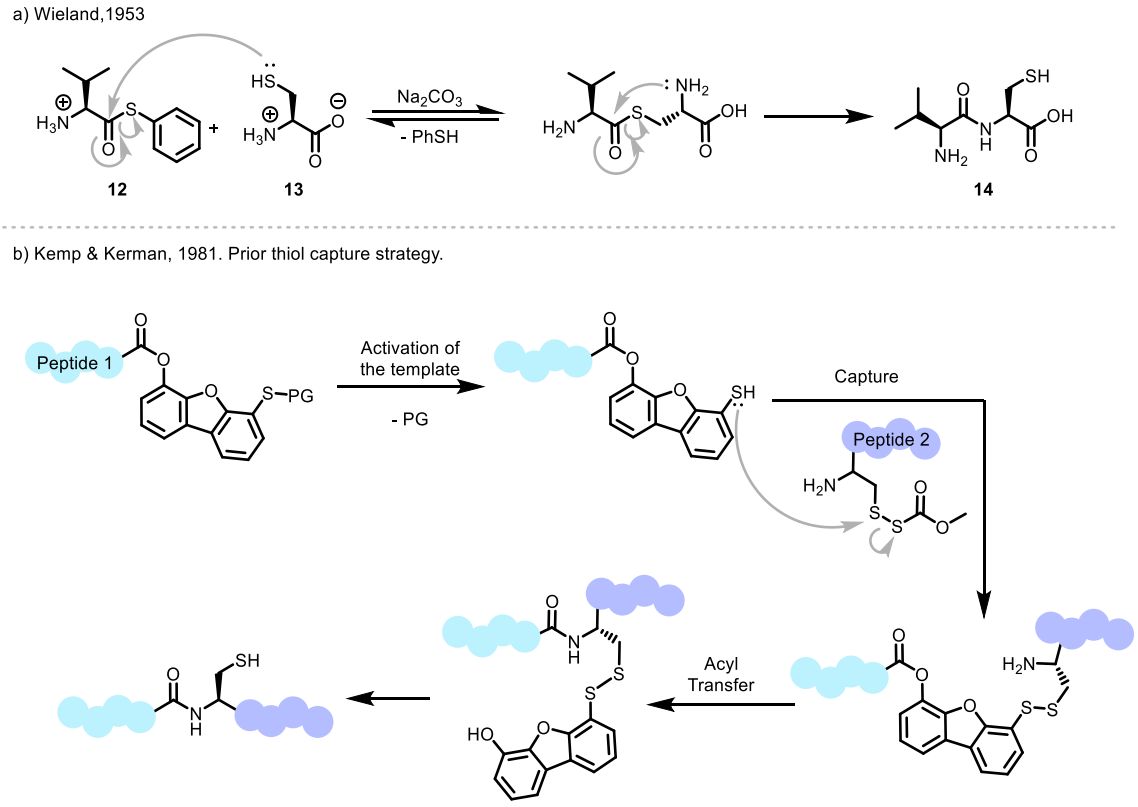

Figure 1.7: Mechanism of: a) The first example of amide coupling *via* an acyl shift by Wieland in 1953. b) The principle of the 'prior thiol-capture strategy' by Kemp and Kerman in 1981.[8] PG= Protecting Group.

Following this work, several chemical ligation strategies were developed, among which native chemical ligation (NCL) became the most important and widely used, as reported by Kent and co-workers in 1994.[70] NCL involves the chemoselective reaction between an N-terminal Cys and a C-terminal thioester. The process begins with a transthioesterification step at pH 7, forming a labile thioester intermediate, followed by

an intramolecular *S*-to-*N*-acyl shift to furnish the native amide bond (**Scheme 1.2**). In comparison with the previously reported technique by Kemp and co-workers, this strategy also enables the coupling of two unprotected peptide fragments in aqueous solution. However, in this case, the ligation reaction results in the formation of a 'native' amide bond at the ligation site.[8] Despite its advantages, this methodology is limited by the requirement for a Cys residue at the ligation junction, a significant drawback, since Cys is relatively rare in natural proteins.[71] To overcome this limitation, a variety of related methodologies inspired by NCL have been developed. These include the substitution of a non-essential AA with Cys, as demonstrated by Dawson *et al*.,[72] applied to the synthesis of the 110-residue enzyme Cys49 barnase and auxiliary-mediated ligation (AML), which enables ligation at non-Cys sites.

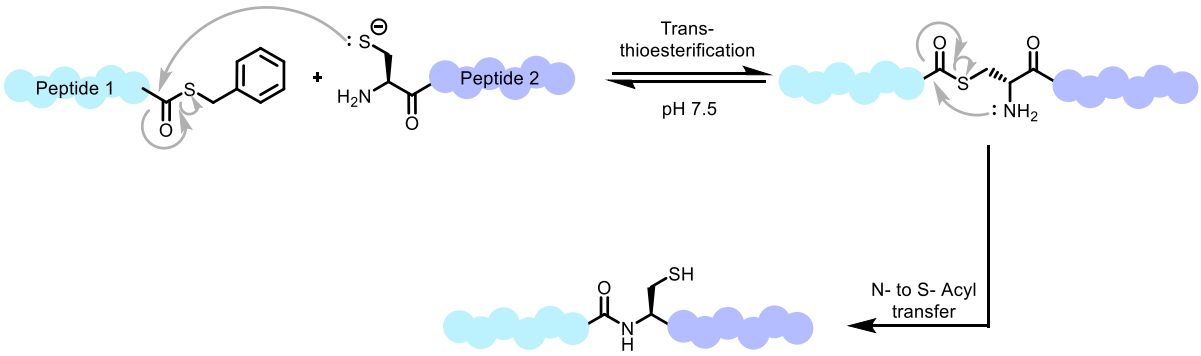

Scheme 1.2: NCL mechanism.

1.3 Peptide Modifications

Synthetic modifications, which are often analogous to post-translational modifications (PTMs), can be achieved by several methods, depending on the biomedical objective. For example, the addition of polymers,[73] carbohydrates,[74, 75] or lipids[76-78] to the peptide, or the formation of antibody–peptide drug conjugates[79] can promote cellular targeting and uptake of the drug. These modifications can also facilitate bioimaging[80] and have applications in material science.[81] In 2019, oral Semaglutide became the first glucagon-like peptide-based receptor agonist (GLP-1RA) with C_{18} fatty diacid chain is attached to Lys26 *via* a spacer, to receive marketing authorisation for the treatment of type 2 diabetes.[5] Among 2024 approvals, examples include Palopegteriparatide, which uses PEGylation to extend circulation time, and Pegulicianine, which is enzymatically activated within the tumour microenvironment.[5]

Modified peptides have been used as drug candidates in the treatment of cancer, enzyme deficiency or metabolic disorders and infectious diseases.[18] Creating additional methods targeting to individual AAs holds great potential to enable researchers in chemical biology, life sciences, and clinical medicine to use these techniques for targeted applications.[82,83] Furthermore, targeting weakly nucleophilic or poor surface-exposed AA residues has also been a primary aim for the researchers in these areas. An example of this was the chemoselective bioconjugation of methionine (Met) residues *via* photoredox reaction by Lin *et al.*[84] More recently, there has been focused on the activation of AA residues by the addition of reactive reagents for relatively inert AA or the addition of electrophiles that can react with AA residues such as Lys and Cys.[85-87]

1.3.1 Cysteine-selective Chemical Peptide Modification

Cys is one of the least abundant AA in human proteins[88] and is therefore an ideal functional handle to achieve selective modification of therapeutic peptides. Cys thiol is both reduction/oxidation (redox)-active and highly nucleophilic.[89] In proteins, Cys participates in numerous chemical reactions such as catalysis, redox and metal trafficking due to its high nucleophilicity and variable oxidation states.[90] The nucleophilicity of the Cys residue is governed by the pKa and ionisation state of the thiol,[91] whereas the oxidative capacity depends on the redox potential of a disulfide pair.[92] The pKa of a surface-exposed Cys thiol is around 8.0,[93] however the pKa values range can be from 3.5 to 12 depending on the local protein environments.[94] For this reason, Cys modification using selective electrophiles has been developed in the recent years with the use of alkyl halides, Michael acceptors and alkynes (**Figure 1.8**).[95]

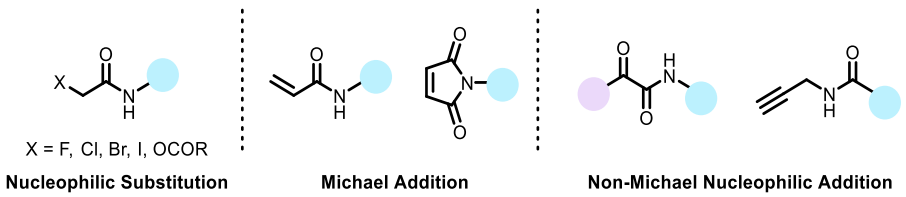

Figure 1.8: Traditional electrophiles for Cys modification.

The most extensively explored electrophilic group for reaction with thiols are the haloacetamides, which are compounds containing a halide in the α position of a carbonyl moiety. This reaction was first reported in the 1930s with a ligation between glutathione (GSH) and iodo-, bromo-, and chloroacetyl reagents.[96] Several years later, this reaction,

which is spontaneous at basic pH, was employed for peptide cyclisation, occurring between a chloroacetyl group at the N-terminus and an internal Cys residue of the peptide. This approach was widely used in the Random non-standard Peptides Integrated Discovery (RaPID) platform for the discovery of biologically active peptide macrocycles *via* mRNA display.[97]

The thia-Michael addition reaction has also become a valuable tool for Cys modification in a wild range of fields in chemical and biological systems. The thia-Michael reaction consists of the nucleophilic attack of an induced thiolate anion onto the electron deficient alkene, shown to be the rate-determining step of the thia-Michael addition reaction pathway (**Figure 1.9**). The initiation process can begins with the abstraction of a proton from a thiol which acts as a Brønsted acid by a Brønsted base catalyst, resulting in the *in situ* generation of a thiolate anion and its corresponding conjugate acid (**Figure 1.9a**).[98] The efficiency of this deprotonation step is governed primarily by the pKa of the thiol and the basicity of the catalyst. A lower thiol pKa or a stronger base facilitates more efficient formation of the thiolate, which is a highly nucleophilic with typically unstable intermediate.[99] This reactive thiolate subsequently performs a nucleophilic attack on the electron-deficient β-carbon of an activated alkene, forming a carbanion intermediate (**Figure 1.9b**). In the final step, the carbanion abstracts a proton from the previously formed conjugate acid, leading to the formation of the thioether product and regeneration of the thiolate species, thereby enabling catalytic turnover.

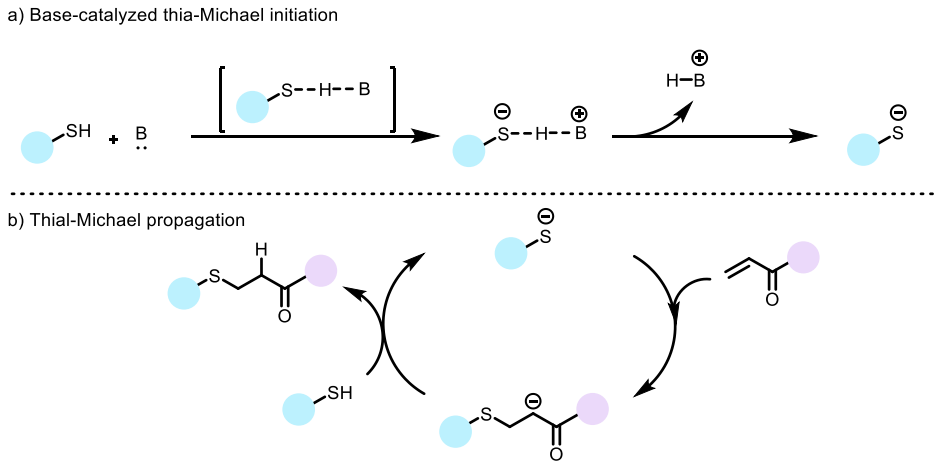

Figure 1.9: Thia-Michael addition mechanism. a) Base-catalysed thia-Michael initiation b) Propagation step of the thiolate to the β-carbon of an activated alkene and consequent proton abstraction from another thiol with the thiolate regeneration.[100]

Maleimide motifs are the most commonly used modification for Cys residues in proteins,[100] since they are considered to be highly reactive and selective conjugate acceptors. The importance of maleimide chemistry was demonstrated in 1949 with the antimitotic activity of maleimide in tissue cultures of chick fibroblasts,[101] and the first conjugation reaction between maleimide and a Cys residue was published in 1956 with *N,N'-(*1,3-phenylene)-bis-maleimide, which was used as a crosslinking agent.[102] Several applications have been developed following this approach and they have been used for imaging Cys residues in proteins and for the bioconjugation of drugs onto macromolecules.[103]

Finally, some advances in the applications of Cys-reactive small molecules have been developed as diagnostic and therapeutic tools for cancer. Some proteins such as oxidoreductases, proteases, kinases, transcription factors, and metabolic enzymes that regulate cancer pathogenesis have been identified as potential theragnostic targets.[90] Owing to the presence of a highly reactive Cys residue in these proteins, targeting these functional Cys with Cys-reactive small molecules represents a common strategy to modulate activity. Other methodologies have recently been developed, including photochemical peptide reactions as modification and bioconjugation strategies for Cys residues in proteins.

1.3.2 Photochemical Peptide Modifications

Photochemical bioconjugation methods possess spatial and temporal control with their reagent-free and selective nature. These types of reaction require the use of light which initiates the reaction, generating highly reactive intermediates *in situ*. The first investigations of this method utilised high-energy ultraviolet (UV) light which was very efficient for certain applications in chemical biology.[104] However several disadvantages were found as a result of the UV exposure, such as the observation of side-reactions or the damage of biomolecules, cells and whole organisms.[105] Switching from UV to visible light was shown to be milder even in complex matrices and in the case of far-red or near-infrared (NIR) light, high tissue penetration with minimum cellular damage has been achieved.[106]

Photochemical peptide modification can typically be grouped in two categories, based on whether the photoexcited state is generated by i) direct excitation or ii) indirect excitation *via* a photoactive additive. By direct excitation, the molecule itself achieves

the desired excited state. This method has been used in biomacromolecular modification and in peptide macrocyclisation.[107] However, this process has limited application and is often used with conjugated systems to lower their excitation energies into the range of visible light.[104] Therefore, indirect excitation is the more commonly employed photochemical modification method used with biomolecules. It involves the activation of a surrogate visible-light antenna chromophore to its excited state, such as a photocatalyst (PC) or photoinitiator. Three main methodologies have been studied for indirect excitation: hydrogen atom transfer (HAT), single electron transfer (SET), and energy transfer (EnT) (**Figure 1.10**).

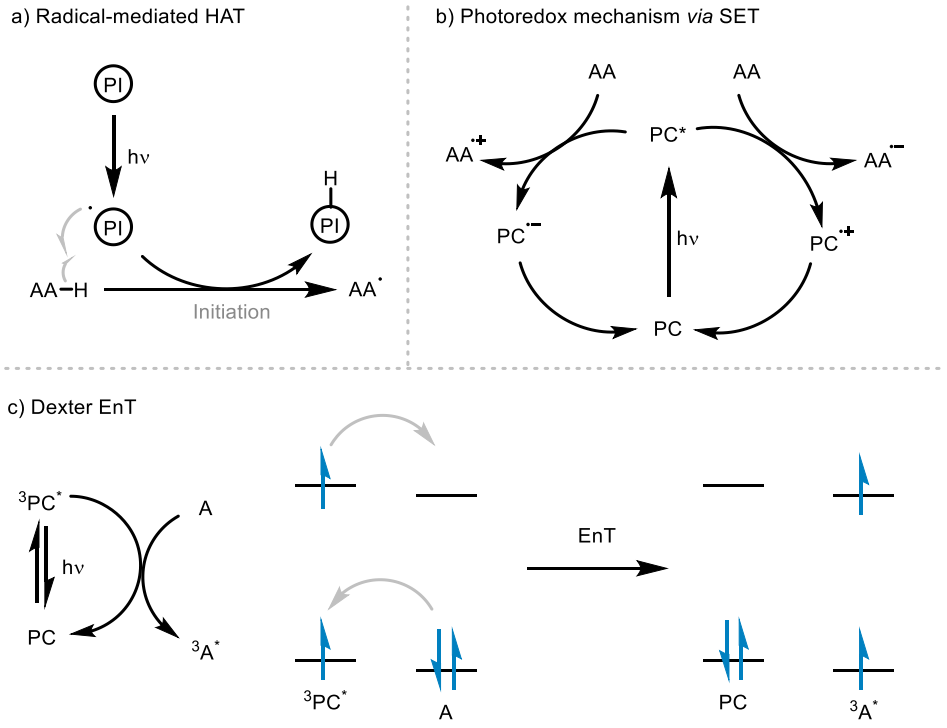

Figure 1.10: Indirect methodologies mechanisms for reactive intermediates *via* photosensitation. PI = photoinitiator, PC = photocatalyst, AA = amino acid, A = Acceptor.[104]

HAT involves the abstraction of a hydrogen atom from the substrate by an initiator to generate a reactive intermediate. SET occurs when a high-energy excited state interacts with the substrate, typically mediated by a PC. A wide variety of PCs exist, each with distinct photochemical properties. When electron transfer occurs from the excited PC to the substrate, the process is referred as a photoredox reaction.[108] EnT involves the transmission of energy from an excited donor, usually in a high-energy triplet state, to a substrate.[109] In this process, the donor relaxes to its ground state while transferring its energy to the acceptor, promoting the acceptor to its own triplet excited state. In contrast with SET, HAT is not recovered since the photoinitiator breaks down into a two different

radical species and they are cleaved by the hydrogen extraction of the substrate, although this not always the case.[110]

Photoactivable moieties are widely employed in the field of bioconjugation, particularly in photoaffinity labelling strategies. Commonly used photoreactive groups, such as diazirines and aryl azides, generate highly reactive intermediates upon light activation. These species can covalently modify proximal biomolecules in a broadly reactive and non-selective manner. A notable example being the thiol–ene click (TEC) reaction, which offers broad applicability for peptide and protein modification. Thiols are commonly used in nucleophilic reactions such as alkylation,[111] arylation,[112] and disulfide bond formation.[113] However, nucleophilic TEC reactions often suffer from limited selectivity, as they typically require activation and may involve electrophilic alkenes that can undergo side reactions with other nucleophilic residues, such as Lys.[114] In contrast, the photoinduced TEC mechanism, which proceeds *via* the generation of thiyl radicals that selectively add onto unactivated alkenes, provides a more chemoselective and efficient alternative.[107]

1.4 Thiol-Ene Click reaction

Free-radical mediated reactions have emerged as one of the most powerful tools for the modification of peptides and proteins at Cys.[115] TEC has emerged as the preeminent methodology in recent years.[116] This reaction is considered a 'click' reaction as defined by Sharpless.[117] A 'click' reaction must fulfil several criteria including (i) possess wide scope (ii) generate readily removable by-products (iii) be stereospecific (iv) high yielding (v) atom efficient and (iv) compatible with ambient conditions (H_2O or O_2).[117] The thiol-ene reaction requires an initiator in order to facilitate thiyl radical formation. Thermal initiation or photoinitiation can be used, although the latter is preferred for peptide substrates in order to avoid undesirable side reactions under heating.[118,119] The most commonly employed initiators reported in peptide radical chemistry are 2,2-dimethoxy-2-phenylacetophenone (DPAP, **15**), 2-hydroxy-4'-(2-hydroxyethoxy)-2-methylpropiophenone (Irgacure 2959, **16**) and 2,2'-azobis[2-(2 imidazolin-2-yl) propane]-dihydrochloride (VA-044, **17**) (**Figure 1.11**).[107]

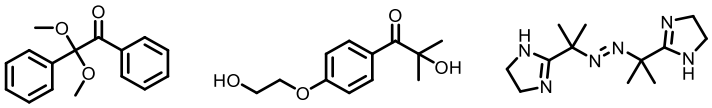

Figure 1.11: Molecular structure of common initiators: DPAP **15**, Irgacure 2959 **16**, and VA-044 **17.**

The radical-mediated thiol-ene mechanism involves three distinct stages (i) initiation: which involves generation of a thiyl radical by an homolytic cleavage of the S-H bond (ii) propagation: whereby the thiyl radical undergoes anti-Markovnikov addition onto an alkene to furnish a carbon-centered radical. The carbon-centered radical then extracts a hydrogen from another thiol to give the thioether product and a new thiyl radical capable of propagating the cycle and finally (iii) termination: whereby any unreacted radical species dimerise, notably, termination products are usually undetectable in thiol-ene reactions due to the high overall efficiency of the process (**Figure 1.12**).[120]

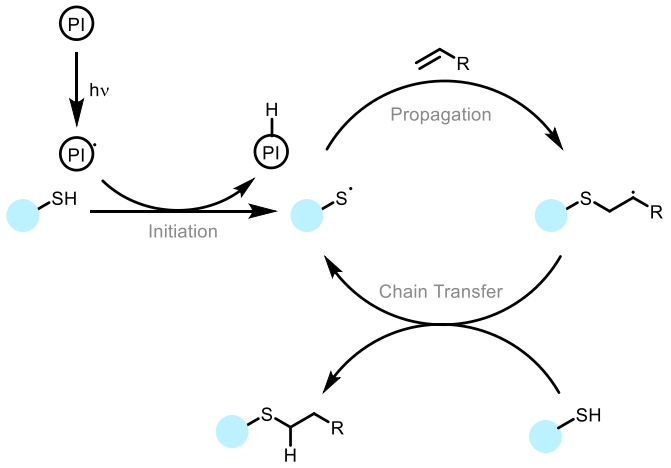

Figure 1.12: Radical chain mechanism of the thiol-ene reaction.[121] PI= Photoinitiator.

1.4.1 Mechanistic Considerations

The radical chain mechanism of the thiol–ene reaction is governed by the ease of hydrogen atom abstraction to generate thiyl radicals, as well as its compatibility with both organic and aqueous solvents. The relatively low bond dissociation energy (BDE) of the thiol S–H bond, approximately 87 kcal·mol^{-1}, is significantly lower than that of a typical C–H bond. This facilitates efficient radical formation, making thiols effective initiating species in radical processes. Depending on the thiol nature BDE differs in significant units. As an example, aryl thiols BDE are around 79 kcal mol^{-1} whereas in the alkyl thiols

can achieve 70 or 84 kcal·mol^{-1} in the case of 4-aminothiolphenol and pentafluorothiophenol, respectively.

The key steps for rate determination are the attack of the thiyl radical on the alkene (propagation) and the chain transfer of the reaction *via* thiol proton abstraction by the carbon-centred radical. The nature of the alkene plays a very significant role in governing the efficiency and outcome of the thiol-ene reaction.[107] Experimental investigations of photoinitiated thiol-ene reactions have shown that alkene structure can affect the rate of the reaction. Norbornene and electron rich alkenes, such as vinyl ether and allyl ether, are the most reactive while electron poor and conjugated alkenes are the least reactive due to the respective stabilities of the *C*-centred radical intermediates in each case.[115] In addition, when the radical attack is significantly slower than the chain transfer, the concentration of alkene is the determining factor, as in the case of less reactive or electron poor alkenes.[122] In contrast, the thiol becomes the rate limiting reactant when the chain transfer is the limiting step. This occurs with thiols with a low propensity to form thiyl radicals such as sterically hindered or less stable thiols due to the lack of resonance stabilisation.[123] All of these kinetic factors have been studied over the years by the correlation between the propagation (k_P) and chain transfer rates (k_{CT}), first published by Griesbaum in 1970.[124]

1.4.2 Thiol-yne Reaction

The analogous reaction thiol-yne click (TYC) reaction involves the addition of a thiyl radical to an alkyne. In some instances, it is followed by a second addition of either the same or a different thiol undergoing a sequential thiol-ene reaction (**Scheme 1.3**). As in the case of TEC reaction, TYC requires use of an initiator to induce the thiyl radical and start the cycle. The initiators typically employed for this reaction are typically the same as those employed for TEC.

Scheme 1.3: TYC reaction workflow.

Several potential side products can arise from competing termination pathways. Compared to the thiol-ene reaction, the intramolecular thiol-yne reaction has been less extensively studied, with only a limited number of examples reported in the

literature.[125,126] As a disadvantage, the *Z*/*E*-isomers of TYC varies, but some examples have been reported where formation of the *Z*-isomer is favoured.[127,128] Generally considered complementary to thiol-ene and copper-catalyzed azide-alkyne cycloaddition (CuAAC) reactions, the thiol-yne reaction may offer unique advantages for peptide science where dual modification is an advantage, for example in the case of glycosylation.[129] Peptide conjugation *via* TYC has proven particularly useful for network polymer synthesis,[130] post-polymerization modification,[131] hyperbranched and dendritic (co)polymer synthesis,[132] and surface functionalization.[133]

1.5 Applications of Thiol-Ene in Peptide Chemistry

Chemical modifications have become an efficient tool for synthesis of modified peptides and proteins. Chemical modifications give rise to precise and uniform alterations for the development of therapeutics.[120] One of the most common approaches involves targeting native AAs such as Lys or Cys, which possess functional side chains amenable to chemical modification. Numerous methodologies have been reported demonstrating chemoselective targeting of specific functional groups or AA residues. Among these, the most widely explored and established approach is the CuAAC, developed by Meldal and Tornøe, who were awarded the Nobel Prize in 2022.[134] Thiol-ene chemistry offers some advantages over other related 'click' methodologies by forming an irreversible thioether bond between the target protein or peptide and the desired probe (**Figure 1.13**). This robust linker, which is also found naturally in nature, for example in methionine, is resistant to degradation by enzymes, rendering the thiol-ene reaction a highly selective and efficient strategy for bioconjugation. Thiol-ene chemistry has been most commonly used for chemical peptide and protein modification applications including glycosylation, lipidation and macrocyclisation.

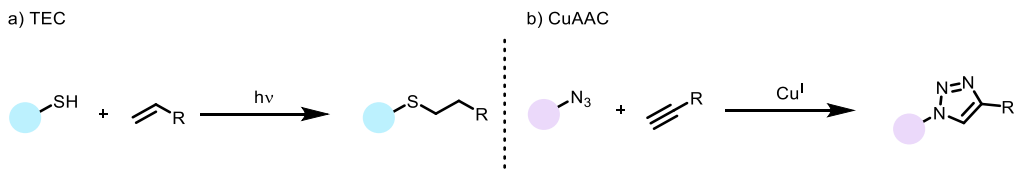

Figure 1.13: Comparison of covalent 'click' linker reactions: a) TEC reaction, b) CuAAC.

1.5.1 Peptide Bioconjugation

Both ionic and radical-mediated chemistries have been successfully employed in peptide and protein bioconjugation to achieve the formation of modified substrates displaying distinct chemical entities linked by thioether bonds. Due to the mild reaction conditions the thiol-ene reaction, the high degree of functional group compatibility and the complete chemoselectivity, the TEC reaction suited to the study of biomolecules including peptides, proteins, carbohydrates, nucleotides and lipids.

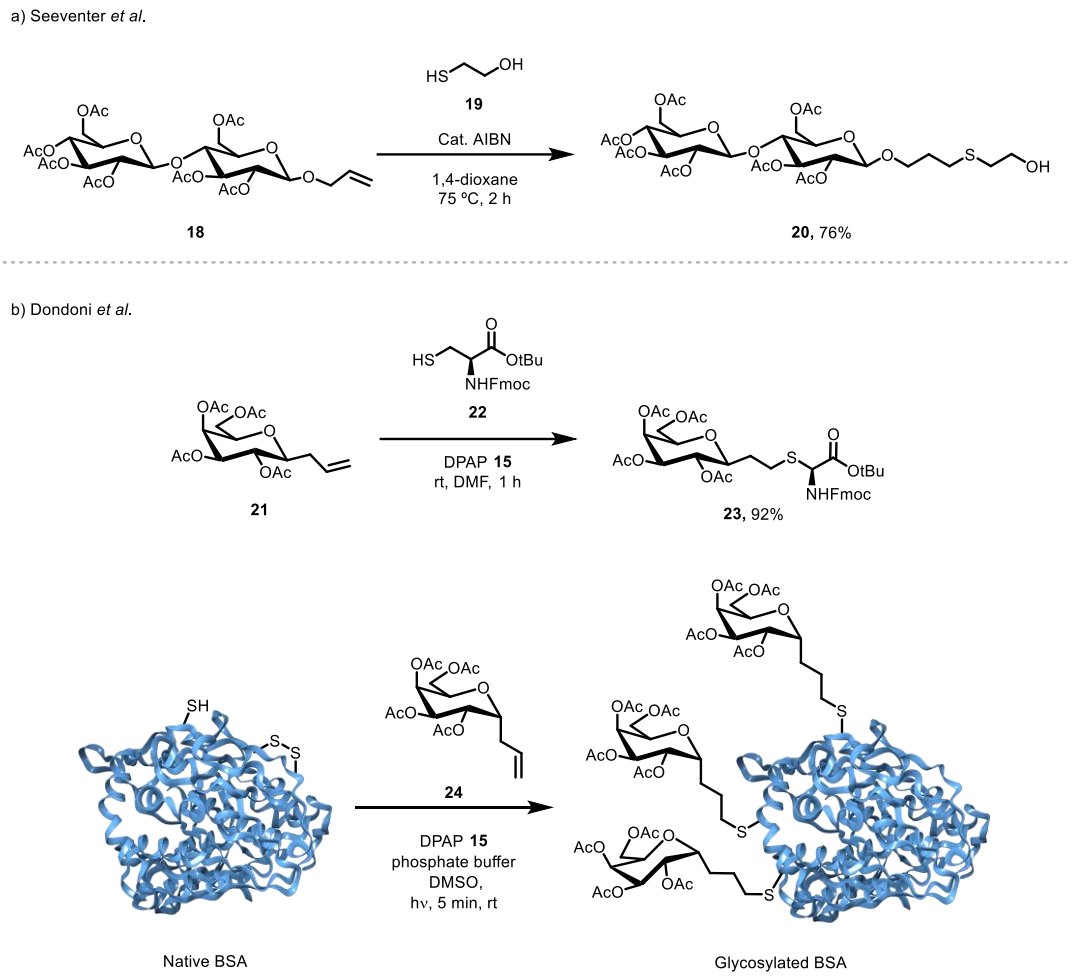

Figure 1.14: a) First glycosylation reaction *via* TEC chemistry by Seeventer *et al.* b) Work by Dondoni *et al.* with the previous optimisation of allylated monosaccharide **24** with protected Cys and the optimised conditions applied to the Cys-containing protein BSA.

It has been estimated that more than 50% of the human proteins are glycosylated, making glycosylation one of the most common post-translational modifications (PTMs) of proteins.[135] The first example of a thiol-ene mediated glycosylation reaction was reported in 1974 by Lee *et al.,*[136] and expanded by Van Seeventer and coworkers in the

1990's.[137] The reaction consisted of an allylated disaccharide **18** with mercaptoethanol **19** to furnish the target thioether product **20** in a 76% yield (**Figure 1.14a**).

Following these early studies which demonstrated compatibility of TEC with glycans, thiol-ene chemistry has been widely applied in glycoscience, for example it has been used for the synthesis of thiosugar monomers and *S*-disaccharides as enzymatic probes,[136] for the synthesis of glycosylated AAs for use in SPPS,[138] and even for oligosaccharides and carbohydrate derived biomaterials.[139] Dondoni and coworkers first applied radical mediated thiol-ene to the glycosylation of protected Cys derivates. The reaction consisted of *C*-allyl glycoside **21** reacting with Fmoc and ^{t}Bu protected Cys **22** using DPAP **15** as photoinitiator to furnish the glycosylated monomer **23** in 92% yield (**Figure 1.14b**).[140] This methodology was later applied to the glycosylation of bovine serum albumin (BSA) which contains three distinct Cys residues (**Figure 1.14b**).[140] These optimised conditions were then applied to the thiolate monosaccharide **24** and alkene-based unnatural amino acids (UAAs), including protected allylglycine (Agl) and protected vinylglycine, achieving the corresponding thioether glycoconjugates in yields greater than 80% (**Figure 1.14b**).[141]

Floyd *et al*. demonstrated direct thiosugar conjugation onto unsaturated proteins *via* TEC chemistry by incorporating the UAA L-homoallylglycine (Hag) in place of Met residues.[142] Initially, they optimised the reaction conditions between a thiosugar **25** and Hag **26** using VA-044 **17** as a photoinitiator, achieving a 79% isolated yield of the glycoconjugate **27** (**Figure 1.15a**). This chemistry was subsequently applied to three different protein substrates: Np276, SsβG, and the Qβ virus capsid, each expressed in *E. coli* with a single Met codon replaced by Hag through site-directed mutagenesis. All inputs were performed at pH 4 and achieved over 95% conversion as determined by RP-HPLC (**Figure 1.15b**). This work demonstrated the first application of the thiol-ene reaction for site-specific protein modification using a 'tag-and-modify' strategy.

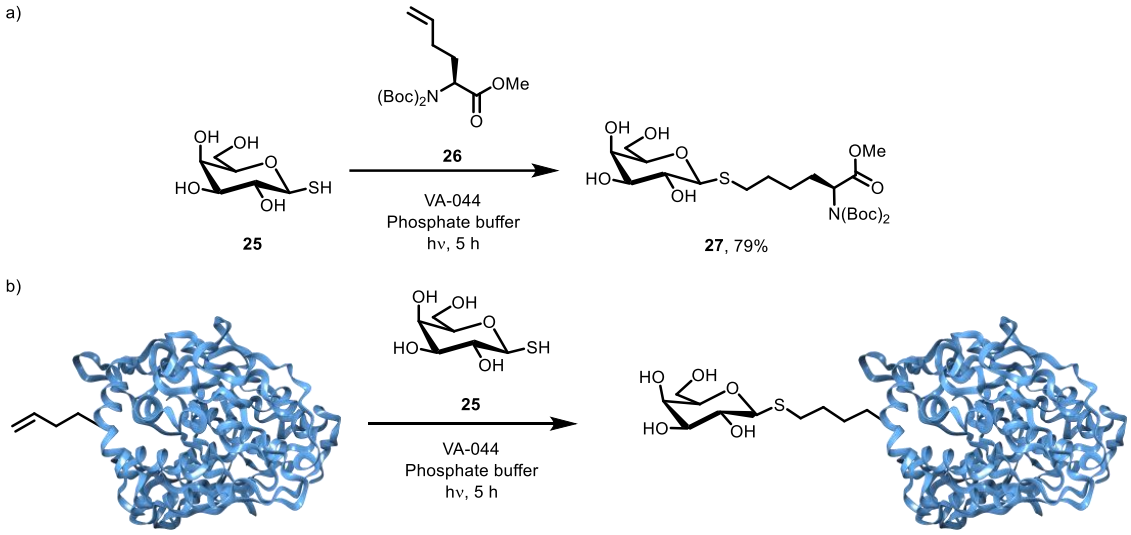

Figure 1.15: The work of Floyd *et al.*; a) the optimisation of thiosugar **25** with L-homoAgl **26** in presence of VA-044 **17** as photoinitiator in phosphate buffer. b) Demonstration of this chemistry applied to an allylated protein such as SsβG-Hag43.

Lipidation is a key chemical modification affecting the physiochemical properties of peptides and is widely used in the design of drug candidates.[143] The addition of lipids onto peptides is utilised to increase the stability, bioavailability and membrane stability of therapeutics.[144-146] Lipopeptides have been employed to combat microbial infections,[147,148] and have been synthesised by the inclusion of lipids during SPPS.[149] The use of TEC chemistry for the synthesis of lipo-AAs for use in SPPS has been demonstrated by Triola *et al.* in a two-step process.[150] The first step is the deprotection of the trityl-protected Cys, followed by the addition of the lipid chain alkene. This approach has been proved to decrease the racemization on the α position in comparison with other methods. Based on this, the Cysteine Lipidation on a Peptide or Amino Acid (CLipPA) approach developed by Brimble group in 2013 has become one of the most prominent tools for peptide lipidation (**Figure 1.16**).[151] The unprotected peptide is lipidated with vinyl palmitate **28** using DPAP **15** as photoinitiator, achieving lipidated antigenic peptide *via* TEC chemistry (**Figure 1.16a**). This approach involves vinyl esters **28** with a bonded lipid chain, which can modify the Cys residues using TEC chemistry.[151] This methodology was optimised and applied to longer-chain peptides by Yang *et al.*, including a 44-residue peptide, achieving a lipidated peptide in 81% yield (**Figure 1.16b**).[152] Finally, Brimble group expanded their methodology combining NCL and CLipPA. Yim *et al.* carried out the NCL of the linear peptide with a thioester in the C-terminus and Cys residue at the N-terminus. The reaction was conducted at pH 7.5 in the

presence of dithiothreitol DTT obtaining cyclised peptide in 30 min**.** Using vinyl palmitate **28** as the unsaturated lipid derivative and DPAP **15** as photoinitiator in acidic conditions for 1 h, the iturin analogue was prepared in 85% conversion **(Scheme 1.16c)**.[153,154]

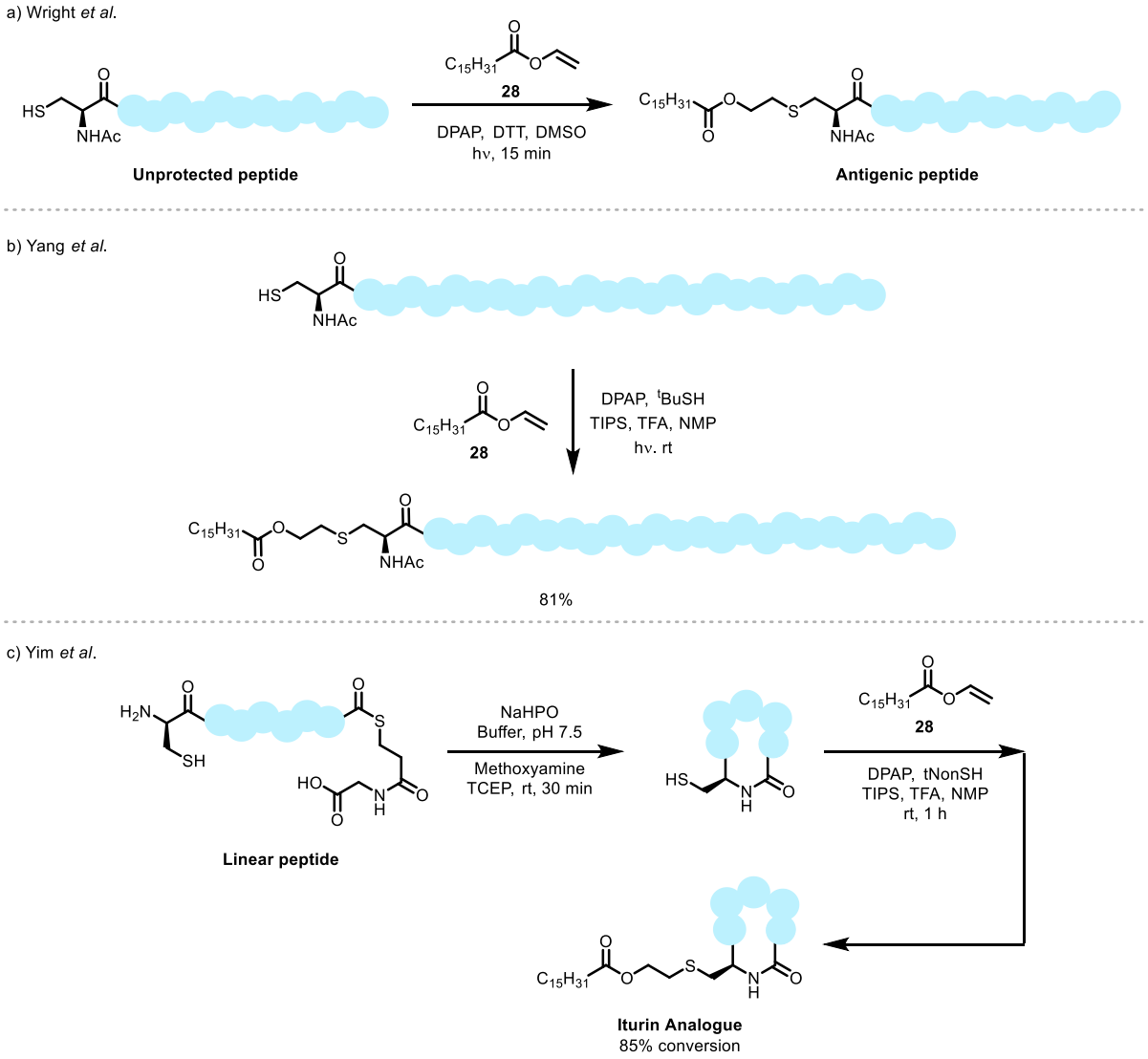

Figure 1.16: CLipPA approach by Brimble group. a) TEC reaction towards peptide lipidation for SPPS by Wright *et al.*[151] b) Lipidation *via* TEC of 44-residue peptide with vinyl palmitate **28** by Yang *et al.*[152] c) NCL-CLipPA *via* TEC chemistry yielding lipidated cyclic Iturin analogue by Yim *et al.*[153,154]

1.5.2 Peptide Macrocyclisation and Stapling

The most widely explored application to date for radical mediated thiol-ene chemistry on peptides is peptide macrocyclisation and stapling in order to increase the durability, stability, selectivity and permeability of biologically active peptides.[155] Macrocyclic peptides are primarily peptide-based molecules characterised by one or more ring structures that include several AA residues.[156] On the other hand, stapled

peptides consist of peptide chains that bring an external brace, the 'staple', that forces the peptide structure into an α-helical arrangement.[157] In addition, thiol-yne mediated reactions have recently been explored in the context of peptide macrocyclisation and stapling and have been found to be equally as versatile as thiol-ene while furnishing useful vinyl-sulfide containing cyclic peptide products.[127] Interestingly, in many of these applications catalytic amounts of initiator are often sufficient for full conversion, which is usually not the case for other intermolecular reactions. Trapping of thiyl radicals in an intermolecular process is a useful approach that has been employed as an effective method for peptide stapling in both one- and two-component systems, with successful applications both in solution and for solid support synthesis.[120]

The one-component methodology requires the presence of both a thiol and an alkene within the same molecule. Therefore, the alkene moiety must be strategically incorporated into the peptide sequence in advance. A common example is the use of Lys side-chain with an Alloc-protecting group or norbonene functionalisation.[158] In 2010, Aimetti *et al.* reported the first thiol-ene mediated on-resin peptide macrocyclisation, which was also the earliest example of photochemical thiol-ene mediated peptide macrocyclisation. The Cys residue of an integrin-binding cyclic Arg-Gly-Asp (RGD) peptide and internal alkene, incorporated through a Lys sidechain, were reacted with DPAP **15** as photoinitiator in DMF under UV-light.[158] The cyclised peptide was achieved in 37% and 24% yield respectively, with yields based on SPPS standards (**Figure 1.17a**). Photoactivation was shown to be more efficient and a quicker approach than the use of thermal activation. Following this work, the same authors demonstrated that a sequential thiol-ene macrocyclization followed by thiol-yne addition could be employed for the formation of multivalent cyclic peptides.[159] This approach enabled conjugation of a cyclic-RGD motif onto a multivalent polymer backbone in a chemoselective process. Interestingly, a combination of cyclic and multivalent peptides was found to act synergistically to enhance the inhibition of fibrinogen binding to glycoprotein IIb/IIIa, a key integrin found on the surface of platelets, by up to two orders of magnitude. On-resin thiol-ene macrocyclisation was subsequently expanded by Zhao *et al.* with the use of UAAs bearing but-4-enyl, pent-5-enyl, or hex-6-enyl sidechains (**Figure 1.17b**). Peptides were cyclised using Irgacure 2959 **16** as photoinitiator in DMF under UV-light conditions achieving 79-90% RP-HPLC conversions.[160]

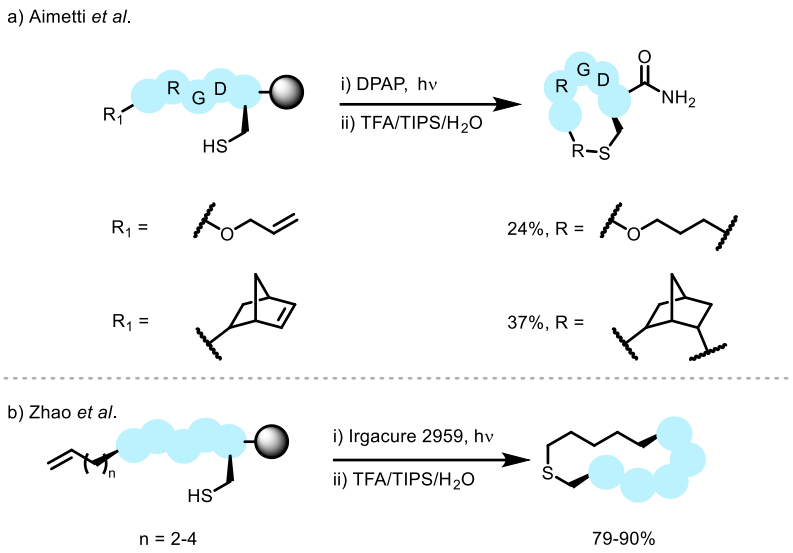

Figure 1.17: On-resin peptide cyclisations *via* TEC by: a) Aimetti *et al.*,[158] b) Zhao *et al.*[160]

This approach has been explored in both on-resin and for solution-phase cyclisation. Hoppmann *et al.* reported the incorporation of a photoswitchable click AA (PSCaa) with a terminal alkene, enabling the TEC reaction.[161] The PSCaa was introduced into the peptide by SPPS and cyclised with a Cys residue located at position 9 of the peptide. TEC cyclisation was then carried out using VA-044 **17** as a photoinitiator, triggering a trans-to-cis isomerisation of the azo group (**Figure 1.18a**). Full conversion to the cyclised peptide was confirmed by RP-HPLC. More recently, Nolan *et al.* applied TEC-based peptide cyclisation to develop thioether-bridged neuropeptide analogues of the well-known hormone oxytocin.[162] While oxytocin is susceptible to reduction *in vivo*, the introduction of a stable thioether linkage could enhance its suitability for drug development. In their study, the authors introduced an Agl residue at position 6 *via* SPPS, and, using DPAP **15** as the photoinitiator, achieved cyclisation with RP-HPLC conversions exceeding 90%, as well as confirming the structure by ^{1}H NMR spectroscopic analysis (**Figure 1.18b**).

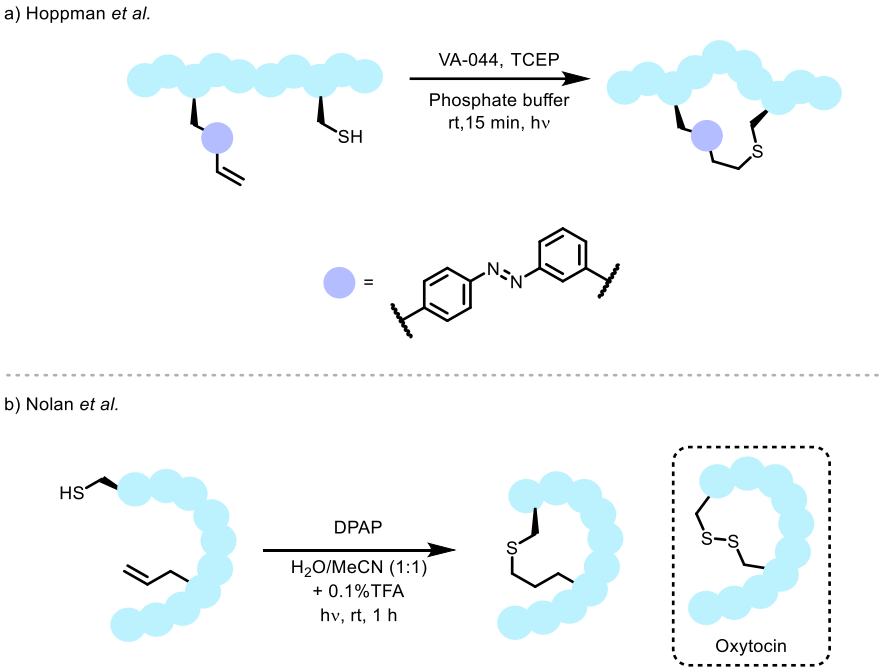

Figure 1.18: One component TEC stapling in solution by: a) Hoppman *et al.*,[161] b) Nolan *et al.*[162]

Two-component methodologies involve both the peptide of interest and an external modifier, resulting in a two-step cyclisation process. The first step consists of a TEC reaction between the peptide and the external stapling agent, which subsequently undergoes an intramolecular TEC reaction to form the second staple.[163] Compared to one-component cyclisation, this approach offers the advantage that no modifications are required within the peptide itself, as native Cys residues can be used in combination with a variety of dienes. The pioneers of this approach were Wang *et al.*, who employed diene **29** and a peptide containing two Cys residues, along with DPAP **15** as a photoinitiator, to obtain the stapled peptide in 90% yield under UV-light irradiation.[164] The same authors later extended this chemistry to diallylurea-type dienes **30** and peptides, this time employing aqueous conditions with the water-soluble photoinitiator VA-044 **17**. In this case, the stapled peptide was obtained in 95% yield (**Figure 1.19**).[165] This study was then extended to a TYC stapling and a combination of TYC-TEC stapling, where the first step is TYC-mediated to form a vinyl sulfide linkage which was subsequently modified by TEC under UV-light conditions to furnish bicyclic stapled peptides and proteins.[165]

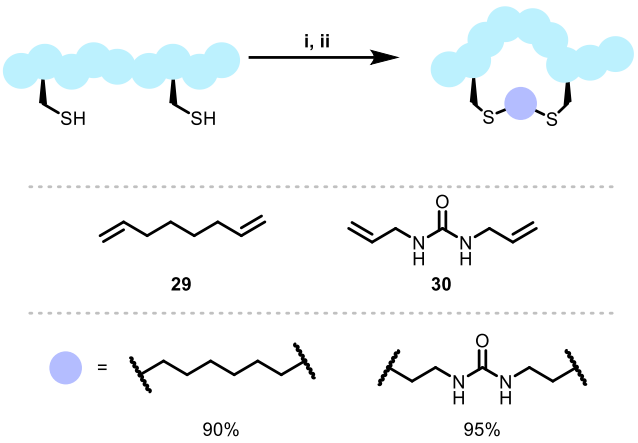

Figure 1.19: Two component TEC-stapling by Wang *et al.*[156, 164, 165] i) The peptide was reacted with the diene linker **29** to yield stapled peptide in the presence of DPAP **15** and NMP for 15 min under UV-light conditions.[157] ii) The peptide was reacted with urea diene **30** in aqueous conditions with VA-044 **17** and TCEP for 15 min to yield the stapled peptide.[158]

1.5.3 Other Applications

TEC and TYC chemistries have been widely explored in various fields beyond peptides, including sugars and proteins.[166,167] The acyl–thiol–ene (ATE) reaction shares a similar mechanism with the previously mentioned TEC reaction and has recently gained significant attention. ATE involves the reaction between a thioacid and an alkene in the presence of a thermal initiator or photoinitiator. This reaction yields a thioester product, which serves as a valuable intermediate for accessing the corresponding thiol due to its ease of hydrolysis. Numerous reports in the literature have highlighted the utility and versatility of this transformation. In 2018, McCourt *et al.* reported the synthesis of thiolactones *via* ATE and acyl–thiol–yne (ATY) cyclisation.[168] The authors synthesised thioacid **41** containing a terminal alkene, and reacted it under UV irradiation for 2 h using DPAP **15** as the photoinitiator and MAP as the photosensitizer to selectively obtain the final γ-thiolactone **42** in 88% yield. The same approach was extended to the ATY reaction: an unsaturated thioacid **43** was cyclized in the presence of DPAP **15** and MAP, affording γ-unsaturated thiolactones **44** in 51% yield (**Scheme 1.4**). Interestingly, they also reported that the 5-exo-trig product was more favoured in the case of thiolactones due to the stability of the corresponding carbon-centred radical. However, in case of thiol–ene thioether products, the 6-endo-trig product was more stable.

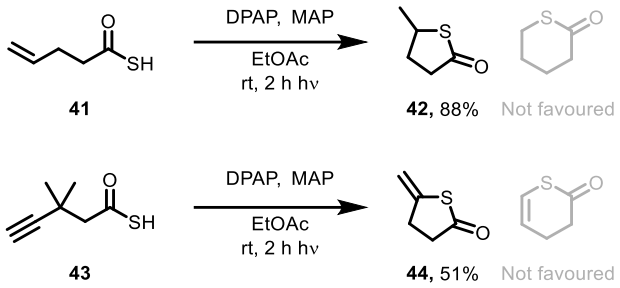

Scheme 1.4: ATE and ATY cyclisation of γ-alkenyl and alkynyl thioacids by McCourt *et al.*[168]

Inter- and intramolecular ATE has also been applied to peptide macrocyclisation. Benny *et al.* reported the cyclisation of a linear peptide **45** *via* ATE, introducing an alkene moiety through the incorporation of an Agl residue, and synthesizing Boc-Asp(STrt)-OTMS to generate the corresponding thioacid upon deprotection/cleavage.[169] Peptide cyclisation was then carried out in the presence of DPAP **15** as a photoinitiator under UV-light irradiation for 15 min (**Figure 1.20a**). Crude RP-HPLC analysis showed complete consumption of the starting material and 90% conversion to the final thiolactone peptide **46**. The methodology was further expanded to a series of bioactive peptides containing diverse chemical functionalities. All the cyclised peptides were achieved in high conversion according with RP-HPLC analysis. A recent study by Ostrovitsa *et al.* developed a new strategy for on-resin direct peptide hydrothiolation employing intermolecular ATE and *S*-deacetylation chemistries.[170] This study synthesised several Vasopressin and Somatostatin analogues by the addition of a Fmoc-Agl residue during the SPPS. This methodology, implementing TEC, was performed by the addition of thioacid **47**, DPAP **15** and MAP as photoinitiator and photosensitiser respectively in DMF for 15 min. This reaction was then followed by *S*-deacetylation using DTT and H-Cys-OMe in DMF/PBS at pH 8.5 for 1 h at rt. The thiolated product was cleavage from the resin and cyclised by the disulfide bond formation. The final cyclised product was yielded in 24% isolated yield (**Figure 1.20b**).

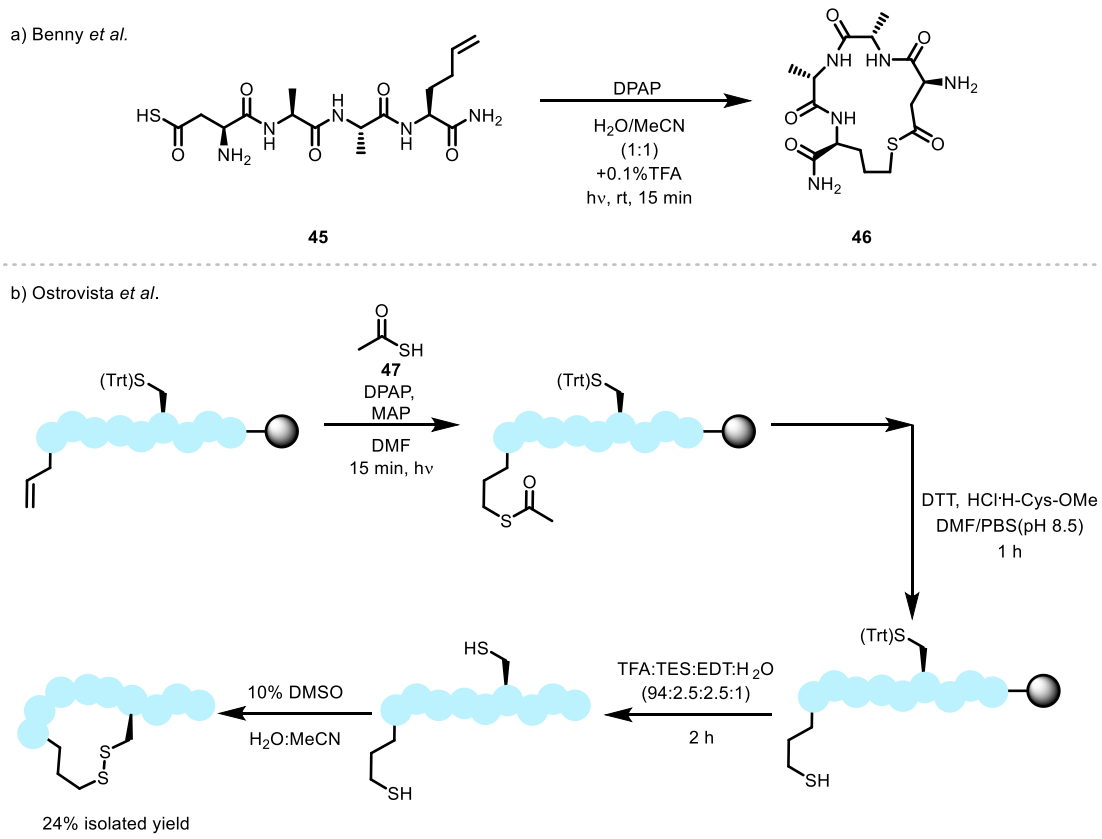

Figure 1.20: a) Intramolecular peptide cyclisation *via* ATE by Benny *et al.*,[169] b) On-resin hydrothiolation methodology *via* intermolecular ATE reaction and followed *S*-deacetylation for the synthesis of Vasopressin and Somatostatin analogs.[170]

TEC chemistry has also found application in the study of native protein post-translational modifications (PTMs), particularly ubiquitination. Ubiquitination is a fundamental PTM that involves the covalent attachment of ubiquitin, a 76-AA protein, to modify proteins through the coordinated action of the E1, E2, and E3 enzyme cascade. This modification plays a critical role in regulating protein function, subcellular localisation, and proteasomal degradation.[171] Given the high selectivity of TEC, this is a valuable method for site-selective Cys labelling in proteins. Deubiquitinating enzymes (DUBs), which catalyse the removal of ubiquitin from substrate proteins, represent a diverse family of approximately 100 members.[167] These enzymes are classified into seven subfamilies, six of which are Cys proteases.[172] Neil *et al.* reported the design of an alkene-functionalised ubiquitin activity-based probe (ABP), referred to as HA-1-75Ub-alkene probe, which undergoes a TEC reaction to selectively label DUBs (**Figure 1.21**).[173] In this study, an alkene moiety was introduced at the C-terminal isopeptide linkage of ubiquitin, enabling a covalent reaction with the Cys residue within the DUB active site. The TEC reaction was initiated under UV-light irradiation in the presence of DPAP **15** as photoinitiator and MAP as photosensitiser. Notably, successful labelling was highly

dependent on a degassing step along with the UV explosion. Building on this approach, Campaniço *et al.* optimised the TEC labelling strategy by evaluating alternative initiation conditions.[167] They explored UV-, visible-light-, and redox-initiated TEC using Irgacure 2959 **16**, 9-mesityl-10-methylacridinium perchlorate (Mes-Acr^{+}), and manganese(III) acetate ($Mn(OAc)_3$), respectively. The authors demonstrated that all initiators effectively triggered TEC-mediated DUB labelling. However, Irgacure 2959 **16** was found to be particularly advantageous for experiments involving cell lysates, due to its ability to achieve rapid and efficient bond formation under atmospheric conditions.

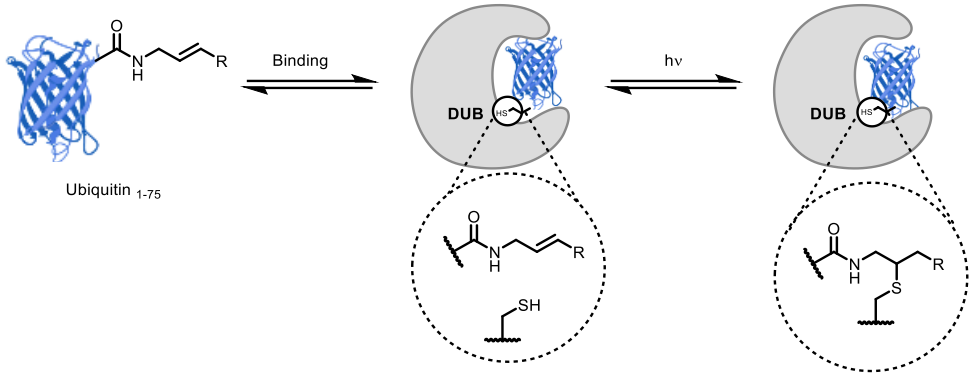

Figure 1.21: Covalent bond formation of probes to DUBs *via* a thiol–ene reaction by Neil *et al.*[173]

1.6 Work Presented in this Thesis

As discussed in this chapter, TEC reaction has been demonstrated as a selective and broadly applicable strategy for protein and peptide modification. Nevertheless, there are certain applications of thiol-ene reaction that have not yet been explored.

Chapter 2 describes a novel methodology that involves the development of TEC-mediated 'green' peptide bioconjugation under continuous flow. Building on previous work from the Scanlan group which established the potential of 'green' peptide conjugation. This study extends the 'green' chemistry dogma to a continuous flow approach. Glutathione (GSH) was utilised as a model peptide and, once its conjugation under continuous flow was optimised, the scope was expanded to include a variety of alkenes in 'green' solvents such as Deep Eutectic solvents (DES), bio-based solvents and fully aqueous conditions. This approach was then applied for the glycosylation of bioactive peptides, culminating with the glycosylation of an anticancer RGD peptide under continuous-flow conditions in both DES and aqueous media.

In **Chapter 3**, the development of one-pot peptide disulfide rebridging *via* TYC was investigated inspired by previous work of Griebenow *et al*.[174] To date, phosphines have been the predominant disulfide-reducing agents employed in this context. However, this work introduces $NaBH_4$ as an unexplored disulfide reducing agent in peptide chemistry. First, optimisation of this strategy was undertaken for both disulfide reduction and TYC reaction. A broad scope was investigated with a range of synthetised alkynes and, this approach was finally applied to the modification of the Somatostatin analogue octreotide **4** with a view towards cellular bioimaging applications.

Chapter 4 explores an emerging methodology employing a new class of organic photocatalyst for thiol-ene reaction. While naphthalimides have been previously reported as photoinitiators for polymer chemistry, herein we demonstrate its reactivity suitable as photocatalyst for organic molecules and peptide modifications *via* TEC-mediated photoredox. Optimisation studies of naphthalimides as photocatalyst for thiol-ene chemistry was carried out in both organic and aqueous conditions as homo- and heterogeneous catalysis, respectively in order to understand its mechanisms under UV-light irradiation. This approach allows us to develop a variety of applications from organic photochemistry to peptide modifications in biological environments.

Chapter 5 describes a novel approach for site-selective, peptide-based protein-protein interactions (PPI) inhibitors using TEC. mRNA display has been established as a powerful platform for discovering peptide ligands *via* affinity-based selection of a target protein. However, no evidence of site-specific inhibition can be obtained by this method. To address this limitation, in this chapter a selective chemistry such as TEC chemistry was integrated into the standard mRNA protocol. By introducing covalent warheads such as the thiol group from a Cys residue of the target protein and an encoded alkene moiety in the DNA library, site-selective covalent inhibition can be achieved. Initially, optimisation of the thiol-ene reaction under mRNA display conditions was undertaken in order to confirm compatibility with the TEC reaction using a mRNA display parameters, such as small-scale reactions. Finally, this approach was applied to a first round of mRNA display selection as proof-of-concept of this method.

Chapter 6 presents a final summary of the work presented throughout this thesis.

Chapter 7 contains experimental details and characterisation data for the compounds synthesised over this thesis.

Chapter 2

‘Green’ thiol–ene mediated peptide bioconjugation under continuous flow†

2.1 Introduction

The traditional perception of radicals as highly reactive intermediates over which little selectivity and control can be wielded has evolved significantly in recent years, largely due to the development of highly selective reagents and catalysts that can modulate radical reactions under mild reaction conditions through, fast, well-understood mechanistic pathways.[175] The application of radical species in organic chemistry began over 120 years ago with the discovery of *C*-centred radicals.[176] Extensive use of metals including Sn, Sm and Hg for radical generation persists within contemporary organic syntheses, despite issues with toxicity and disposal.[177] This has severely limited the potential for radical chemistry to adhere to the principles of 'green chemistry', especially within an industrial context.

From a green chemistry perspective, the large requisite quantities of solvents used in both industry and academia remains highly problematic. Green chemical syntheses are governed by regulations to minimise the use of organic solvents, instead favouring non-hazardous alternatives.[178] The thiol-ene reaction has the potential to be considered an archetypal green reaction due to its numerous advantages, as previously discussed in **Chapter 1**.**4**. One of the most prominent limitations of this reaction, from the perspective of sustainability, is the requisite use of harmful organic solvents. This is to ensure sufficient solubility of organic photoinitiators such as DPAP **15** and organic biomolecules used for peptide bioconjugation, both of which possess negligible aqueous solubility.[121] For substrates possessing some organic solubility, the addition of alcohol or ethereal solvents such as methanol (MeOH), butan-1-ol (BuOH) or tetrahydrofuran (THF) is sufficient to permit efficient thiol-ene addition. Peptide chemistry is also in need of an ecological makeover, as current synthetic methods commonly rely on dimethylformamide (DMF), dimethylsulfoxide (DMSO) and related hazardous solvents to ensure initiator solubility.[179] *N*-methylpyrrolidone (NMP) and DMF are defined as substances of very high concern by the European Chemicals Agency (ECHA) and have serious and irreversible effects on human health and the environment.[180]

In order to address these limitations, the use of greener solvents, such as water, bio-based solvents, and deep eutectic solvents (DESs), in place of noxious organic solvents. Water is the prototypical green solvent as it is non-toxic, readily available and cheap. Peptide chemistry presents an ideal opportunity for the use of aqueous conditions

in synthesis due to the fact that native peptides tend to be water soluble. Deep eutectic solvents (DESs) consist of two components: a hydrogen bond acceptor, usually an ammonium salt, and a hydrogen bond donor. These individual components form strong interactions, resulting in an overall decrease in the melting point compared to an ideal mixture.[181] The use of DESs is highly advantageous as they can be reused, biodegradable, they have low toxicity and natural origin, thereby reducing solvent waste in organic syntheses. It has also been shown that DESs are compatible with TEC chemistry.[182] Bio-based solvents, such as glycerol, ethyl lactate, D-limonene, and methyl soyate are isolated from renewable raw materials or waste feedstock.[183] DESs and bio-based solvents possess advantages such as safer use, greater biodegradability and reduced toxicity in comparison with conventional organic solvents.

2.1.1 Continuous-Flow Chemistry

Fundamentally, continuous-flow chemistry refers to chemical reactions undertaken through a continuous flow of solvent, reagents and substrates which are pumped through tubing at a constant rate. Reagents, flow rate, solvents, reaction time, and temperature are fixed over the course of the reaction. Reaction efficiency is controlled by flow rate and the residence time of the reactor.[184] The type of reactor is selected based on the type of chemical reaction that is being carried out (**Figure 2.1**).

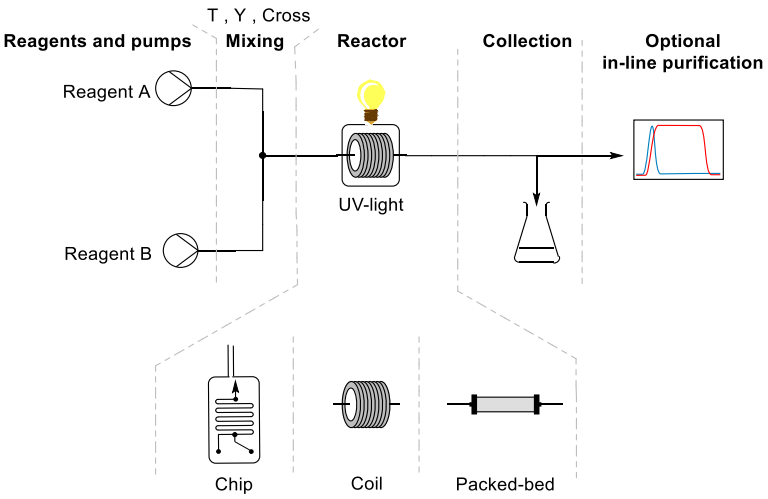

Figure 2.1: Flow system reported by Kerry Gilmore and co-workers.[185] The system begins with reagent delivery where all the reagents are introduced in the system and subsequent mixing is carried out if more than one reagent is included. The mixture is then introduced into a reactor. Quenching and pressure regulation can be included in the system. Finally, collection or connection to an analytical or purification system.

Chip type reactors are commonly used for organic processes in solution. Chips are designed to ensure laminar flow dominates over the course of the reaction, achieving more efficient mixing. The use of smaller chip reactors is beneficial due to the prevention of undesired local overheating ('hot spots'), giving greater selectivity and higher yields,[186] however, they are significantly more expensive than simpler coil-based reactors. Coil reactors consist of a long length of tubing coiled around a central support, permitting greater reaction scales. Coil reactors are also easier to set up and more cost efficient. Packed bed reactors feature immobilised reagents or catalysts in heterogeneous catalysis and other reaction processes.[187] Once the reaction has been carried out, analytical or purification strategies such as high-performance liquid chromatography (HPLC), liquid chromatography-mass spectrometry (LC-MS), infrared (IR) spectroscopy, and nuclear magnetic resonance (NMR) spectroscopy may be incorporated in-line to easily monitor reaction completion and aid in product characterisation (**Figure 2.1**).[187, 188]

The goals of flow chemistry and green chemistry are closely aligned in prioritising the development of highly efficient synthetic approaches.[189] Flow chemistry has contributed to making chemical processes more sustainable and safer in both industry and academic settings.[190] Flow chemistry offers numerous advantages over traditional batch synthesis, including greater control over selectivity and reproducibility, safer reaction setups, and more precise regulation of parameters such as temperature, reagent equivalents, and solvent volume.[188] It also facilitates easier scale-up, making it especially well-suited for the large-scale synthesis of pharmaceuticals.[185] As a highly efficient two-component reaction requiring only catalytic quantities of initiator, the radical mediated thiol-ene reaction is an ideal candidate for adaptation to a continuous flow set-up.

TEC under continuous flow has been reported for the synthesis of alkylic thioesters,[191] lipidated Cys derivatives,[192] substituted cinchona alkaloids,[193] thiomorpholines[194] and polyamidoamines.[195] To date, however, radical mediated thiol-ene modification of biologically pertinent unprotected peptides has not been demonstrated either under continuous flow or in fully aqueous or 'green' conditions. This concept is explored in the following chapter through the radical-mediated hydrothiolation of small molecules displaying a terminal alkene functionality with Cys containing peptides under continuous-flow.

2.2 Previous Work Within the Scanlan group and Aims

Previous work within the Scanlan group demonstrated the compatibility of the TEC reaction with DESs under batch conditions. The TEC reaction was optimised to afford excellent yields using either organic photoinitiators or molecular oxygen to propagate the reaction. Following the successful application of this system to small molecules, its application to a peptide binder for the SARS-CoV-2 spike protein was performed using this green platform to generate conjugated analogues.[182]

In this project, the primary aim is to establish the first application of a green, photoactivated, radical-mediated thiol-ene reaction for peptide bioconjugation under continuous-flow conditions. A series of bioconjugation reactions were carried out using DESs, bio-based solvents, and fully aqueous systems to demonstrate their compatibility with a range of biologically relevant peptide substrates. The incorporation of the water-soluble photoinitiator Irgacure 2959 **16** enables the efficient synthesis of bioactive glycosylated peptides under entirely aqueous conditions, thereby eliminating the need for organic solvents and improving the overall environmental sustainability of the process. The chapter concludes with a study on the glycosylation and biotinylation of an anticancer RGD peptide under continuous flow conditions in both DES and aqueous media.

2.3 Results and Discussion

Glutathione (GSH) **48** was selected as a model thiolated substrate due to the therapeutic potential of GSH conjugates (GSX)[196] and its commercial availability. GSH is a tripeptide that consists of glutamic acid (Glu), Cys, and glycine (Gly) residues (Glu-Cys-Gly). GSH is a major antioxidant in cellular homeostasis that maintains the cellular redox status to enable efficient physiological functions such as detoxifying xenobiotics and drug metabolism.[197] Decreased GSH levels are commonly associated with the aging process, as well as in a wide range of pathological conditions, such as neurodegenerative disorders.[198] Notably, GSH depletion and/or alterations in GSH metabolism appear to be crucial in the onset of Parkinson's disease.[197,198]

2.3.1 Optimization of the Thiol-ene Reaction with GSH Under Batch Conditions

Initial investigations into radical mediated thiol-ene chemistry to access GSX conjugates were carried out under conditions previously reported by Conway and co-workers.[196] DPAP **15** was used as a photoinitiator in THF/H_2O (1:1) in order to ensure sufficient solubility of both GSH **48** and DPAP **15**. Allyl alcohol **49** was selected as a model alkene substrate as it is readily available and exhibits good solubility in the solvent system. Optimisation reactions were performed using GSH **48** and allyl alcohol **49** with DPAP **15** as photoinitiator in a 112 W Luzchem UV photoreactor under stirring (**Table 2.1**).

Table 2.1: Optimization table of GSH **48** and allyl alcohol **49** with DPAP **15** as photoinitiator in THF/H_2O under entry 1-11 conditions.

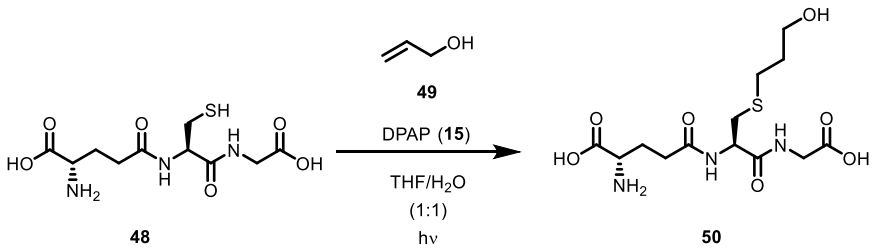

Entry	GSH:Alkene (eq.)	DPAP (eq.)	GSH Concentration [M]	Time (min)	Power (W)	Yield[a] (%)
1	1:1	0.05	0.2	60	112	82
2	1 : 2.5	0.05	0.2	60	112	91
3	1 : 2.5	0.1	0.2	60	112	91
4	1 : 2.5	0.2	0.2	60	112	93
5	1 : 2.5	0.05	0.4	60	112	87
6	1 : 2.5	0.05	0.6	60	112	96
7	1 : 2.5	0.05	0.6	5	112	88
8	1 : 2.5	0.05	0.6	10	112	91
9	1 : 2.5	0.05	0.6	20	112	93
10	1 : 2.5	0.05	0.6	20	36	89
11	1 : 2.5	0.05	0.6	30	36	86

[a] % yields are quoted as isolated yields.

The thiol-ene reaction of 1 eq. of GSH **48** and 1 eq. allyl alcohol **49** in the presence of 0.05 eq. of DPAP furnished thioether adduct **50** in 82% yield (entry 1, **Table 2.1**) following purification by column chromatography. Analysis of the ^{1}H NMR spectroscopic spectrum of the crude mixture indicated the presence of unreacted GSH **48**. A further 1.5 eq. of allyl alcohol **49** was added to achieve complete consumption of GSH and 91% yield of conjugated GSH product (entry 2, **Table 2.1**). The number of equivalents of photoiniator DPAP **15** was increased, however, this did not result in any

appreciable increase in yield (entry 3 and 4, **Table 2.1**). Concentration in continuous flow systems has a critically important role. The ability to perform reactions at high concentration is beneficial from a green perspective as the required solvent volume is reduced. To investigate the effect of concentration on this reaction, it was performed at increased GSH **48** concentrations of 0.4 M (entry 5, **Table 2.1**) and 0.6 M (entry 6, **Table 2.1**) with yields of 87% and 96% respectively, with no detected formation of undesirable side products. This confirmed that higher reaction concentrations lead to an overall improvement in yield. The effect of reaction time on reaction yield was also investigated (entry 7, 8, and 9, **Table 2.1**). ^{1}H NMR spectroscopy after 20 min indicated full conversion of GSH **48** and isolation *via* column chromatography gave GSX conjugate **50** in a 93% yield. A change in the UV-light source used for these reactions was necessary to enable easy modification of the continuous flow set up. The reaction of GSH **48** and allyl alcohol **49** was carried out using a 36 W portable UV nail lamp, with only a minor reduction in yield (86-89%) observed upon isolation of the product (entry 10 and 11, **Table 2.1**). With the optimised conditions for this model reaction in hand, application to a continuous flow set up commenced.

2.3.2 Optimisation of the Thiol-ene Reaction with GSH Under Continuous Flow Conditions.

Optimisation reactions under continuous flow employed a system consisting of two HPLC pumps and a microchip reactor (1000 µL) covered by a 36 W UV lamp (**Figure 2.2**).[a]

a) b)

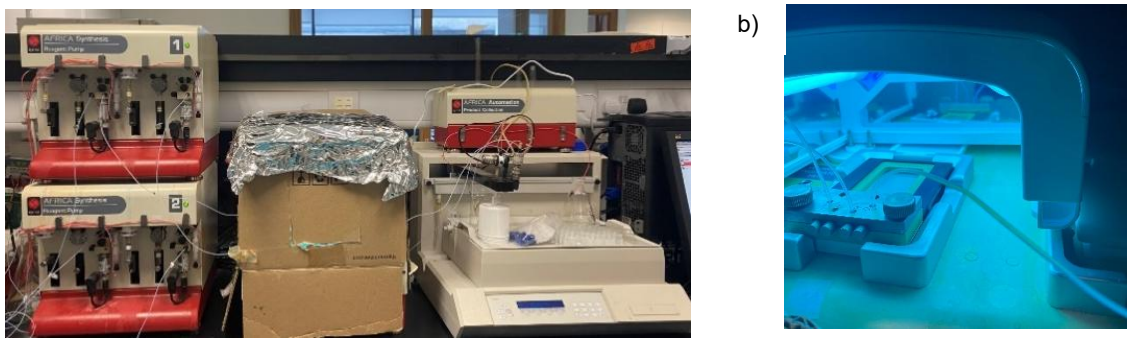

Figure 2.1: a) Integrated Syrris Ltd. continuous flow system in the O'Shea Laboratory (RCSI) on which initial radical mediated thiol-ene chemistry optimisation was carried out. b) Chip reactor used in this project.

[a] Access to the continuous flow system discussed in this section was provided by Prof. Donal O'Shea, Royal College of Surgeons in Ireland (RCSI), York House, York Street, Dublin 2, Ireland.

The radical mediated thiol-ene reaction of GSH **48** and allyl alcohol **49** under continuous flow conditions was optimised as shown in **Table 2.2**. All reactions were repeated in quadruplicate and stated isolated yields are an average.

The reaction of GSH **48** (1 eq.) with allyl alcohol **49** (1 eq.) in the presence of DPAP **15** (0.05 eq.) under UV light in continuous flow for 20 min resulted in 83% yield of thioether adduct **50** following isolation by aqueous work up (entry 1, **Table 2.2**). However, crude ^{1}H NMR spectroscopic analysis revealed unreacted residual GSH. An increase to 2.5 eq. of allyl alcohol **49** was performed (entry 2, **Table 2.2**) in order to promote GSH **48** consumption and to provide a direct comparison between flow and batch reactions. Increased equivalents of DPAP **15** result in a decrease in yield (entry 3, **Table 2.2**), possibly due to mixing difficulties caused by the higher concentration of DPAP in THF diminishing mixing and subsequent reaction efficiency.

Table 2.2: Thiol-ene reaction optimisation of GSH **48** and allyl alcohol **49** in flow under entry 1-5 conditions.

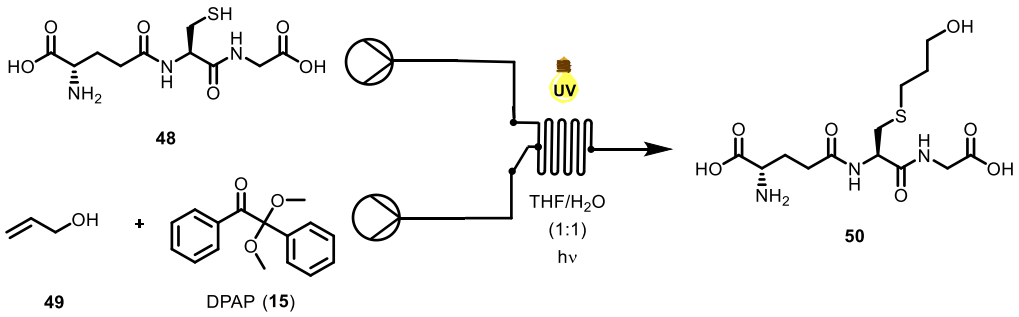

Entry	GSH:Alkene (eq.)	DPAP (eq)	Temp. (°C)	Time (min)	Yield[a] (%)
1	1 : 1	0.05	rt	20	83
2	1 : 2.5	0.05	rt	20	91
3	1 : 2.5	1	rt	20	85
4	1 : 2.5	0.05	rt	10	34
5	1 : 2.5	0.05	40	10	99

[a]Yield quoted as mean yield obtained from replicates of each reaction (n = 4).

Decreasing the reaction time from 20 min to 10 min resulted in a significant reduction in yield from 91% to 34% (entry 4, **Table 2.2**), however, near quantitative yields were restored when a 10 min reaction was coupled with an increase in temperature from rt to 40 °C (entry 5, **Table 2.2**). As the increased temperature required the addition of a heating source under the reactor, which would complicate the scale up and negatively

impact the environmental impact of this approach, the optimal conditions selected for a reproducible GSH thiol-ene reaction involved a 20 min reaction time, with the reaction being performed at rt (entry 3, **Table 2.2**).

2.3.3 Scope of the Thiol-ene Reactions of GSH in Batch

With optimal reaction conditions established both in batch and under continuous flow using allyl alcohol **49**, a series of alkenes were selected to explore the scope of the reaction. Each alkene was selected to demonstrate the applicability of thiol-ene chemistry to biochemically relevant substrates.

The synthesis of protected allyl monosaccharide **52** was achieved through the allylation of per-acetylated galactose derivative **51** with allyl alcohol **49** in the presence of $BF_3 \cdot OEt_2$ in CH_2Cl_2 (**Scheme 2.1**). The reaction was monitored by TLC and after 3.5 h the starting material was fully consumed. Following an aqueous work up and column chromatography, the product **52** was obtained in 56% yield. Acetyl deprotection was performed using NEt_3 in MeOH and the desired product **53** was isolated in 92% yield.

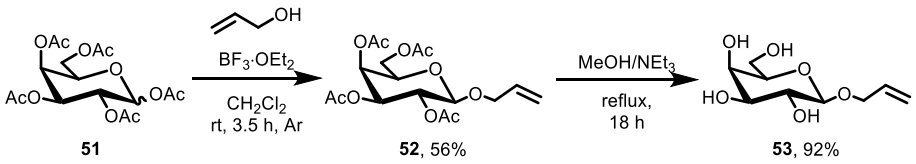

Scheme 2.1: Synthesis of unprotected monosaccharide **53.**

Further water-soluble alkenes were used to broaden the scope of the reaction, including allyl alkenes including allyl alcohol **49** and 4-pentenol **54**. Allyl AA derivatives including Fmoc-Lys(OAll)-OH, Fmoc-Glu(OAll)-OH and Fmoc-Asp(OAll)-OH were also used. Finally, unprotected allyl monosaccharide **53**, allyl urea, and allyl thiourea completed the scope of selected alkene containing reactants.

Fmoc deprotection of allyl AAs was performed upon treatment with 20% piperidine in DMF (v/v) (**Scheme 2.2**). The deprotected AA was then precipitated by trituration with cold Et_2O to furnish desired compounds **55** (40%), **56** (40%) and **57** (53%).

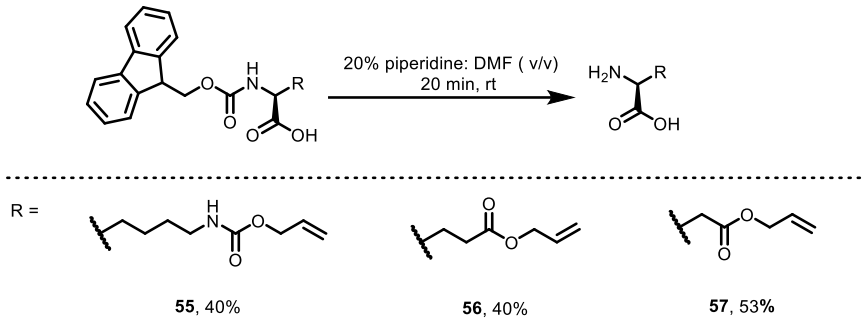

Scheme 2.2: Allyl AA's **55**, **56** and **57** *via* Fmoc deprotection.

The comparison of yields obtained from the reaction of GSH with water soluble alkenes **49, 53**, **54**, **55**, **56**, **57**, allyl thiourea **58,** allyl urea **59** and vinyl glycine **60** under both flow and batch conditions is shown in **Figure 2.2**.

As a general observation, yields obtained under continuous flow conditions tended to be higher than those obtained from standard batch reactions (**50**, **61**, **62**, **63**, **64**, **65, 67** and **68**, **Figure 2.2**). This is likely due to increased mixing efficiency and decreased attenuation of UV irradiation, which is comparable to a decrease in irradiation path length. In the case of hydroxyl GSX conjugates **50** and **61** and unprotected monosaccharide GSX conjugate **62**, no prominent difference was observed between batch and continuous flow as the yields of batch reactions were already >80%. Yields were particularly enhanced (~30% increase from batch to continuous flow) in reactions involving electron-poor alkenes **63** and **67**, derived from aspartic acid and allylurea, respectively. Electron-poor alkenes suffer from decreased TEC reactivity due to the poor stability of the corresponding *C*-centered radical intermediate (**Figure 2.2**).[199] The yields of GSX conjugates **64**, **65** and **68** (**Figure 2.2**) increased significantly under continuous flow due to the greater reactivity and faster reaction kinetics of the respective alkene precursors **56**, **57** and **60** (**Figure 2.2**). However, in the case of compound **66**, quantitative conversion was observed for the batch reaction, dropping to 84% under continuous flow conditions.

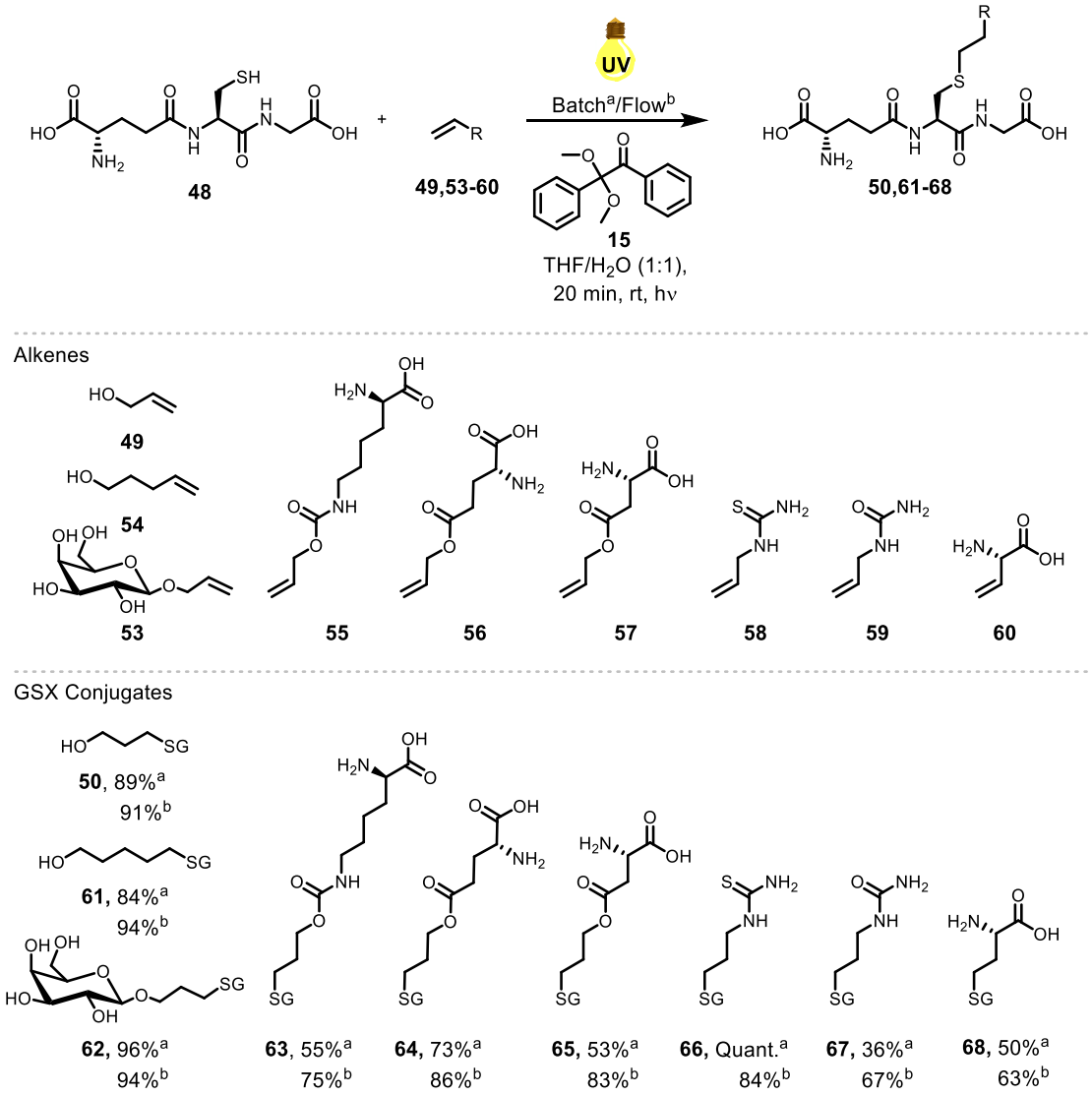

Figure 2.2: Scope of GSH thiol-ene reaction with water soluble alkenes in batch (a) and under continuous flow (b). Yields were measured by ^{1}H NMR spectroscopic analysis with dimethyl sulfone as internal standard (100% mol).

The significant improvement in conversion for thiourea derivative **66** relative to the urea **67**, in particular for the batch reaction, may be due to improved solubility and reactivity of the thiourea substrate **66**.[200] In the case of vinylglycine **68**, the shorter allyl chain positions the carbon-centred radical closer to the heteroatom and therefore potentially stabilises the carbon-centred radical and, as a result, the homopolymerisation can occur at a faster rate. Therefore, the difference in batch versus flow yields is notable in comparison to the rest of the alkene derivatives (*c.f.* **Figure S9.1-S9.9**).[121,201]

2.3.4 Radical Mediated Thiol-ene Reactions in DESs, Bio-based and Less Harmful Solvents

With the efficiency of the TEC mediated GSH bioconjugation reactions under continuous flow demonstrated successfully, further optimisation of this method was undertaken in order to enhance its 'green' properties. This was done by employing green solvents. The use of DESs in the radical mediated TEC reaction has previously been reported by the Scanlan group and circumvents the requirement for organic solvents.[182] However, due to the higher viscosity of DESs in comparison to the H_2O/THF solvent system, the use of the continuous flow system in a chip reactor was not possible. In place of this, based on previous work from Seeberger[185,187] and Baker,[202] a simple, high volume flow system was developed using a 2-channel syringe pump and a coil reactor (9.65 m length and 0.8 mm internal diameter length). This setup was placed in a UV oven with a sample collector for analysis (**Figure 7.1**). In addition to DESs, a number of bio-based solvents were also investigated (**Figure 2.3**). The use of the chosen bio-based solvents has been previously reported under continuous flow,[203] but not in the context of the radical mediated thiol–ene reaction for peptide bioconjugation.

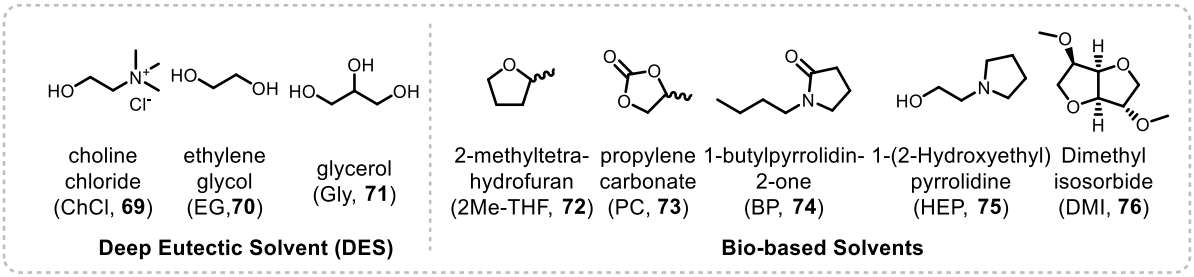

Figure 2.3: Chemical structure of DES and bio-based components used in this project.

An initial study was performed using DES/H_2O in a ratio of 3:2 based on previous studies carried out in the Scanlan lab. This ratio was chosen in order to achieve the substrate solubility and reduce viscosity whilst retaining the hydrogen bonding characteristics of the DESs.[182] TEC reactions were performed with GSH **48** and unsaturated alcohols **49** and **54**. DPAP **15** was used as a photoinitiator and the reaction was performed under UV irradiation at 254 nm with the previously optimised continuous flow conditions (**Table 2.3**).

Table 2.3: Radical mediated thiol-ene reaction with allyl alcohol **49** and 4-pentenol **54** in DESs and bio-based solvents in batch[a] and under continuous flow[b].

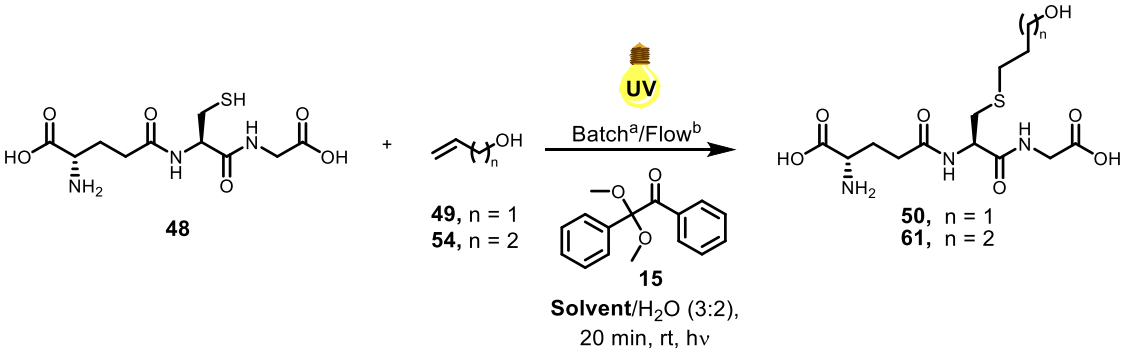

Entry	Solvent	Conv 50[a]	Conv 61[b]	Conv 50[a]	Conv 61[b]
1	ChCl: EG (2:1) **69**:**70**	>99%	83%	98%	91%
2	ChCl: Gly (2:1) **69**:**71**	Quant.	84%	>99%	Quant.
3	2 Me-THF + BHT **72**	>99%	95%	>99%	86%
4	Propyl Caro **73**	Quant.	96%	>99%	>99%
5	BP **74**	Quant.	93%	>99%	>99%
6	HEP **75**	98%	96%	Quant.	Quant.
7	DMI **76**	>99%	96%	Quant.	Quant.

* % yields were measured by RP-HPLC area integration utilising a calibration curve.

Conversion of GSH **48** to the GSXs **50** and **61** was determined by RP-HPLC analysis by area integration utilising a calibration curve (Appendix **Fig. S9.17**). In batch reactions, conversions were >95% (columns 3 and 5, **Table 2.3**) in all solvent systems investigated highlighting the compatibility of DESs with the radical mediated thiol-ene reaction. Conversions under continuous flow (columns 4 and 6, **Table 2.3**) were slightly lower than those obtained in batch, although they remained >80% in all cases. This is likely due to the higher viscosity of DESs, bio-based and less harmful solvents creating distortions in the flow system, preventing effective reagent mixing.[121] The lowest reaction conversions were observed with choline chloride **69** based DESs (entry 1 and 2, **Table 2.3**), less harmful solvent HEP **75** (entry 6, **Table 2.3**) and bio-based solvent DMI **76** (entry 7, **Table 2.3**). These solvent systems possess the highest viscosity. With these promising results in hand, the next step was to achieve peptide bioconjugation under continuous flow in fully aqueous conditions.

2.3.5 Substrate Scope of the Thiol-Ene Reaction in Water Under Continuous-Flow

In order to circumvent the use of hazardous organic solvents, water-soluble photoinitiator, Irgacure 2959 **16,** was employed for the following reactions under fully aqueous conditions. Irgacure 2959 **16** has been used principally in dental and biomedical

applications for the crosslinking of hydrogels and polymers.[204] However, **16** is not widely used synthetically and has not previously been used to initiate thiol-ene additions in a synthetic context.[121] Radical mediated thiol-ene reactions of GSH **48** and alkenes **49** and **53**–**60** were undertaken in the presence of water-soluble initiator **16** in batch and under continuous-flow conditions (**Figure 2.4**).

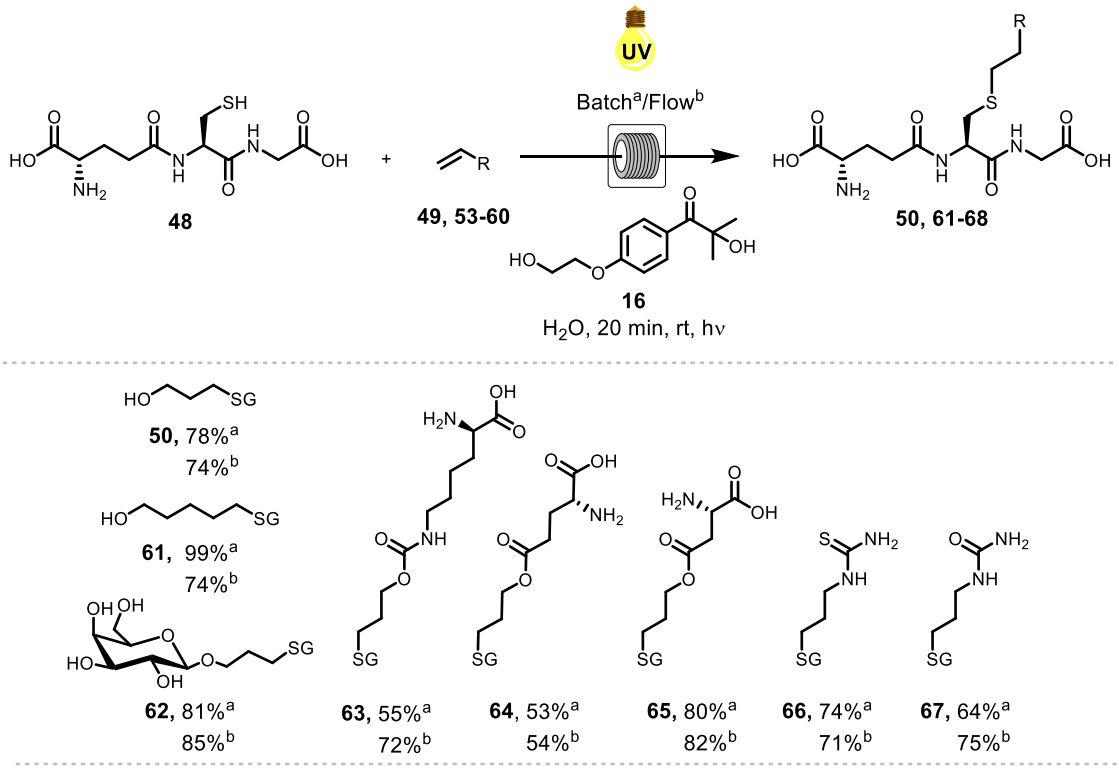

Figure 2.4: Substrate scope of radical mediated TEC using Irgacure **16** as photoinitiator under a) batch and b) continuous-flow conditions. Yields were calculated by ^{1}H NMR spectroscopy using dimethyl sulfone as an internal standard (100 mol%).

Upon first observation, the product yields obtained from reactions initiated with **16** under continuous flow were lower than the corresponding reactions initiated with DPAP **15** (**Figure 2.4**). This is as a result of the slower rate of homolytic cleavage to form the corresponding initiating radical species of **16** in comparison to DPAP **15** (**Figure 2.5**).[205] The secondary alkyl radical species resulting from cleavage of **16** (**Figure 2.5,** D) exhibits significantly lower stability than the stabilised benzoyl radical resulting from the cleavage of DPAP **15** (**Figure 2.5**, B), thereby limiting the rate of homolytic fission.[121]

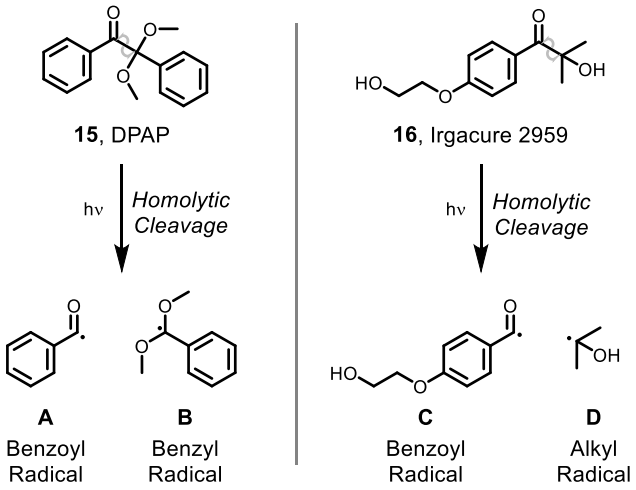

Figure 2.5: Homolytic cleavage of photoinitiators **15** and **16**.

Comparison of the crude ^{1}H NMR spectra of the thiol–ene reactions of GSH **48** and aspartic acid derived alkene **55** using DPAP **15** and Irgacure 2959 **16** indicated that the reaction mixture initiated by Irgacure 2959 **16** contained a greater proportion of signals corresponding to unreacted initiator. This suggested that the slower homolytic fission of initiator **16** is indeed responsible for the lower yields observed in comparison to reactions with DPAP **15**. Nevertheless, satisfactory reaction yields of the peptidic substrates were obtained. Continuous flow proved to generate greater yields in the majority of the cases compared to the standard batch conditions. With the applicability of the thiol-ene reaction demonstrated, this method was carried out using a biologically relevant target peptide substrate.

2.3.6 Thiol-Ene Mediated Glycosylation of Biologically Active Peptides in Water Under Continuous-Flow

Tumour homing peptide, CREKA **77**, containing the sequence H-Cys-Arg-Glu-Lys-Ala is known for to its high specificity for cancer cells.[206] CREKA **77** is used to target tumour extracellular matrix (ECM). In tumour cells, CREKA **77** forms an integral component of the intracellular matrix, therefore increasing its tumour-homing potential.[206] Conjugation of CREKA peptide **77** to maleimide at the Cys residue of the peptide has been commonly been performed to facilitate the imaging of cancer cells.[207] CREKA peptide **77** represents an ideal model substrate for aqueous radical mediated thiol-ene bioconjugation due to the presence of a terminal Cys residue and its inherent aqueous solubility. Allylated

monosaccharide **53** was selected as a model alkene substrate. This saccharide-based substrate was chosen as the synthesis of CREKA peptide **77** glycoconjugates have not been previously reported in the literature and may be of considerable interest for biological applications due to the unique properties of glycoconjugates, including cell uptake and lectin binding.[121] CREKA peptide **77** was prepared *via* manual SPPS and purified by RP-HPLC. TEC addition of galactoside **53** (20 eq.) to CREKA peptide **77** was carried out in the presence of **16** as photoinitiator under UV irradiation in H_2O (+ 0.1% formic acid (FA)) under continuous flow (**Scheme 2.3**). Mild acidic conditions were used to avoid the oxidation of the starting material to a disulfide bond.[208,209] The progress of the reaction was monitored by RP-HPLC analysis and indicated full consumption of the starting material **77** in 2 h. Subsequent freeze drying and semi-PREP HPLC analysis permitted isolation of the target glycosylated peptide **78** in a 44% isolated yield (*c.f.* **Figure S9.10** and **S9.12**).

Peptide **79** was selected as a second biologically relevant peptide of interest given that antifungal proteins (AFP) are useful for the treatment of fungal infections such as Candidiasis, Cryptococcosis and Aspergillosis.[210] The sustainability, high efficacy, low toxicity, and relatively cheap production of AFPs grant their suitability to peptide bioconjugation.[210] CKYKAQ peptide **79** is an AFP sequence located in bacterial type 3 chitin-binding domains.[211] This sequence is also located in the chitin-binding domains of fungi, such as *A. giganteus*.[210] CKYKAQ peptide **79** was prepared *via* manual SPPS and purified by RP-HPLC. The progress of the thiol-ene reaction with **53** under aqueous continuous flow conditions was monitored by RP-HPLC analysis and full consumption of starting material **79** was observed in 2 h (**Scheme 2.3**). HPLC purification permitted isolation of the target glycosylated peptide **80** in a 58% isolated yield (*c.f.* **Figure S9.11** and **S9.13**). The addition of 6 M Guanidine HCl to the reaction mixture, as reported by Wang and co-workers,[165] to disrupt intramolecular and intermolecular hydrogen bonding and improve the solubility of reagents was investigated, however, no notable increase in the yield of products **78** or **80** was observed.

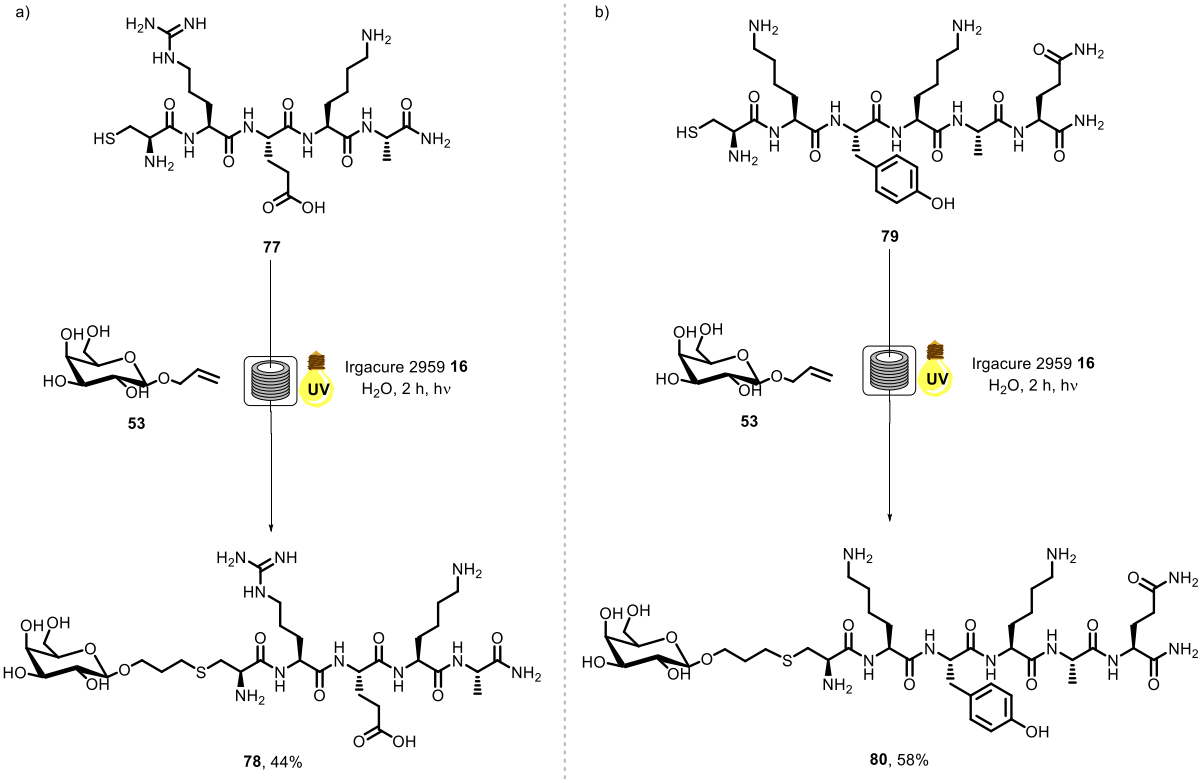

Scheme 2.3: Radical mediated TEC reaction of allylated monosaccharide **53** and: a) CREKA peptide **77** b) CKYKAQ peptide **79** under continuous-flow conditions in aqueous media.

Finally, the RGD peptide **81** which comprises 11 AA residues was selected to prove the applicability of the green approach on longer-chain peptides. RGD-peptides are known to be over-expressed in cancer cells.[212] The RGD motif targets integrins expressed on the tumour vasculature, enabling targeting of imaging agents, therapeutics, and gene delivery systems.[213] RGD peptide conjugates are therefore of considerable interest for medicinal chemistry and drug development. H-PQVTRGDVFTEG-NH_2 peptide **81** was synthesised by SPPS using a Liberty Blue® peptide synthetiser.[b] In an attempt to improve ligation yields, a strategy was reported by Alexander and co-workers[214] whereby the alkene moiety is installed on the peptide substrate, thereby limiting any side reaction with Cys residues.

In order to perform this reaction, a thiolated GlcNAc derivative **84** was selected and synthesised from glucosamine in a two-step synthesis (**Scheme 2.4**).

[b] RGD peptide **81** was synthesized by Dr. Nikita Ostrovitsa.

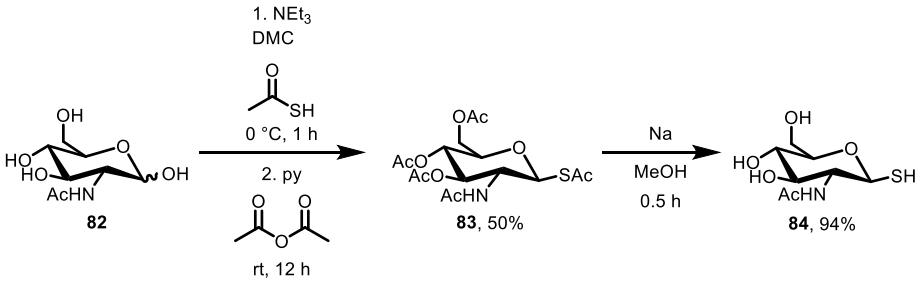

Scheme 2.4: Synthesis of the thiolated derivative **84** through glucosamine modification.

The first step consisted of the thioacetylation of glucosamine **82** in the presence of triethylamine (TEA), this was followed by the universal protection of the monosaccharide in the presence of acetic anhydride. The thioacetylated product **83** was purified by flash-column chromatography and obtained in a 50% yield. Subsequently, thioacetylated product **83** was selectively deprotected at the 1,3,4,5-positions in the presence of $Na_{(s)}$. Dowex® 50WX8 (H+) ion exchange resin was added to the crude mixture and final product was filtered and concentrated *in vacuo* achieving a 94% yield of deprotected thiosugar **84** (*c.f.* **Figure S9.14** and **S9.15**).

The TEC reaction was then carried out between RGD-peptide **81** and thiolated GlcNAc derivative **84** (5 eq.), with Irgacure 2959 **16** (2.5 eq.) as photoinitiator, under continuous flow for 2 h in EG:H_2O (3:2) (**Figure 2.6**). The crude material was analysed and purified by RP-HPLC, furnishing conjugated-peptide **85** in a 62% isolated yield. The use of the DES:H_2O system was optimal for the RGD peptide and compatibility of this green solvent system with the chosen initiator **16** has previously been demonstrated in section **2.3.3.** These examples represent the first application of the radical mediated thiol-ene reaction in the bioconjugation of biologically active peptides, in green solvents, under continuous flow. This is an extremely promising result as this method significantly reduces the environmental impact of traditional thiol-ene bioconjugation methodologies.

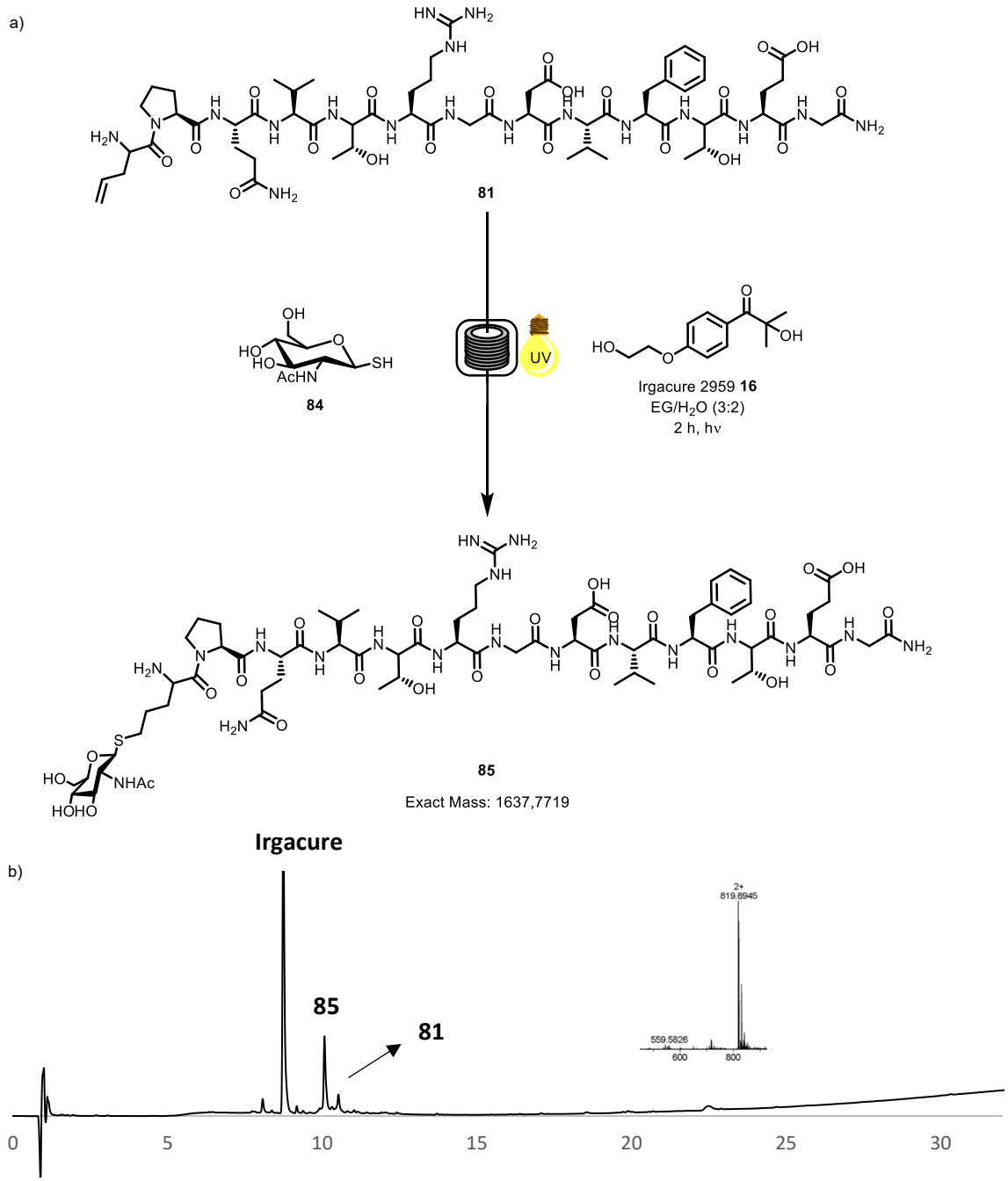

Figure 2.6: a) TEC reaction of RGD peptide **81** and thiolated sugar **84** with Irgacure 2959 **16** as photoinitiator under continuous flow conditions. b) Crude RP-HPLC trace (220 nm, 5-95% MeCN/H_2O + 0.1% TFA) of the reaction between RGD peptide **81** and thiolated sugar **84** after 2 h.

For the culmination of this chapter TEC under continuous-flow conditions was demonstrated for biotinylation. In molecular biology and biochemistry, biotinylation is a highly important modification involved in selective labelling, detection, and manipulation of proteins and other bioactive molecules.[215] In this project biotin-PEG-

thiol **86** was selected to investigate this reaction.[c] In the first instance, the reaction was conducted with RGD peptide **81** under standard batch conditions using EG/H_2O (3:2) as solvent for 2 h under UV-light irradiation. The crude mixture was analysed by RP-HPLC and 50% conversion to the biotinylated peptide **87** was achieved (**Figure 2.7b**). Subsequently, the same reaction was performed under continuous flow conditions to assess whether the conversion could be improved, using the same reaction parameters. However, no formation of the desired product **87** was observed by RP-HPLC. This negligible conversion may be attributed to the nature of the strongly hydrophilic PEG moiety, which likely adhered to the tubing of the flow reactor, despite its hydrophobic nature and polytetrafluoroethylene (FEP) composition, highlighting a potential limitation for continuous flow processing of large hydrophilic molecules. Future studies will investigate how these limitations may be overcome through judicious selection of materials for the continuous flow system.

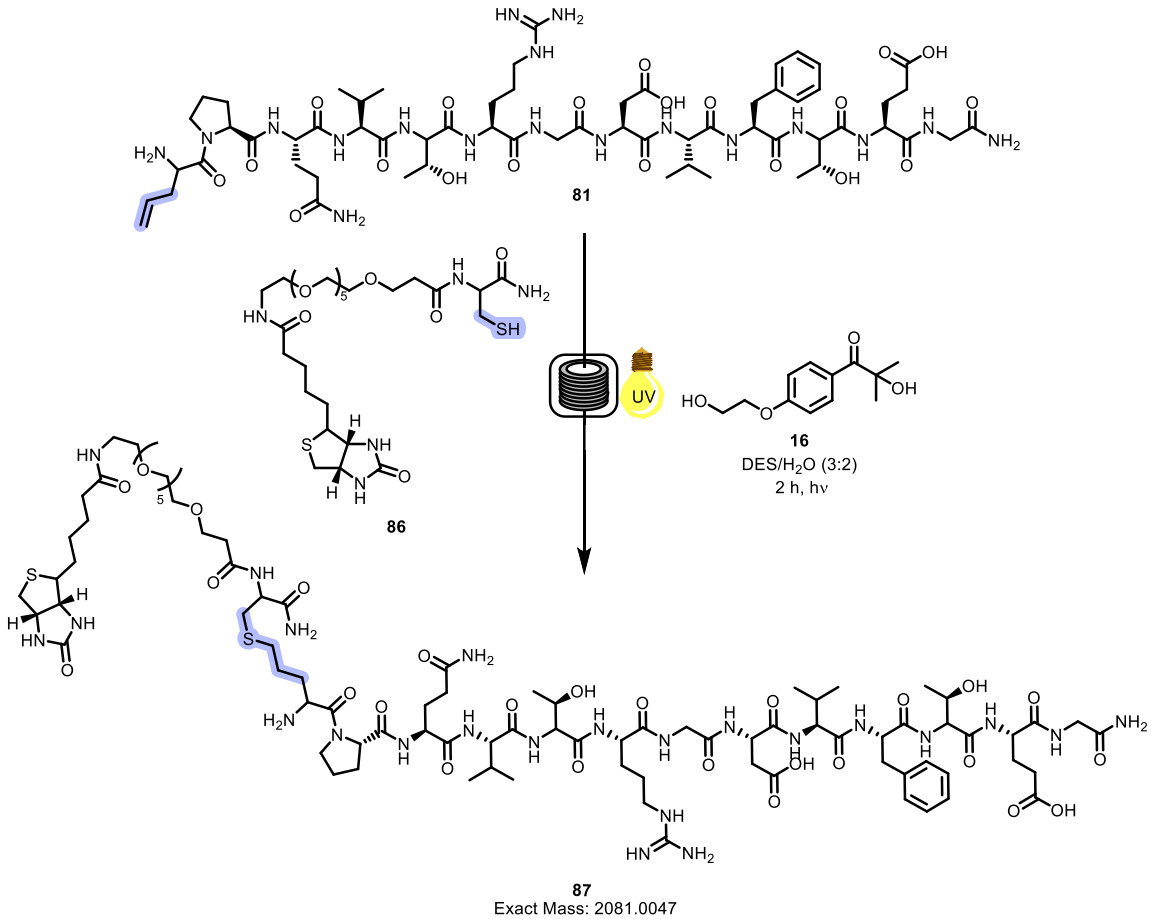

Figure 2.7: TEC reaction between biotin-PEG-thiol **86** and RGD peptide **81** in the presence of Irgacure **16** as photoinitiator in DES/H_2O.

[c] Biotin-PEG-thiol **86** was synthetized by Lucy McCormack.

2.4 Conclusions

This research has established the viability of the radical-mediated thiol-ene reaction under continuous-flow conditions in environmentally friendly solvents with peptide-based substrates. By initially optimising the batch conditions reported by Conway and colleagues in THF/H_2O,[196] it was shown that continuous flow could effectively produce GSX conjugates in excellent yields. Further exploration of the reaction scope with various alkenes revealed that continuous flow generally afforded higher yields compared to traditional batch methods, underscoring the potential of the continuous-flow system to enhance the efficiency and sustainability of widely used organic reactions. Several novel GSX peptide derivatives of biological relevance were successfully synthesised using this method. This study demonstrated that DESs, as well as other bio-based and less hazardous solvents, are compatible with radical-mediated thiol-ene chemistry in continuous-flow, thereby eliminating the reliance on toxic organic solvents. Notably, the use of the water-soluble photoinitiator Irgacure 2959 **16** enabled efficient synthesis under entirely aqueous conditions, eliminating the need for organic solvents and significantly reducing the environmental effect of the reactions. The developed continuous-flow approach was further validated through the successful glycosylation of three biologically significant peptides, furnishing the desired glycoconjugates in good yields. Overall, this work highlights the effectiveness and broad applicability of a ‘green’, radical-mediated peptide bioconjugation strategy. Furthermore, it showcases the enhanced sustainability achieved over traditional techniques through integration of continuous-flow techniques and ‘greener’ solvent selection.

Chapter 3

One-pot peptide disulfide rebridging *via* thiol-yne 'click' chemistry†

3.1 Introduction

Amongst the myriad of synthetic peptide modifications available, peptide cyclisation and stapling offer a promising approach to enhance stability and improve binding affinity. Stapled peptides contain one or more specific macrocycles that help stabilise the α-helical conformation.[216] This involves the formation of a linkage between two side chain residues of the same peptide to maintain and stabilize its helical structure. The external brace restricts the flexibility of the molecule, lowering the entropic cost of binding the peptide, thereby increasing its affinity and selectivity for the target. Additionally, this conformation obscures the amide bond within the helix, improving protease stability and facilitating easier cell membrane permeation.[217,218]

Over time, several different methods of peptide stapling have been developed, including ring-closing methasis,[219] copper-catalysed azide-alkyne cycloaddition[134], lactamisation[220] and Cys stapling. Disulfide functionalisation has emerged as one of the most useful approaches for site-selective protein modifications towards the generation of peptide/protein hybrids.[221-223] Disulfide 'rebridging' strategy involves the functionalisation of the disulfide bond *via* reduction followed by a covalent reaction with a bis-reactive reagent and is demonstrated to enhance the pharmacokinetics and properties of proteins, peptides and antibodies (**Figure 3.1**).[224-227] The functional rebridging of native disulfides was first introduced by Brocchini *et al*.[228, 229] and it has gained considerable attention in recent years, leading to the development of various new approaches.

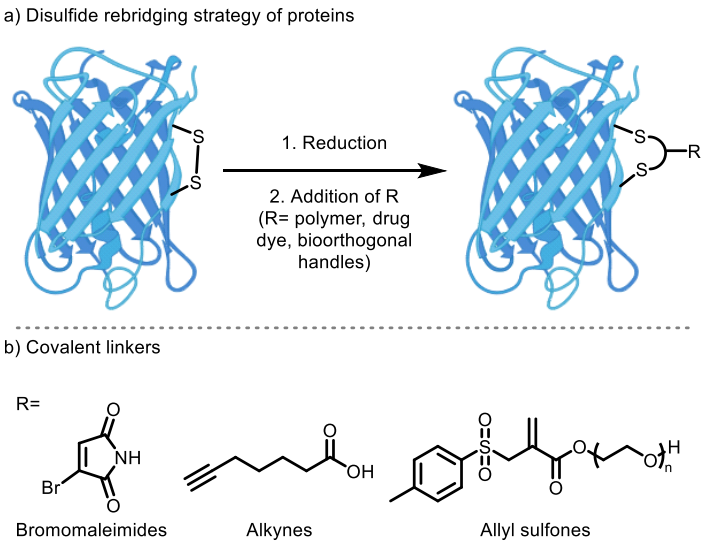

Figure 3.1: a) Surface-exposed disulfide bond rebridging in proteins. b) Representative covalent linkers from literature.[221, 227, 230]

Chemical rebridging of a reduced disulfide bond will inevitably cause some structural alteration to the peptide or protein, as the number and hybridisation of atoms in the new bridge will differ from the natural geometry of the original linkage. However, the biological properties of a native peptide can be maintained or even enhanced through disulfide rebridging, in particular *via* increase in the stability of the peptide.[231,232] Developing a method to photochemically rebridge peptides includes several advantages such as (a) facile attachment of tags; (b) fast and high-yielding photochemical reactions; and (c) functional group selectivity during irradiation, maximizing the potential for reforming the pharmacophore.[233] The thiol-yne click (TYC) reaction is known as a 'click' reaction due to its adaptability to aqueous environments, its biorthogonal characteristics, and its modularity with the added benefit of being a metal-free process (**Figure 3.2**).[234] TYC reactions offer a unique opportunity to extend the chemistry of related thiol-ene reactions (discussed earlier in this thesis), enabling the creation of a wide variety of novel materials with diverse properties.[235] However, the TYC reaction presents some limitations, such as its sensitivity to steric hindrance and the tendency to form mixtures of stereoisomers.[165] The general mechanism of TYC reaction (**Figure 3.2**) involves the addition of a thiyl radical (generated *via* a thermal- or photoinitiator as discussed previously for the thiol-ene reaction) to a C≡C bond to give an intermediate vinyl thioether radical. The next step involves a hydrogen atom transfer (HAT) between the intermediate vinyl-based radical and a thiol. A second hydrothiolation occurs on the intermediate vinyl thioether to furnish the target 1,2-bisaddition of the thioether product.[130]

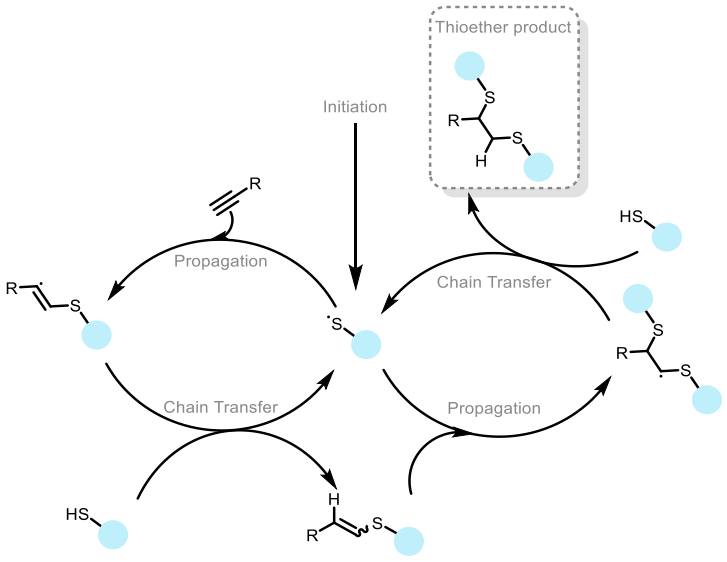

Figure 3.2: Thiol-yne chain reaction mechanism workflow.[130]

TYC has been employed by Y. Wang *et al.*[165] in protein macrocyclization along with D. A. Richards *et al.*[236] for stapling helical peptides. While one-pot methods offers several advantages such as the reduced waste and high mass efficiency,[237] a common limitation is the incompatibility between the reagents for the distinct reactions as in the case of rebridging chemsitry.[230]

Thiol-yne conjugation of peptide and proteins *via* disulfide rebridging has been previously reported by Griebenow *et al.*[174] The authors demonstrated their strategy on a range of disulfide-containing systems, including the disulfide bonds of the telipressin peptide and antibodies. However, to the best of our knowledge, no additional reducing agents have been investigated for this methodology, and the range of alkynes studied remains limited.

3.2 Aims

The objective of this project was to develop a one-pot peptide rebridging strategy with a suitable disulfide reducing agent and to apply the optimised methodology to a broad range of alkynes to further demonstrate the versatility of this strategy beyond the current literature (**Figure 3.3**). Initially, we set out to investigate the use of $NaBH_4$ as a potential reducing agent for the first step of the disulfide rebridging process, owing to the ease of quenching of excess reagent and facile removal of the corresponding salts. By contrast, Griebenow and co-workers reported the use of tris(2-carboxyethyl)phosphine (TCEP) as a reducing agent which is known to undergo desulfurization reactions under light mediated conditions.[238] An extensive investigation was carried out to assess the rebridging potential of our modified strategy on various biomolecules and is reported herein. The chapter concludes with the application of this chemistry to a synthetic analogue of the peptide hormone Somatostatin (octreotide **4**), aimed at advancing bioimaging techniques.

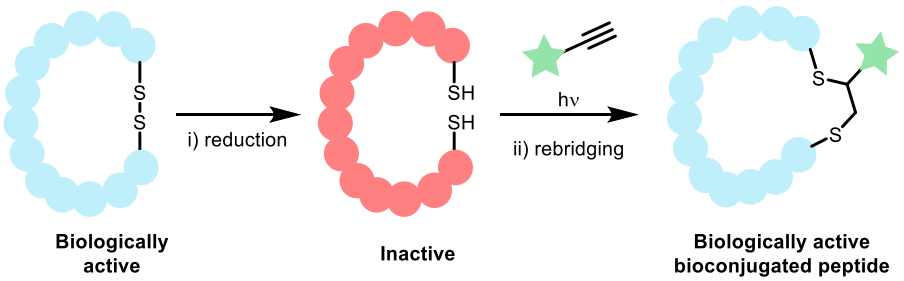

Figure 3.3: One-pot disulfide peptide rebridging methodology.[174, 233]

3.3 Results and Discussion

3.3.1 Synthesis of disulfide peptide analogue

The selected model peptide for this study was a 5-AA cyclic model peptide **89** which contains a generic sequence of AAs along to two terminal Cys residues to mimic the natural disulfide bonds found in proteins.

To commence the initial investigations, the model pentapeptide H_2N-Cys-Ala-Tyr-Gly-Cys-$CONH_2$ **88** was synthesised using manual Fmoc SPPS on Rink Amide resin, with Fmoc deprotection achieved using 20% (v/v) piperidine in DMF (2 x 10 min) (**Figure 3.4a**). Coupling of the deprotected peptide amine was achieved through use of PyBOP coupling agent in the presence of *N*-methyl morpholine base (NMM). The initial AA was coupled using a solution of Fmoc-Cys(Trt)-OH (4 equiv.), DIC (4 equiv.) and Oxyma Pure (8 equiv.) in DMF for 45 min, so as to ensure efficient and complete coupling to the resin. The following three residues were coupled using a solution of Fmoc-AA-OH (3 equiv.), PyBOP (3 equiv.) and NMM (6 equiv.) and the final residue coupled using, Fmoc-Cys(Trt)-OH (3 equiv.), DIC (3 equiv.) and Oxyma Pure (3 equiv.) for 45 min. Following chain assembly, the peptide was deprotected and cleaved from the resin using a cleavage cocktail consisting of TFA:TES:H_2O:DTT (90:2.5:2.5:5) for 2 h to furnish the linear peptide **88**. The isolated crude peptide was obtained in >95% purity by analytical RP-HPLC (**Figure 3.4b**) which was sufficiently pure for use in the following steps. Peptide **88** was cyclised *via* disulfide bond formation between the Cys residues located at both the C- and N-terminus of the sequence. The cyclisation was based on the conditions outlined by Kröling *et al.*,[239] employing DMSO as an oxidative reagent. The peptide was dissolved in MeCN:H_2O (1:1) + 0.1% FA along with 10% (v/v) DMSO. The reaction was stirred at rt and monitored by analytical RP-HPLC and after 48 h full conversion to the intramolecular disulfide product was achieved (**Figure 3.4c**). The final cyclised product **89** was purified on semi-preparative RP-HPLC using a gradient of 0-100% MeCN in H_2O (+ 0.1% TFA) and lyophilised to furnish a white powder (*c.f.* **Figure S9.18** and **S9.19**).

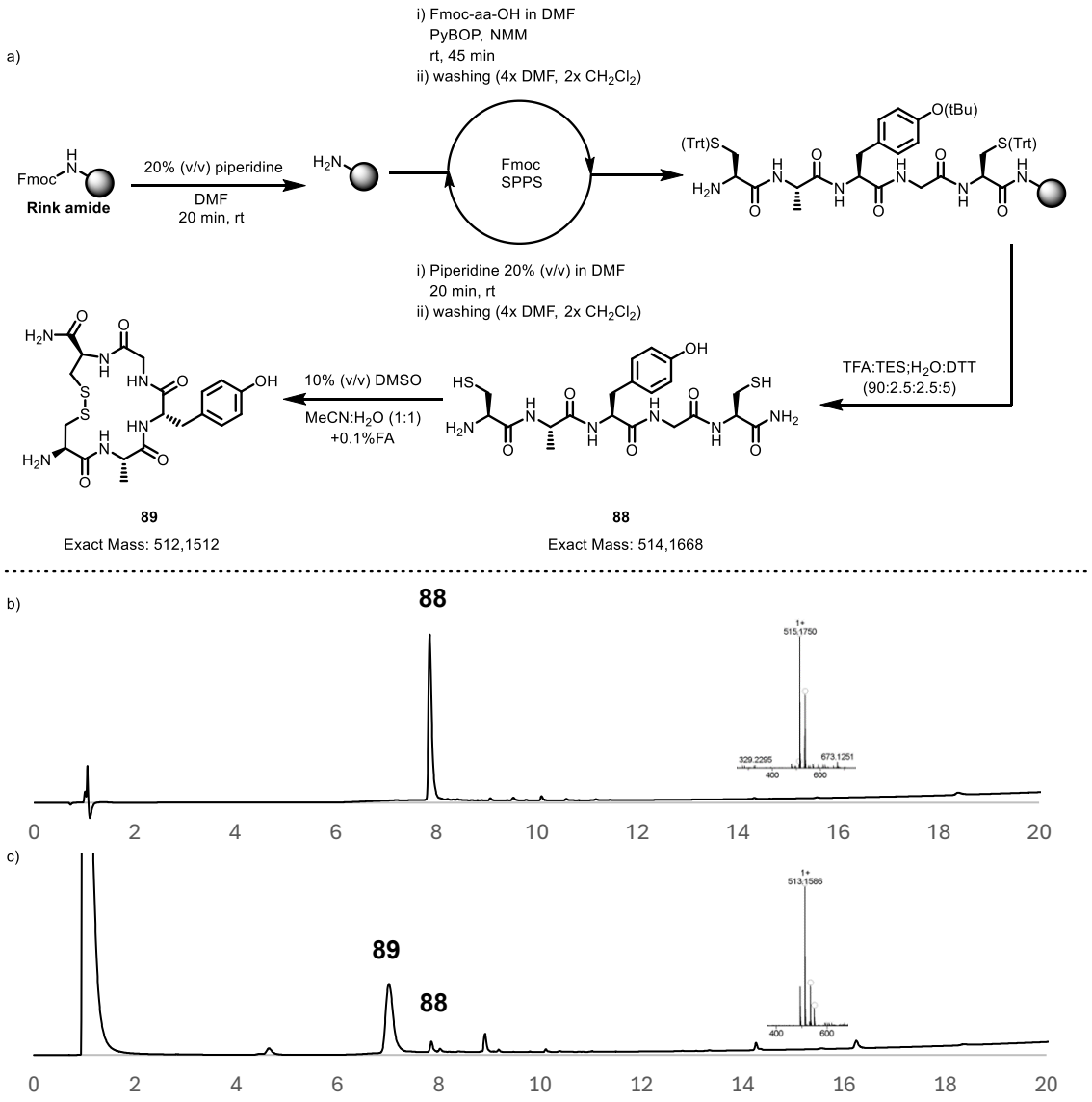

Figure 3.4: a) Synthesis of disulfide-bridged cyclic peptide **89**. b) HPLC trace (220 nm, 5-95% MeCN/H_2O + 0.1% TFA) of the crude linear peptide **88** post SPPS. c) Crude HPLC trace (220 nm, 5-95% MeCN/H_2O + 0.1% TFA) of the cyclisation reaction, forming peptide **89**.

3.3.2 $NaBH_4$ reduction

Three primary classes of disulfide reducing agents have been established in the literature: (i) phosphines, (ii) thiols or dithiols and (iii) $NaBH_4$.[240] In this study we set out to achieve a one-pot rebridging method through use of borohydride reagents. The use of thiols as reducing agents was excluded as an option due to the potential formation of an excessive quantity of uncontrollable thiyl radicals during the thiol-yne reaction. This would interfere with the reaction mechanism, ultimately preventing its progression. In the context of phosphines, although they function efficiently as disulfide reducing reagents, it is well-established that Cys containing peptides, when exposed to TCEP and a radical

initiator, can undergo competing desulfurisation processes (**Scheme 3.1**). The application of TCEP for peptide radical-based desulfurisation was reported by Wan and Danishefsky in 2007,[241] who utilized VA-044 and tert-butyl thiol (^{t}BuSH) to facilitate radical-based, chemoselective desulfurisation for polypeptides. Furthermore, González and Valencia, in 1998,[242] reported the photochemical desulfurisation of Cys in Cys-containing peptides.

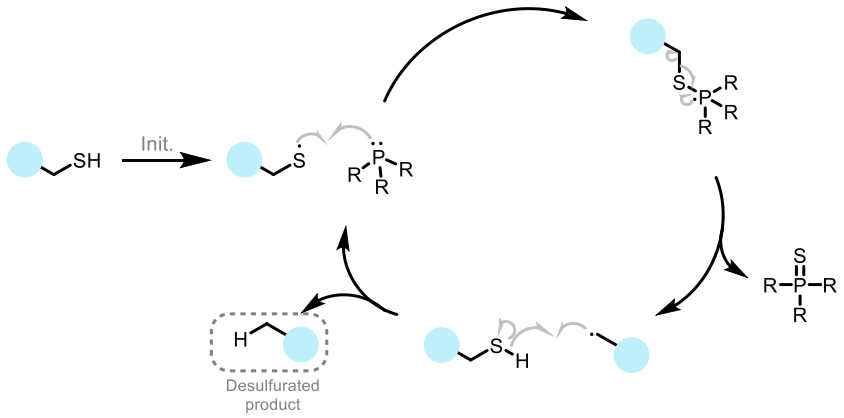

Scheme 3.1: Radical chain mechanism of desulfurisation reaction using phosphines.[243]

$NaBH_4$ has been employed as reducing agent for disulfide bonds in organic molecules, offering advantages over phosphine reagents including its relatively low cost and facile handling and work-up properties. It has been reported that $NaBH_4$ can specifically reduce disulfides to free thiols without affecting other major functional groups in proteins.[244,245] Hermanson developed a protocol for borohydride disulfide reduction for organic compounds that eliminates the need for purification steps to remove the reducing agent after the reaction.[246] As a result, peptides reduced using this protocol can be directly applied in bioconjugation without the need for further purification. To the best of our knowledge, its application in peptide chemistry has not previously been reported to date.

Following the conditions developed by Jocelyn *et al.* for reducing protein disulfides,[247] peptide **89** was dissolved in a 0.75 M solution of $NaBH_4$ in H_2O and then redissolved in H_2O to achieve a final reaction concentration of 0.3 M at pH 9 (**Figure 3.5a**). The reaction was stirred for 1 h at rt while being monitored by analytical RP-HPLC. The reaction was then worked up by acidifying the mixture with 1 M HCl, leading to the decomposition of $NaBH_4$. 25% conversion to the dithiol product **88** was achieved within 15 minutes as determined by analytical RP-HPLC, and after 1 h, the reaction mixture reached a maximum of 38% dithiol product **88** based in RP-HPLC conversion. Based on these results, it was postulated that higher concentrations of $NaBH_4$ may be required to

improve conversion to the desired dithiol product.[240] This was confirmed by dissolving peptide **89** in a 0.75 M $NaBH_4$ in H_2O solution, which successfully achieved 88% product conversion within 15 minutes. When the same reaction was carried out in PBS (pH 7) to simulate cell culture conditions, it was observed that 89% product conversion was achieved within 2 minutes (**Figure 3.5b**). After 30 minutes, the reaction reached >95% dithiol product **88** RP-HPLC conversion. Conversions on this study were based on RP-HPLC area integration of peptide **88** (peptide **88** metrics are included in the appendix **Figure S9.29**).

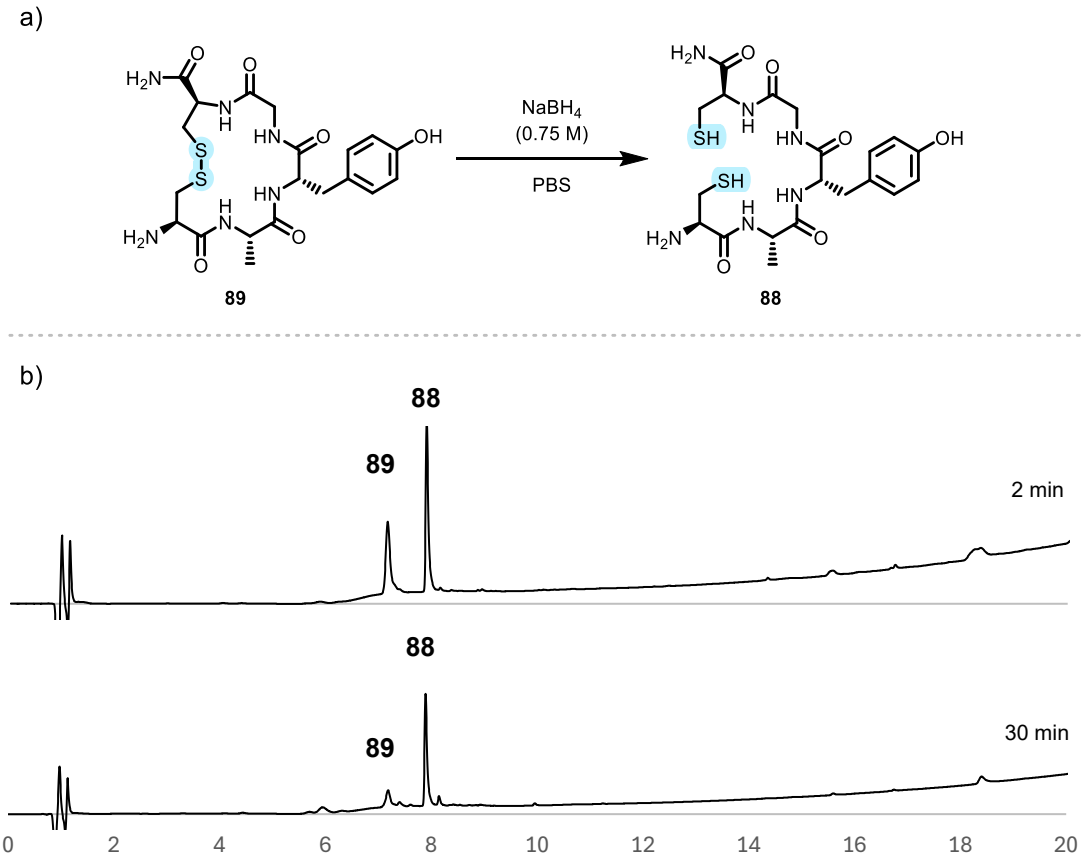

Figure 3.5: a) Reduction of disulfide **89** with $NaBH_4$. b) Comparison of the HPLC trace (220 nm, 5-95% MeCN/H_2O + 0.1% TFA) of the disulfide peptide **89** after 2 min reaction (top) and the crude HPLC trace (220 nm, 5-95% MeCN/H_2O + 0.1% TFA) of the disulfide peptide **89** after 30 min (bottom).

3.3.3 TEC reaction

A thiol-ene-mediated model reaction was developed to evaluate if both thiols in the peptide could undergo radical formation in a reasonable period of time. Allyl alcohol **49** was selected as the alkene due to its ease of handling and small size, along with high yields for thiol-ene ligation as reported in **Chapter 2.** Thus, peptide **88** and allyl alcohol

49 along with Irgacure 2959 **16** as the photoinitiator were dissolved in H_2O + 0.1% FA and stirred at rt for 1 h under UV-light (**Figure 3.6a**). The reaction resulted in complete consumption of the starting material, as confirmed by RP-HPLC analysis, with >95% product conversion (**Figure 3.6b**). No disulfide dimer of peptide **89** was observed thereby demonstrating the suitability of the selected peptide **89** for thiol-yne conjugation (*c.f.* **Figure S9.20**).

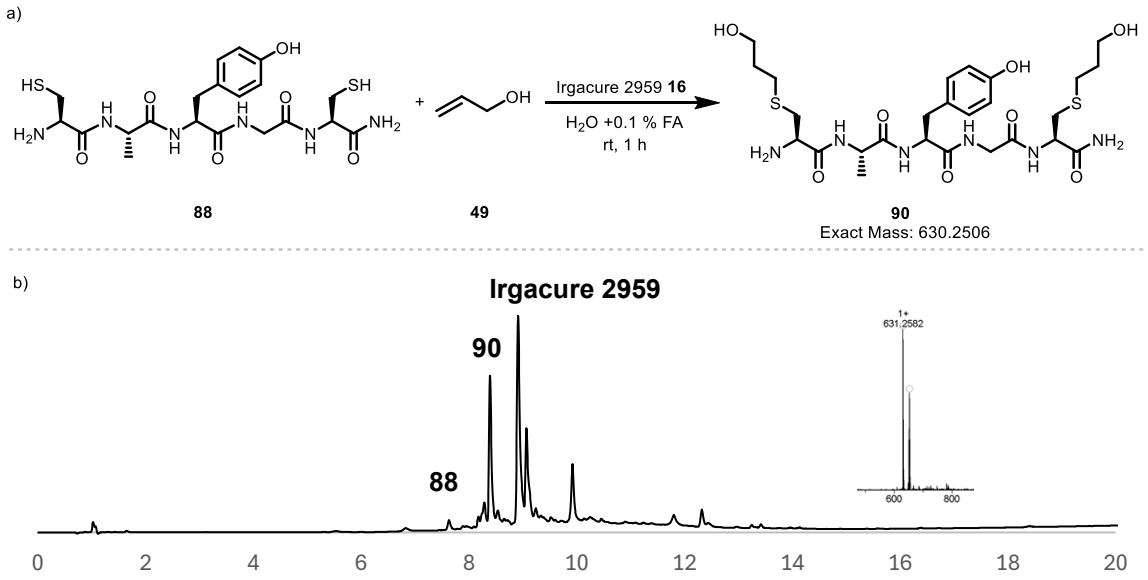

Figure 3.6: a) Thiol-ene test reaction of peptide **88** with allyl alcohol **49**. b) Crude RP-HPLC trace (220 nm, 5-95% MeCN/H_2O + 0.1% TFA) of the thiol-ene test reaction

3.3.4 TYC optimization

In the radical thiol-yne reaction, several side processes can compete during the reaction, including double addition products and disulfide formation along with the various potential stereoisomers formed from thiol-ene addition onto the vinylsulfide product of the initial thiol-yne reaction. Therefore, optimisation of the reaction conditions was performed. The radical TYC reaction was optimised using the linear peptide **88**, and propargyl alcohol **91** as the alkyne due to its ease of handling and relatively small size which should prevent unwanted steric interference during the thiyl radical mediated reactions. The reaction was performed at rt and under UV irradiation. The results of the optimization studies are summarized in **Table 3.1**.

Table 3.1: Optimization of TYC on linear peptide **88**.

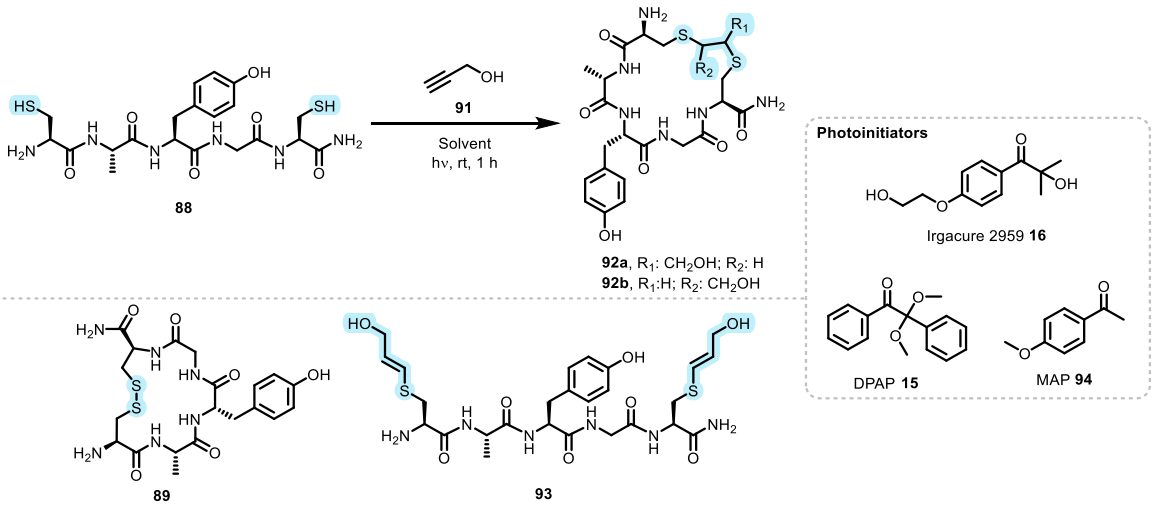

Entry	SH: Alkyne	88 Conc. (mM)	Photoinitiator (0.5 equiv.)	Solvent	Notes	Conv.* (HPLC)
1	1:1	5	Irgacure 2959	H_2O:MeCN (9:1)	+ 0.1% FA	35%
2	1:2	5	Irgacure 2959	H_2O:MeCN (9:1)	+ 0.1% FA	30%
3	1:4.5	5	Irgacure 2959	H_2O:MeCN (9:1)	+ 0.1% FA	20%
4	2:1	5	Irgacure 2959	H_2O:MeCN (9:1)	+ 0.1% FA	25%
5	1:2	5	Irgacure 2959	H_2O:MeCN (1:1)	+ 0.1% FA	5%
6	1:2	5	Irgacure 2959	DMF	+ 0.1% FA	NR
7	1:1	5	DPAP+MAP	H_2O:MeCN (9:1)	+ 0.1% FA	52%
8	1:1	10	DPAP+MAP	H_2O:MeCN (9:1)	+ 0.1% FA	70%
9	1:1	10	DPAP+MAP	PBS:MeCN (9:1)	pH 7	23%
10	1:1	10	DPAP+MAP	H_2O:MeCN (9:1)	No FA	40%
11	1:1	10	-	H_2O:MeCN (9:1)	Dark	NR
12	1:1	10	-	H_2O:MeCN (9:1)	+ 0.1% FA	NR

*Conversions measured by RP-HPLC as a sum of the two resulting isomers **92a** and **92b**. NR= No reaction occurred.

The reaction was conducted with Irgacure 2959 **16** as the photoiniator based on the favourable results reported using this initiator in **Chapter 2**. A ratio of 1:1 thiol:alkyne respectively was used initially, as this ratio was theoretically considered to be sufficient. However, it was observed that the desired conjugated peptide **92a/b** was only obtained in 35% conversion (entry 1, **Table 3.1**). Upon the addition of 1 more equiv. of alkyne **91**, the RP-HPLC conversion remained at 30% (entry 2, **Table 3.1**). Notably, when an additional 2.5 equiv. of alkyne were introduced, the conversion decreased further to 20% (entry 3, **Table 3.1**). This decline in conversion was attributed to the excess alkyne, which likely facilitated dual addition to the peptide, resulting in peptide **93** being obtained in

19% and 44% RP-HPLC conversion (entry 2 and 3, respectively**, Table 3.1**). To investigate the source of proton extraction during the TYC reaction, 2 equiv. of linear peptide **88** were added (entry 4, **Table 3.1**). However, RP-HPLC conversion remained unchanged at 25%. The study was extended by altering the solvent system to a 1:1 ratio of H_2O:MeCN (entry 5, **Table 3.1**) and to DMF (entry 6, **Table 3.1**) in 0.1% FA. In both cases, not only did the conversion to the desired product fail to improve, but disulfide peptide **89** was also obtained in 6% and 18% RP-HPLC conversion, with the dual addition product **93** in 89% and 79%, respectively. These results confirm that the proton extraction originates from the solvent. As discussed in **Chapter 2**, it is established that DPAP **15** exhibits a faster rate of the homolytic cleavage compared to Irgacure 2959 **16**. Given that TYC is a time-dependent reaction, the standard conditions previously optimized were employed, utilising DPAP **15** as the photoinitiator and MAP **94** as a photosensitiser (entry 7, **Table 3.1**). As anticipated, the RP-HPLC conversion of the desired product **92a/b** increased to 52%. As in the case of TEC, the TYC reaction is also concentration-dependent; thus, the linear peptide concentration **88** was increased to 10 mM (entry 8, **Table 3.1**) in order to achieve better yield. Under these modified conditions, a 70% conversion of peptide **92a/b** was achieved. To investigate the important influence of the pH in this process (to maintain the thiol residues in the protonated form required for the radical chain process), reactions were carried out in PBS at pH 7 (entry 9, **Table 3.1**), and without FA (entry 10, **Table 3.1**). The peptide **92a/b** conversions were 19% and 37%, respectively, with disulfide peptide **89** being obtained in RP-HPLC conversion of 77% and 54%. These results suggest that in the absence of formic acid (FA), the thiol can deprotonate, thereby promoting the formation of the disulfide bond more readily and hindering the likelihood of TYC occurring. In the final study, reactions were conducted both without a photoinitiator (entry 11, **Table 3.1**) and without UV irradiation (entry 12, **Table 3.1**) to confirm that the reaction proceeded *via* a radical mechanism rather than a nucleophilic one, as seen in the thiol-michael reaction. Neither of these conditions led to a successful reaction, suggesting that the reaction does indeed proceed *via* a radical mediated TYC reaction. The optimal conditions for the reaction were achieved with a thiol:alkyne ratio of 1:1, using 10 mM of peptide **88**, DPAP **15** as the photoinitiator, and MAP **94** as the photosensitizer (entry 8, **Table 3,1**). A key advantage of this protocol is that disulfide peptide **89**, previously considered a side-product in the TYC optimisation, can now be repurposed as a starting material in the one-pot reaction, enabling the reaction to proceed recurrently. Having demonstrated the efficacy of $NaBH_4$ as a potential

alternative reducing agent to phosphine for disulfide bond reduction and the efficacy of the model dithiol peptide in TYC reactions with propargyl alcohol **91**, we next set out to investigate if these two reactions could be combined into a 'one-pot' protocol suitable for rebridging disulfide containing peptides and proteins.

3.3.5 One-pot, thiol-yne mediated disulfide rebridging reaction

Synthetic chemistry consistently necessitates the development of more efficient and environmentally sustainable techniques aimed at improving mass efficiency, minimising the effort required for intermediate isolation, reducing energy consumption, and decreasing waste generation.[237] The one-pot TYC reaction for disulfide-based peptide rebridging has been previously explored by Griebenow *et al*.,[174] demonstrating distinct behaviours across various peptide-based disulfides, beginning with intermolecular disulfide reduction, followed by intramolecular disulfide rebridging, and culminating in an exploration of antigen scopes.

Based on the previous optimised conditions identified for the stepwise process, a one-pot TYC-mediated disulfide rebridging reaction of disulfide peptide **89** was performed using $NaBH_4$ as the reducing agent for the disulfide bond with propargyl alcohol **91**. Peptide **89** was added to a solution of 0.75 M $NaBH_4$ in H_2O. The reaction mixture was stirred for 15 min at rt. Then a mixture of DPAP **15**, MAP **94** and propargyl alcohol **91** in H_2O:MeCN (9:1) + 0.1% FA was added to this solution and it was let stir at rt under UV-light irradiation for 1 h (**Scheme 3.2a**).

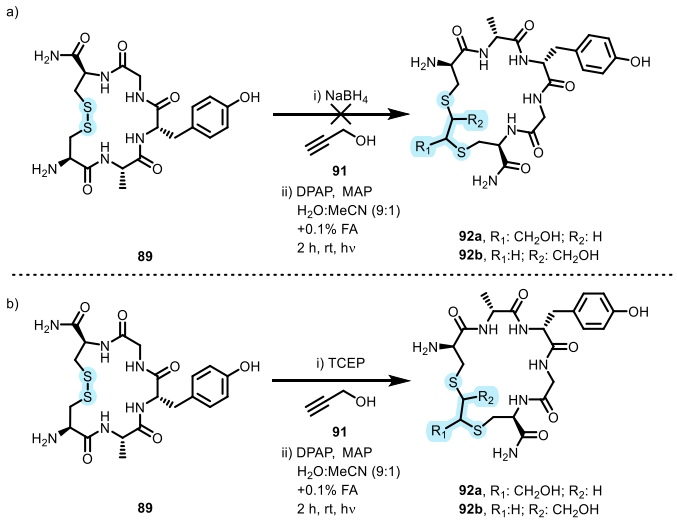

Scheme 3.2: a) One-pot disulfide rebridging of peptide **89** using $NaBH_4$ as reducing agent of disulfide bonds. b) One-pot disulfide rebridging of peptide **89** using TCEP as reducing agent of disulfide bonds.

The addition of acidified buffer would allow the reaction to be worked up *in situ*, enabling the TYC process to proceed. However, the reaction was unsuccessful, likely due to competing crosslinking reactions, such as hydroboration of the alkyne,[248] occurring simultaneously with the TYC-mediated process. Given that this strategy was successful using TCEP as the reducing agent, the study was subsequently continued employing TCEP as the standard disulfide reducing agent under the same procedure (**Scheme 3.2b**). Desulfurisation requires an excess of TCEP and longer reaction times, typically performed with a thermal initiator, compared with the TYC reaction.[241] To prevent desulfurisation, only 1.5 equivalents of TCEP were used, and the reaction time was limited.

A one-pot reaction between peptide **89** and propargyl alcohol **91** was performed. Disulfide reduction of peptide **89** with TCEP in H_2O was achieved within 15 min. Subsequently, a mixture of DPAP, MAP, and propargyl alcohol **91** in H_2O:MeCN (9:1) + 0.1% FA was added to the peptidyl solution and the reaction was stirred at rt under UV irradiation for 1 h. After this period, the dithiol peptide **88** remained with 65% conversion as determined by RP-HPLC. Addition of a second equivalent of propargyl alcohol **91** followed by an additional hour under UV irradiation. Full consumption of the starting material was achieved with >95% RP-HPLC conversion to thioether isomers **92a/b** (*c.f.* **Figure S9.21**). No alkene intermediates were detected by ^{1}H NMR spectroscopy, indicating an optimisation relative to previously reported conditions.[228]

3.3.6 Scope of One-Pot TYC Peptide rebridging with Chemically Diverse Alkynes

To comprehensively examine the behaviour of the chemistry with alkynes of varying size and functionality, the synthesis of alkynes **91, 95-100** (**Scheme 3.3-3.5**) was carried out. For this study, two commercially available alkynes, propargyl alcohol **91** and 4-pentynoic acid **95** were also used. In the case of the sugar alkynes, such as galactose-alkyne **96** and lactose-alkyne **97**, these were synthesized following conditions reported by Hsiao-Wu *et al*.,[249] through the addition of propargyl alcohol **91** onto the sugar in the presence of $BF_3.OEt_2$ in dry CH_2Cl_2 (**Scheme 3.3**). The reaction was monitored by TLC and carried out for 3.5 h. Following an aqueous work up and column chromatography purification, the protected galactose-alkyne **100** and lactose-alkyne **101** were obtained in 67% and 27% isolated yield, respectively. Acetyl deprotection of both monosaccharide and

disaccharide were performed using NEt_3 in MeOH (1:4) and the desired products **96** and **97** were isolated in 82% and 64% yield, respectively (*c.f.* **Figure S9.22-S9.25**).

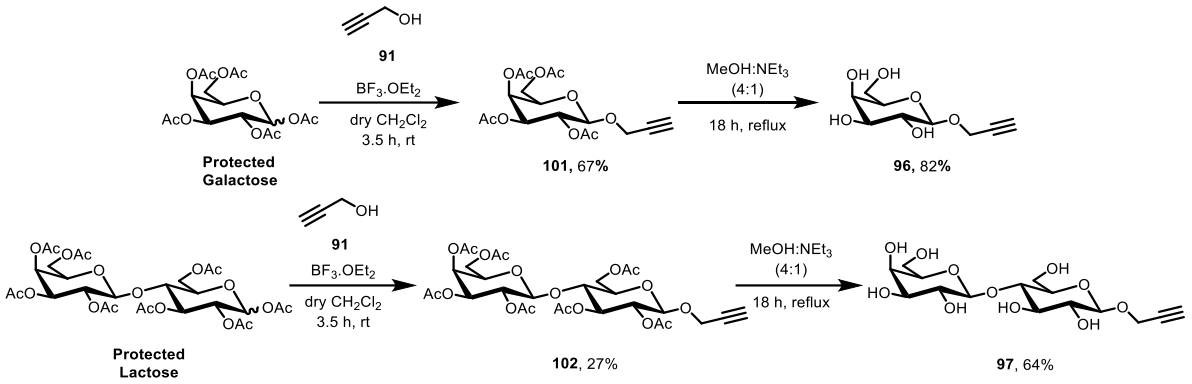

Scheme 3.3: Synthesis of the monosaccharide **96** and disaccharide **97**.

The synthesis of the alkyne-azide **98** was performed by dissolving bromide alkyne **103** in DMF and NaN_3 was added. The mixture was stirred for 18 h at 80 ºC. After the extraction with EtOAc, the product **98** was obtained in 15% isolated yield (*c.f.* **Figure S9.26**).[250]

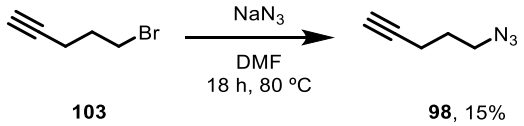

Scheme 3.4: Synthesis of alkyne-azide **98**.

Finally, biotin-alkyne **99** was synthesised by the addition of coupling reagents HCTU, DIPEA and DMAP (1equiv., 1equiv. and catalytic quantity, respectively) to a solution of biotin **104** and propargyl amine in DMF (**Scheme 3.5**). The reaction mixture was stirred at rt overnight. The reaction was worked up through extraction with EtOAc, in order to remove residual DMF. Flash column chromatography was performed and the desired product **99** was obtained in 55% isolated yield (*c.f.* **Figure S9.26**).[251]

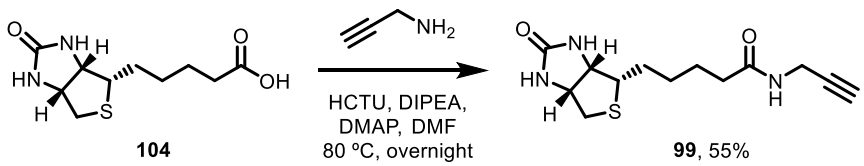

Scheme 3.5: Synthesis of the biotin-alkyne **99**.

The standard protocol as reported by Griebenow *et al.*,[174] was followed for the one-pot reduction-TYC reaction, in this case using the alkynes prepared as outlined above. Disulfide peptide **89** and TCEP (1.5 equiv.) were added to a 1 mL glass vial and dissolved in H_2O. The peptide containing solution was allowed to stir for 15 min to allow complete reduction of the disulfide to dithiol. Next, a mixture of DPAP **15** (1 equiv.), MAP **94** (1 equiv.), and the corresponding alkyne (1 equiv.) in H_2O:MeCN (9:1) + 0.1% FA was added to the peptidyl solution and allowed to stir at rt under UV-light conditions for 1 h (**Figure 3.7**). After this time, a second equiv. of the corresponding alkyne was added and stirred for 1 h under UV irradiation.

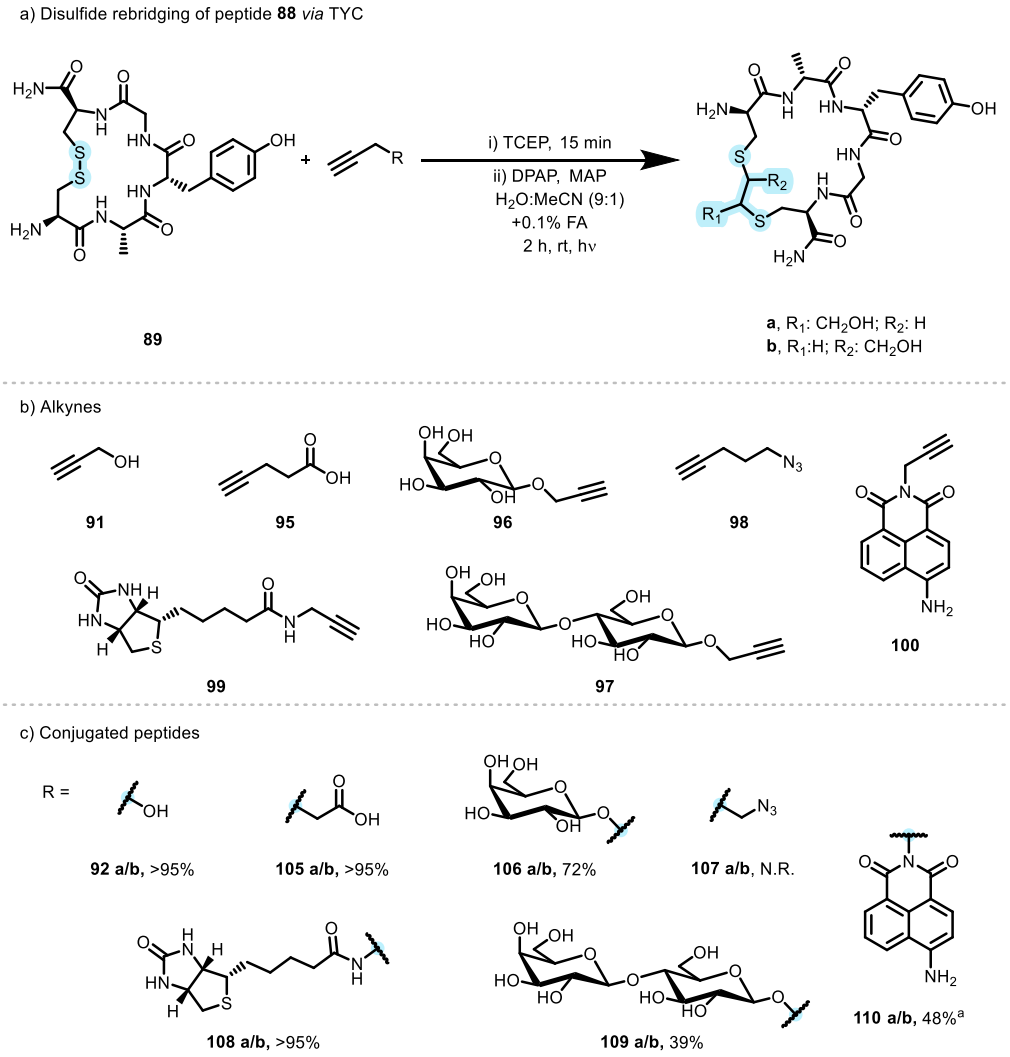

Figure 3.7: Scope of the one-pot TYC-mediated rebridging of the disulfide peptide **88**. % Conversions were measured by RP-HPLC as a summary of the 2 resulting isomers **a** and **b.** [a] Denotating a different solvent system such as H_2O:MeCN (7:3) + 0.1% FA. N.R = No reaction occurred.

When performing the reactions with propargyl alcohol **91** and 4-pentynoic acid **95**, complete consumption of the starting materials was observed, with >95% conversion to isomers **92a/b** and **105 a/b** determined by RP-HPLC. This efficient reactivity was most

likely due to the small steric bulk of the allyl alkynes. In the case of the slightly bulkier monosaccharide alkyne **96**, 25% of the disulfide peptide **89** was also formed. This by-product is likely attributable to partial reoxidation of the dithiol **88**, promoted by the electron-withdrawing groups present on the alkyne **96**, which render it a more electron-poor substrate, resulting in overall slower kinetics for the thiyl radical mediated reaction.

To extend the scope towards the introduction of 'clickable' handles, the alkyne-azide **98** was investigated as a potential linker with capability for further modification, as previously demonstrated by Markey *et al.*[116] However, no product formation was observed when disulfide peptide **89** was treated with alkyne–azide **98**. This is likely attributable to a competing reductive side reaction of the azide moiety in the presence of a dithiol (**Figure 3.8**).

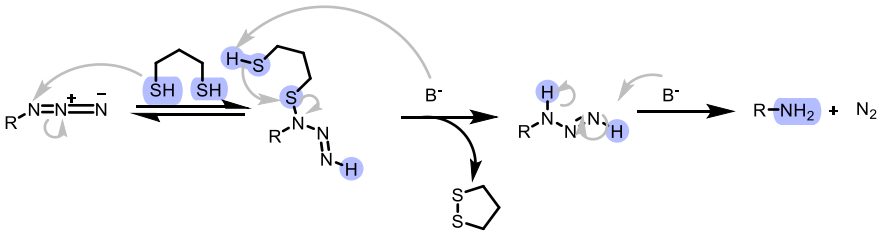

Figure 3.8: Azide reduction by dithiols.[252]

In comparison to the previously mentioned alkynes, biotin–alkyne **99** displayed a selective trend, furnishing a 100:0 ratio of isomers **108a/b**. However, further studies could not be performed to confirm the structural isomerism of the conjugate due to the limited material obtained after purification. On the other hand, full consumption of starting materials was achieved with >95% conversion of biotinylated peptide **108a/b**.

For the disaccharide alkyne **97**, complete consumption of the starting materials was not achieved, with 31% of disulfide **89** and 29% of dithiol **88** obtained. This was likely due to the significantly larger steric bulk of the alkyne group relative to the monosaccharide alkyne **96**. Conjugated peptide **109a/b** was achieved in a 39% RP-HPLC conversion. To promote product conversion, an additional equivalent of TCEP was introduced after 1 h of reaction; however, no substantial improvement was observed. Instead, formation of a desulfurisative by-product was detected by mass spectrometry. A comparable outcome was observed in the case of the naphthalimide–alkyne **100**.[d] In this

[d] Naphthalimide-alkyne **100** was synthetised by Dr. Ramírez-Lázaro.

case, solvent polarity was adjusted by increasing the proportion of MeCN in the H_2O:MeCN mixture from 9:1 to 7:3 in order to achieve maximum solubilisation of the reagents. Despite these changes, only 48% RP-HPLC conversion was achieved for the bioconjugated naphthalimide-peptide **110a/b**, along with traces amounts of desulfurisation by-product.

Future work will fully address the isomeric distribution of products of the TYC reaction and further clarify the stereochemical aspects of this methodology.

3.3.7 Octreotide scaffold

To demonstrate the applicability of this chemistry to larger substrates, the octreotide peptide **4** was selected as a model disulfide bond-containing peptide. Octreotide is a long-acting synthetic octapeptide analogue of the naturally occurring hormone Somatostatin. It functions by inhibiting the secretion of anterior pituitary growth hormone and thyroid-stimulating hormone, as well as a broad range of peptide hormones from the gastroenteropancreatic endocrine system.[253] Compared with the Somatostatin peptide, octreotide exhibits an extended half-life and exerts stronger inhibitory effects.[254] Due to these properties, it has been approved as a first-line treatment for acromegaly[255] and cancer therapy.[256,257] The conjugation of octreotide with a fluorophore has been widely explored for tumour targeting[258] and for its quantification in biological or cellular environments.[258-261]

Octreotide peptide **4** was synthesized *via* Fmoc-SPPS synthesis using the Liberty Blue peptide synthesiser, employing repetitive cycles of Fmoc-AA couplings and Fmoc deprotections under microwave-assisted conditions and elevated temperature. Amide couplings were carried out using DIC (3 equiv.) as a coupling reagent and Oxyma Pure (6 equiv.) as an activating additive, and Fmoc deprotections were achieved upon treatment of the resin-bound peptide with 20% (v/v) piperidine in DMF. The combination of DIC and Oxyma pure in both manual and automated synthesis is an effective racemisation-free method for amide formation.[262] Following peptide cleavage and deprotection as previously described, the crude product was dissolved in MeCN:H_2O (1:1) + 0.1% FA along with 10% (v/v) DMSO without further purification for 48 h at rt. Crude product was then purified by semi-preparative RP-HPLC yielding the final octapeptide **4** with >95% purity as confirmed by analytical RP-HPLC and ESI-MS (**Figure 3.9**).

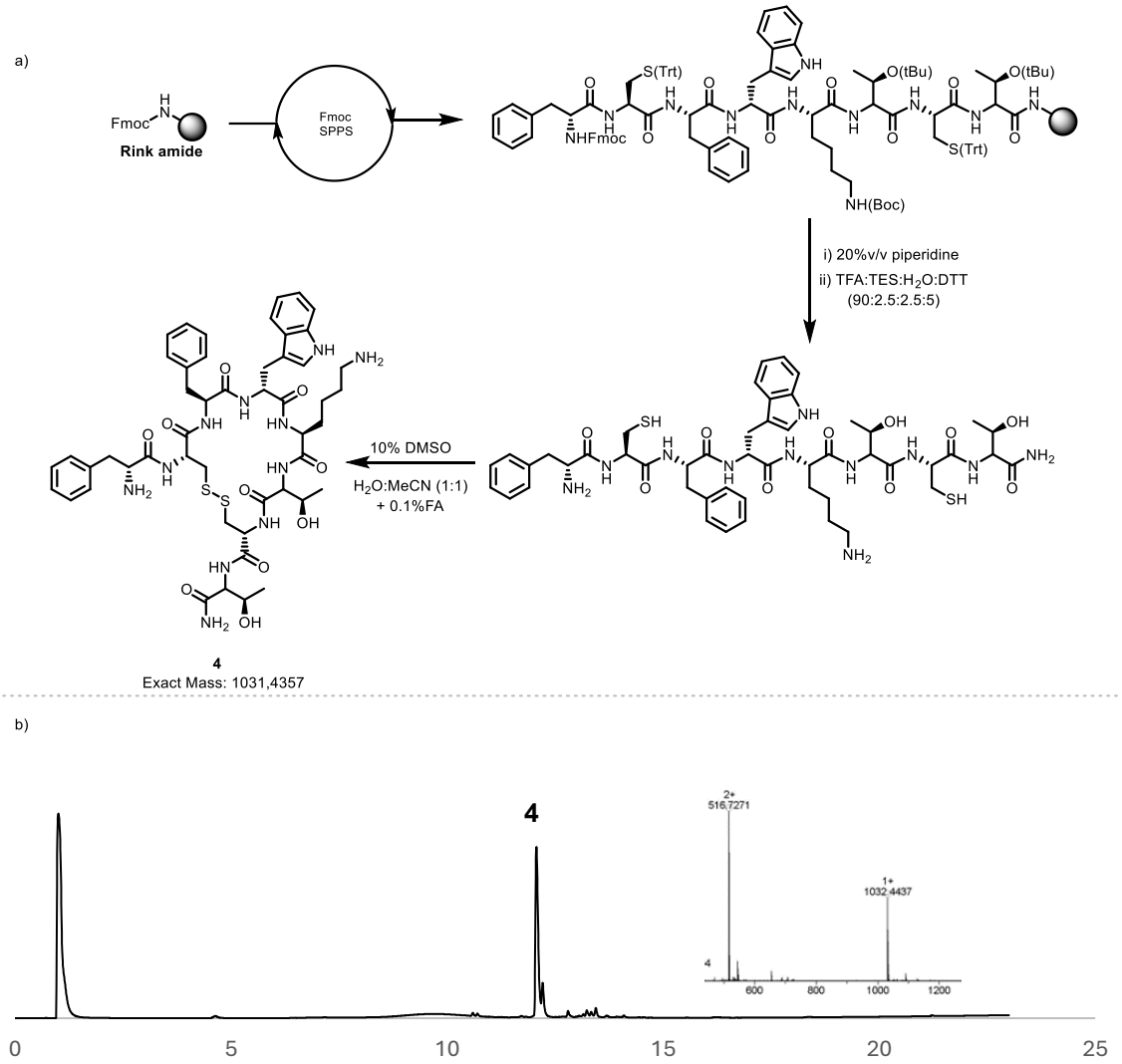

Figure 3.9: a) SPPS synthesis of octreotide peptide **4**. b) Crude RP-HPLC trace (220 nm, 5-95% MeCN/H_2O + 0.1% TFA) of the cyclisation with 10% (v/v) DMSO.

Following our one-pot disulfide reduction and TYC rebridging protocol, naphthalimide-alkyne **100** was used to generate a rebridged fluorescent peptide analogue of octreotide suitable for potential bioimaging applications. Octapeptide **4** and TCEP (1.5 equiv.) were added into a vial and dissolved in H_2O. The peptide solution was allowed to stir for 15 min in order to reduce the disulfide to the dithiol. Next, a mixture of DPAP **15**, MAP **94** and the naphthalimide-alkyne **100** in H_2O:MeCN (7:3) + 0.1% FA was added to the peptidyl solution and let stir at rt under UV-light conditions (**Scheme 3.10**). The crude mixture was monitored by analytical RP-HPLC and purified by semi-preparative RP-HPLC furnishing the final conjugated octapeptide **111a/b** in 62% RP-HPLC conversion. The starting material was completely consumed in the reaction; however, a 38% conversion to the desulfurisation byproduct **112** was also observed. In an attempt to improve the product yield, an additional equiv. of TCEP was added after 1 h of reaction.

However, this resulted in >95% conversion to the desulfurised byproduct **112**, with no detectable formation of the desired product due to the excess of TCEP.

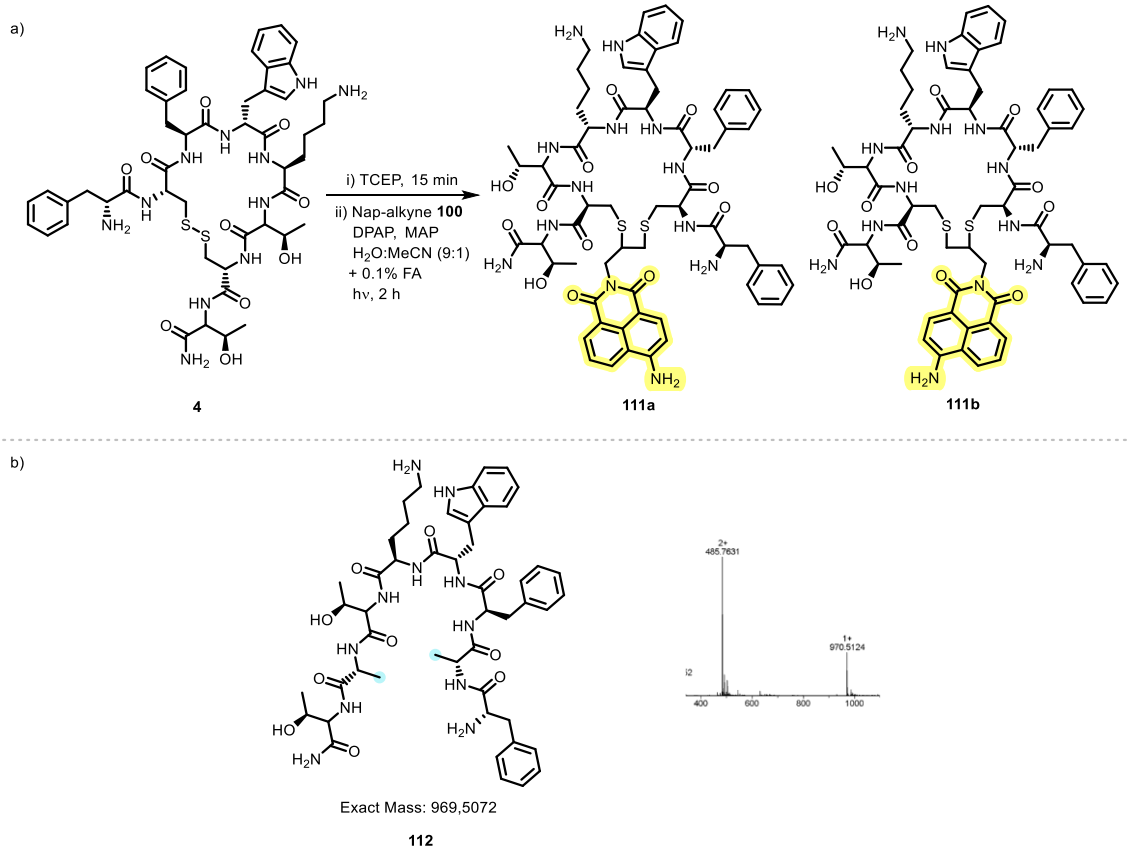

Figure 3.10: a) TYC-mediated rebridging of octreotide peptide **4** with Nap-alkyne **110** in order to yield novel fluorescent peptide conjugates **111a/b.** b) Structure of desulfurisation by-product **112**, as characterised by ESI-MS.

3.4 Conclusions and future work

In this chapter, a TYC-mediated rebridging method was developed for peptide bioconjugation with a focus on applications towards delivering suitably labelled peptide macrocycles as tools for chemical biology. Additionally, use of $NaBH_4$ as a disulfide-reducing agent for use in the stepwise process was identified.

Initially, the optimisation of $NaBH_4$ was undertaken to establish the most efficient conditions for peptide disulfide reduction. Its high efficiency was demonstrated with a model peptide **89**, achieving >95% dithiol conversion by RP-HPLC within 15 minutes in PBS buffer. A subsequent TEC-based model reaction confirmed the feasibility of performing thiyl-radical mediated reactions at both thiols, furnishing >95% of the diconjugated product after 1 h. Optimisation of the TYC reaction was also performed to

gain mechanistic insights into the rebridging reaction and to minimise side-product formation. The optimum conditions were identified as 10 mM of the disulfide peptide **89** with DPAP **15** and MAP **94** as photoinitiator and photosensitiser, in H_2O:MeCN (9:1) + 0.1% FA, yielding 70% conversion of the desired product **92a/b** after 1 h.

However, attempts to perform a one-pot reduction–rebridging using $NaBH_4$ and TYC failed to furnish the desired rebridged product, likely due to potential side reactions between alkynes and $NaBH_4$. Consequently, the one-pot approach was adapted to employ the previously reported reducing agent TCEP, which afforded high RP-HPLC conversions in an expanded alkyne scope study.

As a proof of concept, the one-pot method was successfully applied to the rebridging and fluorescent labelling of a biologically active peptide, octreotide **4**. Treatment of octreotide with an alkyne containing fluorophore, namely naphthalimide-alkyne **100** afforded the corresponding conjugate **111a/b** in 62% conversion, demonstrating the potential utility of this approach.

Moving forward, future work will involve a detailed stereochemical study of the TYC reaction, given that the initial reactivity can occur at either Cys residues. Furthermore, fluorophore–octreotide conjugate **111a/b** will be explored for bioimaging applications in cellular environments, thereby expanding the scope and relevance of this strategy, as has been demonstrated in previous studies.[259-261]

Chapter 4

Naphthalimide-mediated thiol-ene photoredox catalysis †

4.1 Introduction

As previously discussed in **Chapter 1**, TEC is a versatile photochemical 'click' reaction that often relies on light irradiation and the presence of a photoinitiator to induce the radical chain process, although thermal initiation is also a viable option. Thus, the use of light has a distinctive role in the photomediated approach to generate thiyl radicals. Methods for the thiyl radical formation comprise a diverse range of photoinitiators including direct photoinitiation, nanoparticle-based photoinitiators and molecular photoinitiatiors. Development of novel photoinitiators remains an active field of research as more sophisticated methods for proximal thiyl-radical formation are required for applications of thiol-ene ligation in biological systems.[263] Indeed, for applications of thiol-ene ligation in biological milieu, where an abundance of different thiols exist, often within high concentrations of glutathione, selective thiyl radical initiation remains the only logical approach towards achieving selective processes. Direct photolysis of the S-H bond is the simplest method to generate thiyl radicals; however, it requires longer exposure times and higher energy photons compromising the molecules stability.[264,265] In the case of nanoparticle-based photoinitiators, they generally function as heterogeneous catalysts for chemical synthesis and modification.[266] They offer advantages such as reusability, sustainability and ease of separation which fit with the concepts of 'click' and 'green' chemistry. Commonly used nanoparticles in current research include transition metal oxides (e.g., TiO_2, Bi_2O_3) and metal nanoparticles such gold (Au) and silver (Ag).[267, 268] However, the most widely used method for generating thiyl radicals is through the use of molecular photoinitiators. These are commonly known as HAT photoinitiators and can be classified in two groups: (i) bond-cleavage photoinitiators (type I), such DPAP **15** and Irgacure 2959 **16** as previously showed in **Section 2.3.4** and (ii) bimolecular photoinitiating systems (type II), such as benzophenone.[107,269] HAT photoinitiators are the most widely utilised photoinitiators for peptide chemistry involving UV-light. However, shifting to lower excitation energies offers the possibility of milder excitation sources with reduced potential for radical induced damage when performing ligation reactions in biological systems.[263] Therefore, novel methodologies such as photoredox catalysis focused in longer wavelength such as blue and visible light are under investigation due to their improved compatibility with biological systems.[270]

4.1.1 Photocatalysis

Photoredox catalysis is a relatively recent 'tool' that fits well with the 'green-chemistry' dogma owing to its compatibility with room temperatures conditions and low energy photons.[271] The general mechanism of photoredox catalysis involves the absorption of light of by photocatalyst (PC) entering in a photoexcited state (PC*). Once the PC has been excited, it can transfer the electron *via* two different pathways (**Figure 4.1**): the oxidative quenching cycle where PC* transfers an electron to an acceptor species (A) and is consequently oxidised to $PC^{+\bullet}$ which is then reduced back to the ground-state (GS) PC by accepting an electron from a donor (D) or *via* the reductive quenching cycle where PC* is reduced to a $PC^{-\bullet}$ by a D followed by the oxidation back to the GS-PC through electron transfer to the A.[263]

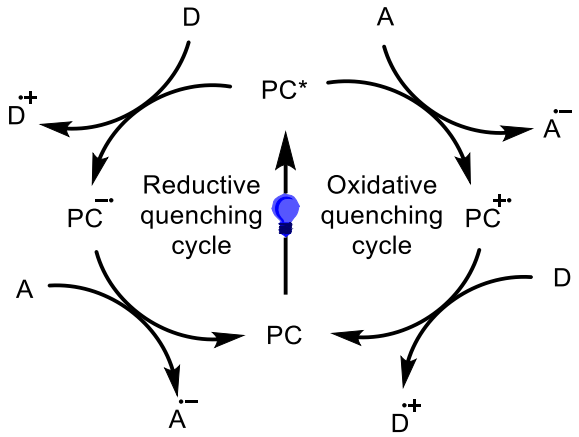

Figure 4.1: Reported catalytic quenching cycles of a photoexcited photoredox catalyst PC*.[272]

The most widely explored photocatalytic redox methodology for thiol-ene reaction is the visible-light-mediated ruthenium (Ru) PC due to its atmospheric redox activity in reductive or oxidative cycles.[273, 274] However, various catalytic structures are also used, including transition metal polypyridyl complexes,[108] lanthanide ions,[275] metal-organic frameworks[275] and organic molecules such as naphthalimides.

4.1.2 Naphthalimides

1,8-naphthalimides (naps) are ben[de]isoquinolin-1,3-diones that possess a naphthalene core connected to a third ring formed by an imide bond (**Scheme 4.1**).

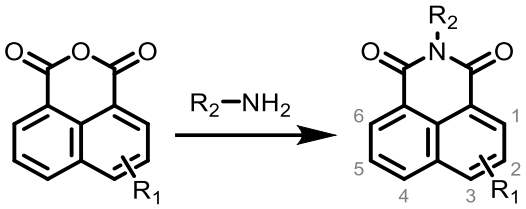

Scheme 4.1: Generic scheme for the synthesis of 1,8-Naphthalimides.

The R_1 group is commonly functionalised with various organic groups which modulate the photophysical properties of these molecules. In 1986, Middleton *et at*. first reported the internal charge transfer (ICT) behaviour of naps.[276] This study showed how naps can adjust the ICT excited state to produce a ratiometric fluorescence response. The naphthalene ring acts as a π-bridge between the electron-accepting imide R_2 group and R_1 group. When R_1 is installed at the 4-position with an electro-withdrawing group such as NO_2, the resulting compound exhibits minimal fluorescence.[277] This is likely due to the high electronegativity of the oxygen atoms which disrupts the conjugation between the donor nitrogen and the rest of the fluorophore, thereby effectively obstructing its ICT. In contrast, substitution of R_1 by electron-donating group (e.g., NH_2) results in 'unrestricted' naps that display 'push-pull' ICT excited-state, where the electrons delocalisation occurs from the NH_2 group to the electron-withdrawing imide (**Figure 4.2**).[277] This leads to a broad emission bands centred around 450 and 550 nm, respectively.

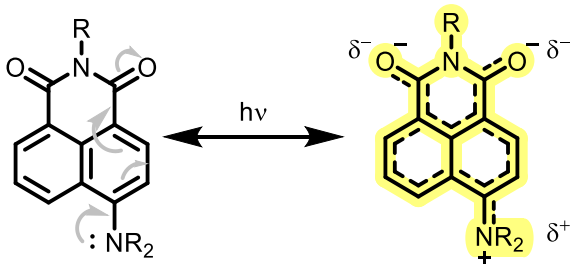

Figure 4.2: Electron delocalization causing ICT within the Nap ring.

Applications of naps have been reported in antitumor research,[278] fluorescent markers in biochemistry,[279] analgesics in medicine,[280] fluorescent switchers,[281] and laser dyes.[282] Henwood *et al.*, reported a novel aggregation-induced emission (AIE) strategy in which nap **113** (**Scheme 4.2**), in the presence of the clinically approved amphiphilic poloxamer P188 developed a co-assembly strategy.[283] This could demonstrate the 'on' (emissive) or 'off' (quenched) behaviour in cells.

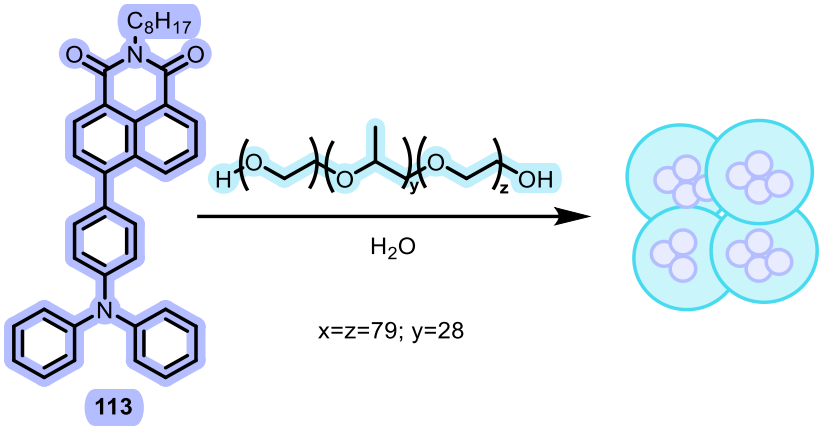

Scheme 4.2: Co-assembly strategy to develop water-soluble nanoparticles in aqueous P188.[283]

This strategy involves the use of P188, a tri-block copolymer composed of two hydrophilic polyethylene glycol chain flanking and a central hydrophobic core (polypropylene oxide), which encapsulates hydrophobic compounds such **113**.[283] Compound **113** is completely insoluble in water and thus serves as a hydrophobic template around which the hydrophobic core of the polymer can assemble, causing the hydrophilic segments to orient outward and make the resulting particles water-soluble.[284] This approach has been further employed to image Hela cells as demonstrated by Ramírez Lázaro *et al*.[285]

Finally, while various naps derivatives have been reported as efficient photoinitiators in polymer chemistry,[286, 287] their use as PC in peptide chemistry is yet to be reported.

4.2 Aims

Certain naps, such as compound **113**, possess an AIE behaviour. This phenomenon often described as 'turn-off/turn-on', involves changes in fluorescence due to molecular aggregation. Aggregation restricts intramolecular motions, resulting in enhanced emission of the fluorophore.[288] The nap **113** is fluorescent in 100% THF, however, as the H_2O content increases, fluorescence is quenched ('turn-off') due to reduced solubility and the onset of aggregation. At 60% water content, aggregation and subsequent restriction of the bonds start to occurs among the nap **113** molecules, recovering the fluorescence ('turn-on').[283] This phenomenon is illustrated in **Figure 4.3**, reproduced here with permission from Henwood *et al*.[283]

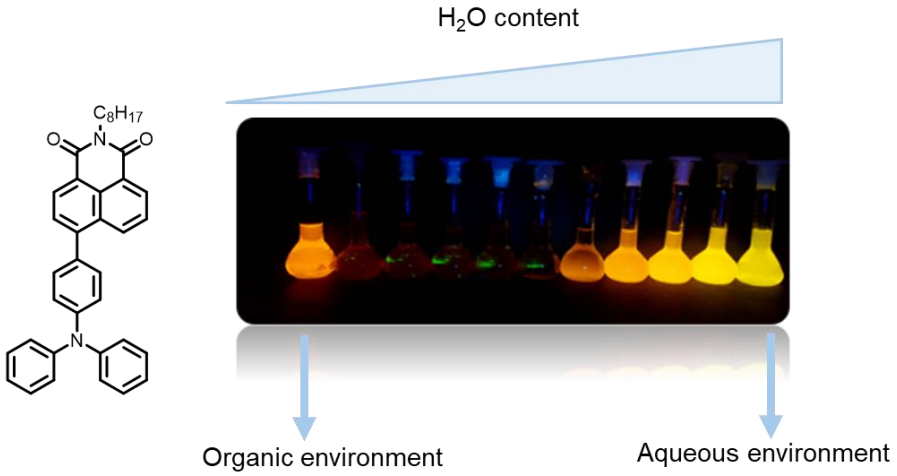

Figure 4.3: Turn-off/turn-on phenomenon by increasing the H_2O content. Picture obtained from ref.[283]

With these characteristics in mind, this project aimed to develop a novel methodology of nap-mediated TEC applicable in both organic and aqueous media, for the bioconjugation of organic molecules and peptides focused on drug discovery (**Figure 4.4**). Initially, optimisation studies were carried out in both solvent environments to identify suitable conditions for the thiol-ene reaction and towards development of a putative mechanistic understanding of nap-mediated TEC. Once optimised, a series of structurally diverse AIE naps[e] were employed to investigate the applicability of this method. This approach will enable the development of a new versatile strategy for nap-mediated TEC photoredox in organic-soluble systems. Furthermore, under aqueous conditions, the objective is to generate the previously described water-soluble particles, thereby facilitating intracellular internalisation of the conjugated drug obtained *via* TEC. Simultaneously, nap **113** will, in theory, serve as a PC mediating the thiol-ene reaction within the cellular environment (**Figure 4.4**). The internalisation can be confirmed by confocal cellular imaging.

[e] All naps used in this project were synthetised by Louisa Constance Sigurvinsson, Dr. Laura Ramírez Lázaro and Dr. Adam Henwood.

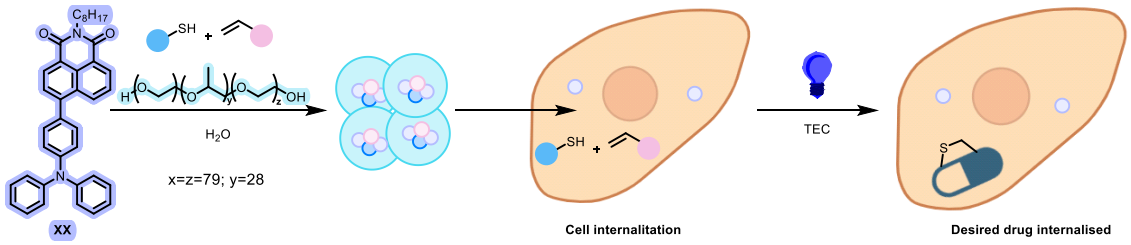

Figure 4.4: Encapsulation of thiols and alkenes along with nap **113** in water-soluble nanoparticles, which are subsequently internalised within the cellular environment. The cells are then irradiated with blue light to trigger the thiol-ene reaction, leading to the formation of the desired intracellular drug.

4.3 Results and Discussion

Nap **113**, reported by Henwood *et al*. was selected to be a representative example for this methodology.[283] Previous studies conducted by Henwood in Trinity Biomolecular Sciences Institute, demonstrated its UV-vis absorption and emission spectra in THF, with its absorption observed at ca. 300-400 nm and emission within the 550–700 nm range, indicating the requirement of blue or visible light for its excitation. Although UV light could also be suitable for this project, a milder irradiation source was chosen due to the focus on cellular applicability. In addition, the use of UV light in combination with electron transfer is limited by the presence of AA residues such as Tyr and Trp that also absorbs in the same wavelength range and which might lead to side-chain oxidation potential.[107] Given the higher photonic energy of blue light, a 2 Kessil LED PhotoReaction Light (KSPR160L-440) centred at 440 nm light source was employed in this project.

4.3.1 Optimisation in Organic Solvents

Previous investigations by the Scanlan group demonstrated a photocatalytic TEC reaction between allyl benzoate **114** and thioacetic acid **115** using a carbon/Bi_2O_3 nanocomposite as PC.[267] The authors reported the novel application of a catalyst that is simple to prepare and allows straightforward purification, affording excellent yields. The same optimised conditions were selected for the naps-mediated TEC reaction.

In an initial experiment allyl benzoate **114** (1.0 equiv.) and thioacetic acid **115** (4.0 equiv.) with nap **113** (0.05 equiv.) as the PC were combined in moderate polar solvent such as THF (**Figure 4.5**). The reaction was performed at rt for 1 h under blue light

irradiation. The desired thioester product **116** was purified by flash column chromatography and achieved in 76% isolated yield (*c.f.* **Figure S9.30**).

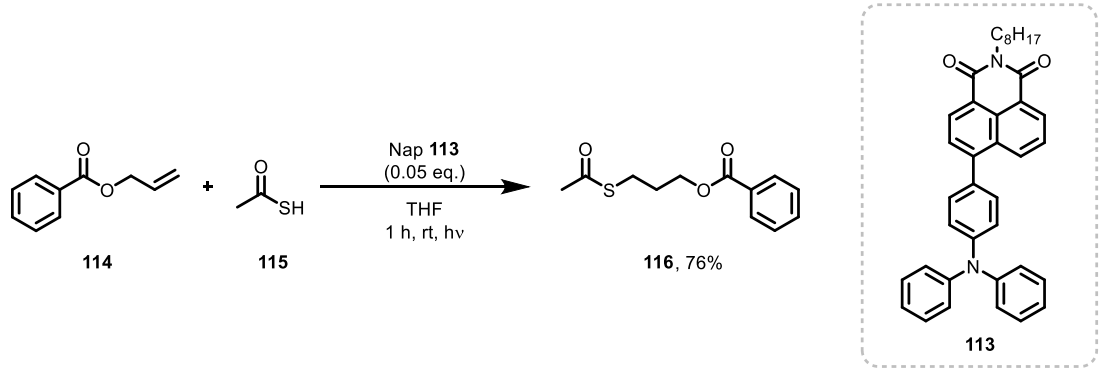

Figure 4.5: Synthesis of thioester **116** *via* nap-mediated TEC reaction.

The first hypothesis suggested that the nap indeed played a role as a catalyst of the reaction but further experiments also showed a second potential radical source which could come from peroxide decomposition arising from the THF. To address this, a full optimisation study was conducted in a moderately polar organic solvent such as CH_2Cl_2.The reaction was carried out following the conditions displayed in entries 1-10 (**Table 4.1**).

Table 4.1: Optimisation of TEC reaction between allyl benzoate **114** and thioacetic acid **115** under blue light irradiation in entries 1-10 conditions

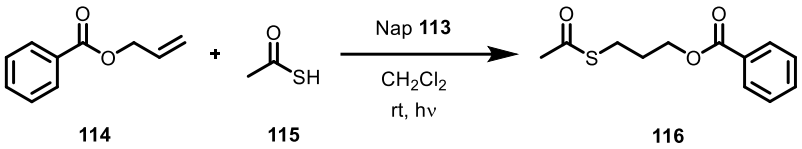

Entry	Time (min)	Nap 113	O_2	Light	Thioester conversion[a]
1	60	0.05 equiv.	Yes	Yes	86%
2	5	0.05 equiv.	Yes	Yes	N.R
3	30	0.05 equiv.	Yes	Yes	67%
4	60	--	Yes	Yes	4%
5	60	0.05 equiv.	--	Yes	61%
6	60	0.05 equiv.	Yes	--	N.R
7	60	--	--	Yes	N.R
8	60	--	Yes	--	N.R
9	60	0.05 equiv.	--	--	3%
10	60	--	--	--	N.R

All the reactions were carried out with allyl benzoate **114** in 1 equiv. and thioacetic acid **115** in 4 equiv. in CH_2Cl_2 at rt. [a] % yields are quoted as isolated yields. N.R = No reaction occurred.

The same conditions previously applied to THF as discussed above were employed, achieving an 86% isolated yield of the desired thioester product **116** (entry 1, **Table 4.1**). In an effort to develop faster reaction conditions, the reaction time was reduced, given that TEC is considered a click-type reaction. Reactions conducted for 5 and 30 minutes resulted in no product formation and a 67% yield of thioester **116**, respectively (entries 2 and 3, **Table 4.1**). Thus, 1 h was established as an optimal reaction time for completion of the photocatalytic cycle. The role of nap **113** as a PC in the TEC reaction was then investigated. The reaction was performed at rt under blue light irradiation in the absence of nap **113** (entry 4, **Table 4.1**). Only 4% of the desired thioester adduct was obtained, confirming the critical importance of the nap **113** as a PC. Previously, the Scanlan group reported O_2-mediated thiol-ene reaction.[289] The authors demonstrated that heating the reaction to 66 ºC in the presence of atmospheric oxygen (O_2) led to quantitative ^{1}H NMR conversion and >95% isolated yields. To assess the role of atmospheric O_2 in the current system, the reaction was conducted with 0.05 equiv. of PC for 1 h at rt under degassed conditions (entry 5, **Table 4.1**). A notable decrease in yield to 61% of the desired product was observed, confirming the important role of O_2 in the photocatalytic process. Furthermore, the same reaction was carried out with 0.05 equiv. of nap **113** under atmospheric O_2, but in the dark (entry 6, **Table 4.1**). No thioester product **116** was observed, confirming that the reaction proceeds *via* excitation of nap **113**. Additional experiments were performed to assess the individual roles of the three key parameters: nap **113**, atmospheric O_2, and light (entries 7, 8, and 9, **Table 4.1).** Almost no product formation was observed in the absence of any of these components. Finally, to confirm that the reaction proceeds *via* a radical pathway rather than a nucleophilic mechanism, as in the case of the thiol–Michael reaction, the reaction was repeated under degassed conditions, in the absence of nap **113** and light (entry 10, **Table 4.1**) where, as expected, no reaction was observed.

Following these optimisation studies, which confirmed the essential role of each variable, and following previous reported mechanisms for organic PC such as for the role of Eosin Y,[290, 291] a proposed mechanism for the nap-mediated TEC reaction is presented in **Figure 4.6.** The mechanism begins with nap **113** in its GS. Upon irradiation, nap **113** is promoted to its excited state (PC*), where it undergoes a single electron transfer (SET) *via* oxidative quenching, resulting the formation of the thiyl radical cation from the thiol. Subsequently, $PC^{-\cdot}$ is oxidised back to its ground state by atmospheric O_2, which

develops into a superoxide species. Further studies such as electron paramagnetic resonance (EPR) spectroscopy will be required to conclusively report a definitive mechanism.

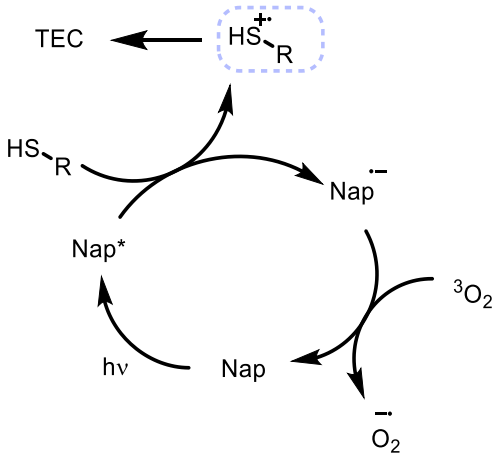

Figure 4.6: Suggested photoredox mechanism for nap-mediated TEC reaction.[292]

The ICT phenomenon occurs when electrons are transferred from an electron-rich region to an electron-deficient region within the same molecule.[283] This π cloud of electrons can be easily stabilised or destabilised by the dipole moment of a given solvent. Therefore, the ICT properties of a molecule will be affected based on the polarity nature of the solvent in question. (**Figure 4.7a**).[25,33] Herein, the previous optimised reaction between allyl benzoate **114** and thioacetic acid **115** was then repeated using different organic solvents to confirm nap **113** efficiency for thiol-ene reaction in a set of different polarity solvents. Thioacetic acid **115** and allyl benzoate **114** were dissolved in hexane, CH_2Cl_2 and EtOAc. Nap **113** was then added to the solution and the reaction was stirred for 1 h under blue light irradiation at 440 nm (**Figure 4.7b**). The polarity phenomena of the different solvents were observed when the reaction was irradiated under blue light. The reaction mixture was shown with yellow colour (closer to blue) than in the case of CH_2Cl_2 that presented a red coloured mixture (**Figure 4.7b**). This can be explained by the fact that, in more polar organic solvents, π–π* transitions exhibit a red shift as solvent polarity increases, resulting in a smaller transition energy 'gap'. In contrast, in less polar solvents, these transitions present blue-shifted, corresponding to a higher transition energy. The thioester product **116** was obtained in 80%, 86% and >95% isolated yields, respectively demonstrating the great efficiency of nap **113** in all the different organic solvent polarities.[283,285,293] Future work will focus on the photophysical studies of nap **113**

in the different solvents in order to address the difference within the yield achieved of the product.

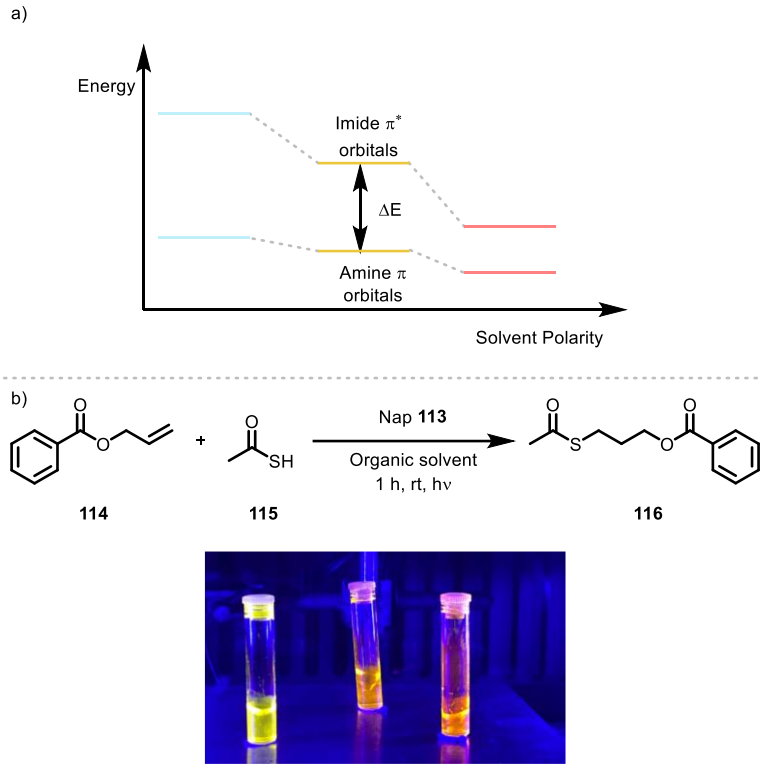

Figure 4.7: a) Influence of solvent polarity on the energy gap. b). TEC reaction of allyl benzoate **114** and thioacetic acid **115** in hexane (yellow), EtOAc (orange) and CH_2Cl_2 (red).

4.3.2 Scope of Naphthalimides

With the nap **113**-mediated TEC conditions optimised as discussed in the previous section, a series of different nap derivatives exhibiting AIE behaviour were investigated to demonstrate their efficiency and suitability in thiol–ene chemistry.

Naps **113**, **117, 118, 119** were used as PC for the photoredox catalysis TEC reaction.[f] Allyl benzoate **114 (**1.0 equiv.) and thioacetic acid **115 (**and 4.0 equiv.) were used with naps **113**, **117-119** (0.05 equiv.) at rt for 1 h under blue light irradiation at 440 nm. $CDCl_3$ was used in this experiment to quantify product conversion *via* ^{1}H NMR spectroscopy using 1,3,5-trimetoxybenzene as an internal standard (**Figure 4.8**).

[f] Synthesis of naps **113**, **117**, **118** and **119** used in this project were carried out by Louisa Constance Sigurvinsson, Dr. Laura Ramírez Lázaro and Dr. Adam Henwood.

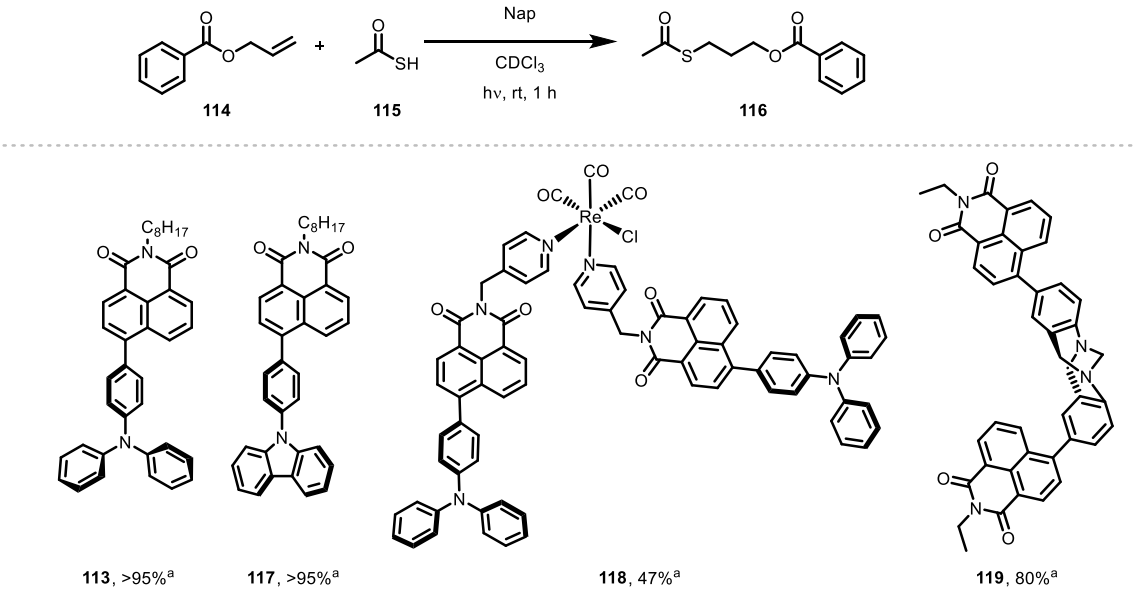

Figure 4.8: TEC reaction performed with nap **113**, **117**, **118** and **119**. [a] Yields were calculated by ^{1}H NMR spectroscopy using 1,3,5-trimetoxybenzene as an internal standard (100 mol%).[b]

Excellent yields were obtained for naps **113** and **117** (**Figure 4.8**) with >95% ^{1}H NMR spectroscopy conversion of the desired thioester product **116**. In the case of Re-nap **118,** thioester product **116** was obtained in 47%, as determined by ^{1}H NMR spectroscopy conversion (**Figure 4.8**). As a final example Tröger's base nap **119** was utilised as photoinitiator for the reaction and thioester product **116** was obtained in 80% ^{1}H NMR conversion (**Figure 4.8**). Further photophysical studies will be carried out in order to address the distinct reaction efficiencies for naps **113**, **117**, **118** and **119** as PC of TEC. Nevertheless, these naps demonstrated efficient activity as PCs for nap-mediated TEC, comparable to standard HAT photoinitiators, culminating in the establishment of a promising novel PC for the photoredox cycle of nap-mediated thiol-ene reaction in organic solvents.

4.3.3 Optimisation in Aqueous Solvents

Water-soluble naps salts have been previously used in biological system as PC for the photooxidative cleavage of proteins and DNA.[294,295] Naps have also been reported as heterogenous PC when immobilised on mesoporous silicas for applications such as textile dye degradation.[266] However, to the best of our knowledge, there are no reports of naps being employed as heterogeneous PC for peptide bioconjugation in the context of drug discovery.

Following the successful results in organic solvents and with the aim of enabling nap-mediated TEC reactions at the cellular scale, optimisation under aqueous conditions was undertaken. Up to this point, all reactions had been performed under homogeneous conditions. However, nap **113** is not a water-soluble molecule, although it remains fluorescent, as previously demonstrated. Therefore, a novel methodology for nap-mediated TEC was developed under heterogeneous conditions.

Building upon the conditions reported by Conway *et al.* and the promising results obtained in **Chapter 2** of this thesis,[121, 196] GSH **48** and allyl alcohol **49** were selected to carry out the heterogeneous nap-mediated TEC reaction (**Table 4.2**).

Table 4.2: Thiol-ene reaction in aqueous conditions with GSH **48** and allyl alcohol **49** with nap **113** as a PC in the reaction.

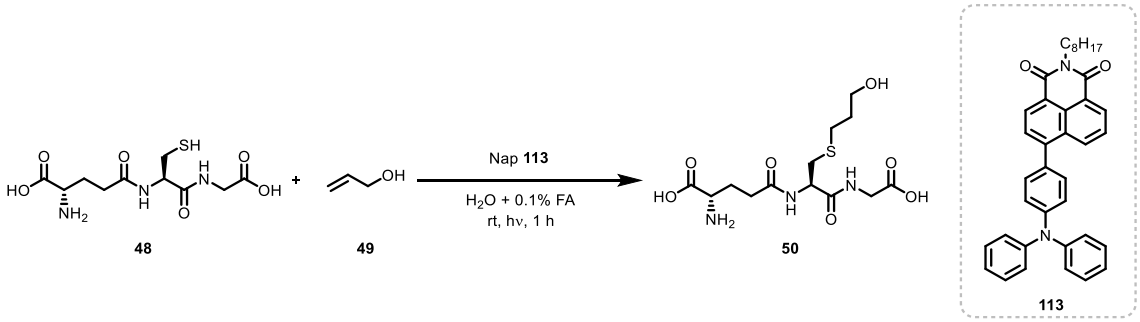

Entry	Thiol:Alkene equiv.	Nap 113 (equiv.)	Time (h)	Thioester conversion
1	1:2.5	1	1	NR
2	2.5:1	0.5	2	75%[a]
3	2.5:1	0.05	1	>95%[b]

[a] % yields are quoted as ^{1}H NMR conversion. [b] % yields are quoted as RP-HPLC conversion. NR = No reaction occurred.

Initially, identical conditions as reported in **Chapter 2** were applied. GSH **48** (1.0 equiv.), allyl alcohol **49** (2.5 equiv.), and nap **113** (1.0 equiv.) were added into a solution of H_2O + 0.1% FA. The reaction was conducted for 1 h at rt under blue light irradiation at 440 nm (entry 1, **Table 4.2**). The reaction was filtered to remove nap **113** from the crude mixture which was then analysed by RP-HPLC and ^{1}H NMR spectroscopy. Unfortunately, no desired product formation of compound **50** was observed under these conditions.

Since TEC chemistry is initiated through the formation of thiyl radicals, an excess of thiol was employed to help promote the initiation of the reaction. Using an excess of GSH **48** (2.5 equiv.), allyl alcohol **49** (1.0 equiv.) and nap **113 (**0.5 equiv.) were added to the reaction mixture and the reaction was stirred for 2 h at rt under blue light irradiation (entry 2, **Table 4.2**). In the crude ^{1}H NMR spectrum (400 MHz, D_2O, **Figure 4.9**), residual alkene peaks from 6.07-5.06 ppm can be observed, suggesting incomplete consumption of the starting materials. Additionally, peaks in the region of 3.36–3.26 ppm correspond to the formation of the disulfide dimer of GSH **48**, likely due to the excess of GSH **48** used in the reaction and the long reaction time (**Figure 4.9**). The presence of the disulfide was further confirmed by RP-HPLC and MS. Nevertheless, the desired product **50** was observed in 75% conversion determined by ^{1}H NMR, confirming the successful heterogeneous thiol–ene reaction mediated by nap **113**.

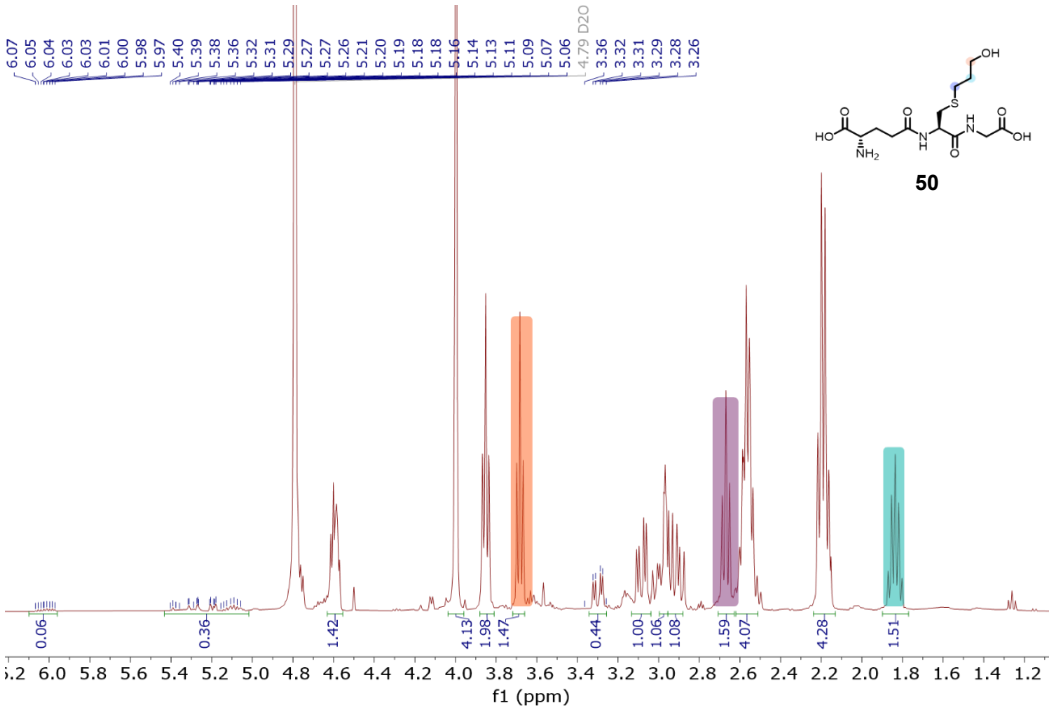

Figure 4.9: ^{1}H NMR spectrum (400 MHz, D_2O) of the crude reaction mixture with GSH **48** and allyl alcohol **49** after 2 h reaction under aqueous conditions**.**

Given that the excess of thiol promotes successful product formation, along with a reduced amount of nap equivalents, a final optimisation attempt was carried out using GSH **48** (2.5 equiv.) and allyl alcohol **49** (1 equiv.), with nap **113** serving as the PC in only 0.05 equiv. The reaction was irradiated with blue light for 1 h (entry 3, **Table 4.2**). The crude reaction mixture was then filtered and analysed by analytical RP-HPLC, ^{1}H NMR, and mass spectrometry. To our delight, a >95% RP-HPLC conversion to product

50 was observed under these conditions, (**Figure 4.10b**), strongly highlighting the synthetic potential for heterogeneous catalysed thiol–ene reactions under aqueous conditions.

Future studies will focus on encapsulating the target Cys-based peptide with an alkene probe to perform the reaction mediated by nap **113** in a cellular environment, as outlined in **Figure 4.4**.

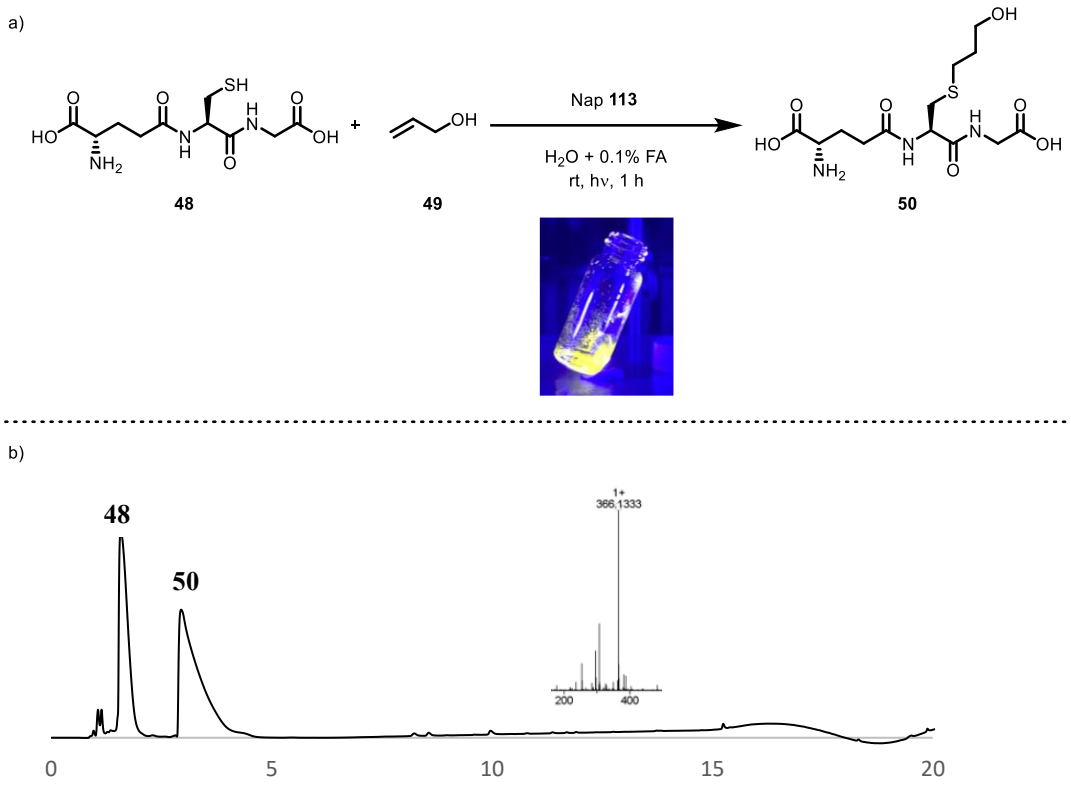

Figure 4.10: a) Scheme of Thiol-ene reaction in aqueous conditions with GSH **48** and allyl alcohol **49** with nap **113** as a PC in the reaction. b) RP-HPLC trace (220 nm, 2-15% MeCN/H_2O + 0.1% TFA) of the crude mixture after filtration of the nap **113**.

4.4 Conclusion and Future Work

This chapter presents the initial development of a novel approach towards nap-mediated thiol–ene reaction under both homogeneous and heterogeneous conditions. Initially, the reaction was successfully optimised in organic solvents using simple thiols, such as thioacetic acid **115**, and aromatic alkenes, such as allyl benzoate **114**, to gain a comprehensive understanding of the possible role of nap **113** acting as a PC under homogeneous conditions. A putative catalytic mechanism is proposed based on the

obtained results; however, more detailed studies are required to elucidate individual steps within the catalytic cycle. Subsequently, a study involving organic solvents with higher polarity was performed to confirm the ICT phenomenon of nap **113**. In addition, the scope of AIE naps was explored, including distinct structural naps such as **117**, **118** and **119** to investigate the different suitability to TEC reaction.

Once the reaction was optimised under homogeneous organic conditions, a novel heterogeneous thiol–ene reaction was developed with nap **113** to enable the ligation process under aqueous conditions. The reaction, using GSH **48** in 2.5 equiv. and allyl alcohol **50** in 1 equiv. with nap **113** in 0.05 equiv. was carried out in H_2O containing 0.1% FA. The thioether product **50** was obtained with >95% conversion as determined by RP-HPLC.

As hypothesised, nap **113** exhibited the most suitable behaviour for this application, enabling photocatalysis of the TEC reaction in both organic and aqueous media. Future studies will focus on optimising the nap-mediated TEC reaction within a cellular environment. The capacity of the polymer P188 to form water-soluble nanoparticles encapsulating nap **113**, combined with its ability to catalyse the TEC reaction, allows for the co-encapsulation of thiol-based targets and alkene-based probe biomolecules, thereby facilitating the cellular internalisation of these biomolecules for advanced biological applications as outlined in **Figure 4.4**.

Chapter 5

Covalent site-selective screening platform to discover protein-protein interactions inhibitors

5.1 Introduction

Protein-protein interaction (PPI) networks play essential roles in the regulation of numerous biological processes, including cell proliferation, signalling, and pathogen-host interactions.[296] Recent structural and biochemical studies have demonstrated that key immune checkpoint pathways, such as PD-1/PD-L1, are mediated by high-affinity PPIs that facilitate immune evasion in cancer and chronic infections.[297] Furthermore, emerging pathogens, such as SARS-CoV-2, are known to exploit PPIs; in particular, they utilise the interaction between the viral spike protein and host ACE2 receptor to enable viral entry and establish infection.[10] Efficient disruption of these interactions requires drug molecules that not only bind tightly to their target proteins, but also engage selectively with the specific interfacial contact sites. Since peptides intrinsically signal molecules for many physiological functions, research efforts have sought to exploit the inherent biocompatibility of AA and peptides, combined with the vast customisability of their individual sequencings, for therapeutic interventions that closely mimic natural pathways.[298,7] Major advancements in synthetic methodologies have enabled the production of peptide drugs exhibiting high specificities and low immunogenicities *via* efficient, low-cost manufacturing methods.[4] However, despite their promising attributes, the enthusiasm for peptide therapeutics has been tempered by certain limitations such as their *in vivo* stability and low cell permeability.[299]

Cyclic peptides are a well-known modality to target challenging PPI surfaces due to their ability to engage the relatively flat protein binding surfaces.[300] In addition, cyclic peptide possess advantages such as increased enzymatic stabilities and improved target selectivity, affinity and cell permeability.[301] The growing interest in the therapeutic application of peptides has driven the development of advanced screening platforms, such as the Random non-standard Peptides Integrated Discovery (RaPID) system, as previously mention in **Chapter 1.1.2**. However, all current screening methods lack the precision to evaluate direct binding to specific functional 'hot-spots'.

The RaPID system is a type of mRNA display that consists of a powerful platform to discover new protein inhibitors (**Figure 5.1)**.[97] This system is able to screen a library of more than 10^{12} macrocyclic peptides binding to a desired protein.

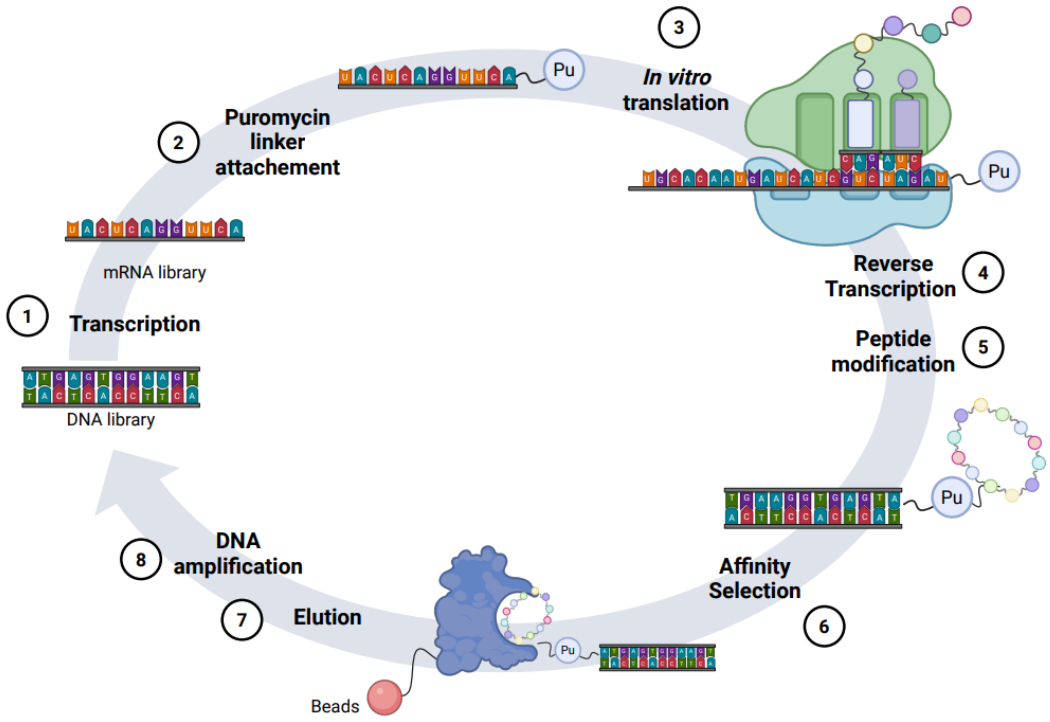

Figure 5.1: Conventional RaPID system workflow. Briefly, DNA is transcribed to RNA (1), connected with puromycin by ligation (2), and then translated in vitro (3). The resulting mRNA-peptide conjugates are copied to cDNA (4) and optionally chemically modified (5). The mature library is then panned for affinity to a protein target (6) and the cDNA encoding binders is eluted (7) for amplification by PCR (8) to generate a new DNA library enriched in binders.

The mRNA display procedure is carried out entirely *in vitro*, which makes it possible to select under a wide range of interesting conditions that would be incompatible with traditional *in vivo* selection methods.[302] In the RaPID system, a DNA library is first transcribed to mRNA. A linker containing puromycin (Pu) is attached to the 3' end of the mRNA *via* a molecular spacer. Pu is an antibiotic that mimics the 3' end of an aminoacylated tRNA and is used as a bridge between the RNA and the peptide. The resulting mRNA-Pu template is subjected to an *in vitro* translation. The translated peptide (phenotype) is therefore covalently linked to its own genetic information in the form of mRNA (genotype). After reverse transcription of the genotype and peptide modification, the phenotype-Pu-genotype hybrid is then exposed to the target protein for the affinity selection. Its purpose is to enable recovery of the genotype of binding peptides through affinity-based enrichment against the desired immobilised protein. Elution washes followed by DNA amplification are conducted in order to generate a new library for the next round with peptides that presents high affinity for the target protein.[303]

The RaPID system can incorporate non-canonical building blocks, either replacing canonical AA with a close structural homologue, or for more exotic AA by

attaching them to synthetic tRNAs using catalytic RNA called 'flexizymes' (**Figure 5.2**).[304] The flexizymes mechanism consists of unique molecular recognition of aromatic motifs which can be present in the sidechain or the activating group of the non-canonical AA.[305] The flexizyme-catalysed acylation then occur between the activated non-canonical AA and the hydroxyl group of the completely conserved 3' CAA sequence of any tRNA.[306, 307] Incorporation of non-canonical AA's enables the generation of modified peptides such as cyclic peptides,[308] or those displaying backbone modification.[309] These modified peptides allow the library to be progressively enriched with high-affinity binders before sequencing.[310]

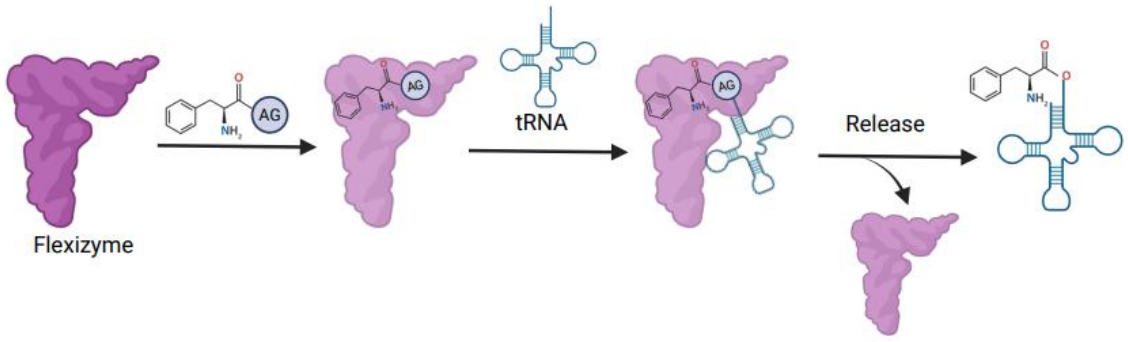

Figure 5.2: Mechanism of flexizyme-mediated tRNA acylation.[311] AG = Activating Group.

To date, the RaPID system enables screening of the largest known library size for peptide discovery, comprising over 10^{12} cyclic peptides. Numerous successful examples of RaPID-mediated identification of bioactive cyclic peptides have been reported in the literature,[299,308] demonstrating its effectiveness for the discovery of potent peptide ligands. However, RaPID possesses a major limitation as it gives no information regarding where a peptide hit binds. In order to target specific PPIs, the peptide needs to bind at the functional interface otherwise the desired inhibition will not occur.

5.2 Aims

The aim of this project is to develop a novel strategy that integrates the powerful RaPID system with proximity-driven, site-selective covalent capture by Thiol-ene Click (TEC) mediated chemistry. By introducing complementary orthogonal chemical handles on the target protein and within the peptide library (Cys and an alkene, respectively), this covalent cross-link will be dependent on strong non-covalent binding, specifically in the target site. As a result, only peptides that bind at the protein functional interface will be

enriched (**Figure 5.3**). The use of peptide discovery methods that rely on a covalent warhead for binding has been previously reported in literature.[312] This is a viable strategy in drug discovery but comes with risks such as non-specific reactivity and problems with warhead stability. In this project, the hits resulting from the covalent selection strategy will be re-synthesized without the covalent warhead, and non-covalent binding to the original (Cys-free) protein will be confirmed. Once optimised, this will be the first method capable of selective targeting of PPI regions. This method will be broadly applicable and will enable site-specific peptide discovery with high precision.

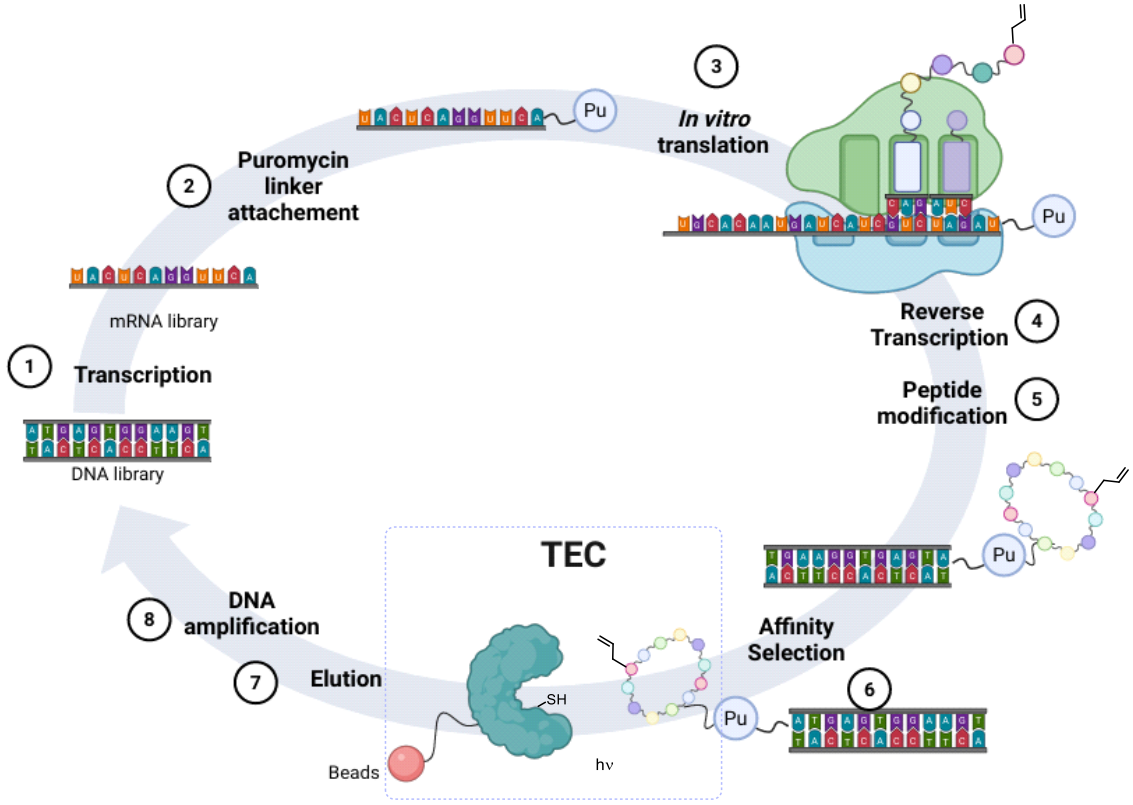

Figure 5.3: TEC-mediated RaPID selection workflow. As compared to the standard workflow in Figure 5.1, the affinity selection step (6) involves a photoinitiated thiol-ene click reaction between the Cys in the target protein's binding interface and the alkene in any library members that bind in close proximity (boxed).

5.3 Results and discussion

This methodology was first investigated using the well-established target protein, human nicotinamide *N*-methyl transferase (hNNMT), which already contains a Cys in its active site. A broad range of peptide inhibitors have previously been reported for NNMT protein, with allosteric and orthosteric binding.[299,313] This will allow rapid proof of concept before moving to a more biologically relevant target.

5.3.1 Preliminary studies

5.3.1.1 Compatibility test

To begin this project, a compatibility test between thiol-ene reaction conditions and the RaPID system was carried out. In the RaPID selection cycle, following the *in vitro* translation, reverse transcription is conducted in order to add a cDNA counterpart to the mRNA strand. This stabilised complex can then be chemically altered before enrichment through binding to an immobilized target protein.[310] In order to apply the TEC reaction to the RaPID selection, it was first necessary to confirm the stability of the mRNA/cDNA complex under UV light irradiation and in the presence of radical species. Yoshisada *et al.*, reported the mRNA/cDNA complex stability studies under a broad range of fundamental chemical conditions.[310] Based on this work, a mRNA/cDNA complex was synthesised by reverse transcription of a random mRNA library with an encoding binding site for the ribosome, a peptide encoding region with a start codon, a random region (NNK_{15}), a Cys codon, and a flexible 'GSGSGS' peptide spacer before a stop. A fluorescently (FAM) labelled reverse transcription primer was used to facilitate the detection of product after conducting the experiment. The reverse transcription mixture was then incubated for 42 ºC for 1 h. Phenol-chloroform-isopropanol (PCI) extraction was conducted, followed by EtOH precipitation. This complex is applicable since in mRNA display, modification reactions are performed after the purification of the reverse transcription product.

Once synthesised, the mRNA/cDNA complex was dissolved in ultrapure (MQ) H_2O to a concentration of 0.5 µM. Samples were exposed to UV-light (254/365 nm) for 5, 10, 15, 30 min at rt (**Figure 5.4**). To further assess stability under radical conditions, the complex (0.5 µM) was incubated with Irgacure 2959 **16 (**50 µM) and irradiated with UV-light for 30 min at rt. As a reference for the complex size within the gel, an additional sample of the complex (0.5 µM) was treated with 1 M NaOH at 37 ºC for 30 min, yielding pure cDNA. The resulted products were visualised by 8% urea-SDS-PAGE for qualitative analysis.

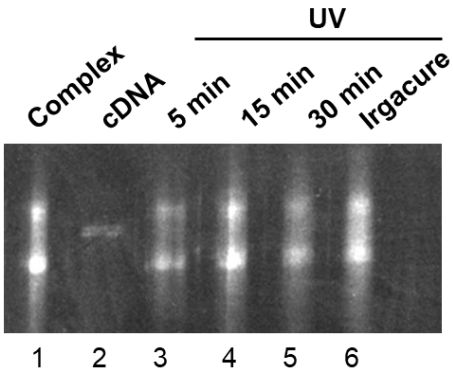

Figure 5.4: 8% Urea-SDS-PAGE of mRNA/cDNA complex samples alone (lane 1), in the presence of NaOH (line 2), under UV irradiation for 5, 15, 30 min (lanes 3, 4, 5, respectively) and 30 min in the presence of Irgacure 2959 (lane 6).

In the urea-SDS-PAGE it was confirmed that stability after 30 min UV-irradiation (lanes 3, 4 and 5) and tolerance to the radical initiator Irgacure 2959 (lane 6) was achieved. The mRNA/cDNA complex and cDNA (lane 1 and 2) were sampled as a control for the urea-PAGE. The mRNA/cDNA complex exhibited full compatibility under TEC conditions, representing the first step towards establishing the RaPID–TEC platform.

5.3.1.2 Affinity measurement of peptide

Hayashi *et al*. reported a variety of novel NNMT inhibitors based on peptide **120** (**Figure 5.5a**) which demonstrated potent inhibitory activity (IC_{50}) against both human and mouse NNMT.[313] Based on this, peptide **121** was suggested as an analogue of peptide **120** using conventional SPPS AA owing to the cost and synthetic challenges associated with non-canonical AA for this peptide. Furthermore, according to a crystal structure of the desired protein, the modified Tyr residue of the peptide **120** lies in close proximity to a Cys residue in the NNMT binding pocket (**Figure 5.5b**).[g] To enable the thiol–ene reaction, the non-canonical Tyr was replaced with allyl glycine (Alg) as the closest proximity residue of peptide **121** to the Cys residue located in the active site of the protein. The N-terminal residue 1 was also changed to tyrosine and residue 6 to phenylalanine, to facilitate ease of later *in vitro* translation using building blocks available on-hand.

[g] Crystal structure analysis was made by Dr. Seino A.K. Jongkees.

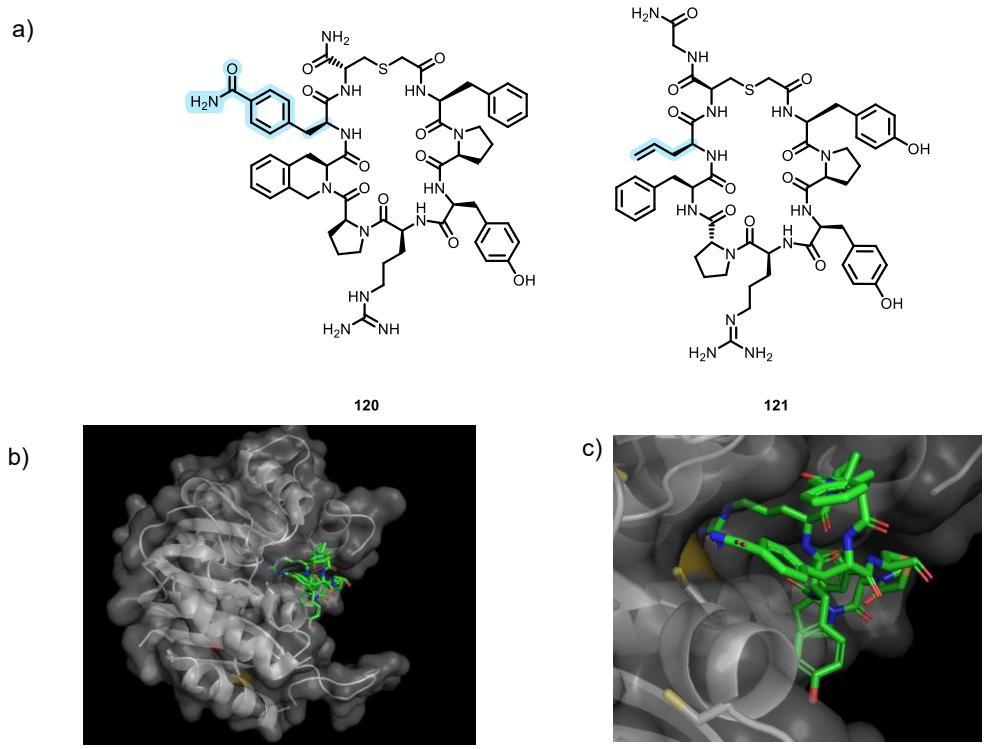

Figure 5.5: a) Chemical structures of peptides 120 and 121. b) Crystal structure of hNNMT (grey) in complex with peptide 120 as an inhibitor (green). (c) Zoom-in view highlighting the interaction between the modified Tyr residue from the peptide 120 and the Cys residue of NNMT (shown in yellow).

Fluorescence polarisation (FP) is a technique that relies on the principle that a fluorescently labelled molecule, when excited with polarised light, emits light whose polarisation depends on how fast the molecule rotates. Small molecules rotate quickly and give low polarisation signals, whereas larger complexes rotate more slowly and give higher signals (**Figure 5.6**). This property enables the detection of interactions between a small, labelled ligand (or peptide) with a larger protein, forming the basis for both direct and competitive binding assays. In this project, peptide **123** was chemically modified through addition of a fluorophore in order to be able to study its interaction with the NNMT protein.

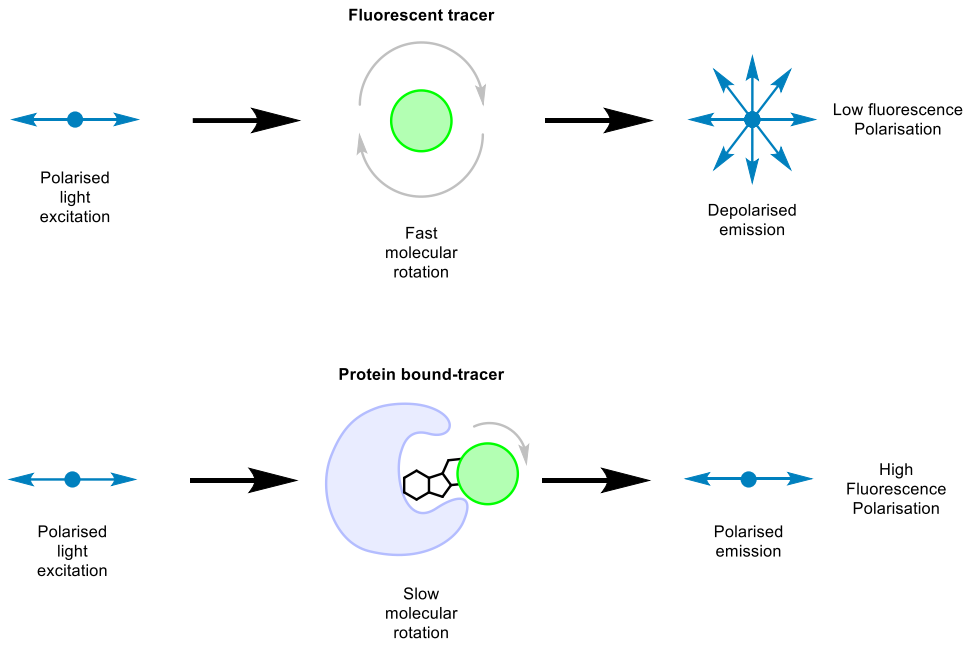

Figure 5.6: Mechanism of FP method.

Inhibitor peptide ClAc-Tyr-Pro-Tyr-Arg-Pro-Phe-Gly-Cys-Gly-Peg_4-azidohomoalanine (Aha)-Gly was synthesised on a Rink amide resin, using a SPPS synthesiser. Fmoc deprotection was carried out with 20% (v/v) piperidine in DMF (2 × 10 min) (**Figure 5.7**). AA coupling was performed using a solution of Fmoc-AA-OH (3 equiv.), DIC (8 equiv.), and Oxyma (4 equiv.) in DMF for 45 min, to ensure efficient and complete coupling to the resin. Following chain assembly, the peptide was deprotected and cleaved from the resin with a cleavage cocktail consisting of TFA:TIPS:H_2O:DTT (90:2.5:2.5:5) for 2 h, furnishing the linear peptide. The crude product was >95% pure by analytical RP-HPLC, which was sufficient for subsequent steps. For the spontaneous ClAc–SH cyclisation, the crude peptide was dissolved in DMSO (2 mL) in the presence of DIPEA (10 µL) to provide basic conditions. After 30 min stirring, the cyclised peptide **122** was obtained with >95% conversion by RP-HPLC. The crude product was then purified by PREP RP-HPLC. The purified peptide was redissolved in DMSO and reacted with DBCO-FAM **123** to achieve the 'click' reaction. After 30 min, the fluorescent peptide **124** was obtained with >95% conversion by RP-LCMS.

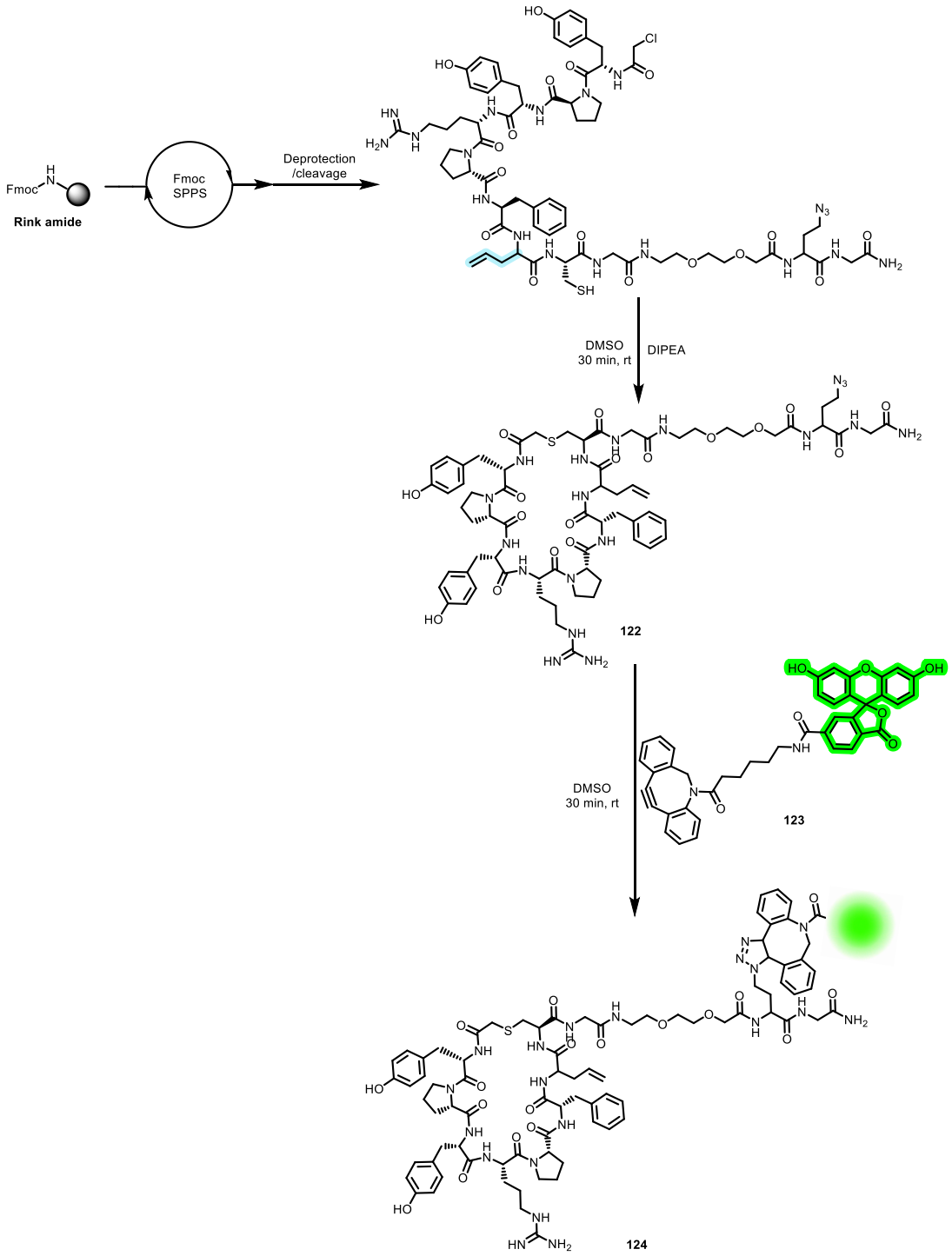

Figure 5.7: Synthesis of fluorescent peptide **124**.

The non-covalent interaction between fluorescent peptide **124** and NNMT protein was measured by FP. Fluorescent peptide **124** showed an affinity of 510 nM for the NNMT protein (**Figure 5.8**).[h] While this indicates moderate affinity, it is not sufficiently strong for stable complex formation, suggesting that covalent linkage could enhance binding stability and overall interaction strength. This binding affinity is, however, strong

[h] FP assay was carried out by Antonius J. P. Hopstaken.

enough for recovery in an mRNA display experiment, making this variant peptide a suitable tool for reaction development.

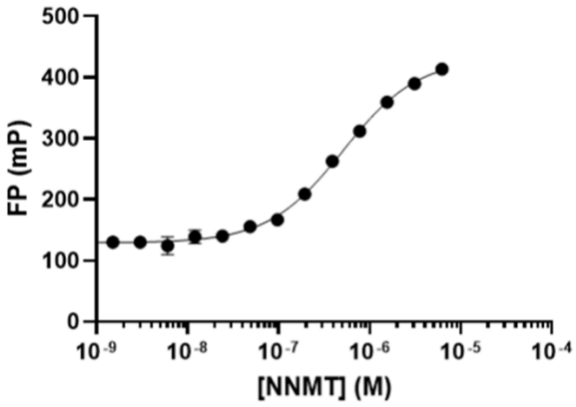

		95% CI
Hillslope	1.055	0.9609 to 1.158
Kd (M)	5.108E-07	4.535e-007 to 5.845e-007

Figure 5.8: Fluorescence polarization measurements from 1:1 serial dilution of NNMT protein with 10 nM FAM labelled peptide **123**. Error bars show ± standard deviation of three technical repeats.

5.3.2 Thiol-Ene Optimisation

Once the compatibility between TEC reaction and a RaPID library was confirmed, TEC reaction was optimised in order to achieve the best conditions for RaPID display. In recent years, targeted covalent inhibitors (TCIs) have attracted considerable attention owing to their outstanding pharmacological properties.[315] Compared with non-covalent inhibitors, TCIs offer notable advantages, including enhanced potency, improved selectivity, and extended duration of action.[316] Commonly, Cys residues serve as the primary targets.[317]

As previously discussed in **Chapter 1**, Campaniço *et al*. demonstrated the ability to performed radical thiol-ene activation of DUB proteins with Ub-alkene probes through the use of Irgacure 2959 **16** as photoinitiator.[167] The authors optimised incubation time between protein and probe, reaction time and photoinitiator concentration. Based on these reported findings, the TEC reaction was carried out between hNNMT target, which possesses a Cys residue on its active site and fluorescent cyclic peptide **123**, with Irgacure 2959 **16** as a water-soluble photoinitiator to initiate the reaction (**Figure 5.9**). The fluorescent property from the peptide allowed us to follow the reaction between the target protein and the cyclic peptide.

hNNMT protein (1.8 μM) was incubated with the fluorescent peptide **124** at different concentrations (70, 100 and 150 μM) on ice for 20 min. We expect this

incubation step played a crucial role in facilitating the reaction, as it positioned the alkene moiety of peptide **124** in close proximity to the active-site Cys residue of NNMT. The TEC reaction was subsequently carried out in the presence of Irgacure 2959 **16** (50 µM) for 2 min at rt under UV-light irradiation (254/365 nm) in tris HCl buffer at pH 7.4. Results were analyzed by SDS-PAGE and visualized by fluorescence (A and C, **Figure 5.9**) and silver staining (B and D, **Figure 5.9**).

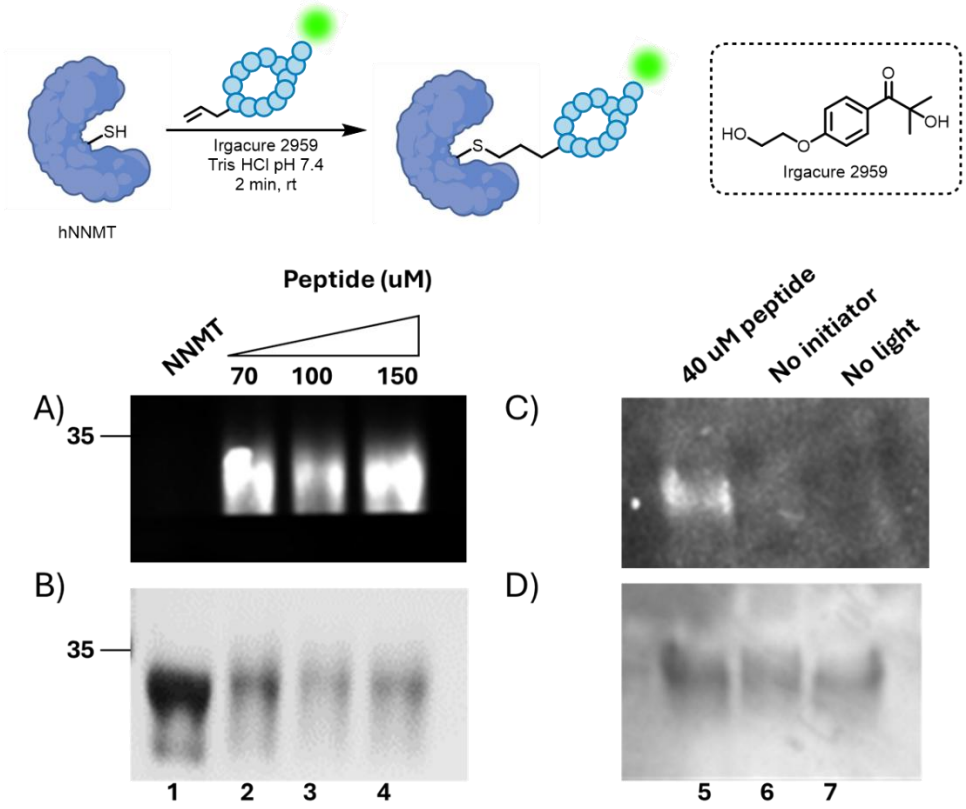

Figure 5.9: Thiol-ene reaction between human NNMT (hNNMT) and cyclised peptide **124** in the presence of a water-soluble photoinitiator. 10% SDS-PAGEs visualized by fluorescence (A and C) and silver staining (B and D).

Successful hNNMT labelling was confirmed by comparison of fluorescence and silver staining. hNNMT alone was loaded as a control (lane 1). TEC reaction was performed in 70, 100 and 150 µM peptide concentration (lane 3, 4 and 5) with Irgacure 2959 as the photoinitiator. Bands were observed in both fluorescent and silver stain visualisation, suggesting successful conjugation between the protein and the probe. Interestingly, slightly higher molecular-weight bands were observed upon coupling (lanes 3, 4, and 5), consistent with the increased mass of the labelled protein. A second attempt was performed with 40 µM of peptide **124** (lane 5) where successful peptide labelling was also observed. In addition, negative controls lacking either the photoinitiator or UV-

light exposure (lane 6 and 7) were undertaken and sampled in a 10% SDS PAGE. The absence of labelling in the negative controls confirmed that the reaction proceeded *via* a radical mechanism.

In mRNA display, the reaction scale is typically in the nanogram range. The protein component can be supplied in excess, but the peptide is always the limiting reagent as it is generated through *in vitro* translation. For this reason, the TEC reaction was specifically adapted to accommodate these constraints. hNNMT at 0.5 μM was incubated with fluorescent peptide **123** at 1 μM for 20 min on ice. Then, Irgacure 2959 **16** was added, and the reaction mixture was irradiated with UV-light for 2, 5, 10 and 15 min (lane 2, 3, 4 and 5, **Figure 5.10**).

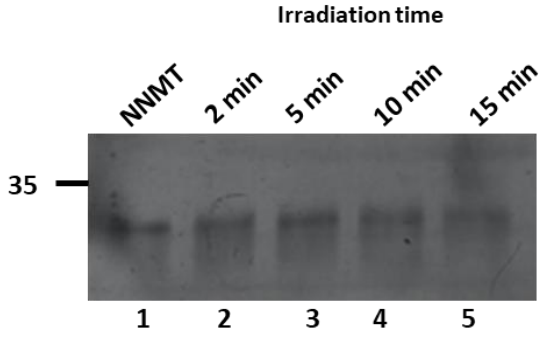

Figure 5.10: 10% SDS-PAGE visualised by silver stain.

No fluorescent visualisation of the SDS-PAGE was possible due to the lower concentrations of the peptide **124**. In this assay, no successful reaction was observed after 2 min (lane 2). On the other hand, a slight upward shift of the band can be appreciated in lane 3, 4 and 5 compared with lane 2, consistent with longer reaction times used. These observations suggest that the reaction may have occurred; however, the results were not conclusive. A different methodology was then utilised in order to better demonstrate the capacity of the TEC to occur under RaPID conditions.

The streptavidin–biotin interaction is considered one of the strongest non-covalent bonds in biochemistry and chemical biology.[318] The streptavidin-biotin bond has a dissociation constant of around 10^{-14} M.[319] If a biotinylated peptide is used, successful reaction between the protein and peptide will be captured by streptavidin beads. This method can then be visualised by comparing bead-bound material with its supernatant (SN) content using SDS-PAGE. The biotinylated peptide was synthesised through a three-step procedure (**Figure 5.11**). The peptide core was assembled *via* SPPS, as

previously described. The Aha residue was reduced with TCEP (5 equiv.) under aqueous conditions for 2 days, until all of the starting material was consumed.[320] The resulting crude peptide **125** was purified by PREP RP-HPLC. Using the exposed amine residue, conventional liquid-phase amide coupling was performed with biotin (1 equiv.), HCTU (1 equiv.), DIPEA (2 equiv.), and DMAP (0.5 equiv.). The reaction was allowed to proceed overnight, and the biotinylated peptide **126** was purified by PREP RP-HPLC and obtained in 5%.

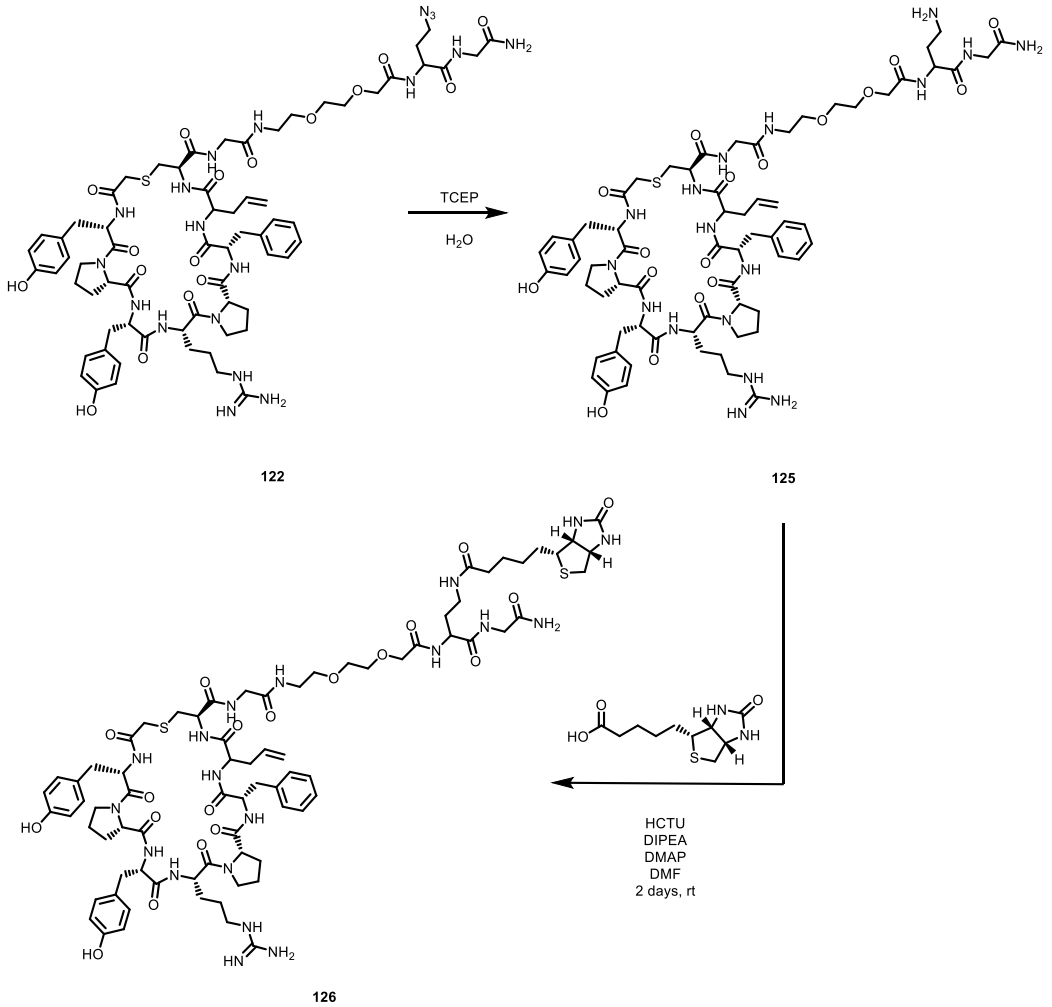

122 125 126

Figure 5.11: Three step-synthesis of biotinylated peptide **126**.

Thiol-ene reaction and streptavidin-beads binding assay was performed by first carrying out TEC reaction with hNNMT at different concentrations (1 and 1.5 μM,) in the presence of biotinylated peptide **126** (1 μM) and Irgacure 2959 **16** (7 μM) as the photoinitiator in tris HCl buffer at pH 7.4 (**Figure 5.12**). The reaction was carried out for 15 min at rt. Subsequently, pull down with 4 μL of streptavidin beads was added to the

reaction mixture in order to capture only the biotinylated protein. Bead binding was performed at 4 ºC with gentle rotation for 30 min. The samples were then analyzed by 10% SDS-PAGE and visualised by silver staining.

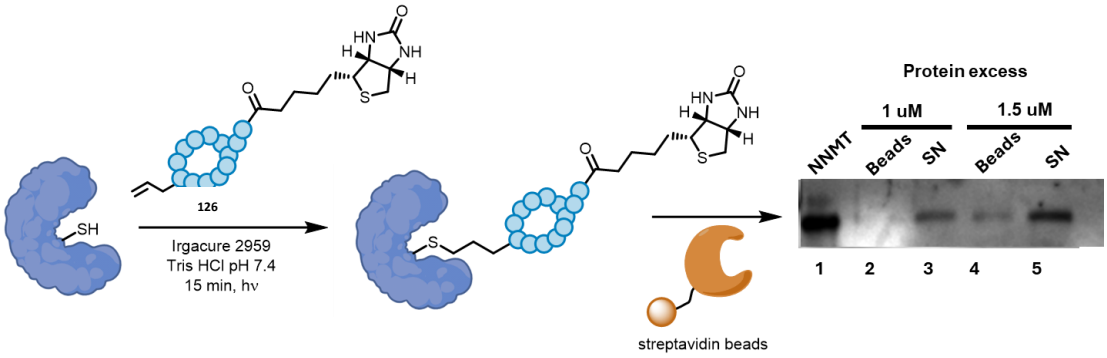

Figure 5.12: Thiol–ene bead-binding assay between the conjugated protein and streptavidin beads. Samples were analysed on a 10% SDS–PAGE gel, with both the beads and their corresponding supernatants (SN) loaded.

No reaction was observed at 1 µM protein, as the protein remained entirely in the SN (lanes 2 and 3). However, upon increasing the protein concentration to 1.5 µM (lanes 4 and 5), a distinct band corresponding to the conjugated protein was detected, suggesting that some TEC reaction had proceeded successfully under RaPID conditions. With all the parameters optimised and a clear notion of the TEC reaction working under RaPID conditions the final step of this project was to proceed with mRNA display selection.

5.3.3 Thiol-ene–Mediated mRNA Selection

The main aim of this project was that peptides identified through the covalent selection strategy will be resynthesised without the covalent warhead, allowing them to bind non-covalently to the native (Cys-free) protein. However, due to time constraints, only TEC-mediated selection was performed as proof-of-concept of this methodology.

To begin this study, chloroacetyl-L-Tyr-cyanomethyl ester (ClAc-L-Tyr-CME) was added to the flexible *in vitro* translation (FIT) system. The CME leaving group facilitated efficient charging onto an initiating model tRNA ($tRNA^{fMet}_{CAU}$) through flexizyme eFx-mediated acylation, as described earlier in this chapter.[312] After 1 h on ice, the amino acetylated tRNA was purified by EtOH precipitation. The ClAc moiety on the Tyr residue promoted spontaneous cyclisation after translation with a Cys programmed later in the sequence.[321] This ClAc–Cys cyclisation has been widely reported in the literature as a robust strategy to achieve macrocyclisation of target-binding sequences,

and has also been applied in the development of NNMT inhibitors.[299,313] Along with this, hNNMT protein was biotinylated by the addition of Biotin-PEG_4-NHS (5 equiv.) to allow the capture of the protein into streptavidin beads for the selection.

A selection experiment was carried out, with some modifications from the standard RaPID protocol to focus on covalent ligand discovery against a biotinylated protein target. Two mRNA-displayed peptide libraries were used in parallel, incorporating either L-homo allyl Gly (Hag) or L-Alg, as a methionine analogue, in order to identify the most suitable alkene residue for TEC-mediated RaPID selection. The selection began with a reprogrammed DNA library encoding peptide **121**, followed by a section encoding CGSGSGS linker was assembled by PCR and subsequently transcribed *in vitro* using T7 RNA polymerase at 37 ºC overnight. The resulting library was ligated by T4 RNA ligase at rt for 30 min to a short oligonucleotide terminating in Pu. EtOH precipitation was carried out with RNAse-free glycogen. *In vitro* translation using PURExpress system was then performed at 37 ºC for 30 min. Reverse transcription of the resulting complex was undertaken at 42 ºC for 1 h to achieve the final construct consisting of a peptide–Pu–mRNA/cDNA complex (with "–" and "/" denoting covalent linkage and nucleotide hybridisation, respectively). Spontaneous cyclisation occurred between the N-terminal ClAc group and the first translated Cys side chain, generating an mRNA-displayed equivalent of the cyclised peptide **121.** Sodium acetate buffer (pH 5) was added to peptide–Pu–mRNA/cDNA complex solution in reverse transcription buffer at pH 8.3 to give a final reaction mixture at pH 7. A 0.5 µL aliquot of the sample was diluted in 500 µL of Milli-Q H_2O and used as an input sample for later qPCR quantification. The biotinylated protein (1.15 µM) was then added to the mixture and incubated for 20 min on ice. Irgacure 2959 **16** (17 µM) was introduced as a photoinitiator, and the mixture was divided into 4 output tubes. Two outputs were irradiated with UV light (254/365 nm) for 15 min at rt. A denaturing solution of 4 M urea was included on two of the tubes (1 each with and without UV treatment) to remove all non-covalently bound peptides. Streptavidin bead pull-down was then performed, followed by three PBS-T washes to ensure complete removal of unbound ligands. Finally, the DNA associated with covalently cross-linked peptides was quantified by quantitative PCR as a measure for DNA recovery, and therefore peptide binding. Results are shown in **Figure 5.13**. As positive control, the non-denatured and non-irradiation output was considered, while non-irradiated but denatured output was considered a negative control.

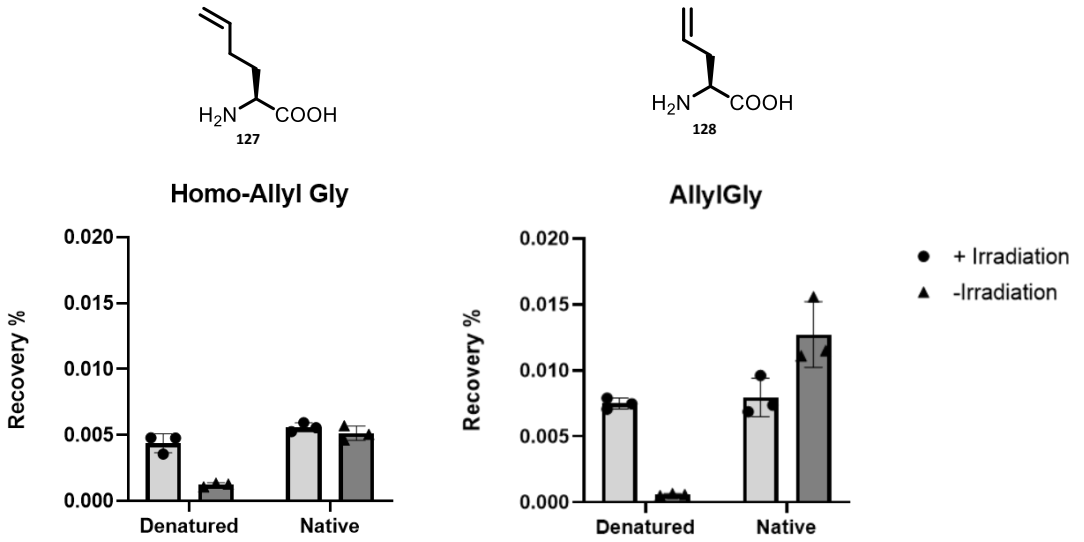

Figure 5.13: Bar charts showing the DNA recovery for both Hag **127** and Alg **128** containing libraries against hNNMT protein. Light grey bars with circle datapoints refer to the recovery upon UV-light irradiation outputs, dark grey bars with triangle datapoints refer to the recovery without UV-irradiation (254/365 nm) outputs. 4 M urea was used as denaturing conditions for this experiment. Native refers to the outputs that were not denatured.

As a first observation, the recovery was lower for the Hag **127** library, with a maximum of 0.005%, compared with 0.013% for the Alg **128** recovery. This difference may be attributed to the greater difficulty of Hag **127** incorporation during translation, possibly due to its longer side chain relative to Alg **128**. On the other hand, a clear difference was observed for both AAs when comparing irradiated *vs*. non-irradiated under denaturing conditions (4 M urea), confirming that successful covalent linkage was achieved *via* the TEC reaction. Furthermore, comparable recovery levels were obtained upon UV-light irradiation under both denatured and non-denatured conditions for both AA's, which is consistent with the advantages previous reported about covalent ligands.

These results provide promising evidence supporting the feasibility of the TEC-mediated RaPID platform. While the standard percentage recovery of mRNA display is estimated between 1-2% recovery, the low percentage recovery observed in this selection may be due to the harsh conditions applied prior to streptavidin pull-down, which may have impaired effective binding of the protein to the beads. Future studies should therefore focus on optimising the recovery conditions, for example by performing the bead pull-down prior to denaturation, as has been reported in the literature.[312]

5.4 Conclusions

In this work, a novel site-selective strategy for the discovery of peptide-based PPI inhibitors was developed. TEC-mediated RaPID selection was demonstrated to be a promising methodology. Although the approach is intended to be applicable to a wide range of targets, hNNMT was selected as a model protein due to the presence of an accessible Cys residue in its active site, which facilitated the feasibility studies.

Preliminary experiments established the physical compatibility of mRNA/cDNA complex with UV irradiation and radical conditions. In parallel, peptide **124**, whose design was based on previously reported NNMT inhibitors,[313] was evaluated and displayed a dissociation constant (K_d) of 510 nM in FP assays, indicating moderate binding affinity with potential for further enhancement through covalent linkage.

Once the compatibility between RaPID and TEC was confirmed, the thiol–ene reaction was optimised under conditions analogous to the standard RaPID protocol. A successful covalent conjugation between hNNMT and fluorophore-labelled peptide **124** was achieved in the presence of Irgacure 2959 under UV irradiation, with an optimal reaction time is <2 min. Furthermore, covalent capture of hNNMT was demonstrated using a biotinylated peptide in a 1:1.5 ratio, yielding satisfactory results as an initial proof-of-concept for the strategy.

Finally, TEC-mediated RaPID selections were performed using two mRNA-displayed peptide libraries incorporating Hag **127** and Alg **128**, respectively, to identify the most suitable alkene residue for covalent capture. Successful enrichment was observed in both cases, with superior recovery obtained using Alg **128**, likely due to its higher translation efficiency or improved alkene positioning compared to Hag **127**. Despite these promising outcomes, the overall recovery remained relatively low, most likely due to the application of denaturing conditions prior to bead binding. Future optimisation will focus on refining the pull-down step, in particular by performing streptavidin capture prior to denaturation, as suggested by previous reports.

Chapter 6

Conclusions

The work outlined in this thesis explores applications of thiyl radical-mediated 'click' reactions for peptide bioconjugation and stapling, with potential applications in drug discovery and development in both academia and in pharma.

As an initial study, discussed in **Chapter 2**, TEC-mediated, continuous-flow methodology was applied to peptide bioconjugation. This work demonstrated, for the first time, the compatibility of TEC reaction with continuous flow system in DES, bio-based solvents and fully aqueous media, offering scalable conditions which address the principles of green chemistry. Firstly, excellent results were obtained for GSH ligation under continuous flow as a-proof-of-concept study, in both DES and biobased solvents under continuous flow. This strategy was applied to a variety of alkenes under both batch and continuous flow with DPAP **15** as a photoinitiator in order to demonstrate the efficiency of the continuous-flow process for peptide bioconjugation and potential scale-up. Product yields under continuous flow were consistently higher than those achieved in batch reactions, ranging from quantitative to 50%. In aqueous conditions, the use of the water-soluble initiator Irgacure 2959 **16** resulted in lower improvements compared to DPAP reactions, due to its slower cleavage rate. Nevertheless, GSH conjugates were obtained in 94%-67% under continuous flow. This approach was successfully extended to the glycosylation of two bioactive peptides, CREKA **77** and CKYKAQ **79** under exclusively aqueous conditions. Finally, the conjugation of an anticancer RGD peptide **81** was achieved in 62% isolated yield under DES and aqueous continuous flow conditions. This chapter highlights the potential of TEC chemistry under continuous flow as a scalable and sustainable platform for peptide bioconjugation and diversification strategies relevant to drug discovery and development.

Chapter 3 presents the application of the related Thiol-yne Click (TYC) chemistry for the purpose of peptide disulfide rebridging. Also in this study, the use of $NaBH_4$ as an emerging peptide disulfide reducing agent was demonstrated. Disulfide reduction of peptide **89** by $NaBH_4$ was achieved within 2 min in nearly 90% product conversion which confirmed its viability as an alternative to other conventional peptide reducing agents. Despite the incompatibility of $NaBH_4$ with TYC chemistry, study of the disulfide rebridging *via* TYC chemistry was achieved using TCEP as the reducing agent. Expanding on previous reported literature and providing new mechanistic insights, a diverse scope of synthesised alkynes was tested for disulfide rebridging of peptide **89** in order to demonstrate the generality of this approach, achieving conversions of between

39% up to quantitative yields. This chapter culminated with the application of this strategy to the Somatostatin analogue, Octreotide **4**, which was conjugated with the fluorophore alkyne **100** to furnish the rebridged product in 62% conversion. Future studies will investigate the applications of the fluorophore octreotide peptide **111** in cellular bioimaging.

In **Chapter 4** naphthalimides were investigated as a novel class of photocatalyst for the TEC-mediated photoredox reaction. For this project, nap **113** was selected as a model naphthalimide based on previous studies from Henwood *et al*. The AIE properties of naphthalimides enabling fluorescence in both organic and aqueous media allowed us to investigate its photoredox mechanism. A detailed optimisation study was conducted based on a model reaction with thioacetic acid **114** and allyl benzoate **115** in organic solvents. A putative photoredox catalysis mechanism was proposed according with the results achieved in the optimisation studies involving the relevant role of atmospheric O_2 and the light irradiation. Further exploration of solvent polarity and a range of AIE-active naphthalimides confirmed the broader applicability of these photocatalysts to TEC reactions. Preliminary studies for the heterogenous naphthalimide-mediated thiol-ene reaction under aqueous conditions were also performed, offering novel insights into this emerging field. Nap **113** can be captured within water-soluble nanoparticles composed of P188 polymer; therefore, future work will focus on the applications of these, nap-containing, water-soluble particles as tenable photocatalysts for thiol-ene mediated reaction within the cellular environment.

Finally, **Chapter 5** describes a proof-of-concept approach for the development of site-selective peptide-based, protein–protein interaction (PPI) inhibitors *via* TEC chemistry. This novel strategy addresses a current limitation of mRNA screening platforms whereby the site of peptide binding is not controlled within the mRNA display platform. Initially, successful compatibility optimisation was carried out by exposure of the mRNA/cDNA complex to TEC conditions, resulting in successful covalent binding of the alkene-modified peptide **124** to the NNMT protein. Following optimisation, TEC reaction was optimised under RaPID selection parameters to confirm the compatibility of both methods. Once compatibility study was confirmed, a TEC-mediated RaPID selection was undertaken as a proof-of-concept for this strategy. Promising preliminary results demonstrated the basis for this novel site-selective strategy to target PPIs.

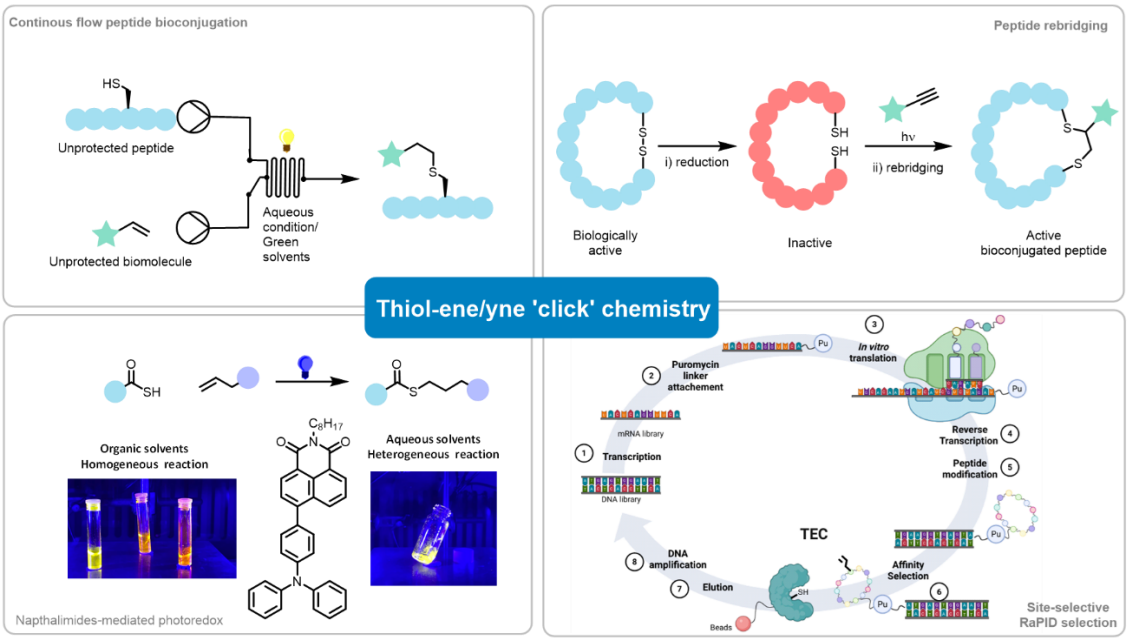

Figure 6.1: Graphical summary of the work described in this thesis.

In summary, this thesis establishes thiyl radical-mediated ligation as a versatile and broadly applicable platform for peptide science. These findings open future directions in therapeutic discovery, cellular imaging, and the selective inhibition of PPIs, positioning thiyl radical chemistry as a valuable tool for both academic research and drug discovery in pharma.

Chapter 7

Experimental

7.1 General Experimental Details

Commercial reagents and materials were purchased from Sigma Aldrich, Fluorochem, VWR, Carbosynth, Rapp Polymere and Tokyo Chemical Industry and used without further purification. Solvents for synthesis were purchased at High Performance Liquid Chromatography (HPLC) grade. Silica gel 60 (Merck, 230-400 mesh) was used for manual flash column chromatography. Automated reverse-phase flash chromatography was performed on a Biotage system using Telos C_{18} flash column cartridges. Room temperature (rt) is classified in this work as 18–21 °C. TLC was performed on Merck 60 F_{254} silica gel plates (fluorescence indicator F_{254}, Merck) and visualised by UV light (λ_{max} = 254 nm), ninhydrin staining (1.5 g ninhydrin, 3 mL acetic acid in 100 mL *n*-butanol), permanganate staining (1.6 g potassium permanganate, 10 g potassium carbonate and 1.25 mL 10% NaOH in 200 mL H_2O) or molybdenum staining (5.0 g ammonium molybdate, 5.3 mL concentrated H_2SO_4 in 100 mL H_2O) or Ellman stains. UV reactions were performed in a Luzchem LZC-EDU (110 V/ 60 Hz) photoreactor housing 12 UV lamps centred at 354 nm. Blue-LED reactions were performed using either a blue LED strip obtained from a domestic supplier or using 2 x Kessil PR160L lamps centred at 440 nm. SPPS was performed in polypropylene syringe vessels (Torviq) fitted with a polypropylene frit and was performed manually with continuous agitation. Melting points (m.p.) are uncorrected and were measured with a Stuart SP-10 melting point apparatus. Infrared spectra (IR) were recorded on a Perkin Elmer Spectrum 100 FT-IR spectrometer. Deuterated solvents for Nuclear Magnetic Resonance (NMR) spectroscopic analyses were purchased from Merck, VWR and Fluorochem. Figures and schemes showed in this thesis were made using ChemDraw 23.1.2.32-bit and Biorender.

Nuclear Magnetic Resonance (NMR) Spectroscopy

^{1}H- and ^{13}C-NMR spectroscopic analyses were performed on a 400 MHz (^{1}H, 400.13 MHz and ^{13}C, 100.61 MHz) Bruker Avance spectrometer or a 600 MHz Bruker Avance spectrometer (^{1}H, 600.13 MHz and ^{13}C, 150.90 MHz). Resonances (δ) are in ppm units downfield from an internal solvent reference. ^{1}H and ^{13}C NMR assignments were confirmed using additional experiments such as 2D COSY, HSQC, HMBC, and NOESY. ^{1}H NMR reaction conversions were measured using ^{1}H NMR spectroscopy with dimethyl sulfone as internal standard (1 equiv.). ^{1}H NMR spectroscopic experiment was executed

utilising a long relaxation time (D1 = 14 s). NMR data was analysed using MestReNova software.

High-performance Liquid Chromatography (HPLC)

Analytical and semi-preparative reverse phase HPLC was performed on a Shimadzu Nexera system equipped with a photodiode array detector. For analytical HPLC, either a C_{18} Jupiter 5 μm, 110 Å, 250 x 4.6 mm column or a C_{18} Jupiter 5 μm, 110 Å, 100 x 4.6 mm column was used, with a flow rate of 1 mL/min. For semi-preparative HPLC a C_{18} Jupiter 5 μm, 110 Å, 250 x 10.0 mm LC column was used. UV absorption signals were detected with a PDA detector at suitable wavelengths as dictated by the resultant absorption spectrum. LC-MS analyses were performed with a UHPLC single quadrupole MS system (Shimadzu LC-MS-2020) using a C_{18} Phenomenex Kinetex 2.1 × 50 mm, 100 Å, 2.6 μm column. Preparative RP-HPLC was performed using a Waters system equipped with a 2489 UV detector on a C_{18} Xterra OBD column (19 × 250 mm, 125 Å, 10 μm).

High Resolution Mass Spectrometry (HRMS)

ESI mass spectra were acquired using a Bruker microTOF-Q III spectrometer interfaced to a Dionex UltiMate 3000 LC in positive and negative modes as required. The instrument was calibrated using a tune mix solution, (Agilent Technologies ESI-l Low concentration tuning mix) this was also used as an internal lock mass. Masses were recorded over the range 100-2000 m/z. Operating conditions were as follows: end-plate offset 500V capillary 4500V, nebulizer 2.0 Bar, dry gas 8.0 L/min, and dry temperature 180 ºC. MicroTof control 3.2 and HyStar 3.2 software were used to carry out the analysis. APCI experiments were carried out on a Bruker micrOTOF-Q III spectrometer interfaced to a Dionex UltiMate 3000 LC or direct insertion probe. The instrument was operated in positive or negative mode as required. Agilent tuning mix APCI-TOF was used to calibrate the system. Masses were recorded over a range of 100-2000 m/z. Operating conditions were as follows: Capillary voltage 4000 V, corona 4000 nA, nebulizer gas 2.0 Bar, dry gas 3.0 L/min, dry gas temperature 100-200 ºC, vap. temperature 100-400 ºC. MicroTof control and HyStar software were used to carry out the analysis.

Carbohydrate positions were numbered from 1 to 6, starting at the anomeric position. In the case of disaccharides, individual glycans are labelled A and B, with A being located at the reducing terminus, as shown in **Figure 7.1**.

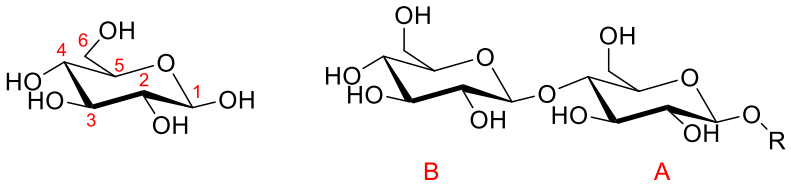

Fig. 7.1: Nomenclature of the carbohydrate moiety.

Continuous Flow Set Up for Initial Optimisation of Radical Mediated Thiol-ene Reactions of Glutathione

The flow reactor used was from Syrris Ltd and consists of two Cavro-type syringe pumps with flow rates ranging from 2.5 to 2500 µL min^{-1}. Reagents were loaded into the reactor chip from two pressurized containers A and B. Glass chip reactors of 1000 µL or 250 µL volume with inner S5 channel diameters of 0.25 mm were used and the temperature was controlled using a cooling/heating plate. For photoinitiation a 36 W Mylee lamp covered was placed over the chip assembly along with a box to prevent radiation leakage. Modules of the system were connected with 0.5 mm internal diameter PTFE tubing. The whole system was computer controlled and pressurized with dry N_2 with a back pressure regulator (1-7 bar).

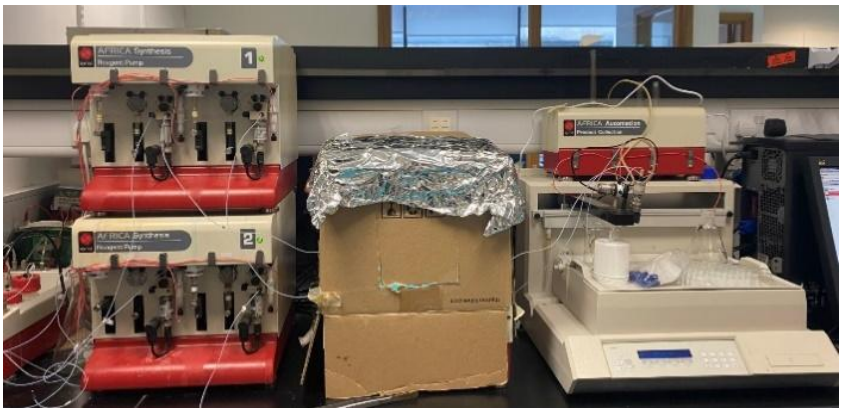

Figure S7.1: Integrated Syrris Ltd. continuous flow system of the O'Shea Laboratory (Royal College of Surgeons in Ireland, RCSI, York House, York Street, Dublin 2, Ireland) on which initial radical mediated thiol-ene chemistry optimisation was carried out.

Continuous Flow Set Up for Investigation the Radical-Mediated Thiol-ene Reactions in THF/H_2O, Bio-based solvents, DESs and H_2O

The flow reactor consisted of a 10 mL syringe pump which was set up with a flow rate of 0.08 mL min^{-1}. Reagents were loaded into dual syringes at atmospheric pressure. FEP tubing with an inner diameter of 0.8 mm was coiled around a glass insert. This insert was placed inside a Luzchem photoreactor, LZC-EDU (110 V/60 Hz) containing 10 UVA lamps centred at 352 nm. The terminus of the tubing was inserted into a glass vial for sample collection and analysis

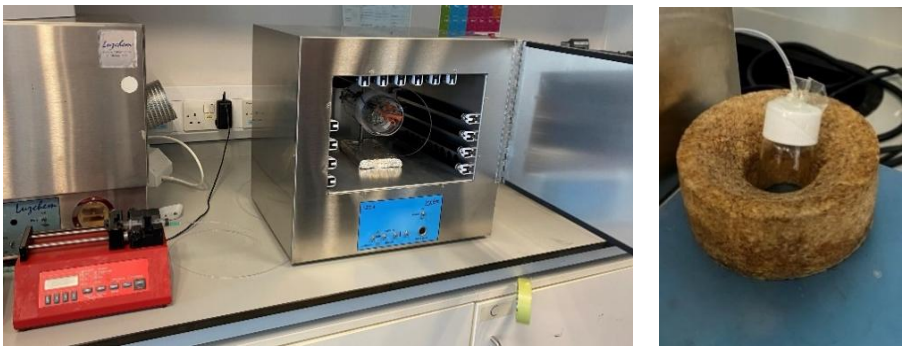

Figure S7.2: Continuous flow system within a 110 V UV oven (Scanlan Laboratory, Trinity Biomedical Sciences Institute, Trinity College Dublin, 152-160 Pearse Street, Dublin 2, Ireland). Investigation of the radical mediated thiol-ene chemistry of a variety of alkenes in THF/H_2O, DESs and bio-based solvents and H_2O under continuous flow was carried out using this apparatus.

7.2 Experimental details for Chapter 2

7.2.1 General procedures

General Procedure A: Radical-Mediated Thiol-ene Reaction of Glutathione <u>in Batch</u>. Alkene (1.63 mmol), glutathione **1** (20 mg, 0.065 mmol) and photoinitiator (0.05 equiv., 0.003 mmol) were stirred at rt in THF/H_2O (1 mL, 1:1) under UV irradiation (352 nm, 110 V) for 20 min. Solvent was removed *in vacuo*. Dimethyl sulfone (6 mg, 0.065 mmol) was added to the mixture and reaction conversions were measured using ^{1}H NMR spectroscopy with dimethyl sulfone as internal standard (1 equiv.). ^{1}H NMR spectroscopic experiment was performed utilising a long relaxation time (D1 = 14 s). All compounds synthesised using this experimental set-up were subsequently isolated by column chromatography and characterised to enable accurate determination of reaction conversions.

General Procedure B: Radical-Mediated Thiol-ene Reaction of Glutathione under Continuous Flow. A solution of glutathione **1** (20 mg, 0.065 mmol), alkene (0.16 mmol) and photoinitiator (0.05 equiv., 0.03 mmol) in THF/H_2O (1 mL, 1:1) or H_2O (1 mL) was pumped at 80 μL min^{-1} through the coil reactor at room temperature under UV irradiation (352 nm, 110 V). Residence time was 20 min. Solvent was removed *in vacuo*. Dimethyl sulfone (6 mg, 0.065 mmol) was added to the mixture and reaction conversions were measured using ^{1}H NMR spectroscopy with dimethyl sulfone as internal standard (1 equiv.). ^{1}H NMR spectroscopic experiment was executed utilising a long relaxation time (D1 = 14 s). All compounds synthesised using this experimental set-up were subsequently isolated by column chromatography and characterised to enable accurate determination of reaction conversions.

General Procedure C: Radical Mediated Thiol-ene Reactions of Glutathione in Deep Eutectic Solvents (DESs) and Bio-Based Solvents in Batch. Alkene (0.16 mmol), glutathione **1** (20 mg, 0.065 mmol) and photoinitiator (0.05 equiv., 0.003 mmol) were stirred at rt in DES/H_2O (3:2, 1 mL) under UV irradiation (352 nm, 110 V) for 20 min. The resulting product containing solutions were collected and analysed by RP-HPLC.

General Procedure D: Radical Mediated Thiol-ene Reactions of Glutathione in Deep Eutectic Solvents (DES) and Bio-Based Solvents under Continuous Flow. A solution of glutathione **1** (20 mg, 0.065 mmol), alkene (0.16 mmol) and photoinitiator (0.05 equiv., 0.03 mmol) in DES/H_2O (3:2, 1 mL) or H_2O (1 mL) was pumped at a flow rate of 80 μL min^{-1} through the coil reactor at room temperature under UV irradiation (352 nm, 110 V). Residence time was 20 min. Solvent was removed *in vacuo* and the resulting crude analysed by RP-HPLC.

General Procedure E: Solid Phase Fmoc Deprotection Utilising Wang Resin. To a polypropylene syringe fitted with a polypropylene frit was added Wang resin (200 mg, 1.0 mmol/g, 0.2 mmol) and DMF (5 mL). The syringe was agitated for 20 min, then drained. To a solution of Fmoc-AA-OH (5 equiv., 1.00 mmol) in DMF (1.5 mL) were added DIC (5 equiv, 1.0 mmol.), HOBt (5 equiv., 1 mmol) and DMAP (0.5 equiv, 0.1 mmol). The resulting solution was preactivated for 5 min prior to addition to the fritted syringe. The syringe was agitated for 1.5 h. Excess reagents were drained from the syringe and the resin was washed with DMF (3 x 5 mL), CH_2Cl_2 (3 x 5 mL) and DMF (3 x 5 mL) again. Fmoc deprotection of the resin bound peptide was accomplished by the

addition of piperidine (20% v/v) in DMF (2 x 10 mL, 20 min). The deprotection solution was expelled from the syringe and the resin washed with DMF (3 x 5 mL), CH_2Cl_2 (3 x 5 mL) and DMF (3 x 5 mL). Cleavage and global deprotection of the resin bound amino acids was undertaken by addition of cleavage cocktail (TFA:TES:H_2O, 95:2.5:2.5 v/v/v, 5 mL) to the syringe which was tightly capped and agitated for 1.5 hours. The syringe was drained, and the filtrate was collected. The resin was washed with TFA (2 x 2.5 mL) and washings combined with the initial filtrate. The solution was concentrated under a stream of N_2 and triturated in cold Et_2O prior to freeze drying to yield the desired amino acid derivative.

General Procedure F: Solid Phase Peptide Synthesis on Rink Amide Resin. To a polypropylene syringe fitted with a polypropylene frit was added Rink amide resin (256 mg, 0.78 mmol/g, 0.20 mmol), and DMF (5 mL). The syringe was agitated for 20 min, then drained. Fmoc deprotection of the resin was accomplished by the addition of piperidine (20% v/v) in DMF (2 x 10 mL, 20 min). The deprotection solution was expelled from the syringe and the resin washed with DMF (3 x 5 mL), CH_2Cl_2 (3 x 5 mL) and DMF (3 x 5 mL). PyBOP (3.0 equiv.), NMM (6.0 equiv.) and Fmoc-AA-OH protected amino acid (3.0 equiv.) were dissolved in DMF (0.2 M) and the resulting solution was preactivated for 5 min prior to addition to a fritted syringe. The syringe was agitated for 45 min. Excess reagents were drained from the syringe and the resin was washed with DMF (3 x 5 mL), CH_2Cl_2 (3 x 5 mL) and DMF (3 x 5 mL). Subsequent amino acid coupling cycles consisted of i) Fmoc deprotection of the resin bound peptide by the addition of 20% (v/v) piperidine in DMF (5 mL) to the resin for 10 min. Following this the solution was expelled from the syringe and replaced by fresh deprotection cocktail and the deprotection repeated, ii) resin washes with DMF (3 x 5 mL), CH_2Cl_2 (3 x 5 mL) and DMF (3 x 5 mL), iii) peptide coupling with addition of PyBOP (3.0 equiv.), NMM (6.0 equiv.) and Fmoc-AA-OH (3.0 equiv.) in DMF (0.2 M) to the peptide resin for 45 min, (iv) resin washes with DMF (3 x 5 mL), CH_2Cl_2 (3 x 5 mL) and DMF (3 x 5 mL), (v) qualitative monitoring of reaction progress with bromophenol blue. Following the final coupling, the resin was treated with 20% (v/v) piperidine in DMF x 2 for 10 min and the resin was washed with DMF (3 x 5 mL) and CH_2Cl_2 (3 x 5 mL). Cleavage and global deprotection of the resin bound amino acids was undertaken by addition of cleavage cocktail (TFA:TES:H_2O, 95:2.5:2.5 v/v/v, 5 mL) to the syringe, which was tightly capped and agitated for 1.5 hours. The syringe was drained and the filtrate was

collected. The resin was washed with TFA (2 x 2.5 mL) and washings combined with the initial filtrate. The solution was concentrated under a stream of N_2 and triturated in cold Et_2O prior to freeze drying. The resulting crude peptide was purified by semi-preparative RP-HPLC.

7.2.2 Characterisation data

Allyl-2,3,4,6-tetra-*O*-acetyl-β-D-galactopyranoside (52).

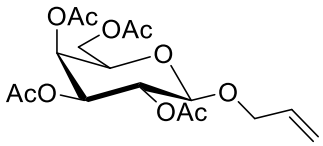

Peracetylated galactose **51** (3.57 g, 9.15 mmol) was dissolved in dry CH_2Cl_2 (15 mL). To the mixture was added $BF_3{\cdot}OEt_2$ (1.24 mL, 10.06 mmol). The mixture was stirred for 1 h before addition of allyl alcohol **49** (0.93 mL, 13.7 mmol). The mixture was left stirring at rt for 3.5 h after which time the reaction was quenched by addition of sat. aq. $NaHCO_3$ solution (20 mL). After stirring for 30 min, the mixture was washed three times with H_2O (3 × 20 mL). The organic layer was dried over $MgSO_4$, filtered and concentrated *in vacuo*. Purification by flash column chromatography using Hex/EtOAc (6:4) as eluent afforded the product **52** (2.00 g, 56%) as a clear colourless syrup. The isolated product was in good agreement with literature.[322] $\mathbf{R_f}$ = 0.44 (Hex:EtOAc, 6:4).**^{1}H NMR** (600 MHz, $CDCl_3$): 5.84 (dddd, *J* = 17.0, 10.8, 6.3, 4.9 Hz, 1H, $OCH_2C\underline{H}=CH_2$), 5.27 (dd, *J* = 17.0, 1.6 Hz, 1H, $CH_2CH=C\underline{H}_{2A}$), 5.22-5.18 (m, 2H, $CH=C\underline{H}_B$ + H3), 5.09 (app. t, *J* = 10 Hz, 1H, H4), 5.02 (dd, *J* = 9.6, 8.0 Hz, 1H, H2), 4.55 (d, *J* = 8.0 Hz, 1H, H1), 4.33 (app. ddt, *J* = 13.1, 4.9, 1.6 Hz, 1H, $O\text{-}C\underline{H}_{2A}CH=CH_2$), 4.25 (dd, *J* = 12.2, 4.8 Hz, 1H, H6a), 4.14 (dd, *J* = 12.2, 2.4 Hz, 1H, $H6_B$), 4.09 (app. ddt, *J* = 13.1, 6.3, 1.4 Hz, 1H, $O\text{-}C\underline{H}_{2B}CH=CH_2$), 3.68 (ddd, *J* = 10, 4.8, 2.4 Hz, 1H, H5), 2.08 (s, 3H, OAc), 2.04 (s, 3H, OAc), 2.01 (s, 3H, OAc), 2.00 (s, 3H, OAc) ppm. **HRMS**: (*m/z* ESI$^+$): found 411.1264 ($[M+Na]^+$, $C_{17}H_{24}NaO_{10}$ requires 411.1262).

Allyl-β-D-galactopyranose (53)

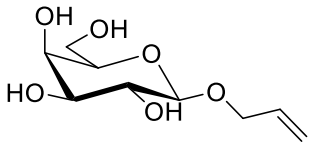

A round bottom flask was charged with compound **52** (3.68 g, 9.48 mmol) and dissolved in MeOH/NEt_3 (4:1, 20 mL) and heated at reflux for 18 h. The solution was cooled down to rt and DOWEX (H+) 50WX8-200 resin was then added until pH = 5 was achieved. The resin was then filtered off and the solvent was evaporated *in vacuo* to yield a light red solid. The crude product was then titrated with CH_2Cl_2 (20 mL) and redissolved in MeOH. Finally, the solvent was removed *in vacuo*. Compound **53** was obtained as a white solid (1.91 g, 92%). The isolated product was in good agreement with literature.[323] **m.p.** 104-106 °C (Lit.[324] m.p. 102-103 °C). $\mathbf{R_f}$ = 0.82 (IPA:ACN:H_2O, 10:9:2). **^{1}H NMR** (400 MHz, MeOD-d_4) δ 6.00 (dddd, J = 17.0, 10.9, 6.1, 5.2 Hz, 1H,$OCH_2C\underline{H}=CH_2$), 5.36 (dd, J = 17.0, 1.7 Hz, 1H, $OCH_2CH=C\underline{H}_{2A}$), 5.19 (dd, J = 10.9, 1.7 Hz, 1H, $OCH_2CH=C\underline{H}_{2B}$), 4.41 (dd, J = 12.8, 5.2 Hz, 1H, $OC\underline{H}_{2A}CH=CH_2$), 4.33 (d, J = 7.8 Hz, 1H, H1), 4.18 (dd, J = 12.8, 6.1 Hz, 1H, $OC\underline{H}_{2B}CH=CH_2$), 3.89 (dd, J = 11.9, 2.0 Hz, 1H, $H6_A$), 3.69 (dd, J = 11.9, 5.3 Hz, 1H, $H6_B$), 3.38-3.27 (m, 3H, H3 + H4 + H5), 3.23 (dd, J = 9.0, 7.8 Hz, 1H, H2) ppm. **HRMS** (*m/z* ESI$^+$): found 243.0837 ($[M+Na]^+$, $C_9H_{16}NaO_6$ requires 243.0839).

N^6-((allyloxy)carbonyl)-D-lysine (55)

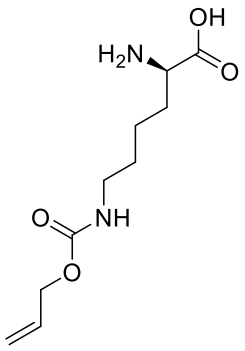

55 was prepared by solid phase Fmoc deprotection of Fmoc-Lys(Alloc)-OH as per **general procedure E** (138 mg, 40%) and was obtained as a white solid. The isolated product was in good agreement with literature.[325] **m.p.** 191-192 °C (dec.) (Lit.[325] m.p. 189-190 °C). **^{1}H NMR** (400 MHz, D_2O): δ 5.96 (ddt, J = 17.0, 10.6, 5.0 Hz, 1H,

C<u>H</u>=CH_2), 5.33 (d, *J* = 17.4 Hz, 1H, CH=C<u>H_{2A}</u>), 5.26 (d, *J* = 10.6 Hz, 1H, CH=C<u>H_{2B}</u>), 4.57 (d, *J* = 5.0 Hz, 2H, OC<u>H_2</u>CH=CH_2), 4.00 (t, *J* = 6.3 Hz, 1H, Lys αCH), 3.17 (app. t, *J* = 6.3 Hz, 2H, Lys βCH_2), 2.05-1.87 (m, 2H, Lys εCH_2), 1.60-1.56 (m, 2H, Lys δCH_2), 1.51-1.40 (m, 2H, Lys γCH_2) ppm. **HRMS** (*m/z* ESI^+); found 231.1235 $(M+H]^+$, $C_{10}H_{18}N_2O$ requires 231.1267).

(*S*)-5-(allyloxy)-2-amino-5-oxopentanoic acid (56)

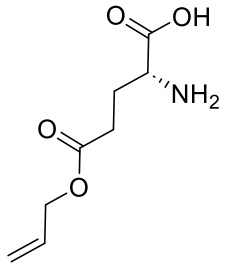

56 was prepared by solid phase Fmoc deprotection of Fmoc-Glu(OAll)-OH as per **general procedure E** (92 mg, 40%) and was obtained as a yellow oil. The isolated product was in good agreement with literature.[325] **^{1}H NMR** (400 MHz, D_2O): δ 5.99 (ddt, *J* = 16.7, 11.1, 5.7 Hz, 1H, OCH_2C<u>H</u>=CH_2), 5.38 (dd, *J* = 16.7, 1.6 Hz, 1H, OCH_2CH=C<u>H_{2A}</u>), 5.31 (dd, *J* = 11.1, 1.6 Hz, 1H, CH=C<u>H_{2B}</u>), 4.66 (d, *J* = 5.7, 2H, OC<u>H_2</u>CH=CH_2), 3.89 (t, *J* = 6.5 Hz, 1H, Glu αCH), 2.67-2.62 (m, 2H, Glu γCH_2), 2.29-2.14 (m, 2H, Glu βCH_2) ppm. **HRMS** (*m/z* ESI^+): found 188.0880 $([M+H]^+$, $C_8H_{13}NO_4$ requires 188.0845).

(*R*)-4-(allyloxy)-2-amino-4-oxobutanoic acid (57)

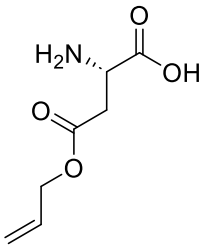

57 was prepared by solid phase Fmoc deprotection of Fmoc-Asp(OAll)-OH as per **general procedure E** (146 mg, 53%) and was obtained as a white solid. The isolated product was in good agreement with literature.[325] **m.p.** 102-105 °C (dec.) (Lit.[325] m.p. 105-108 °C). **^{1}H NMR** (400 MHz, D_2O): δ 5.41 (ddd, *J* = 17.4, 11.0, 6.0 Hz, 1H, CH_2C<u>H</u>=CH_2), 5.34 (d, *J* = 17.4 Hz, 1H, CH=C<u>H_{2A}</u>), 5.34 (d, *J* = 11.0 Hz, 1H, CH=C<u>H_{2B}</u>), 4.50 (d, *J* = 6.0 Hz, 2H, OC<u>H_2</u>CH=CH_2), 3.23 (dd, *J* = 18.4, 5.9 Hz, 1H, Asp

βCH$_{2A}$), 3.23 (dd, *J* = 18.4, 4.3 Hz, 1H, Asp βCH$_{2B}$), 3.03-3.02 (m, 1H, Asp αCH) ppm. **HRMS** (*m/z* ESI$^+$): found 174.0625 ([M+H]$^+$, $C_7H_{11}NO_4$ requires 174.0688).

1-thioacetyl-3,4,6-tri-Oacetyl-2-deoxy-2-acetamido-β-D-glucopyranoside (83).

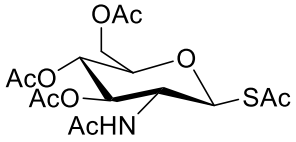

N-Acetyl-D-glucosamine **82** (500 mg, 2.26 mmol) and triethylamine (3.1 mL, 22.6 mmol) were stirred in H_2O (10 mL) and cooled to 0 °C. 2-Chloro-1,3-dimethylimidazolinium chloride (1.2 g, 6.78 mmol) was added. After 0.5 h, thioacetic acid (2.4 mL, 33.9 mmol) was added dropwise, and the reaction mixture was allowed to stir for an additional 0.5 h at 0 °C. The reaction mixture was then diluted with H_2O (10 mL) and washed with CH_2Cl_2 (5 x 20 mL). The aqueous layer was concentrated *in vacuo* and the solid suspended in pyridine (7 mL) under an atmosphere of N_2. The mixture was stirred at rt and acetic anhydride (7 mL, 74.1 mmol) was added. The reaction was stirred for 12 h, after which time TLC (100% EtOAc) indicated the formation of a single major product. H_2O (10 mL) was added, and the mixture was then washed with CH_2Cl_2 (3 x 100 mL). The combined organic extracts were washed with aqueous HCl (1 M, 100 mL), $NaHCO_3$ (sat. aqueous soln., 100 mL), H_2O (100 mL) and brine (100 mL), dried ($MgSO_4$), filtered, and concentrated *in vacuo*. The residue was recrystallised (Hex/CH_2Cl_2) to afford thiolated glucose **83** (453 mg, 50%) as a white solid. The isolated compound was in good agreement with the literature.[214] **m.p.** = 184-186 °C (Lit.[214] m.p. 186-188 °C). **R$_f$** = 0.53 (100% EtOAc). ^{1}H NMR (400 MHz, $CDCl_3$) δ 5.52 (d, *J* = 9.7 Hz, 1H, NH), 5.3-5.0 (m, 3H, H1 + H3 + H4), 4.35 (app. q, *J* = 10.1 Hz, 1H), 4.24 (dd, *J* = 12.5, 4.5 Hz, 1H. H6a), 4.10 (dd, *J* = 12.4, 2.1 Hz, 1H, H6b), 3.80-3.76 (m, 1H, H5), 2.4 (s, 3H,OAc), 2.1 (s, 3H, OAc), 2.0 (s, 6H, OAc), 1.9 (s, 3H, SAc) ppm. **HRMS** (*m/z* ESI$^+$): found 406.116823 ([M+H]$^+$, $C_{16}H_{24}NO_9S$ requires 406.116629).

2-acetamido-2-deoxy-1-thio-β-D-glucopyranose (84).

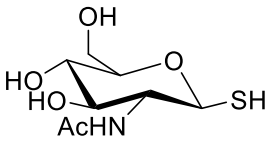

Sodium metal (25.4 mg, 1.1 mmol) was added to MeOH (5 mL) and stirred. 1-Thioacetyl3,4,6-tri-O-acetyl-2-deoxy-2-acetamido-β-D-glucopyranoside **83** (203 mg, 0.50 mmol) was added and the reaction was stirred for 0.5 h, at which point TLC (100% EtOAc) indicated complete consumption of starting material ($\mathbf{R_f}$ = 0.53) and formation of a single product ($\mathbf{R_f}$ = 0). Dowex® 50WX8 (H+) ion exchange resin was added portion-wise until the reaction reached neutral pH. The mixture was then filtered and concentrated *in vacuo* to afford 1-thio-2-acetamido-2-deoxy-β-D-glucopyranose **27** (121 mg, 94%) as a white solid. The isolated compound was in good agreement with the literature.[214] **m.p.** 176-178 °C (lit.[214] 177-179 °C); ^{1}H NMR (400 MHz, $MeOD_4$) δ 4.57 (d, *J* = 10.0 Hz, 1H, H1), 3.88 (dd, *J* = 12.0, 2.0 Hz, 1H, $H6_A$), 3.74-3.65 (m, 2H, H2 + $H6_B$), 3.45-3.36 (m, 3H. H3 + H4 + H5), 2.0 (s, 3H, OAc) ppm. **HRMS** (*m/z* ESI^+): found 238.0746 ($[M+H]^+$, $C_8H_{16}NO_5S$ requires 238.0744).

7.2.3 Characterisation Data of Thiol-ene Products

***N*-((*R*)-1-((carboxymethyl)amino)-3-((3-hydroxypropyl)thio)-1-oxopropan-2-yl)-D-glutamine (50)**

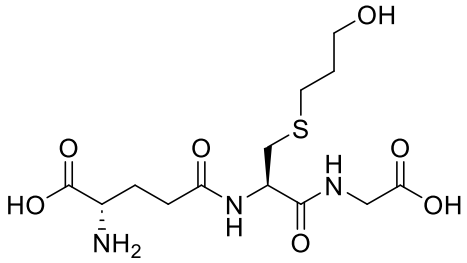

50 was prepared by radical mediated thiol-ene reaction of glutathione **48** and allyl alcohol **49** as per **general procedure A** in batch (21 mg, 89%) and as per **general procedure B** under continuous flow (22 mg, 91%). The reaction mixture was washed with CH_2Cl_2 (2 x 50 mL), and aqueous layer was lyophilized prior to ^{1}H NMR spectroscopic analysis. The isolated product was in good agreement with literature.[196] **m.p.** 131-139 °C (dec.). $\mathbf{R_f}$ = 0.59 (IPA:ACN:H_2O, 10:9:2).**^{1}H NMR** (400 MHz, D_2O): δ 4.59 (dd, *J* = 8.7, 5.1 Hz, 1H, Cys αCH), 3.96 (s, 2H, Gly αCH_2), 3.82 (t, *J* = 6.3 Hz, 1H, Glu αCH), 3.68 (t, *J* =

6.3 Hz, 2H, $CH_2CH_2C\underline{H_2}OH$), 3.09 (dd, *J* = 14.1, 5.1 Hz, 1H, Cys βCH_{2A}), 2.90 (dd, *J* = 14.1, 8.7 Hz, 1H, Cys βCH_{2B}), 2.67 (t, *J* = 7.5, Hz, 2H, Glu γCH_2), 2.58-2.52 (m, 2H, Glu βCH_2), 2.21-2.15 (m, 2H, $\underline{CH_2}CH_2CH_2OH$), 1.88-1.79 (m, 2H,$CH_2\underline{CH_2}CH_2OH$) ppm. **HRMS** (*m/z* ESI^+): found 366.1329 ($[M+H]^+$, $C_{13}H_{24}N_3O_7S$ requires 366.1329).

N-((R)-1-((carboxymethyl)amino)-3-((5-hydroxypentyl)thio)-1-oxopropan-2-yl)-D-glutamine (61)

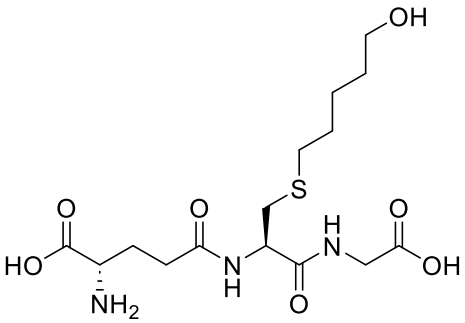

61 was prepared by radical mediated thiol-ene reaction of glutathione (**48**) and 4-penten-1-ol (**54**) as per **general procedure A** in batch (21 mg, 84%) and as per **general procedure B** under continuous flow (24 mg, 94%). The reaction mixture was washed with CH_2Cl_2 (2 x 50 mL) and aqueous layer was lyophilized prior to ^1H NMR spectroscopic analysis. **m.p.** 180-185 °C (dec.). $\mathbf{R_f}$ = 0.56 (IPA:ACN:H_2O, 10:9:2).**^{1}H NMR** (400 MHz, D_2O): δ 4.59 (dd, *J* = 8.7, 5.1 Hz, 1H, Cys αCH), 4.00 (s, 2H, Gly αCH_2), 3.85 (t, *J* = 6.4 Hz, 1H, Glu αCH), 3.62 (t, *J* = 6.5 Hz, 2H, $CH_2CH_2CH_2CH_2C\underline{H_2}OH$), 3.08 (dd, *J* = 14.0, 5.1 Hz, 1H, Cys βCH_{2A}), 2.90 (dd, *J* = 14.0, 8.7 Hz, 1H, Cys βCH_{2B}), 2.63 (t, *J* = 7.4 Hz, 1H, Glu γCH_2), 2.59-2.54 (m, 2H, Glu βCH_2), 2.22-2.16 (m, 2H, $C\underline{H_2}CH_2CH_2CH_2CH_2OH$), 1.64 (dt, *J* = 8.5, 6.8 Hz, 2H,), 1.64-1.54 (m, 4H, $CH_2\underline{CH_2}CH_2CH_2CH_2OH$ + $CH_2CH_2CH_2\underline{CH_2}CH_2OH$), 1.49-1.37 (m, 2H, $CH_2CH_2\underline{CH_2}CH_2CH_2OH$) ppm. **^{13}C NMR** (101 MHz, D_2O): δ 174.8 (C=O), 173.5 (C=O), 173.5 (C=O), 172.8 (C=O), 61.6 ($CH_2CH_2CH_2CH_2\underline{C}H_2OH$), 54.8 (Glu αCH), 53.2 (Cys αCH), 41.3 (Gly αCH_2), 32.7 (Cys βCH_2), 31.5 (Glu γCH_2), 31.2 (Glu βCH_2), 30.8 ($CH_2CH_2CH_2\underline{C}H_2CH_2OH$), 27.9 ($CH_2\underline{C}H_2CH_2CH_2CH_2OH$), 26.0 ($\underline{C}H_2CH_2CH_2CH_2CH_2OH$) 24.2 ($CH_2CH_2\underline{C}H_2CH_2CH_2OH$) ppm. **HRMS** (*m/z* ESI^+): found 392.1487 ($[M+H]^+$, $C_{15}H_{26}N_3O_7S$ requires 392.1496). $\boldsymbol{\nu_{max}}$ (film)/cm^{-1}: 3342 (N-H, O-H), 2929 (CH_2), 1673 (C=O), 1256 (C-O), 684 (C-S).

_N_-((_R_)-1-((carboxymethyl)amino)-1-oxo-3-((3-(((2_R_,3_R_,4_S_,5_R_,6_R_)-3,4,5-trihydroxy-6-(hydroxymethyl) tetrahydro-2H-pyran-2-yl)oxy)propyl)thio)propan-2-yl)-L-glutamine (62)

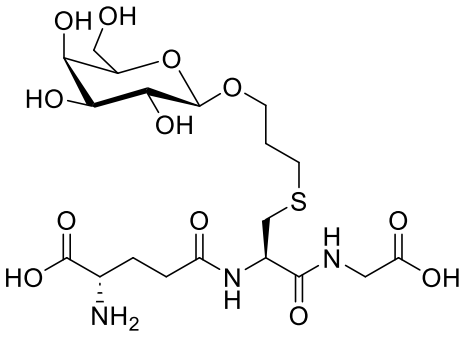

62 was prepared by radical mediated thiol-ene reaction of glutathione **48** and allylated monosaccharide **53** as per **general procedure A** in batch (34 mg, 96%) and as per **general procedure B** under continuous flow (49 mg, 94%). The reaction mixture was washed with CH_2Cl_2 (2 x 50 mL) and aqueous layer was lyophilized prior to ^{1}H NMR spectroscopic analysis. **m.p.** 132-140 °C (dec.). **R_f** = 0.5 (EtOH:H_2O, 8:2).**^{1}H NMR** (400 MHz, D_2O): δ 4.59 (dd, *J* = 8.9, 4.9 Hz, 1H, Cys αCH), 4.46 (d, *J* = 7.9 Hz, 1H, H1), 4.02-3.97 (m, 1H, Glu αCH), 3.92 (dd, *J* = 12.4, 2.2 Hz, 1H, $H6_A$), 3.79-3.73 (m, 5H, Gly αCH_2 + $C\underline{H}_2CH_2CH_2S$ + H5), 3.72-3.62 (m, 1H, $H6_B$), 3.52-3.44 (m, 1H, H4), 3.40-3.36 (m, 1H, H3), 3.27 (dd, *J* = 9.3, 7.9 Hz, 1H, H2), 3.10 (dd, *J* = 14.1, 5.0 Hz, 1H, Cys βCH_{2A}), 2.89 (dd, *J* = 14.1, 8.9 Hz, 1H, Cys βCH_{2B}), 2.70 (t, *J* = 6.9 Hz, 2H, Glu γCH_2), 2.55 (app. td, *J* = 7.5, 2.5 Hz, 2H, $CH_2CH_2C\underline{H}_2S$), 2.20-2.14 (m, 2H, $CH_2C\underline{H}_2CH_2S$), 1.96-1.88 (m, 2H, Glu βCH_2) ppm. **^{13}C NMR** (101 MHz, D_2O): δ 176.2 (C=O), 174.9 (C=O), 174.3 (C=O), 171.7 (C=O), 102.3 (C1), 75.7 (C3), 73.1 (C2), 69.7 (C4), 68.71 (Glu αCH, $C\underline{H}_2CH_2CH_2S$), 60.6 ($CH_2$, C6), 54.1 (C5), 53.9 ($CH_2CH_2\underline{C}H_2O$), 53.2 (Cys αCH), 43.3 (Gly αCH_2), 32.8 (Cys βCH_2), 31.4 (Glu βCH_2), 28.8 ($\underline{C}H_2CH_2CH_2O$), 27.9 (Glu γCH_2), 26.2 ($CH_2\underline{C}H_2CH_2O$) ppm. **HRMS** (*m/z* ESI$^+$): found 550.1674 ([M+Na]$^+$, $C_{19}H_{33}N_3NaO_{12}S$ requires 550.1677). **ν_{max}** (film)/cm^{-1}: 3263 (N-H), 2929 (CH_2), 1634 (C=O), 1235 (C-O).

(2*R*, 7*R*, 20*R*)-2,20-diamino-7-((carboxymethyl)carbamoyl)-5,14-dioxo-13-oxa-9-thia-6,15-diazahenicosanedioic acid (63).

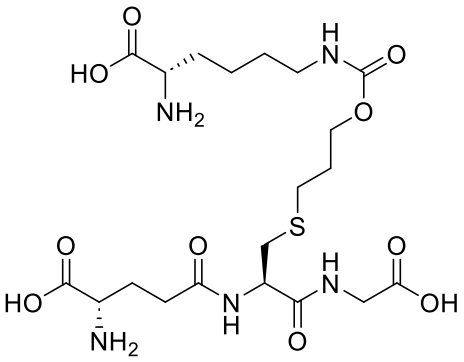

63 was prepared by radical mediated thiol-ene reaction of glutathione **48** and Lys(OAll)-OH **55** as per **general procedure A** in batch (55%) and as per **general procedure B** under continuous flow (75%). The reaction mixture was washed with CH_2Cl_2 (2 x 50 mL), and aqueous layer was lyophilized prior to ^{1}H NMR spectroscopic analysis. **m.p.** 187-195 °C (dec.). **R_f** = 0.66 (H_2O:ACN, 7:3) reverse phase C_{18} TLC.**^{1}H NMR** (600 MHz, DMSO-d_6): δ 8.19 (d, *J* = 6.0 Hz, 1H, Gly NH), 8.05 (d, *J* = 8.5 Hz, 1H, Cys NH), 6.85 (t, *J* = 5.8 Hz, 1H, Lys NH), 4.23 (ddd, *J* = 9.4, 8.5, 4.8 Hz, 1H, Cys αCH), 3.74 (t, *J* = 6.5 Hz, 2H, $SCH_2CH_2C\underline{H}_2O$), 3.66 (app. t, *J* = 6.4 Hz, 1H, Glu αCH), 3.60 (app. t, *J* = 6.2 Hz, 1H, Lys αCH), 3.53 (d, *J* = 6.0 Hz, 2H, Gly αCH_2), 2.74-2.72 (m, 2H, Lys εCH_2), 2.63 (dd, *J* = 13.7, 4.8 Hz, 1H, Cys βCH_{2A}), 2.38 (dd, *J* = 13.7, 9.4 Hz, 1H, Cys βCH_{2B}), 2.34-2.30 (m, 2H, $SC\underline{H}_2CH_2CH_2O$), 2.16 (ddd, *J* = 15.3, 9.4, 6.2 Hz, 1H, Glu γCH_{2A}), 2.08 (ddd, *J* = 15.3, 9.3, 6.2 Hz, 1H, Glu γCH_{2B}), 1.85-1.70 (m, 2H, Glu βCH_2), 1.57-1.47 (m, 4H, $SCH_2C\underline{H}_2CH_2O$ + Lys βCH_2), 1.20-1.12 (m, 2H, Lys γCH_2), 1.09-1.03 (m, 2H, Lys δCH_2) ppm.**^{13}C NMR** (151 MHz, DMSO): δ 171.1 (C=O), 171.1 (C=O), 170.9 (C=O, Lys), 170.8 (C=O), 170.6 (C=O), 156.2 (C=O), 62.3 ($SCH_2CH_2\underline{C}H_2O$), 52.1 (Cys αCH), 52.0 (Lys αCH), 51.8 (Glu αCH), 40.7 (Gly αCH_2), 39.8 (Lys εCH_2), 33.5 (Cys βCH_2), 30.7 (Glu γCH_2), 29.7 (Lys βCH_2), 28.8 (Lys γCH_2), 28.6 ($SCH_2\underline{C}H_2CH_2O$), 27.7 ($S\underline{C}H_2CH_2CH_2O$), 26.1 (Glu βCH_2), 21.6 (Lys δCH_2) ppm. **HRMS** (*m/z* ESI$^+$): found 538.2184 ($[M+H]^+$, $C_{20}H_{36}N_5O_{10}S$ requires 538.2177). **ν_{max}** (film)/cm^{-1}: 3320 (N-H), 2939 (CH_2), 1661 (C=O), 1241 (C-O).

(*R*)-2-amino-5-(3-(((*R*)-2-((*R*)-4-amino-4-carboxybutanamido)-3-((carboxymethyl)amino)-3-oxopropyl)thio)propoxy)-5-oxopentanoic acid (64).

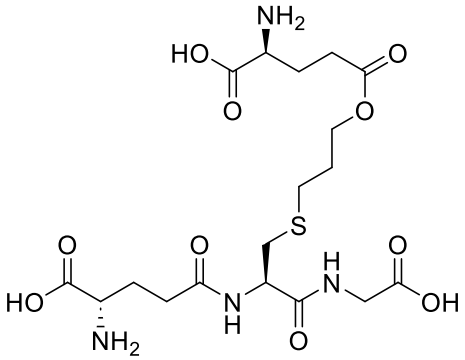

64 was prepared by radical mediated thiol-ene reaction of glutathione **48** and Glu(OAll)-OH **56** as per **general procedure A** in batch (73%) and as per **general procedure B** under continuous flow (86%). The reaction mixture was washed with CH_2Cl_2 (2 x 50 mL) and aqueous layer was lyophilized prior to ^{1}H NMR spectroscopic analysis. **m.p.** 120-135 °C (dec.). **R_f** = 0.94 (H_2O:ACN, 9:1) reverse phase C_{18} TLC. **^{1}H NMR** (600 MHz, DMSO-d_6): δ 8.43 (t, *J* = 5.7 Hz, 1H, Gly NH), 8.27 (d, *J* = 8.5 Hz, 1H, Cys NH), 4.48 (ddd, *J* = 8.9, 8.5, 4.8 Hz, 1H, Cys αCH), 3.98 (t, *J* = 6.4 Hz, 2H, Glu αCH + Glu (GSH) αCH), 3.90-3.83 (m, 2H, $SCH_2CH_2C\underline{H}_2O$), 3.76 (dd, *J* = 5.7, 2.2 Hz, 2H, Gly αCH_2), 2.97-2.94 (m, 2H, $SC\underline{H}_2CH_2CH_2O$), 2.87 (dd, *J* = 13.6, 4.8 Hz, 1H, Cys βCH_{2A}), 2.62 (dd, *J* = 13.6, 8.9 Hz, 1H, Cys βCH_{2B}), 2.57-2.54 (m, 2H, Glu (OAll) βCH_2), 2.40-2.29 (m, 2H, Glu (GSH) βCH_2), 1.80-1.72 (m, 4H, Glu(GSH) γCH_2 + Glu γCH_2), 1.43-1.37 (m, 2H, $SCH_2C\underline{H}_2CH_2O$) ppm. **^{13}C NMR** (151 MHz, DMSO-d_6): δ 207.1 (C=O), 171.6 (2 C=O), 171.44 (C=O), 171.40 (C=O), 171.1 (C=O), 62.8 (Glu αCH), 52.6 (Cys αCH), 52.5 ($SCH_2CH_2\underline{C}H_2O$), 41.2 (Gly αCH_2), 40.4 ($S\underline{C}H_2CH_2CH_2O$), 34.1 (Cys βCH_2), 30.2 (Glu γCH_2), 29.3 (Glu (GSH) βCH_2), 29.2 (Glu βCH_2), 28.20 (Glu (OAll) γCH_2), 22.1 ($SCH_2\underline{C}H_2CH_2O$) ppm. **HRMS** (*m/z* ESI$^+$): found 495.1757 ($[M+H]^+$, $C_{18}H_{31}N_4O_{10}S$ requires 495.1755). **ν_{max}** (film)/cm^{-1}: 2936 (CH_2), 1635 (C=O), 1199 (C-O).

_N_-((_R_)-3-((3-(((_S_)-3-amino-3-carboxypropanoyl)oxy)propyl)thio)-1-((carboxymethyl)amino)-1-oxopropan-2-yl)-L-glutamine (65).

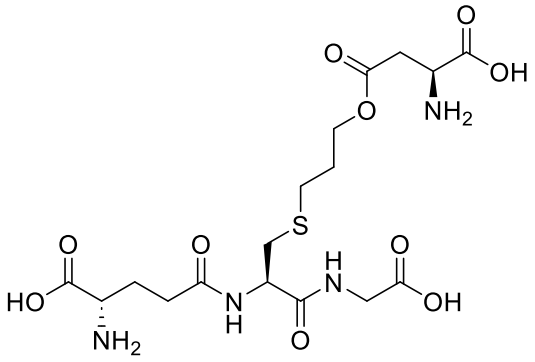

65 was prepared by radical mediated thiol-ene reaction of glutathione **48** and Asp(OAll)-OH **57** as per **general procedure A** in batch (53%) and as per **general procedure B** under continuous flow (83%). The reaction mixture was washed with CH_2Cl_2 (2 x 50 mL) and aqueous layer was lyophilized prior to ^{1}H NMR spectroscopic analysis. **m.p.** 131-139 °C (dec.). **R_f** = 0.67 (H_2O:ACN, 9:1) reverse phase C_{18} TLC.**^{1}H NMR** (400 MHz, D_2O): δ 4.60 (dt, *J* = 8.9, 4.1 Hz, 1H, Asp αCH), 4.49-4.42 (m, 1H, Cys αCH), 4.40 (dd, *J* = 8.9, 7.5 Hz, 1H, Asp βCH_{2A}), 4.35 (dd, *J* = 7.5, 4.1 Hz, 1H, Asp βCH_{2B}), 4.01 (s, 2H, Gly αCH_2), 3.89 (t, *J* = 5.7 Hz, 1H, Glu αCH), 3.20 (dd, *J* = 18.2, 5.8 Hz, 1H, Cys βCH_{2A}), 3.13-3.01 (m, 1H, Cys βCH_{2B}), 2.94-2.87 (m, 2H, $C\underline{H}_2CH_2CH_2O$), 2.69 (t, *J* = 7.3 Hz, 2H, $CH_2CH_2C\underline{H}_2O$), 2.60-2.55 (m, 2H, Glu βCH_2), 2.23-2.17 (m, 2H, Glu γCH_2), 2.05-1.95 (m, 2H, $CH_2C\underline{H}_2CH_2O$) ppm. **^{13}C NMR** (101 MHz, D_2O): δ 174.8 (C=O), 173.6 (C=O), 173.3 (C=O), 172.8 (C=O), 169.2 (C=O), 65.7 (Asp βCH_2), 53.5 (Glu αCH), 53.0 (Asp αCH), 49.5 (Cys αCH), 41.3 (Gly αCH_2), 34.1 (Cys βCH_2), 32.7 ($\underline{C}H_2CH_2CH_2O$), 31.1 (Glu βCH_2), 27.9 ($CH_2CH_2\underline{C}H_2O$), 27.4 ($CH_2\underline{C}H_2CH_2O$), 25.9 (Glu γCH_2) ppm. **HRMS** (*m/z* ESI$^+$): found 481.1599, ($[M+H]^+$, $C_{17}H_{29}N_4O_{10}S$ requires 481.1598). **ν_{max}** (film)/cm^{-1}: 3338 (N-H), 2929 (CH_2), 1671 (C=O), 1222 (C-O).

_N_-((_R_)-1-((carboxymethyl)amino)-1-oxo-3-((3-thioureidopropyl)thio)propan-2-yl)-L-glutamine (66)

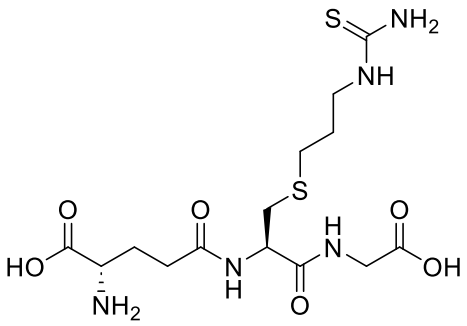

66 was prepared by radical mediated thiol-ene reaction of glutathione **48** and *N*-allylthiourea **58** as per **general procedure A** in batch (quantitative) and as per **general procedure B** under continuous flow (84%). The reaction mixture was washed with CH_2Cl_2 (2 x 50 mL) and aqueous layer was lyophilized prior to ^{1}H NMR spectroscopic analysis. **m.p.** 210-215 °C (dec.). **R_f** = 0.61 (H_2O:ACN, 9:1) reverse phase C_{18} TLC.**^{1}H NMR** (400 MHz, DMSO-d_6): δ 8.53 (d, *J* = 9.6, 5.3 Hz, 1H, Gly NH), 8.34 (d, *J* = 8.6 Hz, 1H, Cys NH), 7.08 (t, *J* = 5.8 Hz, 1H, Thiourea NH), 4.46 (ddd, *J* = 8.7, 8.61, 4.2 Hz, 1H, Cys αCH), 3.97 (t, *J* = 6.3 Hz, 1H, Glu αCH), 3.73 (d, *J* = 5.3 Hz, 2H, Gly αCH_2), 3.60-3.53 (m, 2H, SC$\underline{H}_2CH_2CH_2NH$), 2.88 (dd, *J* = 13.5, 4.6 Hz, 1H, Cys βCH_2), 2.62 (dd, *J* = 13.8, 8.61 Hz, 1H, Cys βCH_2), 2.55 (t, *J* = 7.2 Hz, 1H, Glu γCH_2), 2.37-2.31 (m, 2H, $SCH_2C\underline{H}_2CH_2NH$), 1.97-1.89 (m, 2H, $SCH_2CH_2C\underline{H}_2NH$), 1.78-1.70 (m, 2H, Glu βCH_2) ppm. **^{13}C NMR** (101 MHz, DMSO-d_6): δ 172.1 (C=O), 172.1 (C=O), 170.8 (C=O), 170.8 (C=O), 156.7 (C=S), 62.7 (Glu αCH), 55.5 (Cys αCH), 53.4 ($S\underline{C}H_2CH_2CH_2NH$), 52.9 (Cys αCH), 41.4 (Gly αCH_2), 34.1 (Cys βCH_2), 31.9 ($SCH_2CH_2\underline{C}H_2NH$), 29.3 (Glu β$CH_2$), 28.3 (Glu γ$CH_2$), 27.2 ($SCH_2\underline{C}H_2CH_2NH$) ppm. **HRMS** (*m/z* ESI$^+$): found 424.1319 ($[M+H]^+$, $C_{14}H_{26}N_5O_6S_2$ requires 424.1319). **ν_{max}** (film)/cm^{-1}: 2937 (CH_2), 1645 (C=O), 1133 (C=S).

_N_-((_R_)-1-((carboxymethyl)amino)-1-oxo-3-((3-ureidopropyl)thio)propan-2-yl)-L-glutamine (67).

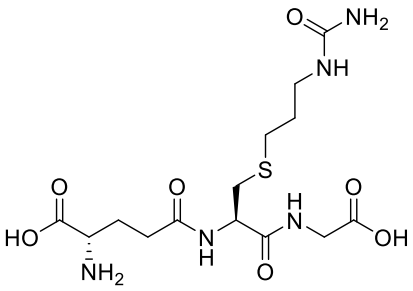

67 was prepared by radical mediated thiol-ene reaction of glutathione **48** and *N*-allylurea **59** as per **general procedure A** in batch (36%) and as per **general procedure B** under continuous flow (67%) as a white solid. The reaction mixture was washed with CH_2Cl_2 (2 x 50 mL) and aqueous layer was lyophilized prior to ^{1}H NMR spectroscopic analysis. **m.p.** 195-200 °C (dec.). $\mathbf{R_f}$ = 0.88 (H_2O:ACN, 9:1) reverse phase C_{18} TLC.**^{1}H NMR** (400 MHz, DMSO-d_6): δ 8.53 (t, J = 5.7 Hz, 1H, Gly NH), 8.48 (d, J = 8.6 Hz, 1H, Cys NH), 6.38 (s, 1H, Urea NH), 5.60 (s, 2H, Urea NH_2), 4.44 (ddd, J = 9.0, 8.6, 4.5 Hz, 1H, Cys αCH), 3.71 (d, J = 5.7 Hz, 2H, Gly αCH_2), 3.47 (t, J = 6.6 Hz, 1H, Glu αCH), 3.02-2.98 (m, 2H, SC$\underline{H}_2$CH_2CH_2NH), 2.87 (dd, J = 13.8, 4.4 Hz, 1H, Cys βCH_2), 2.64 (dd, J = 13.8, 9.0 Hz, 1H, Cys βCH_2), 2.55-2.48 (m, 2H, SCH_2C$\underline{H}_2$CH_2NH), 2.34 (t, J = 7.3 Hz, 2H, Glu γCH_2), 1.95-1.89 (m, 2H, Glu βCH), 1.62-1.54 (m, 2H, SCH_2CH_2C$\underline{H}_2$NH) ppm. **^{13}C NMR** (101 MHz, DMSO-d_6): δ 172.3 (C=O), 171.6 (C=O), 171.5 (C=O), 171.3 (C=O), 159.5 (C=O), 53.5 (Glu αCH), 53.3 (Cys αCH), 41.7 (Gly αCH_2), 38.7 (S$\underline{C}$H$_2$CH$_2$CH$_2$NH), 34.1 (Cys βCH_2), 32.0 (Glu γCH), 30.4 (SCH$_2$CH$_2$$\underline{C}H_2$NH), 29.6 (Glu β$CH_2$), 27.3 (SCH$_2$$\underline{C}H_2CH_2$NH) ppm. **HRMS** (*m/z* ESI$^+$): found 408.155190 ([M+H]$^+$, $C_{14}H_{26}N_5O_7S$ requires 408.1547). $\boldsymbol{\nu_{max}}$ (film)/cm^{-1}: 3280 (N-H), 1644 (C=O).

_N_-((_R_)-3-(((_R_)-3-amino-3-carboxypropyl)thio)-1-((carboxymethyl)amino)-1-oxopropan-2-yl)-D-glutamine (68).

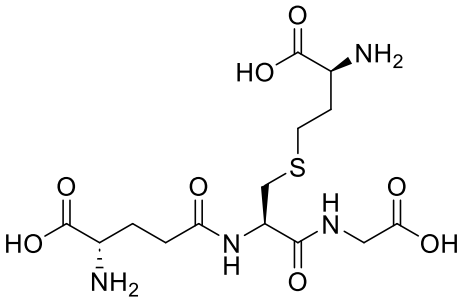

68 was prepared by radical mediated thiol-ene reaction of glutathione **48** and vinylglycine **60** as per **general procedure A** in batch (50%) and as per **general procedure B** under continuous flow (63%). The reaction mixture was washed with CH_2Cl_2 (2 x 50 mL) and aqueous layer was lyophilized prior to ^{1}H NMR spectroscopic analysis. **m.p.** 210-240 °C (dec.). **R_f** = 0.95 (H_2O:ACN, 7:3) reverse phase C_{18} TLC.**^{1}H NMR** (400 MHz, D_2O): δ 4.62 (dd, *J* = 8.4, 5.3 Hz, 1H, Cys αCH), 4.04-4.01 (m, 3H, Gly αCH_2 + SCH_2CH_2C<u>H</u>), 3.93 (t, *J* =6.3 Hz, 1H, Glu αCH), 3.11 (dd, *J* = 14.0, 5.3 Hz, 1H, Cys βCH_{2A}), 2.94 (dd, *J* = 14.0, 8.4 Hz, 1H, Cys βCH_{2B}), 2.75 (t, *J* = 7.5 Hz, 2H, Glu γCH_2), 2.63-2.54 (m, 2H, Glu βCH_2), 2.24-2.18 (m, 4H, SCH_2C<u>H</u>$_2$CH + S<u>C</u>H$_2$$CH_2$CH) ppm. **^{13}C NMR** (101 MHz, D_2O): δ 174.7 (C=O), 173.1 (C=O), 173.0 (C=O), 173.0 (C=O), 172.7 (C=O), 53.3 (Glu *α*CH), 53.0 (Cys *α*CH), 52.8 (SCH_2CH_2<u>C</u>H), 41.2 (Gly αCH), 32.5 (Cys *β*CH_2), 31.1 (Glu *β*CH_2), 29.9 (S<u>C</u>H$_2$$CH_2$CH), 27.0 (Glu *γ*$CH_2$), 25.8 (S$CH_2$<u>C</u>H$_2$CH) ppm. **HRMS** (*m/z* ESI^+): found 409.1389 ($[M+H]^+$, $C_{14}H_{25}N_4O_8S$ requires 409.1387). **ν_{max}** (film)/cm^{-1}: 2924 (CH_2), 1725 (C=O), 1635 (C=O), 1217 (C-O).

(*S*)-5-(((*S*)-6-amino-1-(((*S*)-1-amino-1-oxopropan-2-yl)amino)-1-oxohexan-2-yl)amino)-4-((*S*)-2-((*R*)-2-amino-3-mercaptopropanamido)-5-guanidinopentanamido)-5-oxopentanoic acid (**77**).

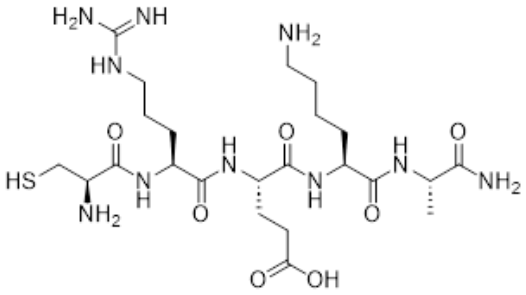

Peptide **77** was prepared as per **general procedure E** utilising Rink amide resin (20 mg, 156 µmoles), Fmoc-Ala-OH, Fmoc-Lys(Boc)-OH, Fmoc-Glu(O^{t}Bu)-OH, Fmoc-Arg(Pbf) and Fmoc-Cys(Trt)-OH. **77** was afforded as a fluffy white solid (60.4 mg, 64%, >95% purity). **m.p.** 202-212 °C (dec.). **Retention time:** 1.62 min (5 - 95% ACN, 20 min 0.1% TFA, λ = 214 nm). **HRMS** (*m/z* ESI$^+$): found 605.3174 ([M+H]$^+$, $C_{23}H_{45}N_{10}O_7S$ requires 605.3188). ν_{max} (film)/cm^{-1}: 3305 (O-H, N-H), 1667 (C=O), 1202 (C-N).

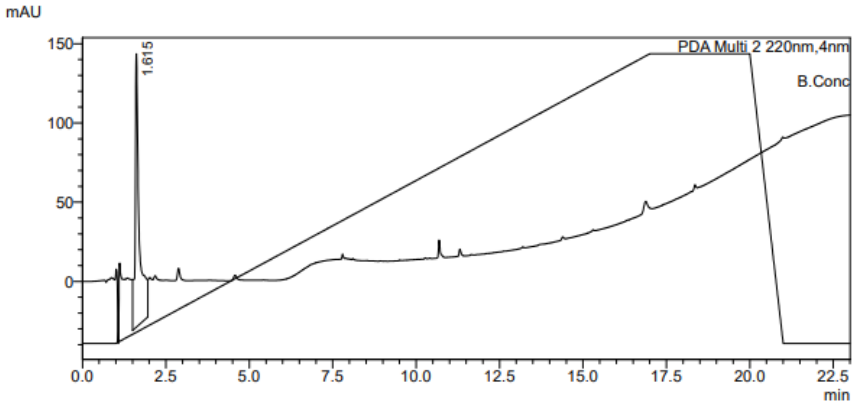

(*S*)-5-(((*S*)-6-amino-1-(((*S*)-1-amino-1-oxopropan-2-yl)amino)-1-oxohexan-2-yl)amino)-4-((*S*)-2-((*R*)-2-amino-3-((3-(((2R,3R,4S,5R,6R)-3,4,5-trihydroxy-6-(hydroxymethyl)tetrahydro-2H-pyran-2-yl)oxy)propyl)thio)propanamido)-5-guanidinopentanamido)-5-oxopentanoic acid (78)

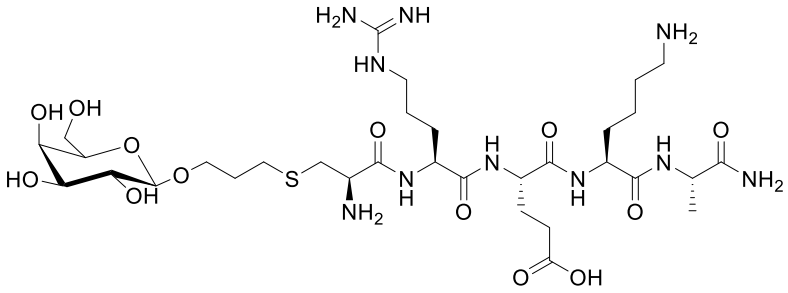

A solution of CREKA peptide **77** (10 mg, 16.5 µmol), alkene **53** (72.8 mg, 0.33 mmol) and photoinitiator **16** (9 mg, 41.3 µmol) in H_2O in 0.1% FA (2 mL) was pumped at 500 µL min^{-1} with 20 mm syringe diameter through the coil reactor at rt under UV irradiation (352 nm, 110 V). Residence time was 120 min. Solvent was removed *in vacuo*. Glycosylated peptide **23** was purified by analytical RP-HPLC (C_{18}, 100 Å x 4.6 mm, 5 µm LC column). Glycosylated peptide **78** was as a flyffly white solid (6.02 mg, 44%). **Retention time:** 10.14 min (5 - 95% MeOH, 20 min 0.1% TFA, λ = 220 nm). **HRMS** (*m/z* ESI^+): found 825.4111 ($[M+H]^+$, $C_{32}H_{61}N_{10}O_{13}S$ requires 825.4135). ν_{max} (film)/cm^{-1}: 3325 (O-H, N-H), 1657 (C=O), 1050 (C-O).

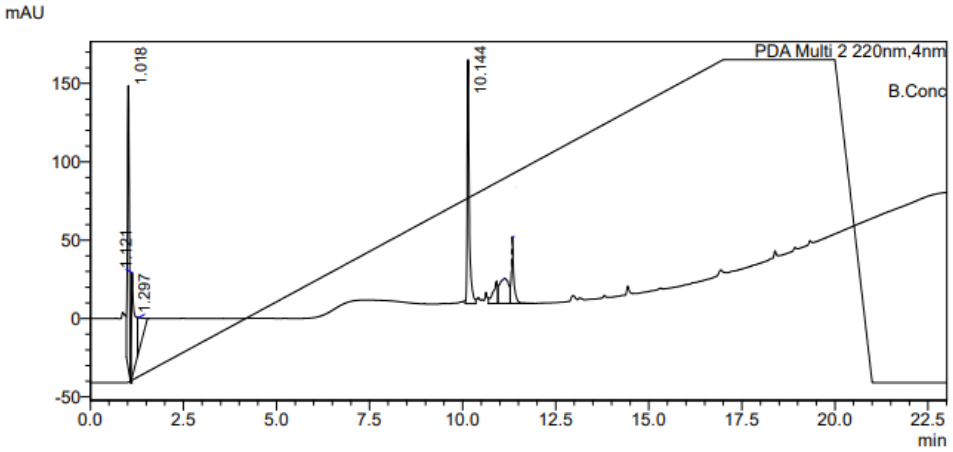

(S)-2-((2S,5S,8S,11S,14R)-14-amino-5,11-bis(4-aminobutyl)-8-(4-hydroxybenzyl)-15-mercapto-2-methyl-4,7,10,13-tetraoxo-3,6,9,12-tetraazapentadecanamido)pentanediamide (79)

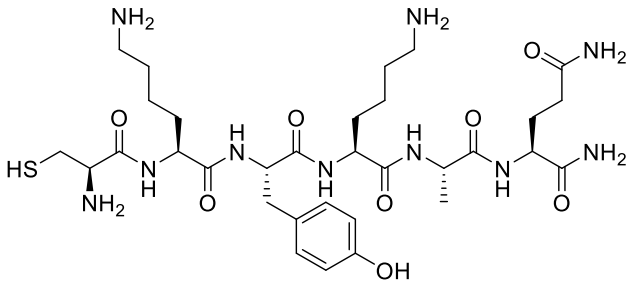

AFP peptide **79** was prepared as per **general procedure E** utilising Fmoc-Gln(trt)-OH, Fmoc-Ala OH, Fmoc-Lys(Boc)-OH, Fmoc-Tyr(tBu)-OH, (x 2), Lys(Boc)-OH and Fmoc-Cys(Trt)-OH. Peptide **79** was afforded as a fluffy white solid. **m.p**: 220-224 °C (dec.). **Retention time:** 14.50 min (2 - 60% ACN, 20 min 0.1% TFA, λ = 254 nm). **HRMS** (*m/z* ESI^{+}): found 739.3925 ([M+H]$^{+}$, $C_{32}H_{55}N_{10}O_8S$ requires 739.3920). ν_{max} (film)/cm^{-1}: 3280 (O-H, N-H), 1675 (C=O), 1625 (C=C), 1457 (C-H), 1202 (C-N), 1138 (C-N), 1024 (C-O), 694 (C=C).

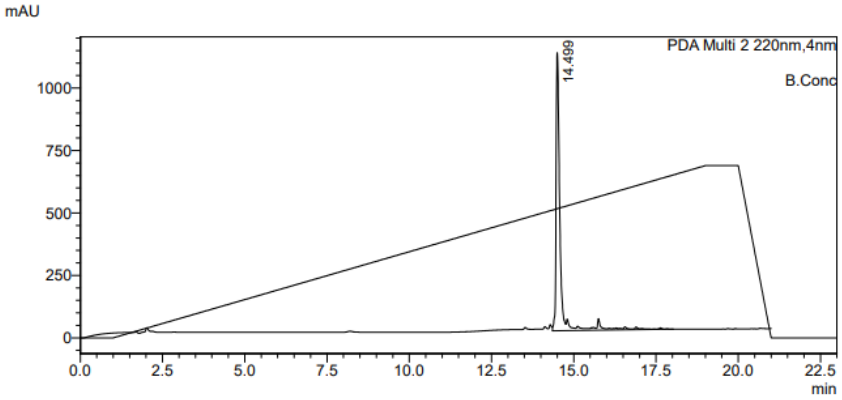

(S)-2-((2S,5S,8S,11S,14R)-14-amino-5,11-bis(4-aminobutyl)-8-(4-hydroxybenzyl)-2-methyl-4,7,10,13-tetraoxo-19-(((2R,3R,4S,5R,6R)-3,4,5-trihydroxy-6-(hydroxymethyl)tetrahydro-2H-pyran-2-yl)oxy)-16-thia-3,6,9,12-tetraazanonadecanamido)pentanediamide (80)

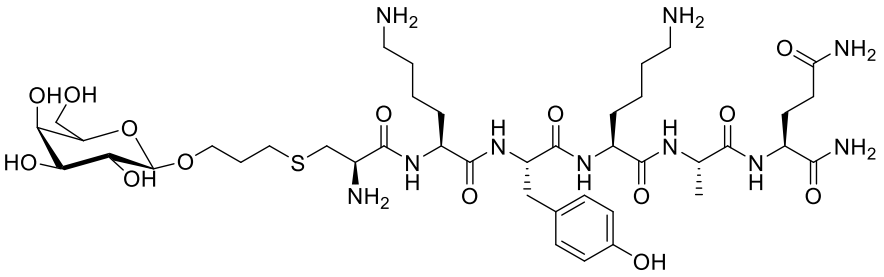

A solution of AFP peptide **79** (10 mg, 13.5 µmol), alkene **53** (0.27 mmol) and photoinitiator **16** (2.5 equiv., 33.8 µmol) in H_2O in 0.1% FA (2 mL) was pumped at 500 µL min^{-1} with 20 mm syringe diameter through the coil reactor at rt under UV-light irradiation (352 nm, 110 V). Residence time was 120 min. Solvent was removed *in vacuo*. Glycosylated peptide **25** was purified by analytical RP-HPLC (C_{18}, 100 Å x 4.6 mm, 5 µm LC column). Glycosylated peptide **25** was afforded as a fluffy white solid (7.4 mg, 58%). **Retention time:** 14.94 min (5 - 95% ACN, 20 min 0.1% TFA, λ = 220 nm). **HRMS** (*m/z* ESI^+): found 480.2477 ($[M+2H]^{2+}$, $C_{41}H_{72}N_{10}O_{14}S$ requires 480.2470). **ν_{max}** (film)/cm^{-1}: 3354 (O-H), 1672(C=O), 1033 (C-O).

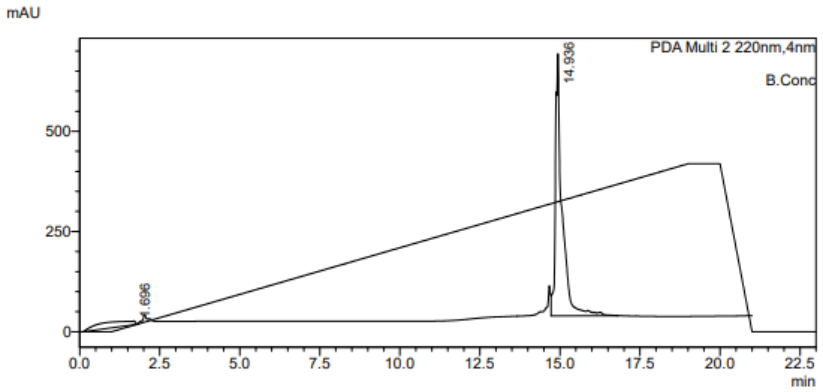

(3S,6S,9S,12S,15S)-3-((3S,6S,9S,12S)-1-((2S)-1-(5-(((2S,3R,4R,5S,6R)-3-acetamido-4,5-dihydroxy-6-(hydroxymethyl)tetrahydro-2H-pyran-2-yl)thio)-2-aminopentanoyl)pyrrolidin-2-yl)-3-(3-amino-3-oxopropyl)-12-(3-guanidinopropyl)-

9-((R)-1-hydroxyethyl)-6-isopropyl-1,4,7,10,13-pentaoxo-2,5,8,11,14-pentaazahexadecan-16-amido)-15-((2-amino-2-oxoethyl)carbamoyl)-9-benzyl-12-((R)-1-hydroxyethyl)-6-isopropyl-4,7,10,13-tetraoxo-5,8,11,14-tetraazaoctadecanedioic acid (85)

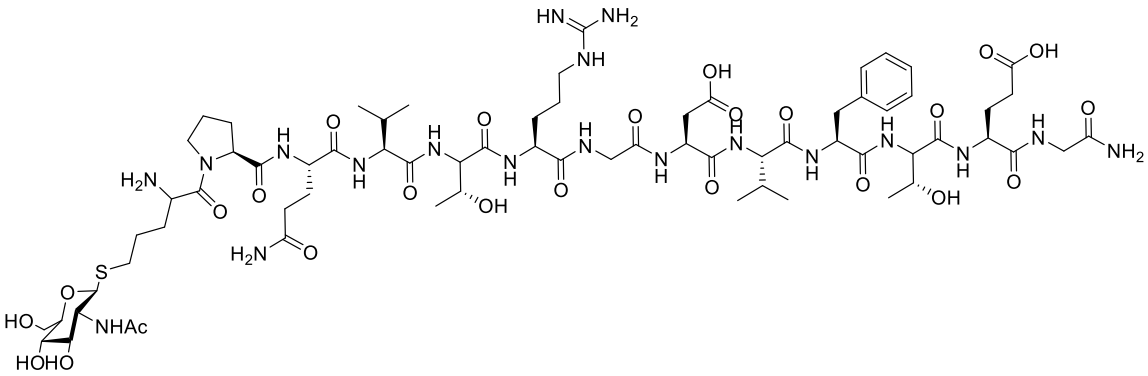

A solution of RGD peptide **81** (10 mg, 3.57 µmol), thiol **84** (4.23 mg, 0.017 mmol) and photoinitiator **16** (2.5 equiv., 8.93 µmol) in DES: H_2O (EG:H_2O) (3:2, 1.5 mL) was pumped at 500 µL min^{-1} with 20 mm syringe diameter through the coil reactor at room temperature under UV irradiation (352 nm, 110 V). Residence time was 120 min. Solvent was removed *in vacuo*. Glycosylated peptide **28** was diluted in H_2O (2 mL) and purified by analytical RP-HPLC (C_{18}, 100 Å x 4.6 mm, 5 µm LC column). Glycosylated peptide **85** was afforded as a fluffy white solid (3.60 mg, 62%). **Retention time:** 9.13 min (5 - 95% ACN, 20 min 0.1% TFA, λ = 220 nm). **HRMS** (*m/z* ESI^+): found 819.8945 ($[M+2H]^{2+}$, $C_{69}H_{113}N_{19}O_{25}S$ requires 819.8932). **ν_{max}** (film)/cm^{-1}: 3270 (O-H, N-H), 1625 (C=O), 1528 (C=C benzene), 1425 (O-H carboxylic) acid), 1200 (C-N), 1133 (C-O), 800 (C=C).

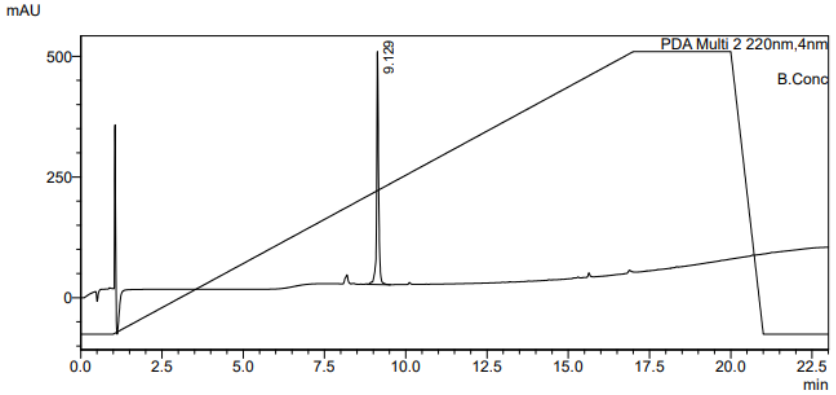

7.3 Experimental details for Chapter 3

7.3.1 General procedures

General procedure G, Sugar propargylation. Peracetylated sugar (1 equiv.) was dissolved in dry CH_2Cl_2 (15 mL). To the mixture was added $BF_3{\cdot}OEt_2$ (1.1 equiv.). The mixture was stirred for 1 h prior to addition of the propargyl alcohol (1.5 equiv.). The mixture was left stirring at rt for 3.5 h after which time the reaction was quenched by addition of sat. aq. $NaHCO_3$ solution (20 mL). After stirring for 30 min, the mixture was washed three times with H_2O (3 × 20 mL). The organic layer was dried over $MgSO_4$, filtered and concentrated *in vacuo*. Purification by flash column chromatography.

General procedure H, Sugar acetyl deprotection. A round bottom flask was charged with the corresponding peracetyl sugars and was dissolved in MeOH/NEt_3 (4:1) and heated at reflux for 18 h. The solution was cooled down to rt and DOWEX(H+) 50WX8-200 resin was then added to the flask until pH = 5 was achieved. The resin was then filtered off and the solvent was evaporated *in vacuo* to yield a light red solid. The crude product was then titrated with CH_2Cl_2 (20 mL) and redissolved in MeOH. Finally, the solvent was removed *in vacuo*.

General procedure I, Disulfide rebridging *via* TYC chemistry. Disulfide (1 equiv.) and TCEP (1 equiv.) were dissolved in H_2O + 0.1% FA and stirred for 15 min. Then, DPAP (1 equiv.), MAP (1.equiv.) and the corresponding alkyne (1 equiv.) were dissolved in MeCN:H_2O (1:1) + 0.1% FA and added to the previous mixture. The mixture was introduced to a UV-oven and stirred for 1 h. After this time, a second equiv. of the corresponding alkyne was added and stirred for 1 h. The crude product was analysed and purified by RP-HPLC (C_{18}, 100 Å x 4.6 mm, 5 μm LC column).

7.3.2 Characterisation data

(R)-2-amino-N-((S)-1-(((S)-1-((2-(((R)-1-amino-3-mercapto-1-oxopropan-2-yl)amino)-2-oxoethyl)amino)-3-(4-hydroxyphenyl)-1-oxopropan-2-yl)amino)-1-oxopropan-2-yl)-3-mercaptopropanamide. (88)

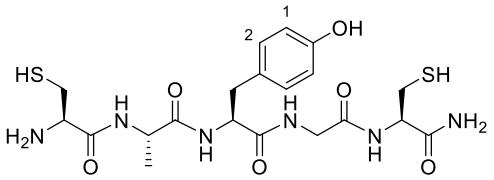

Peptide **88** was prepared as per general **procedure E** utilising Fmoc-Cys(trt)-OH, Fmoc-Ala-OH, Fmoc-Tyr(tBu)-OH, Fmoc-Gly-OH and Fmoc-Cys(Trt)-OH. Peptide **88** was obtained as a fluffy white solid (150 mg, 90%, >95% purity). **m.p**: 171-175°C (dec.). **^{1}H NMR** (600 MHz, DMSO-d_6) δ 9.17 (s, 1H, Ar O<u>H</u>), 8.60 (t, *J* = 5.7 Hz, 1H, Gly NH), 8.35 (d, *J* = 7.0 Hz, 1H, Ala NH), 8.22 (d, *J* = 8.2 Hz, 1H, Tyr NH), 7.87 (d, *J* = 7.9 Hz, 1H, Cys NH), 7.40 (s, 1H, CON<u>H</u>$_2$), 7.22 (s, 1H, CON<u>H</u>$_2$), 7.04 (d, *J* = 8.5 Hz, 2H, Ar H2), 6.64 (d, *J* = 8.5 Hz, 2H, Ar H1), 4.48 (ddd, *J* = 9.9, 8.2, 4.0 Hz, 1H, Tyr CαH), 4.33 (td, *J* = 7.5, 5.0 Hz, 1H, Cys Cα<u>H</u> CONH$_2$), 4.30-4.25 (m, 1H, Ala CαH), 4.00 (t, *J* = 5.3 Hz, 1H, Cys CαH), 3.78 (d, *J* = 5.7 Hz, 2H, Gly CH$_2$), 2.94 (ddd, *J* = 15.0, 10.9, 4.9 Hz, 2H, Cys CH$_{2A}$ + Tyr CH$_{2A}$), 2.86 (dd, *J* = 14.5, 5.0 Hz, 1H, Cys CH$_{2B}$), 2.83–2.71 (m, 2H, Cys C<u>H</u>$_2$ CONH$_2$), 2.65-2.61 (m, 1H, Tyr CH$_{2B}$), 2.22 (s, 1H, Cys S<u>H</u> CONH$_2$), 1.25 (d, *J* = 7.0 Hz, 3H, Ala CH$_3$) ppm. **^{13}C NMR** (151 MHz, DMSO) δ 172.0 (Ala C=O), 171.3 (Cys CONH$_2$ C=O), 171.2 (Tyr C=O), 168.0 (Gly C=O), 167.0 (Cys C=O) , 155.8 (Ar <u>C</u>-OH), 130.1 (Ar <u>C</u>H$_2$), 127.7 (Ar <u>C</u>-CH$_2$), 114.8 (Ar <u>C</u>H1), 54.4 (Cys CαH CONH$_2$), 54.2 (Tyr CαH), 53.8 (Cys CαH), 48.5 (Ala CαH), 41.7 (Gly CαH), 36.8 (Tyr CH$_2$), 26.2 (Cys CH$_2$ CONH$_2$), 25.3 (Cys CH$_2$), 17.7 (CH3) ppm. **Retention time:** 7.87 min (5-95% ACN, 20 min 0.1% TFA, λ = 220 nm). **HRMS** (*m/z* ESI$^+$): found 515.1750 ([M+H]$^+$, $C_{32}H_{55}N_{10}O_8S$ requires 515.1741). **ν_{max}** (film)/cm^{-1}: 3310 (N-H, OH), 1668 (C=O), 1025 (C-O).

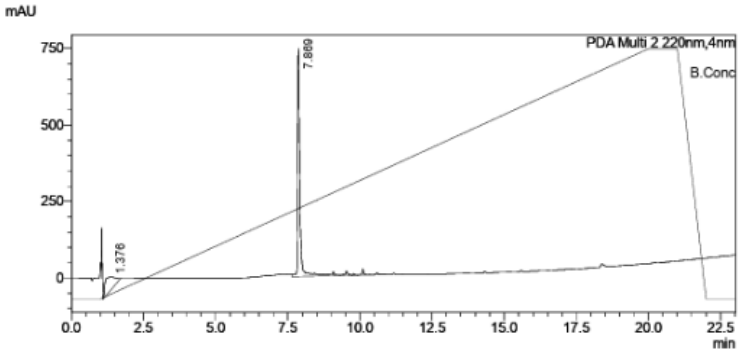

(4R,10S,13S,16R)-16-amino-10-(4-hydroxybenzyl)-13-methyl-6,9,12,15-tetraoxo-1,2-dithia-5,8,11,14-tetraazacycloheptadecane-4-carboxamide (89).

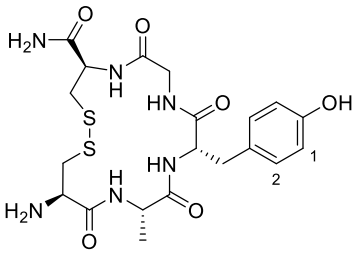

Peptide **89** (20 mg, 38.9 µmoles) was dissolved in 20 mL of MeCN:H_2O (1:1) + 0.1% FA and 10% DMSO at rt for 48 h.[239, 249] The crude peptide was purified by semi-preparative RP-HPLC (C_{18} Φ4.6 × 250 mm column, 1 mL min^{-1} flow rate). Peptide **89** was obtained as a fluffy white solid (9 mg, 46%). **m.p**: 200-202 °C (dec.). **^{1}H NMR** (600 MHz, DMSO-d_6) δ 9.24 (s, 1H, Ar O<u>H</u>), 8.44 (dd, *J* = 7.6, 4.0 Hz, 1H, Gly NH), 8.34 (s, 2H, Cys NH_2), 8.27 (d, *J* = 6.0 Hz, 1H, Tyr NH), 8.06 (d, *J* = 6.6 Hz, 1H, Ala NH), 7.89 (d, *J* = 8.5 Hz, 1H, Cys N<u>H</u> $CONH_2$), 7.26 (s, 1H, CON<u>H</u>$_2$), 7.24 (s, 1H, CON<u>H</u>$_2$), 7.01 (d, *J* = 8.5 Hz, 2H, Ar H1), 6.67 (d, *J* = 8.5 Hz, 2H, Ar H2), 4.34 (app. dt, *J* = 8.5, 4.3 Hz, 1H, Cys CαH $CONH_2$), 4.13 (app. dt, *J* = 8.4, 6.0 Hz, 1H, Tyr CαH), 4.09-4.06 (m, 1H, Ala CαH), 4.03-3.99 (m, 2H, Cys CαH + Gly CH_{2A}), 3.68 (dd, *J* = 15.6, 4.0 Hz, 1H, Gly CH_{2B}), 3.25 (dd, *J* = 13.8, 5.6 Hz, 1H, Cys CH_{2A}), 3.20 (dd, *J* = 13.3, 4.3 Hz, 1H, Cys CH_{2A} $CONH_2$), 3.13 (dd, *J* = 13.8, 6.7 Hz, 1H, Cys CH_{2B}), 3.06 (dd, *J* = 13.3, 9.4 Hz, 1H, Cys CH_{2B} $CONH_2$), 2.91 (dd, *J* = 14.1, 6.0 Hz, 1H, Tyr CH_{2A}), 2.88 (dd, *J* = 14.1, 8.4 Hz, 1H, Tyr CH_{2B}), 1.24 (d, *J* = 7.1, Ala CH_3) ppm. **^{13}C NMR** (151 MHz, DMSO) δ 171.9 (Gly CO), 171.4 (CONH2), 171.2 (Tyr CO), 169.1 (Gly CO),167.3 (Cys CO), 156.0 (Ar <u>C</u>-OH), 130.0 (Ar <u>C</u>H1), 126.9 (Ar <u>C</u>-CH_2), 115.0 (Ar <u>C</u>H2), 56.6 (Tyr CαH), 52.6 (Cys CαH $CONH_2$), 52.2 (Cys CαH), 49.2 (Ala CαH), 42.3 (Gly CαH), 40.7 (Cys CH_2 $CONH_2$), 40.0 (Cys CH_2),

35.8 (Tyr CH_2), 16.8 (Ala CH_3) ppm. **Retention time:** 7.15 min (5-95% ACN, 20 min 0.1% TFA, λ = 220 nm). **HRMS** (*m/z* ESI^+): found 513.1586 ($[M+H]^+$, $C_{32}H_{55}N_{10}O_8S$ requires 513.1584). ν_{max} (film)/cm^{-1}: 3348 (N-H, O-H), 1643 (C=O), 1434 (C-H), 1195 (C-O), 723 (Ar).

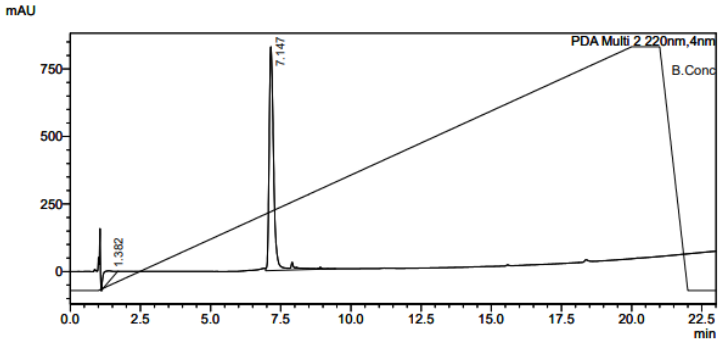

(R)-2-amino-N-((2S,5S,11R)-11-carbamoyl-16-hydroxy-5-(4-hydroxybenzyl)-3,6,9-trioxo-13-thia-4,7,10-triazahexadecan-2-yl)-3-((3-hydroxypropyl)thio)propenamide (90).

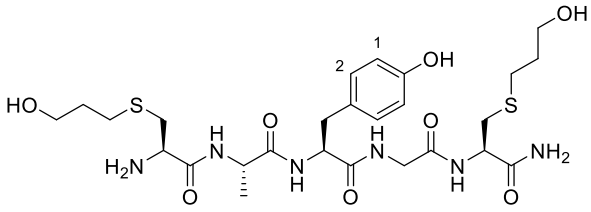

A solution of peptide **88** (5 mg, 9.72 µmoles), allyl alcohol **49** (13.22 µL, 11.29 mg, 194 µmoles) and photoinitiator **16** (5.4 mg, 24.3 µmoles) in H_2O in 0.1% FA (2 mL). Crude mixture was stirred and irradiated for 1 h under UV-light irradiation. The crude peptide was purified by semi-preparative RP-HPLC (C_{18} Φ4.6 × 250 mm column, 1 mL min^{-1} flow rate). Peptide **90** was obtained as fluffy white solid. **^{1}H NMR** (400 MHz, DMSO-d_6) δ 9.17 (s, 1H, Ar OH), 8.63 (s, 1H, Gly NH), 8.32 (d, *J* = 7.1 Hz, 1H, Ala NH), 8.19 (d, *J* = 8.3 Hz, 1H, Tyr NH), 7.87 (d, *J* = 8.1 Hz, 1H, Cys N<u>H</u> $CONH_2$), 7.44 (s, 1H, $CON\underline{H}_2$, 7.20 (s, 1H, $CON\underline{H}_2$), 7.05 (d, *J* = 8.6 Hz, 2H, Ar H1), 6.65 (d, *J* = 8.6 Hz, 2H. Ar H2), 4.53-4.46 (m, 1H, Tyr CαH), 4.35-4.27 (m, 2H, Ala CαH + Cys CαH $CONH_2$), 3.91-3.85 (m, 2H, Cys CαH + Gly $C\alpha H_{2A}$), 3.64 (dd, *J* = 16.8, 5.0 Hz, 1H, Gly $C\alpha H_{2B}$), 3.47-3.44 (m, 4H, $HOCH_2CH_2C\underline{H}_2S$), 2.97-2.88 (m, 2H, Cys CH_{2A} +Tyr CH_{2A}), 2.83 (dd, *J* = 13.6, 5.8 Hz, 1H, Cys CH_{2A} $CONH_2$), 2.76-2.66 (m, 3H, Tyr CH_{2B} + Cys CH_{2B} + Cys CH_{2B} $CONH_2$), 2.61-2.55 (m, 4H, $HOC\underline{H}_2CH_2CH_2S$), 1.69-1.63 (m, 4H, $HOCH_2C\underline{H}_2CH_2S$), 1.20 (d, *J* = 7.4 Hz, 3H, Ala CH_3) ppm. **^{13}C NMR** (151 MHz, DMSO)

δ 172.0 (Cys $CONH_2$), 171.9 (Gly C=O), 171.2 (Cys C=O), 167.8 (Ala C=O), 155.8 (Ar C-OH), 130.2 (C1), 127.9 (Ar C-CH_2), 114.9 (C2), 59.4 ($HOCH_2CH_2CH_2S$), 54.1 (Tyr CαH), 52.2 (Cys CαH $CONH_2$), 51.6 (Cys CαH), 48.5 (Ala CαH), 41.8 (Gly CH_2), 36.9 (Cys CH_2), 33.5 (Cys CH_2 $CONH_2$), 32.3 ($HOCH_2CH_2CH_2S$), 28.9 (Tyr CH_2), 27.7 ($HOCH_2CH_2CH_2S$), 18.0 (CH_3) ppm. **Retention time:** 8.91 min (5-70% ACN, 20 min 0.1% TFA, λ = 220 nm). **HRMS** (*m/z* ESI^+): found 631. 2582 ($[M+H]^+$, $C_{32}H_{55}N_{10}O_8S$ requires 631.2578).

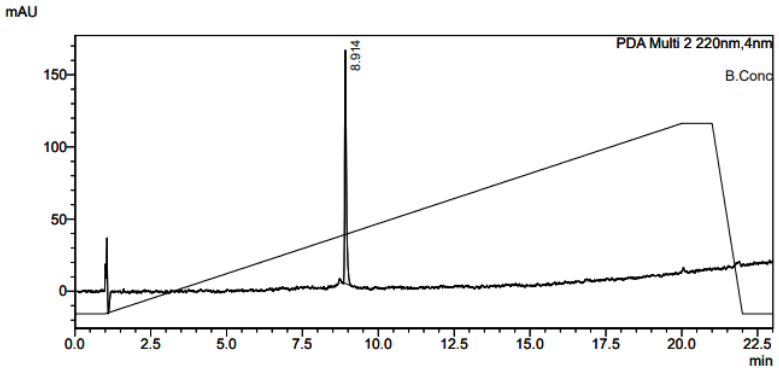

(6R,12S,15S,18R)-18-amino-12-(4-hydroxybenzyl)-3-(hydroxymethyl)-15-methyl-8,11,14,17-tetraoxo-1,4-dithia-7,10,13,16-tetraazacyclononadecane-6-carboxamide (92a/b).

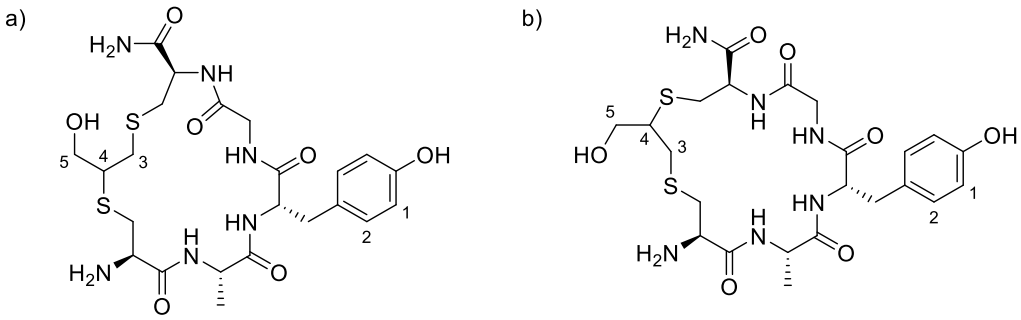

Peptide **92a/b** was prepared as per general **procedure I** (>95%). **89** (5 mg, 9.72 µmoles), propargyl alcohol **91** (2 µL, 2.18 mg, 38.86 µmoles), DPAP (1.25 mg, 4.86 µmoles) and MAP (0.8 mg, 4.86 µmoles) were dissolved in H_2O + 0.1% FA (1 mL). Peptide **92** was isolated as a mixture of **a** and **b** isomers, obtained as a fluffy white solid (0.7 mg, 13%). **^{1}H NMR** (600 MHz, DMSO-d_6) δ 9.25 (s, 1H, Ar OH), 8.47 (s, 1H, Gly NH), 8.34 (s, 1H, Tyr NH), 8.11 (d, *J* = 6.6 Hz, 1H, Ala NH), 7.86 (s, 1H, Cys $CONH_2$ NH), 7.27 (s, 1H, NH_{2A}), 7.23 (s, 1H, NH_{2B}), 7.17 (s, 1H, $CONH_{2A}$), 7.08 (s, 1H, $CONH_{2B}$), 6.99 (d, *J* = 8.5 Hz, 2H, Ar H1), 6.65 (d, *J* = 8.5 Hz, 2H, Ar H2), 5.23 (d, *J* = 3.6 Hz, 1H, CH_2OH),

4.32 (td, J = 8.8, 4.3 Hz, 1H, Cys CαH $CONH_2$), 4.11 (dt, J = 8.3, 6.0 Hz, 1H, Tyr CαH), 4.07-4.03 (m, 1H, Ala CαH), 4.00-3.96 (m, 1H, H4), 3.93 (d, J = 16.8 Hz, 1H, Gly $C\alpha H_A$), 3.69 (d, J = 16.8 Hz, 1H, Gly $C\alpha H_B$), 3.23-3.19 (m, 1H, Cys $CH_{2A}CONH_2$), 3.17 (dd, J = 13.5, 4.2 Hz, 1H, $H3_A$), 3.10 (dd, J = 13.5, 6.6 Hz, 1H, $H3_B$), 3.07-3.01 (m, 3H, Cys $CH_{2B}CONH_2$ + Cys CαH + $H5_A$), 2.90-2.87 (m, 2H, Tyr CH_2), 2.85-2.81 (m, 1H, Cys CH_{2A}), 2.75-2.70 (m, 12H, Cys CH_{2B}+ $H5_B$), 1.20 (d, J = 7.0 Hz, 3H, Ala CH_3) ppm. **Retention time:** 7.457 min (5-95% ACN, 20 min 0.1% TFA, λ = 220 nm). **HRMS** (*m/z* ESI^+): found 571.1989 ($[M+H]^+$, $C_{23}H_{35}N_6O_7S_2$ requires 571.2003).

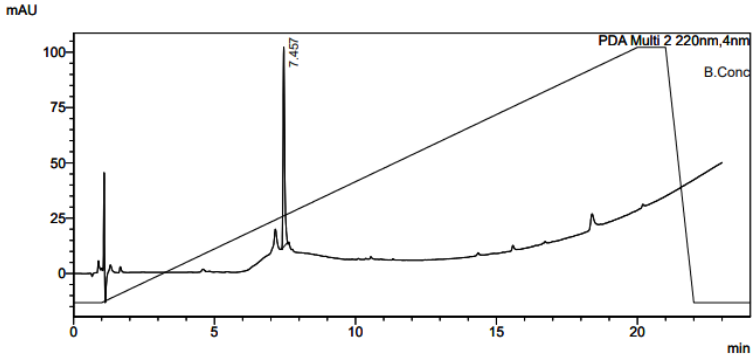

3-((6R,12S,15S,18R)-18-amino-6-carbamoyl-12-(4-hydroxybenzyl)-15-methyl-8,11,14,17-tetraoxo-1,4-dithia-7,10,13,16-tetraazacyclononadecan-3-yl)propanoic acid (105a/b).

a)

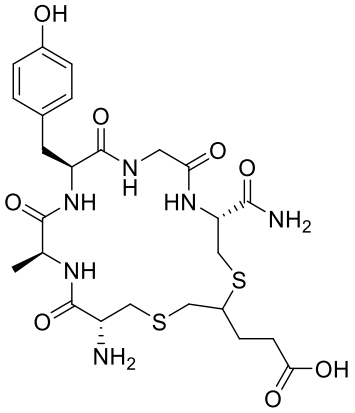

b)

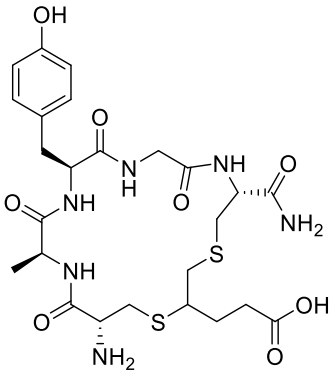

Peptide **105a/b** was prepared as per general **procedure I** (>95%). **89** (3 mg, 5.85 µmoles), 4-pentynoic acid **95** (0.5 mg, 5.85 µmoles), TCEP (2.2 mg, 8.78 µmoles), DPAP (1.50 mg, 5.85 µmoles) and MAP (0.88 mg,5.85 µmoles) were dissolved in H_2O + 0.1% FA (1 mL). **Retention time** (mixture of **a** and **b** isomers)**:** 6.984 min (5-95% ACN, 20 min 0.1%

TFA, λ = 220 nm). **HRMS** (*m/z* ESI$^+$): found 613.2117 ([M+H]$^+$, $C_{25}H_{37}N_6O_8S_2$ requires 613.2109).

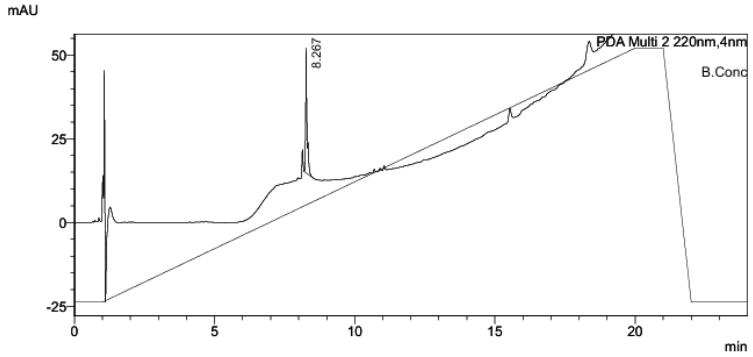

Propargyl-2,3,4,6-tetra-O-acetyl-β-D-galactopyranoside (101)

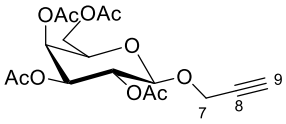

Protected monosaccharide **101** was prepared as per general procedure **G**. Peracetylated galactose (3.00 g, 7.70 mmol), $BF_3{\cdot}OEt_2$ (4.72 mL, 38.50 mmol) and propargyl alcohol **91** (1.84 mL, 30.80 mmol) were dissolved in dry CH_2Cl_2 (20 mL). Purification by flash column chromatography using Hex/EtOAc (6:4) as eluent afforded the product **101** (1.98 g, 67%) as a clear colourless syrup. The isolated product was in good agreement with literature.[250] **R_f :** 0.8 (Hex:EtOAc, 6:4). **^{1}H NMR** (400 MHz, $CDCl_3$) δ 5.46 (dd, *J* = 3.5, 1.4 Hz, 1H, H4), 5.35 (dd, *J* = 10.9, 3.8 Hz, 1H, H2), 5.31 (d, *J* = 3.8 Hz, 1H, H1), 5.16 (dd, *J* = 10.9, 3.5 Hz, 1H, H3), 4.27 (d, *J* = 2.4 Hz, 2H, H7), 4.25-4.23 (m, 1H, $H6_A$), 4.10-4.09 (m, 2H, $H6_B$, H5), 2.45 (t, *J* = 2.4 Hz, 1H, H9), 2.14 (s, 3H, OAc), 2.08 (s, 3H, OAc), 2.04 (s, 3H, OAc), 1.98 (s, 3H, OAc) ppm. **HRMS** (*m/z* ESI$^+$): found 409.1109 ([M+Na]$^+$, $C_{17}H_{22}NaO_{10}$ requires 409.1105).

Propargyl-β-D-galactopyranoside (96)

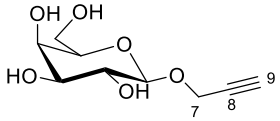

Monosaccharide **96** was prepared as per general procedure **H** with **101** (1.98 g, 5.12 mmol). Reaction was monitored by TLC (Hex/EtOAc (6:4)) indicated complete consumption of starting material (**R_f** = 0.8, Hex:EtOAc, 6:4) and formation of a single

product (R_f = 0, Hex:EtOAc, 6:4). The compound **96** was obtained as a white solid (0.91 mg, 82%). The isolated product was in good agreement with literature.[250] **^{1}H NMR (400 MHz, MeOD$_4$) δ** 4.39-4.37 (m, 3H, H7 +H1), 3.80 (dd, *J* = 3.0, 1.1 Hz, 1H, H2), 3.72-3.69 (m, 3H, H6 + H4), 3.50–3.43 (m, 2H, H3, H5), 2.82 (t, *J* = 2.4 Hz, 1H, H9) ppm. **HRMS** (*m/z* ESI$^+$): found 241.0681 ([M+Na]$^+$, $C_9H_{14}NaO_6$ requires 241.0682).

(6R,12S,15S,18R)-18-amino-12-(4-hydroxybenzyl)-15-methyl-8,11,14,17-tetraoxo-2-((((2R,3R,4S,5R,6R)-3,4,5-trihydroxy-6-(hydroxymethyl)tetrahydro-2H-pyran-2-yl)oxy)methyl)-1,4-dithia-7,10,13,16-tetraazacyclononadecane-6-carboxamide (106a/b)

a)

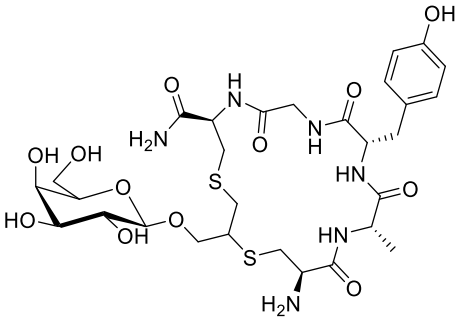

b)

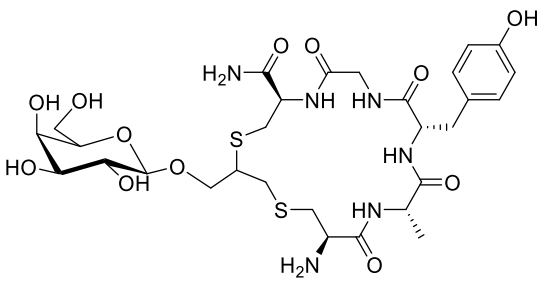

Peptide **106a/b** was prepared as per general **procedure I** (72%). Disulfide **88** (3 mg, 5.85 µmoles), sugar **96** (1.28 mg, 5.85 µmoles), TCEP (2.2 mg, 8.78 µmoles), DPAP (1.50 mg, 5.85 µmoles) and MAP (0.88 mg,5.85 µmoles) were dissolved in H_2O + 0.1% TFA (1 mL). **Retention time** (mixture of **a** and **b** isomers)**:** 8.267 min (5-95% ACN, 20 min 0.1% TFA, λ = 220 nm). **HRMS** (*m/z* ESI$^+$): found 733.2527 ([M+H]$^+$, $C_{29}H_{45}N_6O_{12}S_2$ requires 755.2351).

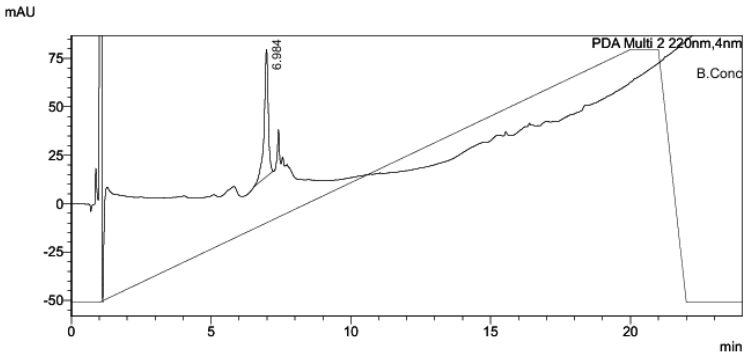

Propargyl β-D-2,3,4,6-tetra-O-acetylgalactopyranosyl-[1->4]-2,3,6-tri-O-acetyl-β-D-glucopyronoside (102)

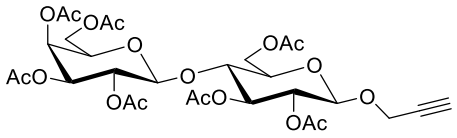

Protected monosaccharide **102** was prepared as per general procedure **G**. Peracetylated lactose (4 g, 5.89 mmol), $BF_3{\cdot}OEt_2$ (678 µL, 0.92 g, 6.48 mmol) and propargyl alcohol **91** (514 µL, 0.5 g, 8.84 mmol) were dissolved in dry CH_2Cl_2 (15 mL). Purification by flash column chromatography using Hex/Acetone (5:5) as eluent afforded the product **102** (1.6 g, 27%) as a crystalline solid. The isolated product was in good agreement with literature.[250, 326] **m.p:** 78-80 °C (Lit. m.p: 80-82 ºC). **R_f:** 0.75 **(**Hex/Acetone (5:5)). **^{1}H NMR** (400 MHz, $CDCl_3$) δ 6.16 (d, *J* = 3.7 Hz, 1H, $H4_B$), 5.39–5.34 (m, 1H, $H5_B$), 5.27–5.25 (m, 1H, $H3_A$), 5.14 (app. t, *J* = 9.3 Hz, 1H, $H3_B$), 5.02 (td, *J* = 10.4, 8.0 Hz, 2H, $H2_A$), 4.92 (d, *J* = 3.7 Hz, 1H, $H3_B$), 4.88 (app. td, *J* = 10.4, 3.4 Hz, 1H, $H4_A$), 4.82 (dd, *J* = 9.3, 8.0 Hz, 1H, $H2_B$), 4.66 (d, *J* = 8.0 Hz, 1H, $H1_B$), 4.44 (dd, *J* = 8.0, 1.7 Hz, 1H, $H1_A$), 4.37–4.34 (m, 1H, $H6'_A$), 4.25 (d, *J* = 2.4 Hz, 2H, H7), 4.09–3.98 (m, 4H, $H6_A$, $H6_B$, $H5'_A$), 3.86-3.81 (m, 1H, $H5_A$), 3.75 (td, *J* = 9.5, 3.1 Hz, 1H, $H4_B$), 3.57 (ddd, *J* = 9.8, 5.0, 2.0 Hz, 1H, $H5_B$), 2.42 (t, *J* = 2.4 Hz, 1H, H9) ppm. **HRMS** (*m/z* ESI^+): found 697.1958 ($[M+Na]^+$, $C_{29}H_{38}NaO_{18}$ requires 697.1950).

Propargyl β-D-galactopyranosyl-[1->4]-β-D-glucopyranoside (97)

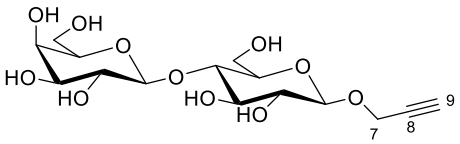

Monosaccharide **97** was prepared as per general procedure **H** with sugar **102** (1.98 g, 5.12 mmol). Reaction was monitored by TLC (Hex/Acetone (5:5)) indicated complete consumption of starting material (R_f = 0.53) and formation of a single product (R_f = 0). The compound **97** was obtained as a brown solid (0.36 mg, 64%). The isolated product was in good agreement with literature.[250, 326] **R_f:** 0 **(**Hex/Acetone (5:5). **^{1}H NMR** (400 MHz, $MeOD_4$) δ 4.52 (d, *J* = 7.8 Hz, 1H, $H2_A$), 4.44 (d, *J* = 2.4 Hz, 2H, H7), 4.38 (d, *J* = 7.6 Hz, 1H, $H2_B$), 3.95-3.75 (m, 8H, $H4_A$, $H4_B$, $H5_A$, $H5_B$, $H6_A$, $H6_B$), 3.62-3.48 (m, 3H,

$H1_A$, $H1_B$, $H3_B$), 3.26-3.11 (m, 1H, $H3_A$), 2.89 (t, *J* = 2.4 Hz, 1H, H9) ppm. **HRMS** (*m/z* ESI^+): found 403.1208 ($[M+Na]^+$, $C_{15}H_{24}NaO_{11}$ requires: 403.1211).

(6R,12S,15S,18R)-18-amino-2-((((2R,3R,4R,5S,6R)-3,4-dihydroxy-6-(hydroxymethyl)-5-(((2S,3R,4S,5R,6R)-3,4,5-trihydroxy-6-(hydroxymethyl)tetrahydro-2H-pyran-2-yl)oxy)tetrahydro-2H-pyran-2-yl)oxy)methyl)-12-(4-hydroxybenzyl)-15-methyl-8,11,14,17-tetraoxo-1,4-dithia-7,10,13,16-tetraazacyclononadecane-6-carboxamide (109a/b).

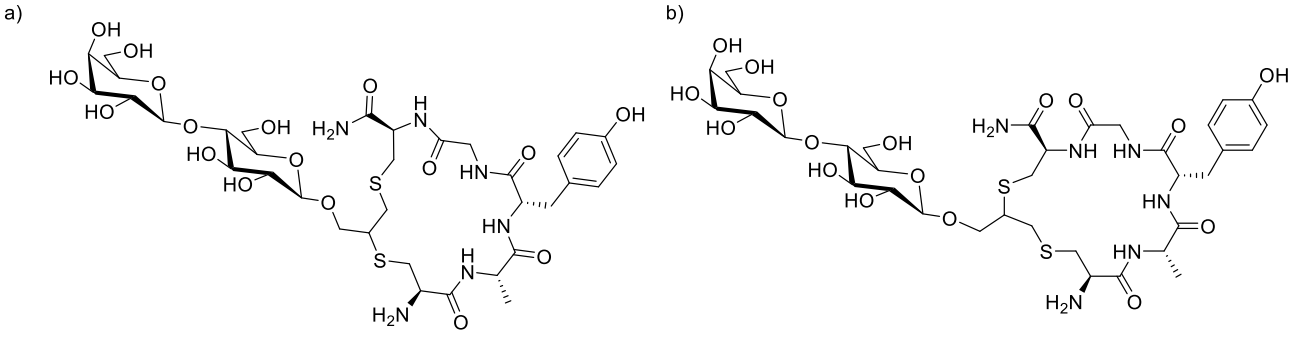

Peptide **109a/b** was prepared as per general **procedure I** (39%). Disulfide **89** (3 mg, 5.85 µmoles), sugar **97** (2.23 mg, 5.85 µmoles), TCEP (2.2 mg, 8.78 µmoles), DPAP (1.50 mg, 5.85 µmoles) and MAP (0.88 mg,5.85 µmoles) were dissolved in H_2O + 0.1% FA (1 mL). **Retention time** (mixture of **a** and **b** isomers)**:** 3.025 min (5-95% ACN, 20 min 0.1% TFA, λ = 220 nm). **HRMS** (*m/z* ESI^+): found 733.2527 ($[M+H]^+$, $C_{29}H_{45}N_6O_{12}S_2$ requires 755.2351).

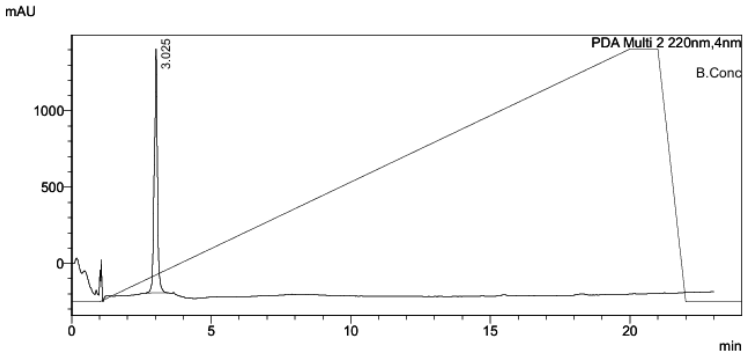

(6R,12S,15S,18R)-18-amino-3-((6-amino-1,3-dioxo-1H-benzo[de]isoquinolin-2(3H)-yl)methyl)-12-(4-hydroxybenzyl)-15-methyl-8,11,14,17-tetraoxo-1,4-dithia-7,10,13,16-tetraazacyclononadecane-6-carboxamide (110a/b).

a)

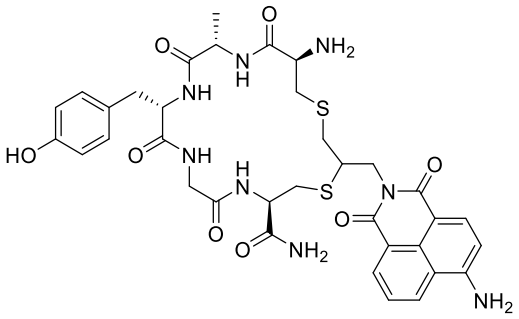

b)

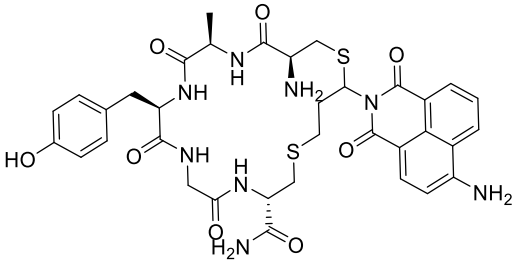

Peptide **110a/b** was prepared as per general **procedure I** (48%). Disulfide **89** (3 mg, 5.85 µmoles), alkyne- nap **100** (0.3 mg, 5.85 µmoles TCEP (2.2 mg, 8.78 µmoles), DPAP (1.50 mg, 5.85 µmoles) and MAP (0.88 mg, 5.85 µmoles) were dissolved in H_2O + 0.1% FA (1 mL). **Retention time** (mixture of **a** and **b** isomers)**:** 8.672 min (5-95% ACN, 20 min 0.1% TFA, λ = 220 nm). **HRMS** (*m/z* ESI^+): found 733.2527 ($[M+H]^+$, $C_{29}H_{45}N_6O_{12}S_2$ requires 755.2351).

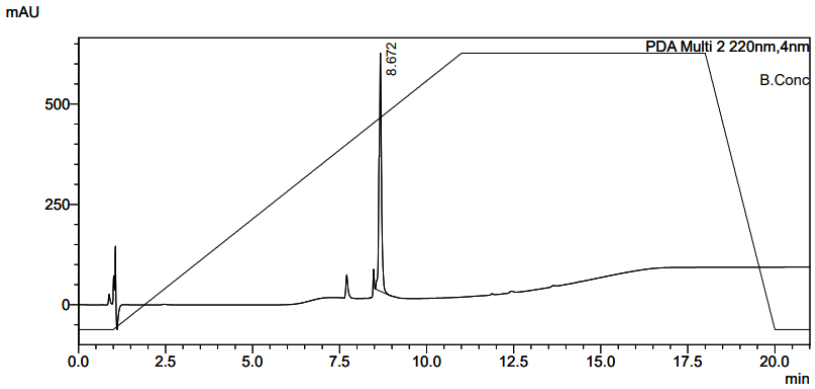

5-azidopent-1-yne (98).

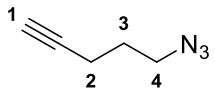

Alkyne bromide **103** (250 mg, 1.70 mmoles) was dissolved in DMF (34 mL) and NaN_3 (442 mg, 6.80 mmol) was added in one portion. The mixture was stirred for 18 h at 80 ºC. After extraction with EtOAc, the solvent was evaporated under vacuo**.**[250] The product **98** was obtained as syrup (8.8 mg, 15%). The isolated product was in good agreement with literature.[327] **^{1}H NMR** (400 MHz, $CDCl_3$) δ 2.85 (t, *J* = 6.6 Hz, 2H, H4), 1.70 (td, *J* = 6.9, 2.6 Hz, 2H, H2), 1.66 (t, *J* = 2.6 Hz, 1H, H1), 1.22-1.15 (m, 1H, H3) ppm. **ν_{max}** (film)/cm^{-1}: 2924 (Csp^3), 2100 (N_3, Csp), 1207 (C-N).

5-((3aS,4S,6aR)-2-oxohexahydro-1H-thieno[3,4-d]imidazol-4-yl)-N-(prop-2-yn-1-yl)pentanamide (99).[328]

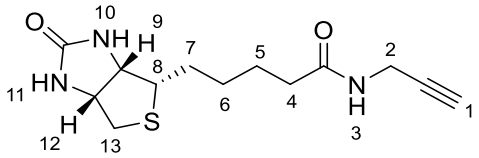

Propargylamine (84 µl, 1.33 mmol) was added dropwise to a cooled solution (0 °C) of D-(+)-biotin **104** (324 mg, 1.33 mmol), HCTU (355 mg, 1.33 mmol), DIPEA (462 µL, 2.65 mmol) and DMAP (81 mg, 663 µmoles.) in DMF (16 mL). The reaction mixture was allowed to reach rt overnight. After reduction of the volume under reduced pressure (~1/2), excess EtOAc was added and the resulting suspension was stored overnight at -20 °C. Filtration and rinsing with EtOAc and Et_2O ultimately afforded the title compound as an white powder (205 mg, 55%). The product **99** was obtained as syrup (8.8 mg, 15%). The isolated product was in good agreement with literature.[251] **^{1}H NMR** (400 MHz, DMSO) δ 8.23 (t, *J* = 5.5 Hz, 1H, H3), 6.47–6.38 (m, 1H, H10), 6.36 (s, 1H, H11), 4.31 (dd, *J* = 7.8, 5.1 Hz, 1H, H12), 4.13 (ddd, *J* = 7.9, 4.3, 2.1 Hz, 1H, H9), 3.84 (dd, *J* = 5.5, 2.5 Hz, 2H, H2), 3.14–3.10 (m, 1H, H8), 3.08 (t, *J* = 2.5 Hz, 1H, H1), 2.83 (ddd, *J* = 12.5, 5.1, 1.0 Hz, 1H, $H13_A$), 2.58 (d, *J* = 12.5 Hz, 1H, $H13_B$), 2.21 (app. t, *J* = 7.4 Hz, 1H, $H7_A$), 2.09 (t, *J* = 7.5 Hz, 1H, $H7_B$), 1.69–1.27 (m, 6H, H4+H5+H6) ppm. **HRMS** (*m/z* ESI^+): found 282.1261 ($[M+H]^+$, $C_{13}H_{20}N_3O_2S$ requires 282.1270).

(6S,12R,15R,18S)-18-amino-12-(4-hydroxybenzyl)-15-methyl-8,11,14,17-tetraoxo-3-((5-((3aR,4R,6aS)-2-oxohexahydro-1H-thieno[3,4-d]imidazol-4-yl)pentanamido)methyl)-1,4-dithia-7,10,13,16-tetraazacyclononadecane-6-carboxamide (108a/b).

a)

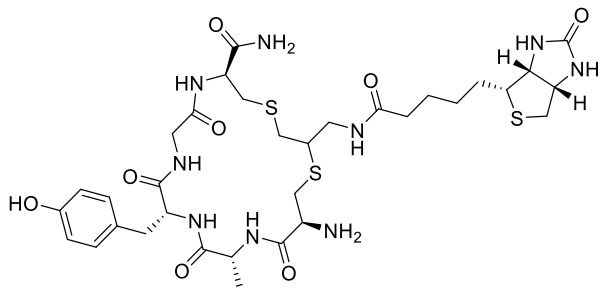

b)

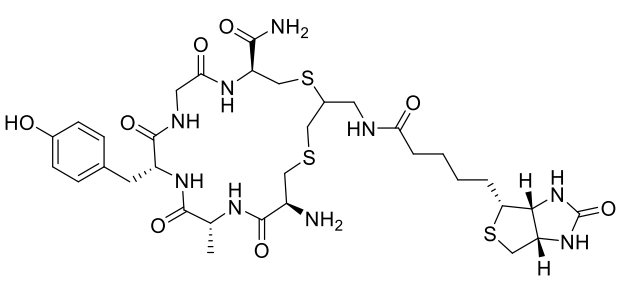

Peptide **108** was prepared as per general **procedure I** (>95%). Disulfide **89** (3 mg, 5.85 µmoles), biotin-alkyne **99** (1.65 mg, 5.85 5.85 µmoles), TCEP (2.2 mg, 8.78 µmoles), DPAP (1.50 mg, 5.85 µmoles) and MAP (0.88 mg,5.85 µmoles) were dissolved in H_2O + 0.1% FA (1 mL). **Retention time** (mixture of **a** and **b** isomers)**:** 8.066 min (5-95% ACN, 20 min 0.1% TFA, λ = 220 nm). **HRMS** (*m/z* ESI^+): found 796.2927 ($[M+H]^+$, $C_{33}H_{50}N_9O_8S_3$ requires 796.2938).

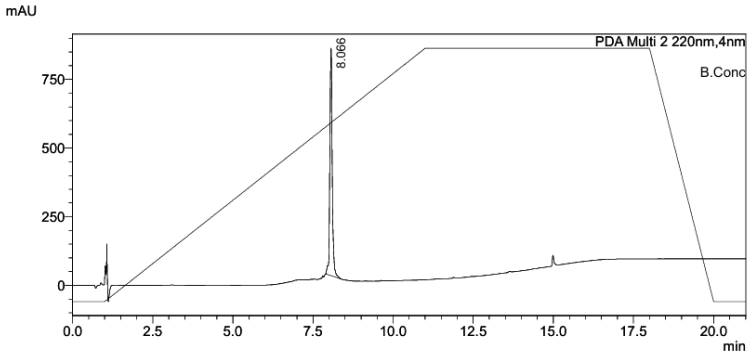

((4R,7S,10S,13R,16S,19R)-13-((1H-indol-3-yl)methyl)-19-((R)-2-amino-3-phenylpropanamido)-10-(4-aminobutyl)-16-benzyl-7-((R)-1-hydroxyethyl)-6,9,12,15,18-pentaoxo-1,2-dithia-5,8,11,14,17-pentaazacycloicosane-4-carbonyl)-L-threonine (4).

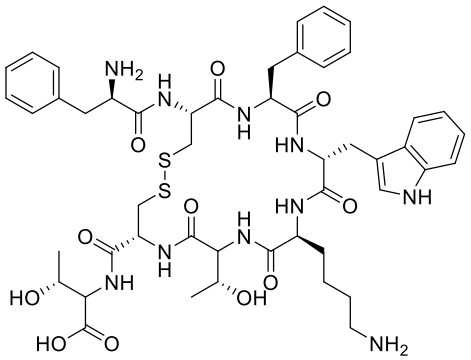

Peptide **4** was prepared as per general **procedure F** utilising Fmoc-D-Phe-OH, Fmoc-Cys(Trt)-OH, Fmoc-Phe-OH, Fmoc-D-Trp(Boc)-OH, Fmoc-Lys(Boc)-OH, Fmoc-Thr(tBu)-OH, Fmoc-Cys(Trt)-OH, Fmoc-Thr(tBu)-OH. Then, crude peptide (21.3 mg, 20.30 μmoles) without further purification was dissolved in 10% DMSO (1 mL) in MeCN:H_2O (1:1, 10 mL) + 0.1% FA at rt for 48 h.[239] The crude peptide was purified by semi-preparative RP-HPLC (C_{18} Φ4.6 × 250 mm column, 1 mL min^{-1} flow rate). Peptide **4** was obtained as fluffy white solid (22 mg, 52%). **Retention time:** 12.064 min (5-95% ACN, 20 min 0.1% TFA, λ = 220 nm). **HRMS** (*m/z* ESI^+): found 1032.4437 ($[M+H]^+$, $C_{49}H_{66}N_{11}O_{10}S_2$ requires 1032.4430).

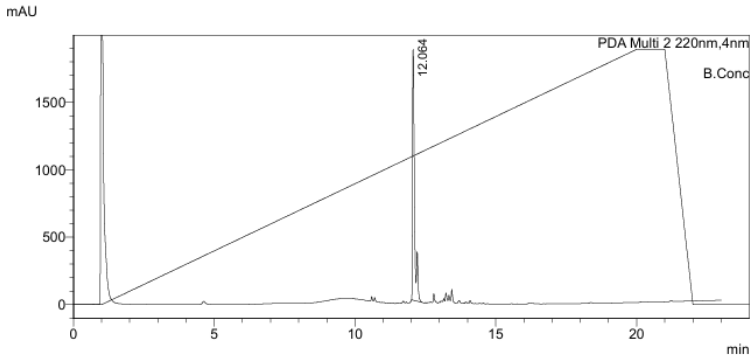

(3S,6R,12S,15R,18S,21R)-15-((1H-indol-3-yl)methyl)-3-((6-amino-1,3-dioxo-1H-benzo[de]isoquinolin-2(3H)-yl)methyl)-N-((3R)-1-amino-3-hydroxy-1-oxobutan-2-yl)-21-((R)-2-amino-3-phenylpropanamido)-12-(4-aminobutyl)-18-benzyl-9-((R)-1-hydroxyethyl)-8,11,14,17,20-pentaoxo-1,4-dithia-7,10,13,16,19-pentaazacyclodocosane-6-carboxamide (111a/b).

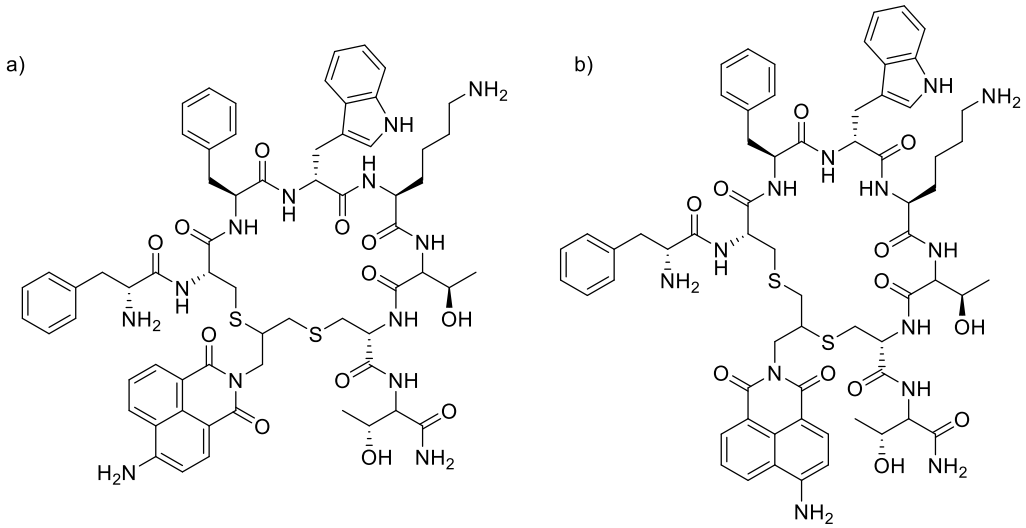

Peptide **111a/b** was prepared as per general **procedure I** (62%). Disulfide **4** (3 mg, 2.91 µmoles), alkyne-nap **100** (1.45 mg, 5.81 µmoles), TCEP (0.80 mg, 2.91 µmoles), DPAP (0.7 mg, 2.91 µmoles) and MAP (0.4 mg, 2.91 µmoles) were dissolved in H_2O + 0.1% FA (409 µL). **Retention time** (mixture of **a** and **b** isomers)**:** 9.838 min (5-95% ACN, 20 min 0.1% TFA, λ = 220 nm). **HRMS** (*m/z* ESI^+): found 1284.5324 ($[M+H]^+$, $C_{64}H_{78}N_{13}O_{12}S_2$ requires1284.5329).

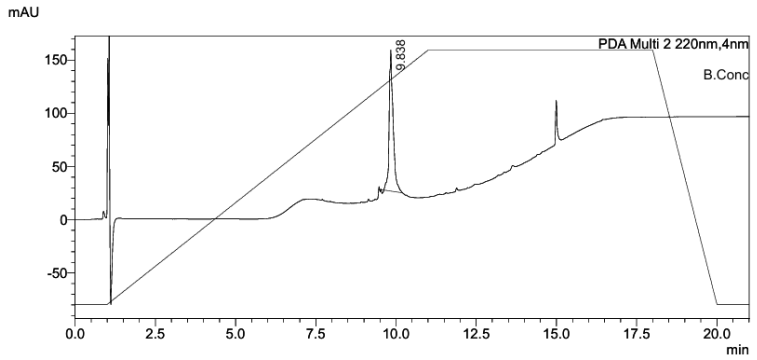

7.4 Characterization product of Chapter 4

7.4.1 Characterisation data

3-(acetylthio)propyl benzoate (116)

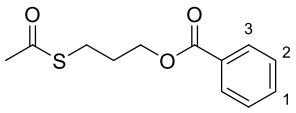

Naphthalimide **113** (3.41 mg, 6.17 μmoles), allyl benzoate **114** (19.05 μL, 20 mg, 123 μmoles) and thioacetic acid **115** (34.8 μL, 37,53 mg, 493 μmoles) were added and dissolved in THF (200 μL). The mixture was stirred under blue LED light for 1 h. Purification by flash column chromatography using Hex/EtOAc (8:2) as eluent afforded the product **116** (22.1 mg, 76%) as a yellow syrup. Product spectroscopic data correlated well to that reported in the literature.[267] **^{1}H NMR** (400 MHz, $CDCl_3$) δ 8.05 (d, *J* = 7.0 Hz, 2H, H3), 7.56 (t, *J* = 7.5 Hz, 1H, H1), 7.4 (app. t, *J* = 7.5 Hz, 2H, H2), 4.38 (t, *J* = 6.2 Hz, 2H, $SCH_2CH_2C\underline{H}_2O$), 3.04 (t, *J* = 7.1 Hz, 2H, $SC\underline{H}_2CH_2CH_2O$), 2.34 (s, 3H, CH_3), 2.10 – 2.03 (m, 2H, $SCH_2C\underline{H}_2CH_2O$) ppm. **HRMS** (*m/z* ESI$^+$): found 261.0563 ($[M+Na]^+$, $C_{12}H_{14}NaO_3S$ requires 261.0556).

7.5 Characterization products of Chapter 5

7.5.1 Sequences

Name	Sequence	Application
T7g10M.F48	TAATACGACTCACTATAGGGTTAACTTTAAGAAGGAGATATACATatg	DNA construction, qPCR
NNK15.R90	GCTGCCGCTGCCGCTGCCGCAMNNMNNMNNMNNMNNMNNMNNMNNMNNMNNMNNMNNMNNMNNMNNCATATGTATATCTCCTTCTTAAAG	mRNA/CDNA complex
FAM-GS3-an2.R36	5'-/56-FAM/TTTCCGCCCCCCGTCCTAGCTGCCGCTGCCGCTGCC-3	Fluorescent primer reverse transcription
GS3an2.R36	TTTCCGCCCCCCGTCCTAGCTGCCGCTGCCGCTGCC	DNA construction, qPCR
NNMTI_121_R65	CGCTGCCGCTGCCGCACATGAATGGTCTATATGGCATATGTATATCTCCTTCTTAAAGTTAACCC	RaPID selection

7.5.2 General Procedures

General Procedure J. Preparation of mRNA/cDNA Complexes. mRNA/cDNA complexes were prepared as a reverse transcribed product of NNK_{15} library. To commence the reverse transcription procedure, the NNK_{15} library was introduced at a final concentration of 1 μM into a preassembled reverse transcription mix. The reverse transcription mix consisted of 1.25 mM dNTPs (Thermo Fisher Scientific, United States of America), 62.6 mM tris.HCl (pH 8.3), 5 μM fluorescent primer (FAM-GS3-an2.R36), 37.5 mM $MgCl_2$, 25 mM KOH, and 200 units/μL reverse transcription enzyme. The reaction mixture was mixed thoroughly by careful pipetting and incubated at 42 °C for 1 h. The reverse transcription product (mRNA/cDNA complex) was purified by phenol-chloroform-isoamyl alcohol (PCI) DNA extraction, adding 1 volume equiv. of 0.6 NaCl and 2 volume equiv. of PCI solution (Amresco K169-400mL) relative to the original reverse transcription mixture. The combined mix was vortexed and then centrifuged at 13,000 rcf for 3 min. The supernatant was transferred to a new tube and mixed with an equal volume of chloroform-isoamyl alcohol (CI) solution (Amresco

X205-450 mL), vortexed and centrifuged at 13,000 rcf for 3 min. The aqueous phase was transferred to a new tube with 2 volume equiv. of EtOH, vortexed and then centrifuged at 13,000 rcf for 15 min. The supernatant was discarded, and the pellet was washed by adding 30 µL of 70% EtOH and centrifuging at 13,000 rcf for 3 min. The precipitate was air-dried. The tube was covered with aluminium foil and stored at −70 °C until use.

General Procedure K. Sodium Hydroxide Control. Reverse transcription product (1 µM) was mixed at 1:1 (v/v) with 1 M sodium hydroxide (NaOH) and incubated at 37 °C for 30 min before quenching with 1 equiv. of AcOH. Samples were then diluted with loading buffer (LB) solution and sampled on Urea-SDS-PAGE.

General Procedure L. UV- Light Control. Reverse transcription product (1 µM) was mixed 1:1 (v/v) with MQ H_2O to give 0.5 µM. Samples were exposed to UV light (UVP UVGL-15, analytikjena, 254/365 nm) from above in an open tube and aliquots were sampled after 5 min, 15 min, and 30 min. Both experiments were carried out under the exclusion of natural light in a cold room at 4 °C. Samples were then diluted with LB solution and sampled on Urea-SDS-PAGE.

General Procedure M. Irgacure 2959 16 Control. The solution consisted of 0.5 µM reverse transcription product and 50 mM Irgacure 2959 **16**. For the preparation of the solution, Irgacure 2959 was dissolved in MQ H_2O before adding the reverse transcription product. Upon incubation at rt for 30 min under UV-light. Samples were then diluted with LB solution and sampled on Urea-SDS-PAGE.

General Procedure N. Peptide Selection. Cyanomethyl ester of chloroacetylated L-tyrosine (separate reactions) were charged with $tRNA_{CAU}$.[299] Based on a previously reported method, selections were carried out against biotinylated hNNMT immobilised on streptavidin magnetic beads for both Homo allyl Gly (Hag) and L-allyl Gly (Alg) initiated libraries in parallel.

The DNA library, which encodes for peptide **121** codons followed by a section encoding a CGSGSGS linker, was assembled by PCR and monitored by 3% agarose gel, followed by transcription to RNA using T7 RNA polymerase (NEB) at 1 mL overnight at 37 °C. Pu ligation [T4 buffer (1.11X), 1.1 mM ATP, 1.1 mM DTT, 1.1 mM PEG8000, Pu linker 1.67 µM, 300 mU/µL of T4 RNA ligase (NEB)], peptide translation (using PURExpress (NEB)) and reverse transcription [0.625 mM dNTPs, 5 µM CGS3an13.R36 primer, 62.5 mM tris.HCl (pH 8.3), 37.5 mM, KOH 25 mM and 2.5X ProtoScript II

Reverse Transcriptase (NEB)] were performed as reported previously.[299] cDNA/mRNA-tagged peptide were diluted with stock solutions of NaOAc buffer (240 mM NaOAc pH 5.2, 375 mM NaCl, 0.0005% tweens) to achieve the final mixture at pH 7, and 0.5 µL of the reverse transcription reaction was diluted in 499 µL MQ H_2O to serve as an input sample for qPCR analysis. Biotinylated hNNMT (1.15 µM) was added to cDNA/mRNA-tagged peptide mixture and incubated during 20 min on ice. Irgacure 2959 **16** (17.5 µM) was then added to the reaction mixture with a total volume of 55 µL mixture in the selection round. Reaction mixture was then divided on 4 tubes in order to carry out positive and negative controls. TEC-mediated outputs were irradiated for 15 min with UV-light (254-365 nm). For the denatured outputs, 4 M urea (17 µL) was added to the reaction mixture. In the case of native outputs PBS-T (17 µL). 4 µL of streptavidin beads was added to each tube and the mixture was gently rotated for 20 min at rt. Stringent washing with 3 x 20 µL PBS-T. Only the denaturing essays were washed one more time with urea 4 M, hepes 25 mM, tween 0,01% for 10 sec. Bound peptides were then eluted by incubation with 50 µl MQ H_2O for 5 min at 95 °C. Samples of the input, positive and negative outputs (1 µL each) were analysed by qPCR alongside a standard curve which was obtained by reverse transcription of the input library. Recoveries were calculated for the positives and negatives selections by dividing the respective amount by the amount of the input sample after compensating for dilution factors.

General Procedure O. **Peptide synthesis.** All peptides of this chapter were synthesized a peptide synthetiser. Fmoc SPPS on a SYRO II (Biotage) using Tentagel rink amide aminomethyl (RAM) resin (25 µmol scale, Rapp Polymere). Each coupling step of 40 min was performed with 5 equiv. of AA, 5 equiv. of HATU and 10 equiv. of DIPEA in DMF. This was followed by a second coupling step using 5 equiv. of PyBOP instead of HATU. Next, uncoupled peptide was capped using 0.5 M acetic anhydride and pyridine in DMF for 5 min at room temperature. Fmoc deprotection was performed using 20% (v/v) piperidine in DMF for 10 min twice. Peptide synthesis was finished by treatment with 0.2 M chloroacetyl *N*-hydroxysuccinimate in DMF for 30 min, twice. Peptide cleavage, global deprotection, and cyclization were performed by the treatment of the cleavage cocktail (TFA:TIPS: H_2O:DTT, 90:2.5:2.5:5). Peptides were subjected to purification *via* PREP-RP-HPLC using a preparative C_{18} column (Gemini C_{18}, 250 x 21.2 mm, 10 µm particle size, Phenomenex). Fractions were analysed by RP-LCMS and those containing the correct peptide mass were pooled and lyophilized. Impure fractions containing product were not re-purified at this stage.

7.5.3 Analysis

Urea-SDS-PAGE. 2 µL of the incubation mix containing 0.5 µM mRNA/cDNA complexe were sampled, in order to load 1 pmol reverse transcription product onto the 8% urea-SDS-PAGE [0.05% (w/v) SDS, 6 M urea, 8% acrylamide/bis mixed solution (37.5:1)]. Samples were mixed with a loading buffer [34.5% (v/v) formamide, 62.5 mM tris.HCl pH 6.8, 5 mM dithiothreitol (DTT), 10 mM EDTA, and 0.05% (w/v) SDS]. The gel electrophoresis was performed at 200 V for 45 min and visualized with UV exposure (at the wavelength 472-513 nm) followed by staining with SYBRTM Green II (10,000x concentrate in DMSO, Invitrogen) and measurement of fluorescence at the wavelength 472-595 nm.

SDS-PAGE. Labelling samples were analysed on a 10% acrylamide gel (2.5 mL MQ H2O, 1.25 mL 40% acrylamide/bis-acrylamide (29:1), 1.25 mL pH 8.8 SDS solution, 50 µL 10% ammonium persulfate (APS), 10 µL Tetramethylethylenediamine (TEMED); stacking gel: 625 µL MQ H_2O, 125 µL acrylamide/bis-acrylamide (29:1), 250 µL pH 6.8 SDS solution, 10 µL 10% APS, 2.5 µL TEMED). PreqGold II Protein Ladder was loaded alongside the samples. Protein separation was performed at 200 V for 45 min in running buffer (25 mM Tris, 190 mM Gly, 1% SDS) and visualised by fluorescence of silver stain.

qPCR. The qPCR mix contained KOD buffer (120 mM tris, 10 mM KCl, 6 mM $(NH4)_2SO_4$, 0.1% Triton X-100, 0.001% bovine serum albumin (BSA) (w/v), adjusted to pH 8 using HCl), 0.25 mM dNTPs, 2 mM $MgCl_2$, 0.25 µM forward primer (F48), 0.25 µM reverse primer (R36) , 1x KOD DNA polymerase (in-house production, stored in 5 mM tris, 5 mM KCl, 0.01 mM EDTA, 0.1 mM DTT, 0.02% Tween-20, 5% glycerol, pH 7.5), and 1x SYBR™ Green I Nucleic Acid Gel Stain (Invitrogen, United States of America) in MQ H_2O. Each sample for qPCR analysis was prepared by adding 0.5 µL of the incubation mix to 499 µL of MQ H_2O to dilute the reactants. In each qPCR reaction, 19 µL of the above qPCR mix was transferred into individual qPCR tubes. Subsequently 1 µL of the specific qPCR sample was added to each tube. Measurements included negative controls containing MQ H_2O instead of sample, and standard curves with a 10X serially diluted reverse transcribed peptide **121**-encoded R65 primer RNA at concentrations ranging from 2 x 10^5 to 2 x 10^9 molecules/µL. The PCR amplification profile encompassed an initial cycle at 95 °C, annealing at 55 °C for 10 sec, and extension at 72 °C for 30 sec, followed by 35 cycles of amplification steps, which consisted of

denaturation at 95 °C for 10 sec, annealing at 62 °C for 10 sec, and extension at 72 °C for 30 sec, with fluorescence measurement after the extension step.

7.5.4 Characterisation data

(6S,12R,18S,20aS,26S,29S,31aS)-15-allyl-N-(1-amino-5-(2-azidoethyl)-1,4,7,16-tetraoxo-9,12-dioxa-3,6,15-triazaheptadecan-17-yl)-18-benzyl-26-(3-guanidinopropyl)-6,29-bis(4-hydroxybenzyl)-5,8,14,17,20,25,28,31-octaoxooctacosahydro-1H,5H-dipyrrolo[1,2-g:1',2'-p][1]thia[4,7,10,13,16,19,22,25]octaazacycloheptacosine-12-carboxamide (122).

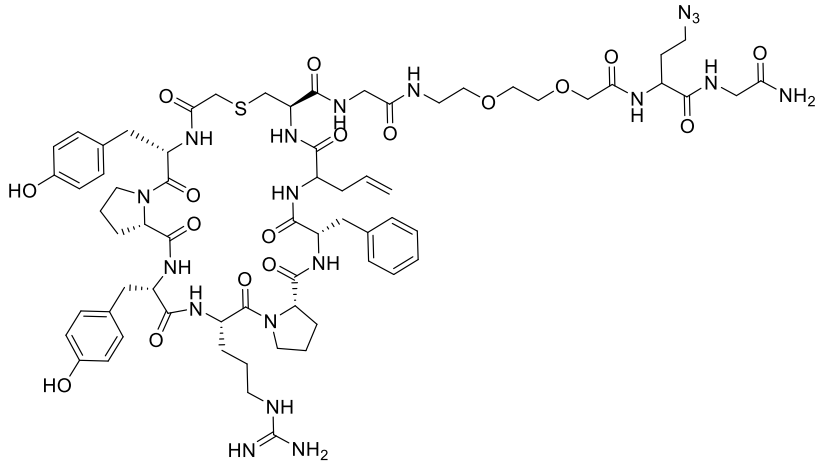

Peptide **122** was prepared as per general procedure **O** utilising ClAc. Fmoc-Tyr(OtBu), Fmoc-Pro-OH, Fmoc-Tyr(OtBu)-OH, Fmoc-Arg(Pbf)-OH, Fmoc-Pro-OH, Fmoc-Phe-Oh, Fmoc-Gly-OH, Fmoc-Cys(trt)-OH, Fmoc-Gly-OH, Fmoc-Peg_4-OH, Fmoc-Aha-OH, Fmoc-Gly-OH). Crude peptide was dissolved in DMSO (2 mL) with DIPEA (10 µL) and the reaction was stirred for 30 min. Cycled product was then purified by preparative RP-HPLC. Peptide **122** was obtained as fluffy white solid. **LC/MS: Retention time:** 6.816 min (5-95% ACN, 10 min 0.1% FA, λ = 280 nm); **MS** (ESpos): m/z = 1466.60 $[M+H]^+$. **HRMS** (*m/z* MALDI): found 1466.265 ($[M+H]^+$, $C_{67}H_{92}N_{19}O_{17}S$ requires 1466.6595).

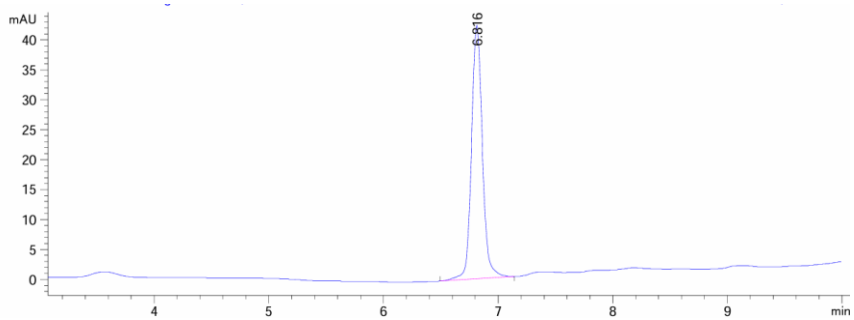

(6S,12R,18S,20aS,26S,29S,31aS)-15-allyl-N-(1-amino-5-(2-(8-(3',6'-dihydroxy-3-oxo-3H-spiro[isobenzofuran-1,9'-xanthene]-6-carbonyl)-3a,8,9,13b-tetrahydro-1H-dibenzo[b,f][1,2,3]triazolo[4,5-d]azocin-1-yl)ethyl)-1,4,7,16-tetraoxo-9,12-dioxa-3,6,15-triazaheptadecan-17-yl)-18-benzyl-26-(3-guanidinopropyl)-6,29-bis(4-hydroxybenzyl)-5,8,14,17,20,25,28,31-octaoxooctacosahydro-1H,5H-dipyrrolo[1,2-g:1',2'-p][1]thia[4,7,10,13,16,19,22,25]octaazacycloheptacosine-12-carboxamide (124)

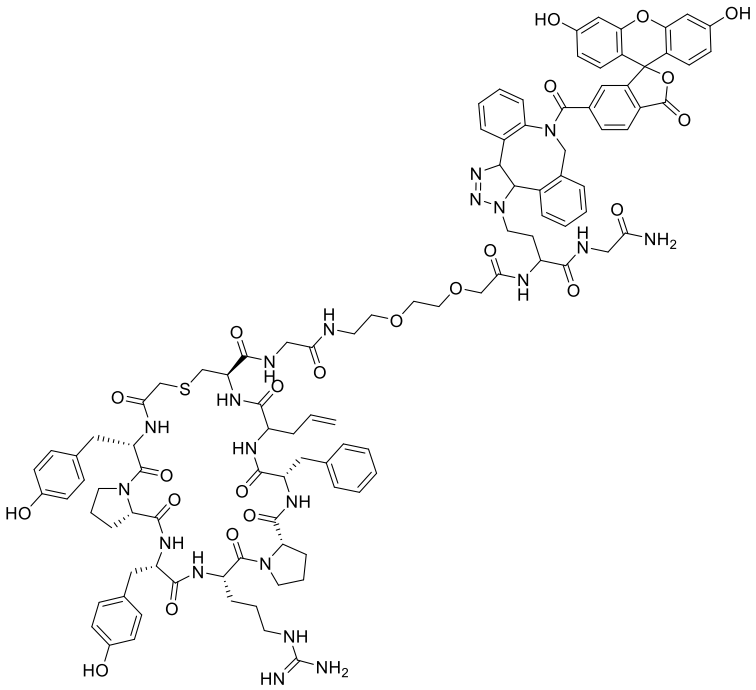

Peptide **124** (1.7 mg, 1.16 µmoles) was dissolved in DMSO with DBCO-FAM (0.784 mg, 1.16 µmoles) and stirred for 30 min. Crude peptide was then purified by preparative RP-HPLC. Peptide **124** was obtained as fluffy yellow solid (0.7 mg, 29%). **LC/MS: Retention time** = 7.156 min (5-95% ACN, 10 min 0.1% FA, λ = 280 nm); **MS** (ESpos): m/z = 2143.06 $[M+H]^+$. **HRMS** (*m/z* MALDI): found 2166.587 ($[M+Na]^+$, $C_{109}H_{126}NaN_{21}O_{24}S$ requires 2166.9028).

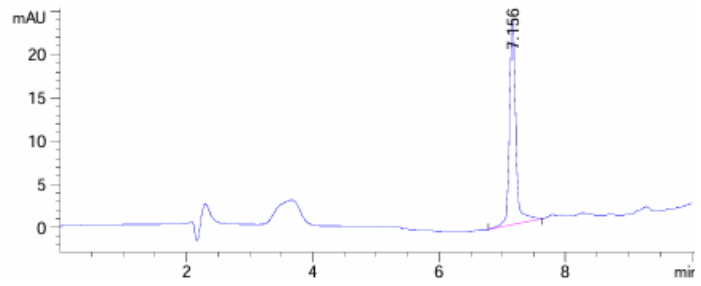

(6S,12R,18S,20aS,26S,29S,31aS)-15-allyl-N-(1-amino-5-(2-aminoethyl)-1,4,7,16-tetraoxo-9,12-dioxa-3,6,15-triazaheptadecan-17-yl)-18-benzyl-26-(3-guanidinopropyl)-6,29-bis(4-hydroxybenzyl)-5,8,14,17,20,25,28,31-octaoxooctacosahydro-1H,5H-dipyrrolo[1,2-g:1',2'-p][1]thia[4,7,10,13,16,19,22,25]octaazacycloheptacosine-12-carboxamide (125).

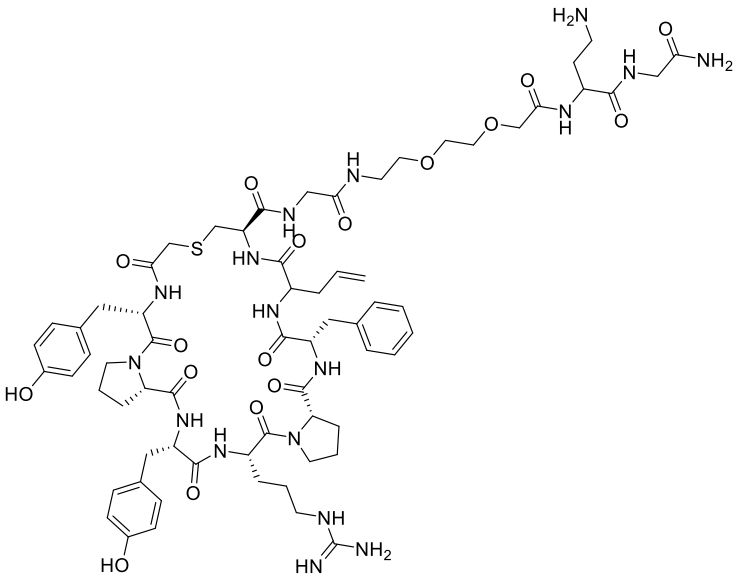

Peptide **122** (1.1 mg, 4.19 µmoles) was dissolved in 500 µL of H_2O. To the peptidyl mixture 7 µL of 1 M TCEP in H_2O + 0.1% FA were added and stirred for 2 days at rt.[320] Crude mixture was then purified by preparative RP-HPLC. Peptide **125** was obtained as fluffy white solid (1.1 mg, 19%). **LCMS: Retention time** = 6.401 min (5-95% ACN, 10 min 0.1% FA, λ = 280 nm); MS (ESpos): m/z = 1440.24 $[M+H]^+$. **HRMS** (*m/z* MALDI): found 1440.420 ($[M+H]^+$, $C_{67}H_{94}N_{17}O_{17}S$ requires 1440.6690).

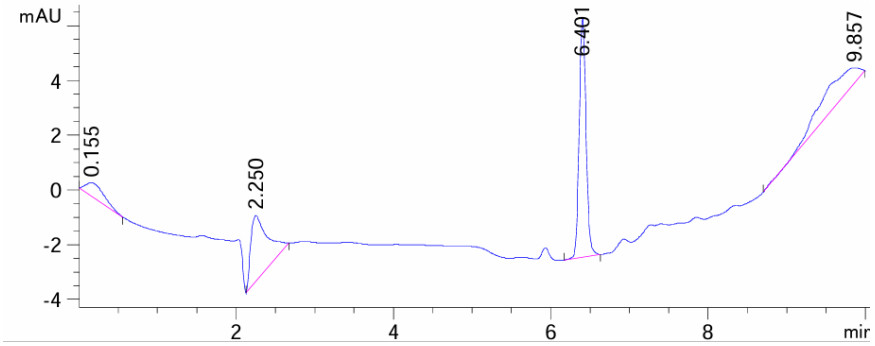

(6S,12R,18S,20aS,26S,29S,31aS)-15-allyl-N-(13-((2-amino-2-oxoethyl)carbamoyl)-2,11,17-trioxo-21-((3aR,4R,6aS)-2-oxohexahydro-1H-thieno[3,4-d]imidazol-4-yl)-6,9-dioxa-3,12,16-triazahenicosyl)-18-benzyl-26-(3-guanidinopropyl)-6,29-bis(4-hydroxybenzyl)-5,8,14,17,20,25,28,31-octaoxooctacosahydro-1H,5H-dipyrrolo[1,2-g:1',2'-p][1]thia[4,7,10,13,16,19,22,25]octaazacycloheptacosine-12-carboxamide (126).

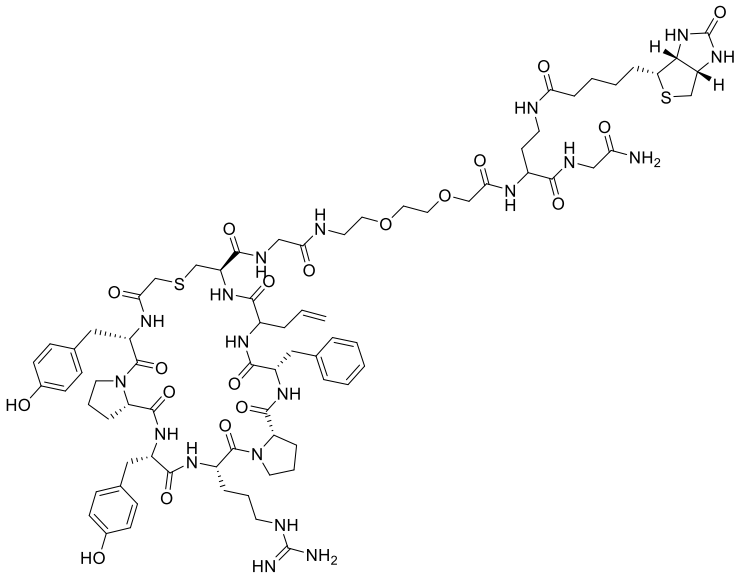

Peptide **125** (1.1 mg, 764 µmoles) was dissolved in 1 mL of H_2O. To the peptidyl solution, 0.35 mM of biotin, 0.35 mM of HCTU, 0.35 mM of DIPEA and 0.17 mM of DMAP were added. The mixture was stirred overnight. Crude peptide **126** was then purified by preparative RP-HPLC. Peptide **126** was obtained as fluffy white solid (0.2 mg, 16%). **LC/MS**: **Retention time** = 7.318 min (5-95% ACN, 10 min 0.1% FA, λ = 280 nm); MS (ESpos): m/z = 1666.56 $[M+H]^+$. **HRMS** (*m/z* MALDI): found 1666.768 ($[M+H]^+$, $C_{77}H_{108}N_{19}O_{19}S_2$ requires 1666.7466).

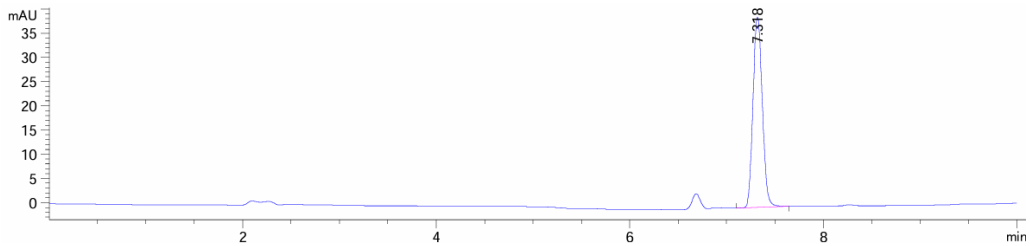

References

1. N. Chaffey, *Ann. Bot.*, 2003, **91**, 401-401.
2. H. Hartley, *Nature*, 1951, **168**, 244-244.
3. M. M. Moiola, M. G. Memeo and P. Quadrelli, *Molecules*, 2019, **24**, 3654.
4. Y. Li, X. Cao, C. Tian and J. S. Zheng, *Chin. Chem. Lett.*, 2020, **31**, 2365-2374.
5. W. Xiao, W. Jiang, Z. Chen, Y. Huang, J. Mao, W. Zheng, Y. Hu and J. Shi, *Signal Transduct. Target. Ther.*, 2025, **10**, 74.
6. R. Hellinger, A. Sigurdsson, W. Wu, E. V. Romanova, L. Li, J. V. Sweedler, R. D. Süssmuth and C. W. Gruber, *Nat. Rev. Methods Primers*, 2023, **3**, 25.
7. M. K. D. Jolene L. Lau, *Bioorg. Med. Chem.*, 2018, **26**, 2700-2707.
8. D. S. Thierry Kimmerlin, *J. Pept. Res.*, 2008, **65**, 229-260.
9. D. L. N. Michael and M. Cox, *Lehninger Principles of Biochemistry*, W. H. Freeman and Company: New York, NY, USA, 2005.
10. N. W. L. Wang, W. Zhang, X. Cheng, Z. Yan, G. Shao, X. Wang, R. Wang and C. Fu, *Signal Transduct. Target. Ther.*, 2022, **7**, 2059-3635.
11. G. Banting, *FEBS Lett*., 1991, **291**, 159-159..
12. F. G. Banting, C. H. Best, J. B. Collip, W. R. Campbell and A. A. Fletcher, *Can. Med. Assoc. J.*, 1922, **12**, 141-146.
13. E.-M. Jülke and A. G. Beck-Sickinger, *Peptides*, 2025, **188**, 171404.
14. C. R. Vincent du Vigneaud, John M. Swan, Carleton W. Roberts, Panayotis G. Katsoyannis, *J. Am. Chem. Soc.*, 1954, **76**, 3115-3121.
15. A. R. Spiegelman, *Jama*, 1964, **187**, 1035.
16. C. S. Carter, W. M. Kenkel, E. L. MacLean, S. R. Wilson, A. M. Perkeybile, J. R. Yee, C. F. Ferris, H. P. Nazarloo, S. W. Porges, J. M. Davis, J. J. Connelly and M. A. Kingsbury, *Pharmacol. Rev.*, 2020, **72**, 829-861.
17. J. G. Shweta Mishra, P. Wal, G. U. Bhivshet, A. K. Tripathi, and V. Walia, *Peptides*, 2024, **174**, 171166.
18. L. Otvos and J. D. Wade, *Front. Chem.*, 2014, **2**.
19. N. A. Khazanov and H. A. Carlson, *PLOS Comput. Biol.*, 2013, **9**, e1003321.
20. D. Thomas, *A big year for novel drug approvals.*, 2013. BIOtechNOW.
21. D. J. Craik, D. P. Fairlie, S. Liras and D. Price, *Chem. Biol. Drug Des.*, 2013, **81**, 136-147.
22. K. Fosgerau and T. Hoffmann, *Drug Discov Today*, 2015, **20**, 122-128.
23. L. Diao and B. Meibohm, *Clin. Pharmacokinet.*, 2013, **52**, 855-868.
24. L. Di, *Aaps j*, 2015, **17**, 134-143.
25. G. Chen, W. Kang, W. Li, S. Chen and Y. Gao, *Theranostics*, 2022, **12**, 1419-1439.
26. X. H. Zhou and A. L. W. Po, *Int. J. Pharm.*, 1991, **75**, 117-130.
27. X. S. Puente, A. Gutiérrez-Fernández, G. R. Ordóñez, L. W. Hillier and C. López-Otín, *Genomics*, 2005, **86**, 638-647.
28. P. Chanson, J. Timsit and A. G. Harris, *Clin. Pharmacokinet.*, 1993, **25**, 375-391.
29. C. Heinis, T. Rutherford, S. Freund and G. Winter, *Nat. Chem. Biol.*, 2009, **5**, 502-507.
30. M. Boehm, K. Beaumont, R. Jones, A. S. Kalgutkar, L. Zhang, K. Atkinson, G. Bai, J. A. Brown, H. Eng, G. H. Goetz, B. R. Holder, B. Khunte, S. Lazzaro, C. Limberakis, S. Ryu, M. J. Shapiro, L. Tylaska, J. Yan, R. Turner, S. S. F. Leung, M. Ramaseshan, D. A. Price, S. Liras, M. P. Jacobson, D. J. Earp, R. S. Lokey, A. M. Mathiowetz and E. Menhaji-Klotz, *J. Med. Chem.*, 2017, **60**, 9653-9663.
31. T. Ishizawa, T. Kawakami, P. C. Reid and H. Murakami, *J. Am. Chem. Soc.*, 2013, **135**, 5433-5440.
32. Y. Huang, M. M. Wiedmann and H. Suga, *Chem. Rev.*, 2019, **119**, 10360-10391.

33. R. M. Franzini, D. Neri and J. Scheuermann, *Acc. Chem. Res.*, 2014, **47**, 1247-1255.
34. N. K. Bashiruddin and H. Suga, *Curr. Opin. Chem. Biol.*, 2015, **24**, 131-138.
35. A. M. Davis, A. T. Plowright and E. Valeur, *Nat. Rev. Drug Discov.*, 2017, **16**, 681-698.
36. S. Brenner and R. A. Lerner, *Proc. Natl. Acad. Sci. USA*, 1992, **89**, 5381-5383.
37. S. Melkko, J. Scheuermann, C. E. Dumelin and D. Neri, *Nat. Biotechnol.*, 2004, **22**, 568-574.
38. B. K. Kay, J. Kasanov and M. Yamabhai, *Methods*, 2001, **24**, 240-246.
39. B. S. Jursic and Z. Zdravkovski, *Synth. Commun.*, 1993, **23**, 2761-2770.
40. E. Fischer and E. Fourneau, *Ber. Dtsch. Chem. Ges.*, 1901, **34**, 2868-2877.
41. E. Fischer, *Eur. J. Inorg. Chem.*, 1905, **38**, 605-619.
42. T. Curtius and H. Curtius, *J. Prakt. Chem.*, 1904, **70**, 158-194.
43. E. Massolo, M. Pirola and M. Benaglia, *Eur. J. Org. Chem.*, 2020, **2020**, 4641-4651.
44. A. El-Faham and F. Albericio, *Chem. Rev.*, 2011, **111**, 6557-6602.
45. P. G. M. Wuts. *Protection for the Amino Group*. In Greene's Protective Groups in Organic Synthesis, 2014, ch. 7, pp. 895-1193.
46. R. Subirós-Funosas, R. Prohens, R. Barbas, A. El-Faham and F. Albericio, *Chemistry*, 2009, **15**, 9394-9403.
47. R. Steinauer, F. M. Chen and N. L. Benoiton, *Int. J. Pept. Protein Res.*, 1989, **34**, 295-298.
48. C. Montalbetti and V. Falque, *Tetrahedron*, 2005, **61**, 10827-10852.
49. J. Wu, G. An, S. Lin, J. Xie, W. Zhou, H. Sun, Y. Pan and G. Li, *Chem. Commun.*, 2014, **50**, 1259-1261.
50. R. B. Merrifield, *J. Am. Chem. Soc.*, 1963, **85**, 2149-2154.
51. J. M. Palomo, *RSC Adv.*, 2014, **4**, 32658-32672.
52. I. Coin, M. Beyermann and M. Bienert, *Nat. Protoc.*, 2007, **2**, 3247-3256.
53. D. s. M. M. Jaradat, *Amino Acids*, 2018, **50**, 39-68.
54. R. B. Merrifield, *J. Org. Chem.*, 1964, **29**, 3100-3102.
55. B. Gutte and R. B. Merrifield, *J. Am. Chem. Soc.*, 1969, **91**, 501-502.
56. H. M. Yu, S. T. Chen and K. T. Wang, *J. Org. Chem.*, 1992, **57**, 4781-4784.
57. S. L. Pedersen, A. P. Tofteng, L. Malik and K. J. Jensen, *Chem. Soc. Rev.*, 2012, **41**, 1826-1844.
58. E. Yahya, A. A. Gerardo, Y. Jad, T. Govender, G. Kruger, A. El-Faham, B. De la torre and F. Albericio, *ACS Sustainable Chem. Eng.,*2016, **4**, 6809-6814.
59. V. Mäde, S. Els-Heindl and A. G. Beck-Sickinger, *Beilstein J. Org. Chem.*, 2014, **10**, 1197-1212.
60. B. L. Pentelute and S. B. H. Kent, *Org. Lett.*, 2007, **9**, 687-690.
61. M. Paradís-Bas, J. Tulla-Puche and F. Albericio, *Chem. Soc. Rev.*, 2016, **45**, 631-654.
62. J. Bedford, C. Hyde, T. Johnson, W. Jun, D. Owen, M. Quibell and R. C. Sheppard, *Int. J. Pept. Protein Res.*, 1992, **40**, 300-307.
63. R. C. d. L. Milton, S. C. F. Milton and P. A. Adams, *J. Am. Chem. Soc.*, 1990, **112**, 6039-6046.
64. G. B. Fields, *Curr. Protoc. Protein Sci.*, 2002, ch. 18, 18.11.11-18.11.19.
65. T. Wieland, E. Bokelmann, L. Bauer, H. U. Lang and H. Lau, *Justus Liebigs Ann. Chem.*, 1953, **583**, 129-149.
66. D. S. Kemp, J. A. Grattan and J. Reczek, *J. Org. Chem.*, 1975, **40**, 3465-3466.
67. D. S. Kemp and D. J. Kerkman, *Tetrahedron Lett.*, 1981, **22**, 185-186.

68. D. S. Kemp, N. G. Galakatos, S. Dranginis, C. Ashton, N. Fotouhi and T. P. Curran, *J. Org. Chem.*, 1986, **51**, 3320-3324.
69. N. Fotouhi, N. G. Galakatos and D. S. Kemp, *J. Org. Chem.*, 1989, **54**, 2803-2817.
70. P. E. Dawson, T. W. Muir, I. Clark-Lewis and S. B. Kent, *Science*, 1994, **266**, 776-779.
71. H. M. Burke, L. McSweeney and E. M. Scanlan, *Nat. Commun.*, 2017, **8**, 15655.
72. P. E. Dawson, M. J. Churchill, M. R. Ghadiri and S. B. H. Kent, *J. Am. Chem. Soc.*, 1997, **119**, 4325-4329.
73. J. Hersh, D. Broyles, J. M. C. Capcha, E. Dikici, L. A. Shehadeh, S. Daunert and S. Deo, *ACS Appl. Bio. Mater.*, 2021, **4**, 229-251.
74. J. Kihlberg, J. Ahman, B. Walse, T. Drakenberg, A. Nilsson, C. Söderberg-ahlm, B. Bengtsson and H. Olsson, *J. Med. Chem.*, 1995, **38**, 161-169.
75. R. Albert, P. Marbach, W. Bauer, U. Briner, G. Fricker, C. Brums and J. Pless, *Life Sci.*, 1993, **53**, 517-525.
76. F. L. Zhang and P. J. Casey, *Annu. Rev. Biochem.*, 1996, **65**, 241-269.
77. P. Orlean and A. K. Menon, *J. Lipid Res.*, 2007, **48**, 993-1011.
78. M. D. Resh, *Biochim. Biophys. Acta.*, 1999, **1451**, 1-16.
79. S. B. van Witteloostuijn, S. L. Pedersen and K. J. Jensen, *Chem. Med. Chem.*, 2016, **11**, 2474-2495.
80. K. Lang and J. W. Chin, *Chem. Rev.*, 2014, **114**, 4764-4806.
81. L. S. Witus and M. B. Francis, *Acc. Chem. Res.*, 2011, **44**, 774-783.
82. N. Stephanopoulos and M. B. Francis, *Nat. Chem. Biol.*, 2011, **7**, 876-884.
83. C. D. Spicer and B. G. Davis, *Nat. Commun.*, 2014, **5**, 4740.
84. S. Lin, X. Yang, S. Jia, A. M. Weeks, M. Hornsby, P. S. Lee, R. V. Nichiporuk, A. T. Iavarone, J. A. Wells, F. D. Toste and C. J. Chang, *Science*, 2017, **355**, 597-602.
85. N. Krall, F. P. da Cruz, O. Boutureira and G. J. Bernardes, *Nat. Chem.*, 2016, **8**, 103-113.
86. J. N. deGruyter, L. R. Malins and P. S. Baran, *Biochemistry*, 2017, **56**, 3863-3873.
87. M. J. Matos, B. L. Oliveira, N. Martínez-Sáez, A. Guerreiro, P. M. S. D. Cal, J. Bertoldo, M. Maneiro, E. Perkins, J. Howard, M. J. Deery, J. M. Chalker, F. Corzana, G. Jiménez-Osés and G. J. L. Bernardes, *J. Am. Chem. Soc.*, 2018, **140**, 4004-4017.
88. L. B. Poole, *Free Radic. Biol. Med.*, 2015, **80**, 148-157.
89. D. W. Bak, T. J. Bechtel, J. A. Falco and E. Weerapana, *Curr. Opin. Chem. Biol.*, 2019, **48**, 96-105.
90. N. J. Pace and E. Weerapana, *ACS Chem. Biol.*, 2013, **8**, 283-296.
91. G. Bulaj, T. Kortemme and D. P. Goldenberg, *Biochemistry*, 1998, **37**, 8965-8972.
92. K. S. Jensen, R. E. Hansen and J. R. Winther, *Antioxid. Redox Signaling*, 2008, **11**, 1047-1058.
93. R. K. Cannan and B. C. J. G. Knight, *Biochem. J.*, 1927, **21**, 1384-1390.
94. S. Pinitglang, A. B. Watts, M. Patel, J. D. Reid, M. A. Noble, S. Gul, A. Bokth, A. Naeem, H. Patel, E. W. Thomas, S. K. Sreedharan, C. Verma and K. Brocklehurst, *Biochemistry*, 1997, **36**, 9968-9982.
95. K. M. Backus, J. Cao and S. M. Maddox, *Bioorg. Med. Chem.*, 2019, **27**, 3421-3439.
96. F. Dickens, *Biochem. J.*, 1933, **27**, 1141-1151.
97. Y. Goto and H. Suga, *Acc. Chem. Res.,* 2021, **54**, 3604-3617.

98. G.-Z. Li, R. K. Randev, A. H. Soeriyadi, G. Rees, C. Boyer, Z. Tong, T. P. Davis, C. R. Becer and D. M. Haddleton, *Polym. Chem.*, 2010, **1**, 1196-1204.
99. S. Chatani, D. P. Nair and C. N. Bowman, *Polym. Chem*, 2013, **4**, 1048-1055.
100. M. Ahangarpour, I. Kavianinia and M. Brimble, *Org. Biomol. Chem.*, 2023, **21**, 3057-3072.
101. E. Friedman, D. H. Marrian and I. Simon-reuss, *Br. J. Pharmacol. Chemother.*, 1949, **4**, 105-108.
102. J. E. Moore and W. H. Ward, *J. Am. Chem. Soc.*, 1956, **78**, 2414-2418.
103. S. D. Fontaine, R. Reid, L. Robinson, G. W. Ashley and D. V. Santi, *Bioconjug. Chem.*, 2015, **26**, 145-152.
104. V. M. Lechner, M. Nappi, P. J. Deneny, S. Folliet, J. C. K. Chu and M. J. Gaunt, *Chem. Rev.*, 2022, **122**, 1752-1829.
105. D. I. Pattison and M. J. Davies, *Exs*, 2006, **96**, 131-157.
106. X. Ai, J. Mu and B. Xing, *Theranostics*, 2016, **6**, 2439-2457.
107. L. Raynal, N. C. Rose, J. R. Donald and C. D. Spicer, *Chem. Eur. J.*, 2021, **27**, 69-88.
108. C. K. Prier, D. A. Rankic and D. W. C. MacMillan, *Chem. Rev.*, 2013, **113**, 5322-5363.
109. Q.-Q. Zhou, Y.-Q. Zou, L.-Q. Lu and W.-J. Xiao, *Angew. Chem. Int. Ed.*, 2019, **58**, 1586-1604.
110. H. Choi, M. Kim, J. Jang and S. Hong, *Angew. Chem. Int. Ed. Engl.*, 2020, **59**, 22514-22522.
111. Y. S. Or, R. F. Clark and J. R. Luly, *J. Org. Chem.*, 1991, **56**, 3146-3149.
112. A. M. Spokoyny, Y. Zou, J. J. Ling, H. Yu, Y.-S. Lin and B. L. Pentelute, *J. Am. Chem. Soc.*, 2013, **135**, 5946-5949.
113. A.-M. Leduc, J. O. Trent, J. L. Wittliff, K. S. Bramlett, S. L. Briggs, N. Y. Chirgadze, Y. Wang, T. P. Burris and A. F. Spatola, *Proc. Natl. Acad. Sci.*, 2003, **100**, 11273-11278.
114. H. Chen, R. Huang, Z. Li, W. Zhu, J. Chen, Y. Zhan and B. Jiang, *Org. Biomol. Chem.*, 2017, **15**, 7339-7345.
115. B. H. Northrop and R. N. Coffey, *J. Am. Chem. Soc.*, 2012, **134**, 13804-13817.
116. L. Markey, S. Giordani and E. M. Scanlan, *J. Org. Chem.*, 2013, **78**, 4270-4277.
117. H. C. Kolb, M. G. Finn and K. B. Sharpless, *Angew. Chem. Int. Ed.*, 2001, **40**, 2004-2021.
118. A. Leydet, P. Barthelemy, B. Boyer, G. Lamaty, J. P. Roque, A. Bousseau, M. Evers, Y. Hénin, R. Snoeck, G. Andrei, S. Iked, D. Reymen and E. De Clercq, *J. Med. Chem.*, 1995, **38**, 2433-2440.
119. A. Murphy, A. Pace and T. D. Stack, *Org. Lett.*, 2004, **6**, 3119-3122.
120. M. D. Nolan and E. M. Scanlan, *Front. Chem.*, 2020, **8**, 583272.
121. I. Rabadán González, J. T. McLean, N. Ostrovitsa, S. Fitzgerald, A. Mezzetta, L. Guazzelli, D. F. O'Shea and E. M. Scanlan, *Org. Biomol. Chem.*, 2024, **22**, 2203-2210.
122. K. F. Long, N. J. Bongiardina, P. Mayordomo, M. J. Olin, A. D. Ortega and C. N. Bowman, *Macromol.*, 2020, **53**, 5805-5815.
123. I. Munar, V. Fındık, I. Degirmenci and V. Aviyente, *J. Phys. Chem.*, 2020, **124**, 2580-2590.
124. K. Griesbaum, *Angew. Chem. Int. Ed. Engl.*, 1970, **9**, 273-287.
125. O. Z. Durham, H. R. Norton and D. A. Shipp, *RSC Adv.*, 2015, **5**, 66757-66766.
126. A. B. Lowe, *Polymer*, 2014, **55**, 5517-5549.

127. Y. Tian, J. Li, H. Zhao, X. Zeng, D. Wang, Q. Liu, X. Niu, X. Huang, N. Xu and Z. Li, *Chem. Sci.*, 2016, **7**, 3325-3330.
128. F. Nador, J. Mancebo-Aracil, D. Zanotto, D. Ruiz-Molina and G. Radivoy, *RSC Adv.*, 2021, **11**, 2074-2082.
129. M. Lo Conte, S. Pacifico, A. Chambery, A. Marra and A. Dondoni, *J. Org. Chem.*, 2010, **75**, 4644-4647.
130. B. D. Fairbanks, T. F. Scott, C. J. Kloxin, K. S. Anseth and C. N. Bowman, *Macromol.*, 2009, **42**, 211-217.
131. B. Yu, J. Chan, C. Hoyle and A. Lowe, *J. Polym. Sci., Part A:Polym. Chem.*, 2009, **47**, 3544-3557.
132. D. Konkolewicz, A. Gray-Weale and S. Perrier, *J. Am. Chem. Soc.*, 2009, **131**, 18075-18077.
133. I. Kaminska, W. Qi, A. Barras, J. Sobczak, J. Niedziolka-Jonsson, P. Woisel, J. Lyskawa, W. Laure, M. Opallo, M. Li, R. Boukherroub and S. Szunerits, *Chem. Eur. J.*, 2013, **19**, 8673-8678.
134. M. Meldal and C. W. Tornøe, *Chem Rev*, 2008, **108**, 2952-3015.
135. R. G. Spiro, *Glycobiology*, 2002, **12**, 43r-56r.
136. L. Lázár, M. Csávás, M. Herczeg, P. Herczegh and A. Borbás, *Org. Lett.*, 2012, **14**, 4650-4653.
137. P. B. van Seeventer, J. A. L. M. van Dorst, J. F. Siemerink, J. P. Kamerling and J. F. G. Vliegenthart, *Carbohydr. Res.*, 1997, **300**, 369-373.
138. G. Piccirillo, A. Pepe, E. Bedini and B. Bochicchio, *Chem. Eur. J.*, 2017, **23**, 2648-2659.
139. J. Mergy, A. Fournier, E. Hachet and R. Auzély-Velty, *J. Polym. Sci., Part A:Polym. Chem.*, 2012, **50**, 4019-4028.
140. A. Dondoni, A. Massi, P. Nanni and A. Roda, *Chem. Eur. J.,* 2009, **15**, 11444-11449.
141. M. Fiore, M. Lo Conte, S. Pacifico, A. Marra and A. Dondoni, *Tetrahedron Lett.*, 2011, **52**, 444-447.
142. N. Floyd, B. Vijayakrishnan, J. R. Koeppe and B. G. Davis, *Angew. Chem. Int. Ed. Engl.*, 2009, **48**, 7798-7802.
143. S.-H. Yang, Y. O. J. Hermant, P. W. R. Harris and M. A. Brimble, *Eur. J. Org. Chem.*, 2020, **2020**, 944-947.
144. J. H. Hamman, G. M. Enslin and A. F. Kotzé, *BioDrugs*, 2005, **19**, 165-177.
145. L. Zhang and G. Bulaj, *Curr. Med. Chem.*, 2012, **19**, 1602-1618.
146. S. Olatunji, X. Yu, J. Bailey, C.-Y. Huang, M. Zapotoczna, K. Bowen, M. Remškar, R. Müller, E. M. Scanlan, J. A. Geoghegan, V. Olieric and M. Caffrey, *Nat. Commun.*, 2020, **11**, 140.
147. S. A. Cochrane and J. C. Vederas, *Med. Res. Rev.*, 2016, **36**, 4-31.
148. K. Al Ayed, R. D. Ballantine, M. Hoekstra, S. J. Bann, C. M. J. Wesseling, A. T. Bakker, Z. Zhong, Y.-X. Li, N. C. Brüchle, M. van der Stelt, S. A. Cochrane and N. I. Martin, *Chem. Sci.*, 2022, **13**, 3563-3570.
149. G. Swinand, M. Rowe, K. Bowen, S. Olatunji, M. Caffrey and E. M. Scanlan, *Chem.l Commun.*, 2025, **61**, 8083-8086.
150. G. Triola, L. Brunsveld and H. Waldmann, *J. Org. Chem.*, 2008, **73**, 3646-3649.
151. T. H. Wright, A. E. Brooks, A. J. Didsbury, J. D. MacIntosh, G. M. Williams, P. W. Harris, P. R. Dunbar and M. A. Brimble, *Angew. Chem. Int. Ed. Engl.*, 2013, **52**, 10616-10619.
152. S.-H. Yang, P. W. R. Harris, G. M. Williams and M. A. Brimble, *Eur. J. Org. Chem.*, 2016, **2016**, 2608-2616.

153. V. V. Yim, A. J. Cameron, I. Kavianinia, P. W. R. Harris and M. A. Brimble, *Front. Chem.*, 2020, **8**, 568.
154. V. Yim, I. Kavianinia, M. K. Knottenbelt, S. A. Ferguson, G. M. Cook, S. Swift, A. Chakraborty, J. R. Allison, A. J. Cameron, P. W. R. Harris and M. A. Brimble, *Chem. Sci.*, 2020, **11**, 5759-5765.
155. C. Bechtler and C. Lamers, *RSC Med. Chem.*, 2021, **12**, 1325-1351.
156. W. Wang, S. C. Khojasteh and D. Su, *Molecules*, 2021, **26**.
157. M. Moiola, M. G. Memeo and P. Quadrelli, *Molecules*, 2019, **24**.
158. A. A. Aimetti, R. K. Shoemaker, C.-C. Lin and K. S. Anseth, *Chem. Commun.*, 2010, **46**, 4061-4063.
159. A. A. Aimetti, K. R. Feaver and K. S. Anseth, *Chem. Commun.*, 2010, **46**, 5781-5783.
160. B. Zhao, Q. Zhang and Z. Li, *J. Pept. Sci.*, 2016, **22**, 540-544.
161. C. Hoppmann, P. Schmieder, N. Heinrich and M. Beyermann, *Chembiochem*, 2011, **12**, 2555-2559.
162. M. D. Nolan, E. M. Scanlan and R. Petracca, *Org. Biomol.Chem.*, 2022, **20**, 8192-8196.
163. Y. H. Lau, Y. Wu, P. de Andrade, W. R. J. D. Galloway and D. R. Spring, *Nat. Protoc.*, 2015, **10**, 585-594.
164. Y. Wang and D. H. Chou, *Angew. Chem. Int. Ed. Engl.*, 2015, **54**, 10931-10934.
165. Y. Wang, B. J. Bruno, S. Cornillie, J. M. Nogieira, D. Chen, T. E. Cheatham, 3rd, C. S. Lim and D. H. Chou, *Chemistry*, 2017, **23**, 7087-7092.
166. A. Prieto-Castañeda, H. Martin, T. Manna, L. Beswick, J. T. McLean, I. Pongener, I. R. González, B. Twamley, G. J. Miller and E. M. Scanlan, *Org. Biomol. Chem.*, 2025, **23**, 5332-5338.
167. A. Campaniço, M. Baran, A. G. Bowie, D. B. Longley, T. Harrison and J. F. McGouran, *Commun. Chem.*, 2025, **8**, 25.
168. R. O. McCourt, F. Dénès, G. Sanchez-Sanz and E. M. Scanlan, *Org. Lett.*, 2018, **20**, 2948-2951.
169. A. Benny, E. M. Scanlan, *Chem. Commun.*, 2024, **60**, 7950-7953.
170. N. Ostrovitsa, C. Williams, K. Raabe, J. T. McLean, M. Muttenthaler and E. M. Scanlan, *Chem. Eur. J.*, **31**, e202501372.
171. P. P. Di Fiore, S. Polo and K. Hofmann, *Nat. Rev. Mol. Cell Biol.*, 2003, **4**, 491-497.
172. M. J. Clague, S. Urbé and D. Komander, *Nat. Rev. Mol. Cell Biol.*, 2019, **20**, 338-352.
173. N. C. Taylor, G. Hessman, H. B. Kramer and J. F. McGouran, *Chem. Sci.*, 2020, **11**, 2967-2972.
174. N. Griebenow, A. M. Dilmaç, S. Greven and S. Bräse, *Bioconjugate Chem.*, 2016, **27**, 911-917.
175. K. J. Romero, M. S. Galliher, D. A. Pratt and C. R. J. Stephenson, *Chem. Soc. Rev.*, 2018, **47**, 7851-7866.
176. M. Gomberg, *J. Am. Chem. Soc.*, 1900, **22**, 757-771.
177. M. S. Galliher, B. J. Roldan and C. R. J. Stephenson, *Chem. Soc. Rev.*, 2021, **50**, 10044-10057.
178. P. T. Anastas and J. C. Warner, *Green Chemistry: Principles and Case Studies*, The Royal Society of Chemistry, 2019, pp. P011-P012.
179. K. Hojo, A. Hara, H. Kitai, M. Onishi, H. Ichikawa, Y. Fukumori and K. Kawasaki, *Chem. Cent. J.*, 2011, **5**, 49.

180. É. Ujaczki, V. Stark-Rogel, M. Olbrich, M. Fuetsch and J. Backmann, *Environ. Sci. Eur.*, 2022, **34**, 101.
181. A. P. Abbott, G. Capper, D. L. Davies, R. K. Rasheed and V. Tambyrajah, *Chem. Commun.*, 2003, 70-71.
182. M. D. Nolan, A. Mezzetta, L. Guazzelli and E. M. Scanlan, *Green Chem.*, 2022, **24**, 1456-1462.
183. Y. Gu and F. Jérôme, *Chem. Soc. Rev.*, 2013, **42**, 9550-9570.
184. K. Schiefelbein and N. Hartrampf, *CHIMIA*, 2021, **75**, 480.
185. M. Guidi, P. H. Seeberger and K. Gilmore, *Chem. Soc. Rev.*, 2020, **49**, 8910-8932.
186. B. P. Mason, K. E. Price, J. L. Steinbacher, A. R. Bogdan and D. T. McQuade, *Chem. Rev.*, 2007, **107**, 2300-2318.
187. M. B. Plutschack, B. Pieber, K. Gilmore and P. H. Seeberger, *Chem. Rev.*, 2017, **117**, 11796-11893.
188. J. A. M. Lummiss, P. D. Morse, R. L. Beingessner and T. F. Jamison, *Chem. Rec.*, 2017, **17**, 667-680.
189. P. J. Dunn, A. S. Wells and M. T. Williams, *Green Chemistry in the Pharmaceutical Industry*, 2010, pp. 1-20.
190. F. Ferlin, D. Lanari and L. Vaccaro, *Green Chem.*, 2020, **22**, 5937-5955.
191. P. Janssens, W. Debrouwer, K. Van Aken and K. Huvaere, *ChemPhotoChem*, 2018, **2**, 884-889.
192. X. Wang, H. Liang, J. Jiang, Q. Wang, Y. Luo, P. Feng and C. Zhang, *Green Chem.*, 2020, **22**, 5722-5729.
193. K. E. Konan, A. Abollé and F.-X. Felpin, *Eur. J. Org. Chem.*, 2023, **26**, e202201055.
194. A. Steiner, R. C. Nelson, D. Dallinger and C. O. Kappe, *Org. Process. Res. Dev.*, 2022, **26**, 2532-2539.
195. F. Wojcik, A. G. O'Brien, S. Götze, P. H. Seeberger and L. Hartmann, *Chem. Eur. J.*, 2013, **19**, 3090-3098.
196. J. Healy, T. Rasmussen, S. Miller, I. R. Booth and S. J. Conway, *Org. Chem. Front.*, 2016, **3**, 439-446.
197. K. Aoyama, *Int. J. Mol. Sci.*, 2021, **22**.
198. T. Homma and J. Fujii, *Curr. Drug. Metab.*, 2015, **16**, 560-571.
199. B. H. Northrop and R. N. Coffey, *J. Am.Chem. Soc.*, 2012, **134**, 13804-13817.
200. A. Tarai and J. B. Baruah, *ACS Omega*, 2017, **2**, 6991-7001.
201. M. Ahangarpour, I. Kavianinia, P. W. R. Harris and M. A. Brimble, *Chem. Soc. Rev.*, 2021, **50**, 898-944.
202. L. Adhikari, N. E. Larm and G. A. Baker, *ACS Sustainable Chem. Eng.*, 2019, **7**, 11036-11043.
203. N. S. Sinclair, X. Shen, E. Guarr, R. F. Savinell and J. S. Wainright, *J. Electrochem. Soc.*, 2021, **168**, 106506.
204. J. R. Choi, K. W. Yong, J. Y. Choi and A. C. Cowie, *Biotechniques*, 2019, **66**, 40-53.
205. A. Sun, X. He, X. Ji, D. Hu, M. Pan, L. Zhang and Z. Qian, *Chin. Chem. Lett.*, 2021, **32**, 2117-2126.
206. A. C. Okur, P. Erkoc and S. Kizilel, *Colloids Surf., B.*, 2016, **147**, 191-200.
207. N. Zhang, B. Ru, J. Hu, L. Xu, Q. Wan, W. Liu, W. Cai, T. Zhu, Z. Ji, R. Guo, L. Zhang, S. Li and X. Tong, *J. Nanobiotechnol.,* 2023, **21**, 77.
208. F. Li, A. Allahverdi, R. Yang, G. B. Lua, X. Zhang, Y. Cao, N. Korolev, L. Nordenskiöld and C. F. Liu, *Angew. Chem. Int. Ed. Engl.*, 2011, **50**, 9611-9614.

209. F. Li, A. Allahverdi, R. Yang, G. B. J. Lua, X. Zhang, Y. Cao, N. Korolev, L. Nordenskiöld and C.-F. Liu, *Angew.Chem. Int.l Ed.*, 2011, **50**, 9611-9614.
210. S. Hagen, F. Marx, A. F. Ram and V. Meyer, *Appl. Environ. Microbiol.*, 2007, **73**, 2128-2134.
211. Y. P. Chen, Y. Li, F. Chen, H. Wu and S. Zhang, *Front. Microbiol.*, 2023, **14**, 1172257.
212. J. L. Sutcliffe-Goulden, M. J. O'Doherty, P. K. Marsden, I. R. Hart, J. F. Marshall and S. S. Bansal, *Eur. J. Nucl. Med. Mol. Imaging*, 2002, **29**, 754-759.
213. F. Wang, Y. Li, Y. Shen, A. Wang, S. Wang and T. Xie, *Int. J. Mol. Sci.*, 2013, **14**, 13447-13462.
214. S. R. Alexander, D. Lim, Z. Amso, M. A. Brimble and A. J. Fairbanks, *Org. Biomol. Chem.*, 2017, **15**, 2152-2156.
215. M. Ingaramo and D. Beckett, *J. Biol. Chem.*, 2011, **286**, 13071-13078.
216. H. J. A. Chandramohan, T. Y. Yuen, R. Duggal, D. Spiegelberg, L. Yan, Y.-C. A. Juang, L. Ge, P. G. Aronica, H. Y. K. Kaan, Y. H. Lim, A. Peier, B. Sherborne, J. Hochman, S. Lin, K. Biswas, M. Nestor, C. S. Verma, D. P. Lane, T. K. Sawyer, R.Garbaccio, B. Henry, S. Kannan, C. J. Brown, A. W. Partridge, *Nat. Commun.*, 2024, **15**, 489.
217. M. Moiola, M. G. Memeo and P. Quadrelli, *Molecules*, 2019, **24**, 3654.
218. P. D. A. Yu Heng Lau, Soo-Tng Quah, Maxim Rossmann, Luca Laraia, Niklas Sköld, Tze Jing Sum, P.J. E. Rowling, T. L. Joseph, C. Verma, M. Hyvönen, L. S. Itzhaki, A. R. Venkitaraman, C.r J. Brown, D. P. Lane and D. R. Spring, *Chem. Sci.*, 2014, **5**, 1804-1809.
219. S. Monfette and D. E. Fogg, *Chem Rev*, 2009, **109**, 3783-3816.
220. M. J. Klein, S. Schmidt, P. Wadhwani, J. Bürck, J. Reichert, S. Afonin, M. Berditsch, T. Schober, R. Brock, M. Kansy and A. S. Ulrich, *J. Med. Chem.*, 2017, **60**, 8071-8082.
221. S. L. Kuan, T. Wang and T. Weil, *Chem. Eur. J.*, 2016, **22**, 17112-17129.
223. S. B. Gunnoo and A. Madder, *Chembiochem*, 2016, **17**, 529-553.
224. C. E. Stieger, A. J. McMillan, M. A. R. de Geus, J. V. V. Arafiles, L. Franz and C. P. R. Hackenberger, *Angew. Chem. Int. Ed.*, 2025, **64**, e202508656.
225. T. A. King, S. J. Walsh, M. Kapun, T. Wharton, S. Krajcovicova, M. S. Glossop and D. R. Spring, *Chem. Commun.*, 2023, **59**, 9868-9871.
226. O. Boutureira and G. J. L. Bernardes, *Chem. Rev.*, 2015, **115**, 2174-2195.
227. G. J. W. M. Nisavic, C. S. Nielsen, S. M. Jeppesen, J. Palmfeldt, Thomas B. Poulsen, *Bioconjugate Chem.*, 2023, **34**, 994.
228. S. Shaunak, A. Godwin, J. W. Choi, S. Balan, E. Pedone, D. Vijayarangam, S. Heidelberger, I. Teo, M. Zloh and S. Brocchini, *Nat. Chem. Biol.*, 2006, **2**, 312-313.
229. S. Brocchini, S. Balan, A. Godwin, J.-W. Choi, M. Zloh and S. Shaunak, *Nat. Protoc.*, 2006, **1**, 2241-2252.
230. M. T. W. Lee, A. Maruani, J. R. Baker, S. Caddick and V. Chudasama, *Chem. Sci.*, 2016, **7**, 799-802.
231. C. Kourra and N. Cramer, *Chem. Sci.*, 2016, **7**, 7007-7012.
232. N. Martínez-Sáez, S. Sun, D. Oldrini, P. Sormanni, O. Boutureira, F. Carboni, I. Compañón, M. J. Deery, M. Vendruscolo, F. Corzana, R. Adamo and G. J. L. Bernardes, *Angew. Chem. Int. Ed. Engl.*, 2017, **56**, 14963-14967.
233. D. A. Richards, M. Nobles, H. Kossen, L. Tedaldi, V. Chudasama, A. Tinkerb and J. R. Baker *Org. Biomol. Chem.*, 2016, **14**, 455-459.
234. Z. W. Shiwei Lü, Shifa Zhu, *Nat. Commun.*, 2022, **13**.

235. C. E. H. a. C. N. B. Andrew B. Lowe, *J. Mat. Chem.*, 2010, **20**, 4745-4750.
236. J. L. Y. Tian, H. Zhao, X. Zeng, D. Wang, Q. Liu, X. Niu, X. Huang, N. Xu and Z. Li., *Chem. sci.*, 2016, **7**, 3325–3330.
237. X. Ma and W. Zhang, *iSci.*, 2022, **25**, 105005.
238. F. R. Smith, D. Meehan, R. C. Griffiths, H. J. Knowles, P. Zhang, H. E. L. Williams, A. J. Wilson and N. J. Mitchell, *Chem. Sci.*, 2024, **15**, 9612-9619.
239. U. Wirth, K. Raabe, P. Kalaba, E. Keimpema, M. Muttenthaler and B. König, *J. Med. Chem.*, 2023, **66**, 14853-14865.
240. S. N. Mthembu, A. Sharma, F. Albericio and B. G. de la Torre, *Chembiochem*, 2020, **21**, 1947-1954.
241. Q. Wan and S. J. Danishefsky, *Angew. Chem. Int. Ed.*, 2007, **46**, 9248-9252.
242. A. González and G. Valencia, *Tetrahedron: Asymmetry*, 1998, **9**, 2761-2764.
243. J. A. Rossi-Ashton, A. K. Clarke, W. P. Unsworth and R. J. K. Taylor, *ACS Catalysis*, 2020, **10**, 7250-7261.
244. W. Duane Brown, *Biochim. Biophys. Acta*, 1960, **44**, 365-367.
245. C. R. Stahl and S. Siggia, *Anal. Chem.*, 1957, **29**, 154-155.
246. G. T. Hermanson, *Bioconjugate Techniques (Third Edition)*, ed. G. T. Hermanson, Academic Press, Boston, 2013, pp. 127-228.
247. P. C. Jocelyn, *Methods in Enzymology*, Academic Press, 1987, vol. 143, pp. 246-256.
248. H. C. Brown and G. Zweifel, *J.Am. Chem. Soc.*, 1961, **83**, 3834-3840.
249. H.-W. Hsieh, R. A. Davis, J. A. Hoch and J. Gervay-Hague, *Chem. Eur. J.*, 2014, **20**, 6444-6454.
250. N. Wolf, L. Kersting, C. Herok, C. Mihm and J. Seibel, *J. Org. Chem.*, 2020, **85**, 9751-9760.
251. M. Verdoes, B. I. Florea, U. Hillaert, L. I. Willems, W. A. van der Linden, M. Sae-Heng, D. V. Filippov, A. F. Kisselev, G. A. van der Marel and H. S. Overkleeft, *Chembiochem*, 2008, **9**, 1735-1738.
252. I. L. Cartwright, D. W. Hutchinson and V. W. Armstrong, *Nucleic Acids Res.*, 1976, **3**, 2331-2340.
253. P. E. Battershill and S. P. Clissold, *Drugs*, 1989, **38**, 658-702.
254. M. D. Katz and B. L. Erstad, *Clin. Pharm.*, 1989, **8**, 255-273.
255. T. Z. Attia, S. G. Abdulrazik and S. M. Derayea, *Luminescence*, 2022, **37**, 1914-1920.
256. E. M. Wolin, *Gastrointest. Cancer Res.*, 2012, **5**, 161-168.
257. G. A. Kaltsas, D. Papadogias, P. Makras and A. B. Grossman, *Endocr. Relat. Cancer*, 2005, **12**, 683-699.
258. S. M. Derayea, S. G. Abdulrazik and T. Z. Attia, *Spectrochim. Acta, Part A*, 2024, **305**, 123546.
259. U. Jaehde, R. Masereeuw, A. G. De Boer, G. Fricker, J. F. Nagelkerke, J. Vonderscher and D. D. Breimer, *Pharm. Res.*, 1994, **11**, 442-448.
260. W. Mier, B. Beijer, K. Graham and W. E. Hull, *Bioorg. Med. Chem.*, 2002, **10**, 2543-2552.
261. A. Vasco Vidal, L. González Ceballos, L. Wessjohann and D. Rivera, *Eur. J. Org. Chem.*, 2022, **2022**.
262. S. R. Manne, A. Sharma, A. Sazonovas, A. El-Faham, B. G. de la Torre and F. Albericio, *ACS Omega*, 2022, **7**, 6007-6023.
263. A. V. Bordoni, M. V. Lombardo and A. Wolosiuk, *RSC Advances*, 2016, **6**, 77410-77426.

264. F. Dénès, M. Pichowicz, G. Povie and P. Renaud, *Chem. Rev.*, 2014, **114**, 2587-2693.
265. G. A. Amaral, F. Ausfelder, J. G. Izquierdo, L. Rubio-Lago and L. Bañares, *J. Chem. Phys.*, 2007, **126**, 024301.
266. B. Castanheira, F. de Jesus Trindade, L. dos Santos Andrade, I. L. Nantes, M. J. Politi, E. R. Triboni and S. Brochsztain, *J. Photochem. Photobiol., A*, 2017, **332**, 316-325.
267. V. Maffeis, R. O. McCourt, R. Petracca, O. Laethem, A. Camisasca, P. E. Colavita, S. Giordani and E. M. Scanlan, *ACS Appl. Nano Mater.*, 2018, **1**, 4120-4126.
268. X. Lang, X. Chen and J. Zhao, *Chem. Soc. Rev.*, 2014, **43**, 473-486.
269. X.-H. Qin, A. Ovsianikov, J. Stampfl and R. Liska, *BioNanoMater.*, 2014, **15**, 49-70.
270. B. Moosmann and P. Hajieva, *Antioxidants*, 2022, **11**, 885.
271. R. A. Angnes, Z. Li, C. R. D. Correia and G. B. Hammond, *Org. Biomol. Chem.*, 2015, **13**, 9152-9167.
272. J. P. Barham and B. König, *Angew. Chem. Int. Ed.*, 2020, **59**, 11732-11747.
273. M. H. Keylor, J. E. Park, C.-J. Wallentin and C. R. J. Stephenson, *Tetrahedron*, 2014, **70**, 4264-4269.
274. E. L. Tyson, M. S. Ament and T. P. Yoon, *J. Org. Chem.*, 2013, **78**, 2046-2050.
275. Y. Qiao and E. J. Schelter, *Acc.Chem. Res.*, 2018, **51**, 2926-2936.
276. R. W. Middleton, J. Parrick, E. D. Clarke and P. Wardman, *J. Heterocycl. Chem.*, 1986, **23**, 849-855.
277. C. Wynne and R. B. P. Elmes, *Front. Chem.*, 2024, **12.**
278. M. F. Braña, J. M. Castellano, C. M. Roldán, A. Santos, D. Vázquez and A. Jiménez, *Cancer Chemother Pharmacol*, 1980, **4**, 61-66.
279. W. W. Stewart, *J. Am. Chem. Soc.*, 1981, **103**, 7615-7620.
280. F. Cosnard and V. Wintgens, *Tetrahedron Lett.*, 1998, **39**, 2751-2754.
281. N. Singh, R. Srivastava, A. Singh and R. K. Singh, *J. Fluoresc.*, 2016, **26**, 1431-1438.
282. E. Martin, R. Weigand and A. Pardo, *J. Lumin.*, 1996, **68**, 157-164.
283. A. F. Henwood, N. Curtin, S. Estalayo-Adrián, A. J. Savyasachi, T. A. Gudmundsson, J. I. Lovitt, L. C. Sigurvinsson, H. L. Dalton, C. S. Hawes, D. Jacquemin, D. F. O'Shea and T. Gunnlaugsson, *Chem.*, 2024, **10**, 578-599.
284. S. Cheung and D. F. O'Shea, *Nat. Commun.*, 2017, **8**, 1885.
285. L. Ramírez Lázaro, L. C. Sigurvinsson, N. Curtin, J. Ho, E. T. Luis, D. A. McAdams, T. A. Gudmundsson, C. S. Hawes, D. Jacquemin, D. F. O'Shea, E. M. Scanlan, T. Gunnlaugsson and A. F. Henwood, *J.Mater. Chem. B*, 2025, **13**, 929-942.
286. N. Zivic, J. Zhang, D. Bardelang, F. Dumur, P. Xiao, T. Jet, D.-L. Versace, C. Dietlin, F. Morlet-Savary, B. Graff, J. P. Fouassier, D. Gigmes and J. Lalevée, *Polym. Chem.*, 2016, **7**, 418-429.
287. J. Zhang, N. Zivic, F. Dumur, P. Xiao, B. Graff, J. P. Fouassier, D. Gigmes and J. Lalevée, *Polym. Chem.*, 2018, **9**, 994-1003.
288. J. Luo, Z. Xie, J. W. Y. Lam, L. Cheng, H. Chen, C. Qiu, H. S. Kwok, X. Zhan, Y. Liu, D. Zhu and B. Z. Tang, *Chem.Commun.s*, 2001, 1740-1741.
289. R. O. McCourt and E. M. Scanlan, *Chem. Eur. J.* , 2020, **26**, 15804-15810.
290. S. S. Zalesskiy, N. S. Shlapakov and V. P. Ananikov, *Chem. Sci.*, 2016, **7**, 6740-6745.

291. M. Rahal, H. Mokbel, B. Graff, V. Pertici, D. Gigmes, J. Toufaily, T. Hamieh, F. Dumur and J. Lalevée, *ChemPhotoChem*, 2021, **5**, 476-490.
292. B. Abraham and L. A. Kelly, *J. Phys. Chem. B*, 2003, **107**, 12534-12541.
293. A. Marini, A. Muñoz-Losa, A. Biancardi and B. Mennucci, *J. Phys. Chem. B*, 2010, **114**, 17128-17135.
294. G. J. Ryan, S. Quinn and T. Gunnlaugsson, *Inorg. Chem.*, 2008, **47**, 401-403.
295. B. M. Aveline, S. Matsugo and R. W. Redmond, *J. Am. Chem. Soc.*, 1997, **119**, 11785-11795.
296. R. González-Muñiz, M. Bonache and M. J. Pérez de Vega, *Molecules*, 2021, **26**.
297. D. S. Chen and I. Mellman, *Immunity*, 2013, **39**, 1-10.
298. M. I. Del Olmo-Garcia and J. F. Merino-Torres, *J. Diabetes Res.*, 2018, **2018**, 4020492.
299. M. J. van Haren, Y. Zhang, V. Thijssen, N. Buijs, Y. Gao, L. Mateuszuk, F. A. Fedak, A. Kij, R. Campagna, D. Sartini, M. Emanuelli, S. Chlopicki, S. A. K. Jongkees and N. I. Martin, *RSC Chem. Biol.*, 2021, **2**, 1546-1555.
300. P. G. Dougherty, A. Sahni and D. Pei, *Chem. Rev.*, 2019, **119**, 10241-10287.
301. H. C. Hayes, L. Y. P. Luk and Y.-H. Tsai, *Org. Biomol.Chem.*, 2021, **19**, 3983-4001.
302. B. Seelig, *Nat.Protoc.*, 2011, **6**, 540-552.
303. G. Kamalinia, B. J. Grindel, T. T. Takahashi, S. W. Millward and R. W. Roberts, *Chem. Soc. Rev.*, 2021, **50**, 9055-9103.
304. T. Passioura and H. Suga, *Chem. Eur. J.*, 2013, **19**, 6530-6536.
305. Y.-K. Choi, T. Katoh, A. Beattie and H. Suga, *Nat. Commun.*, 2025, **16**, 4671.
306. T. Katoh and H. Suga, *Nat. Rev. Chem.*, 2024, **8**, 879-892.
307. H. Saito and H. Suga, *J. Am. Chem.Soc.*, 2001, **123**, 7178-7179.
308. H. Peacock and H. Suga, *Trends Pharmacol. Sci.*, 2021, **42**, 385-397.
309. T. Ozaki, K. Yamashita, Y. Goto, M. Shimomura, S. Hayashi, S. Asamizu, Y. Sugai, H. Ikeda, H. Suga and H. Onaka, *Nat. Commun.* 2017, **8**, 14207.
310. R. Yoshisada, S. Weller, T. S. Çobanoğlu, H. N. de Kock and S. A. K. Jongkees, *Chem. Asian J.*, 2024, **19**, e202400336.
311. J. N. Coronado, P. Ngo, E. V. Anslyn and A. D. Ellington, *Cell Chem. Biol.* 2022, **29**, 1071-1112.
312. Y. Wu, M. T. Bertran, D. Joshi, S. L. Maslen, C. Hurd and L. J. Walport, *Commun. Chem.*, 2023, **6**, 103.
313. K. Hayashi, S. Uehara, S. Yamamoto, D. R. Cary, J. Nishikawa, T. Ueda, H. Ozasa, K. Mihara, N. Yoshimura, T. Kawai, T. Ono, S. Yamamoto, M. Fumoto and H. Mikamiyama, *ACS Med. Chem. Lett.*, 2021, **12**, 1093-1101.
315. R. Lagoutte, R. Patouret and N. Winssinger, *Curr. Opin. Chem. Biol.,* 2017, **39**, 54-63.
316. A. Abdeldayem, Y. S. Raouf, S. N. Constantinescu, R. Moriggl and P. T. Gunning, *Chem. Soc. Rev.*, 2020, **49**, 2617-2687.
317. A. Chaikuad, P. Koch, S. A. Laufer and S. Knapp, *Angew. Chem. Int. Ed.* 2018, **57**, 4372-4385.
318. F. Liu, J. Z. H. Zhang and Y. Mei, *Sci. Rep.*, 2016, **6**, 27190.
319. N. M. Green, *Advances in Protein Chemistry*, eds. C. B. Anfinsen, J. T. Edsall and F. M. Richards, Academic Press, 1975, vol. 29, pp. 85-133.
320. T. Kantner, B. Alkhawaja and A. G. Watts, *ACS Omega*, 2017, **2**, 5785-5791.
321. Y. Goto, A. Ohta, Y. Sako, Y. Yamagishi, H. Murakami and H. Suga, *ACS Chem. Biol.*, 2008, **3**, 120-129.
322. B. J. J. Timmer and O. Ramström, *Chemistry*, 2019, **25**, 14408-14413.

323. A. M. Gómez, C. Uriel, A. Oliden-Sánchez, J. Bañuelos, I. Garcia-Moreno and J. C. López, *J. Org. Chem.*, 2021, **86**, 9181-9188.
324. E. Talley, M. D. Vale and E. Yanovsky, *J. Am.Chem. Soc.*, 1945, **67**, 2037-2039.
325. 1992.
326. A. L. M. Morotti, K. L. Lang, I. Carvalho, E. P. Schenkel and L. S. C. Bernardes, *Tetrahedron Lett.*, 2015, **56**, 303-307.
327. Y. Bandera, H. W. Jones, B. Grant, S. Mell and S. H. Foulger, *RSC Adv.*, 2022, **12**, 29187-29196.
328. M. Verdoes, B. I. Florea, V. Menendez-Benito, C. J. Maynard, M. D. Witte, W. A. van der Linden, A. M. van den Nieuwendijk, T. Hofmann, C. R. Berkers, F. W. van Leeuwen, T. A. Groothuis, M. A. Leeuwenburgh, H. Ovaa, J. J. Neefjes, D. V. Filippov, G. A. van der Marel, N. P. Dantuma and H. S. Overkleeft, *Chem. Biol.*, 2006, **13**, 1217-1226.

Appendix

9.1 Chapter 2

9.1.1 NMR Spectra

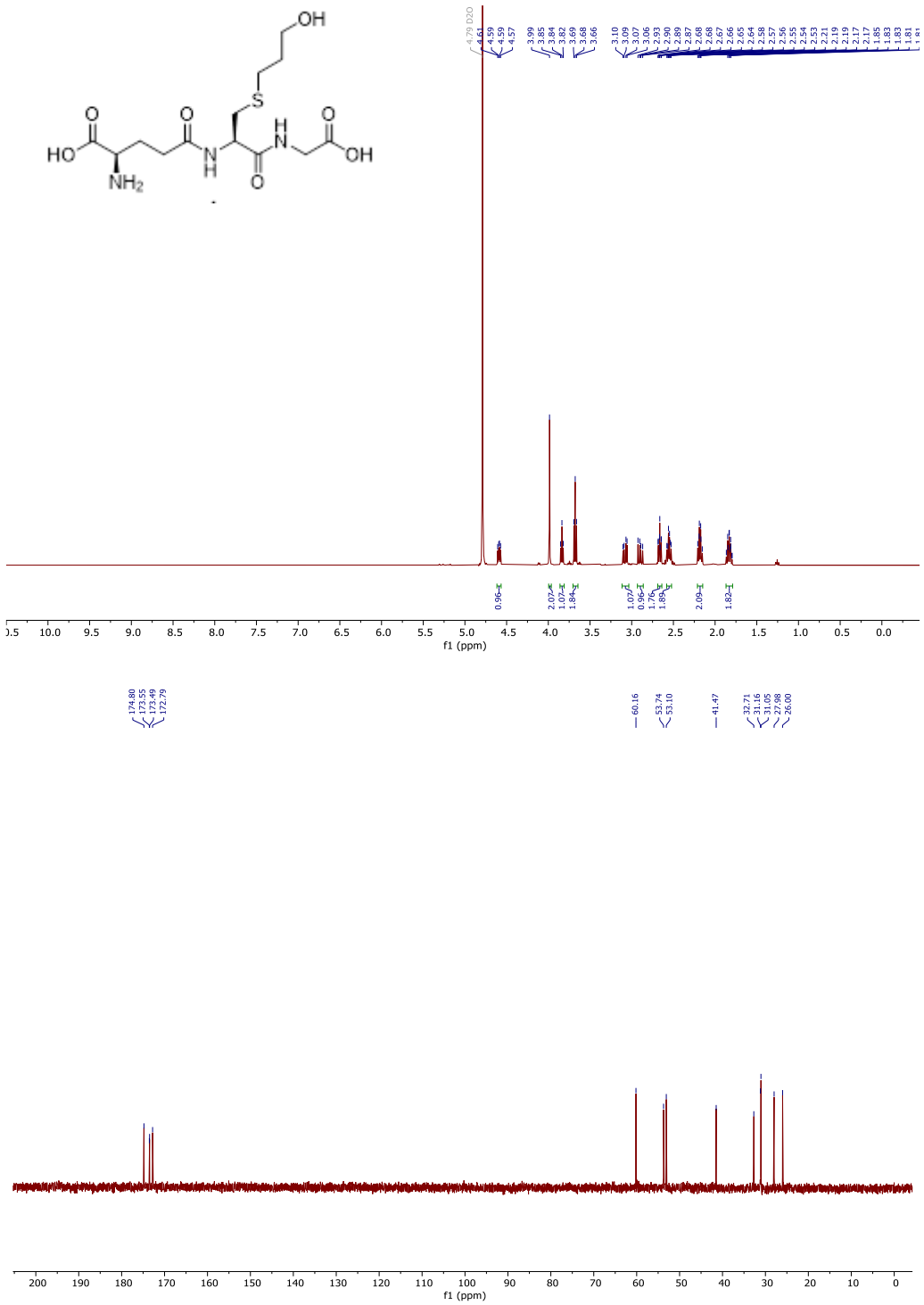

Figure S9.1: ^{1}H and ^{13}C NMR (400 MHz, D_2O) spectra of compound 50

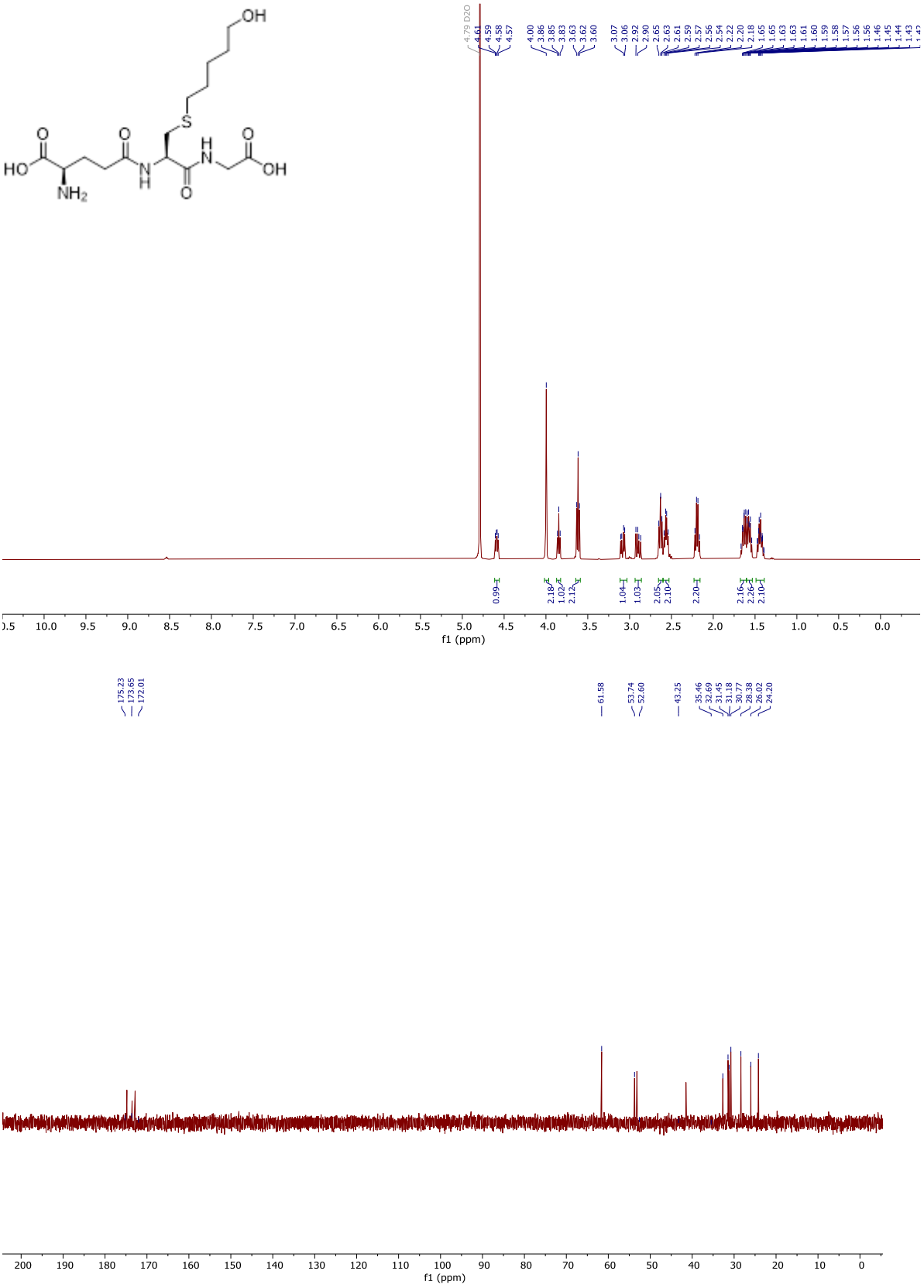

Figure S9.2: ^{1}H and ^{13}C (400 MHz, D_2O) NMR spectra of compound 54

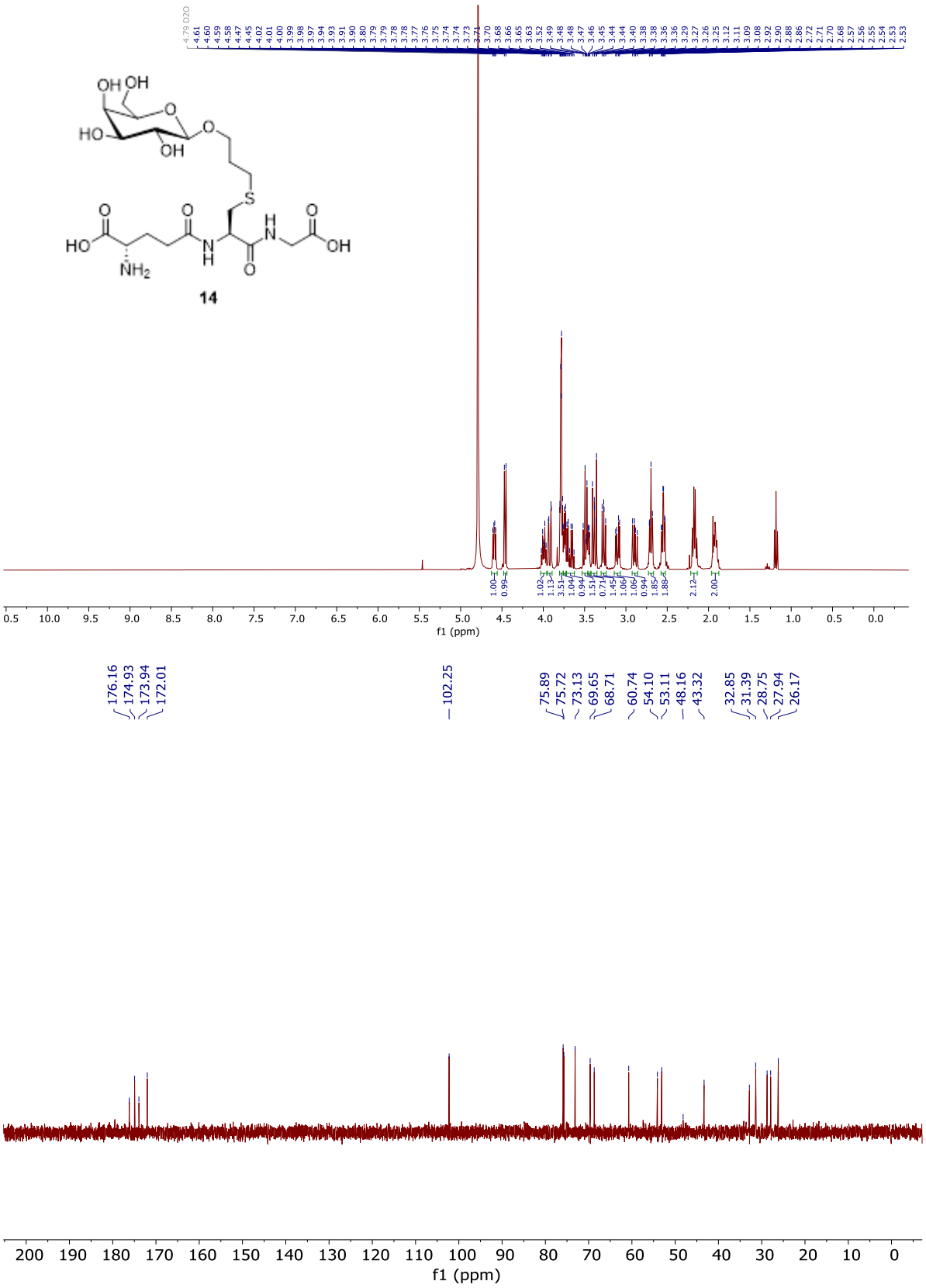

Figure S9.3: ^{1}H and ^{13}C NMR (400 MHz, D_2O) spectra of compound 62

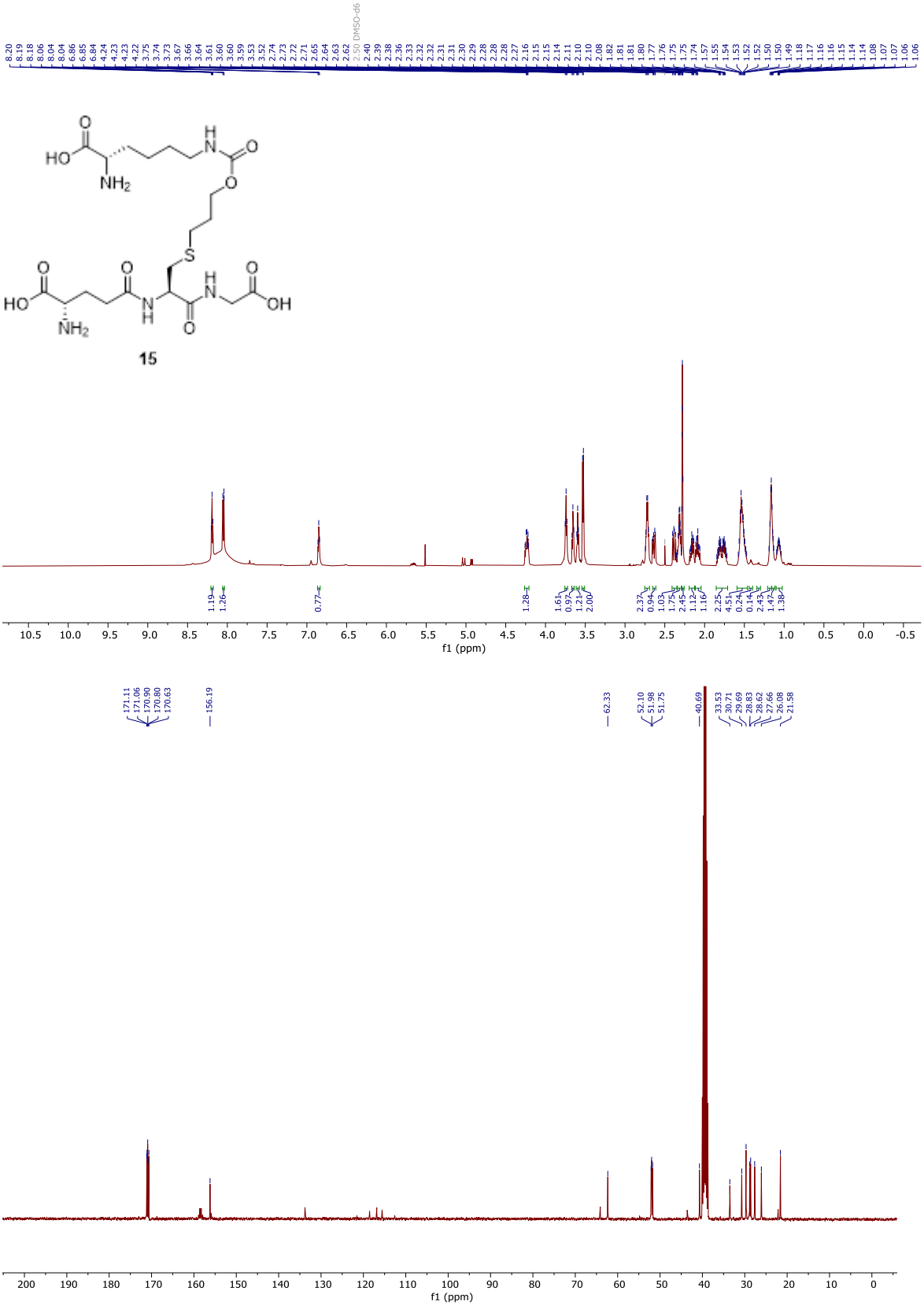

Figure S9.4: ^{1}H and ^{13}C NMR (600 MHz, DMSO) spectra of compound 63

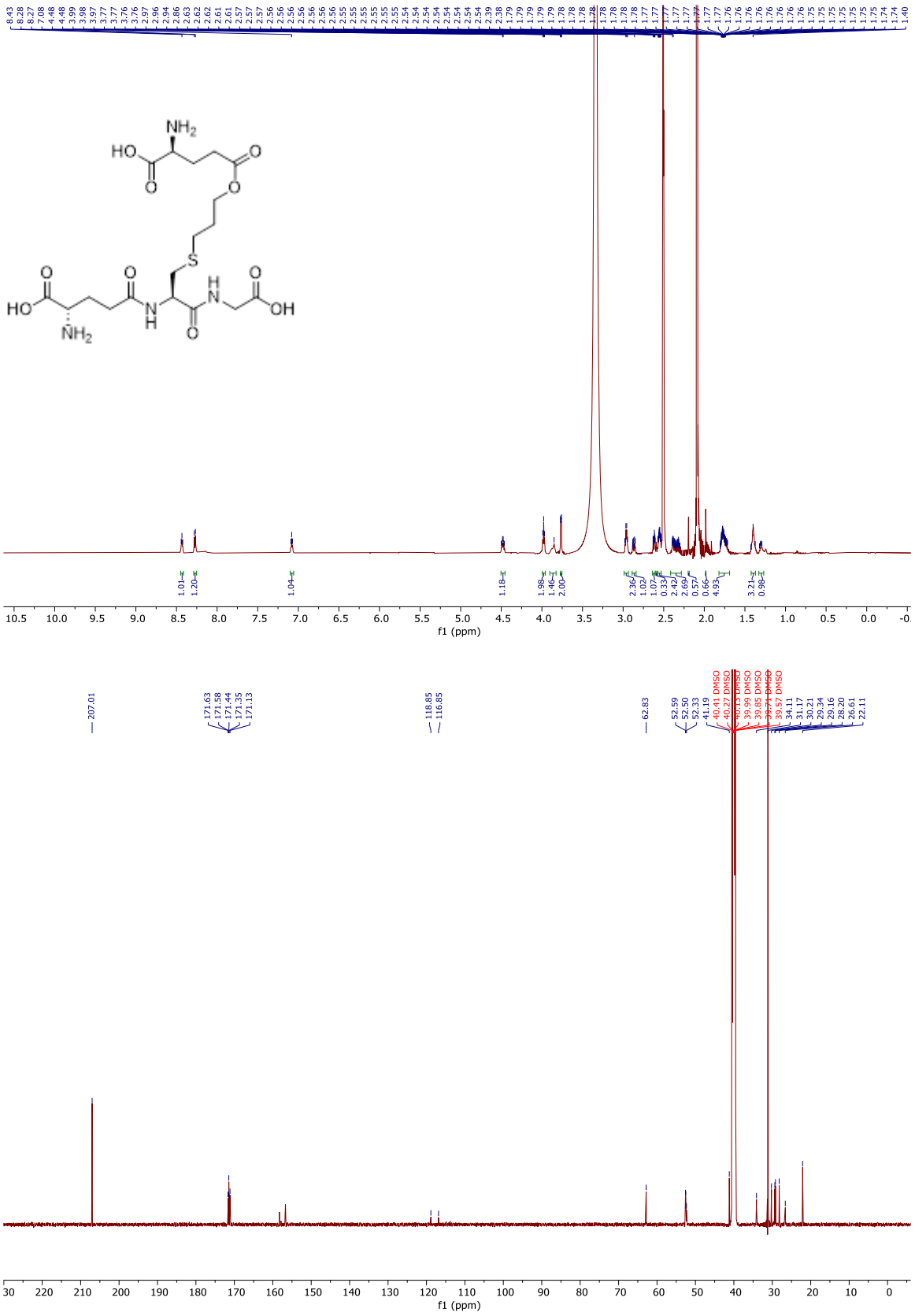

Figure S9.5: ^{1}H and ^{13}C NMR (600 MHz, DMSO) spectra of compound 64

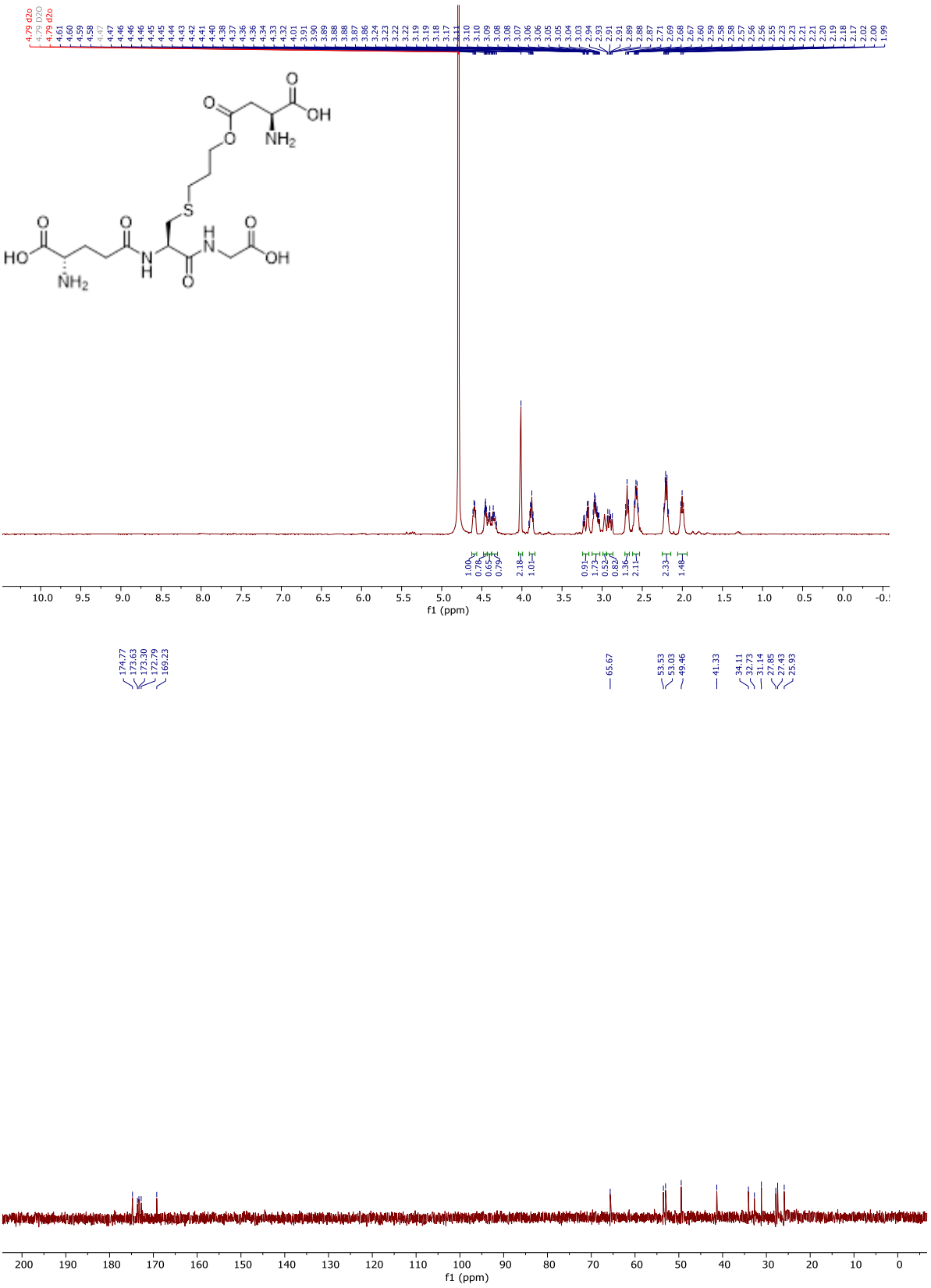

Figure S9.6: ^{1}H and ^{13}C NMR (600 MHz, DMSO) spectra of compound 65

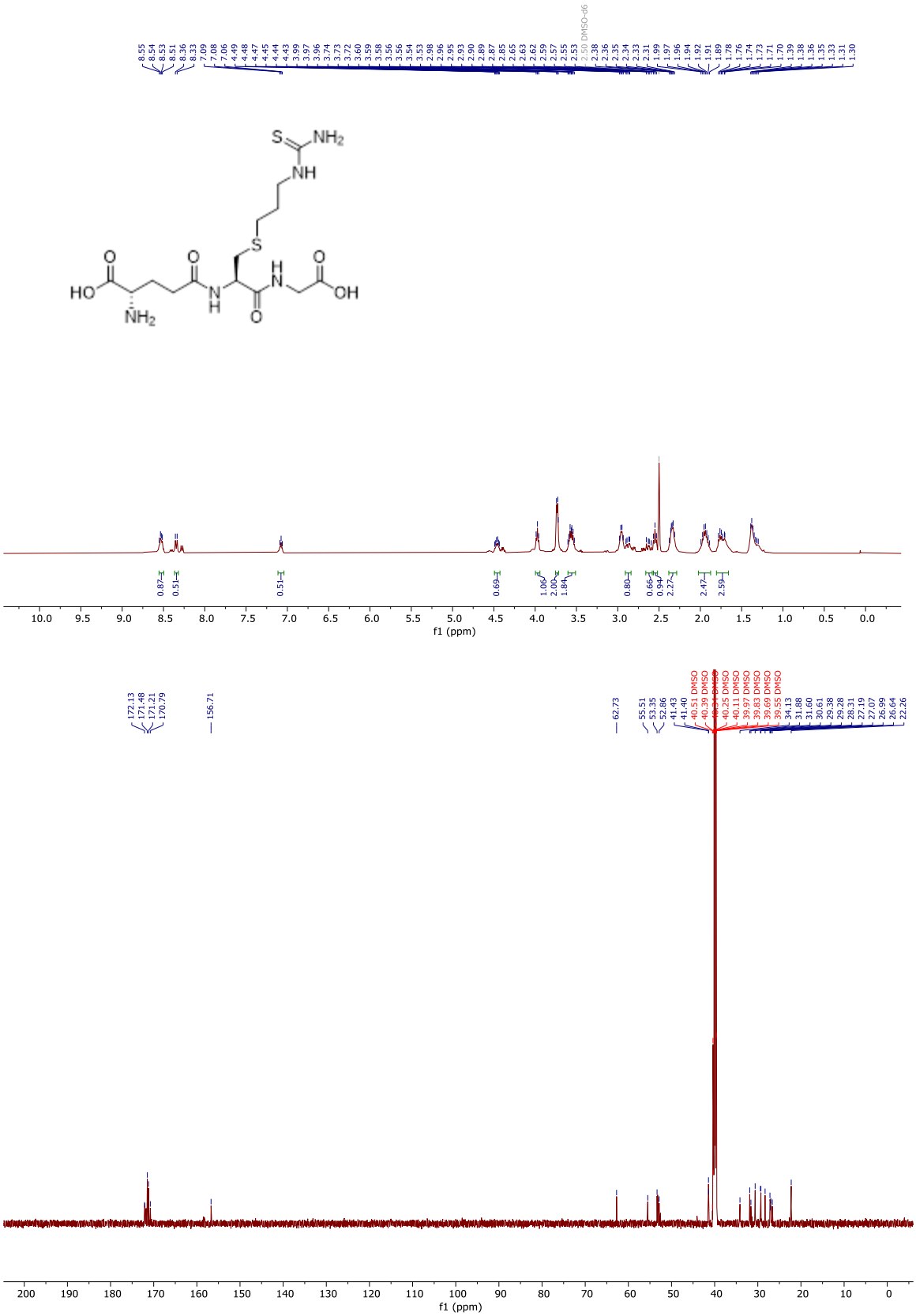

Figure S9.7: ^{1}H and ^{13}C NMR (600 MHz, DMSO) spectra of compound 67

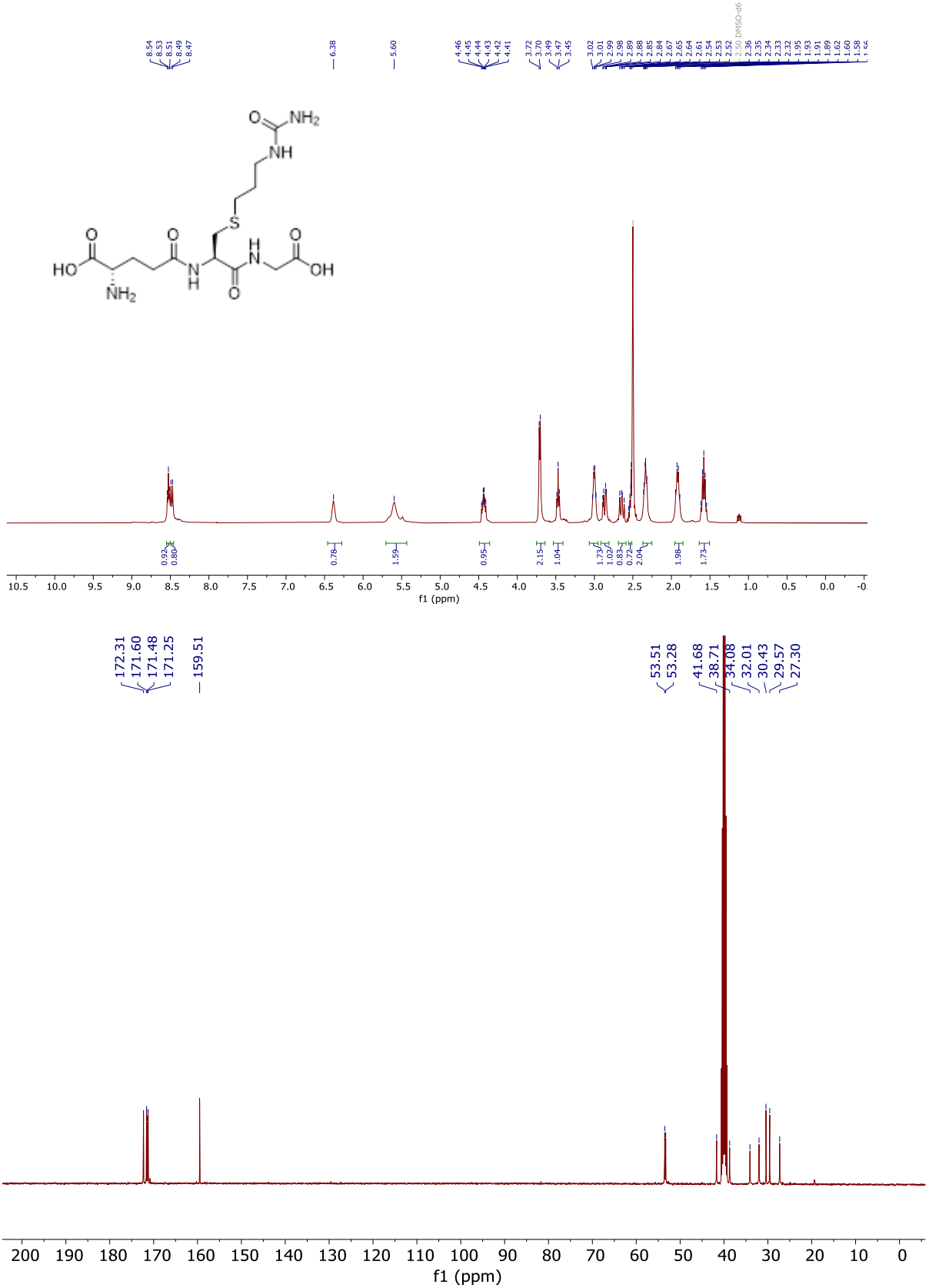

^{1}H Figure S9.8: ^{1}H and ^{13}C NMR (600 MHz, DMSO) spectra of compound 68

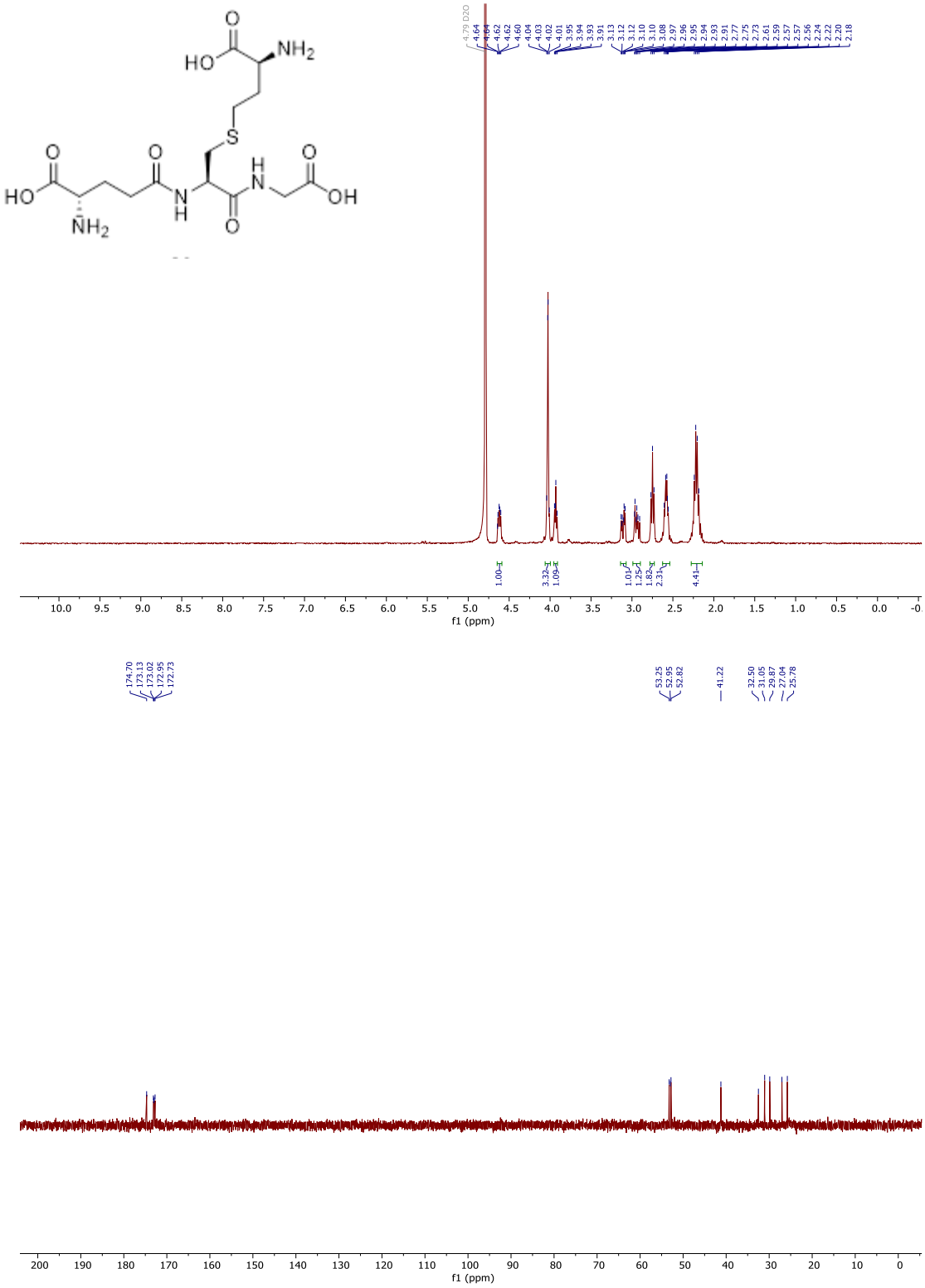

Figure S9.9: ^{1}H and ^{13}C NMR (400 MHz, D_2O) spectra of compound 68

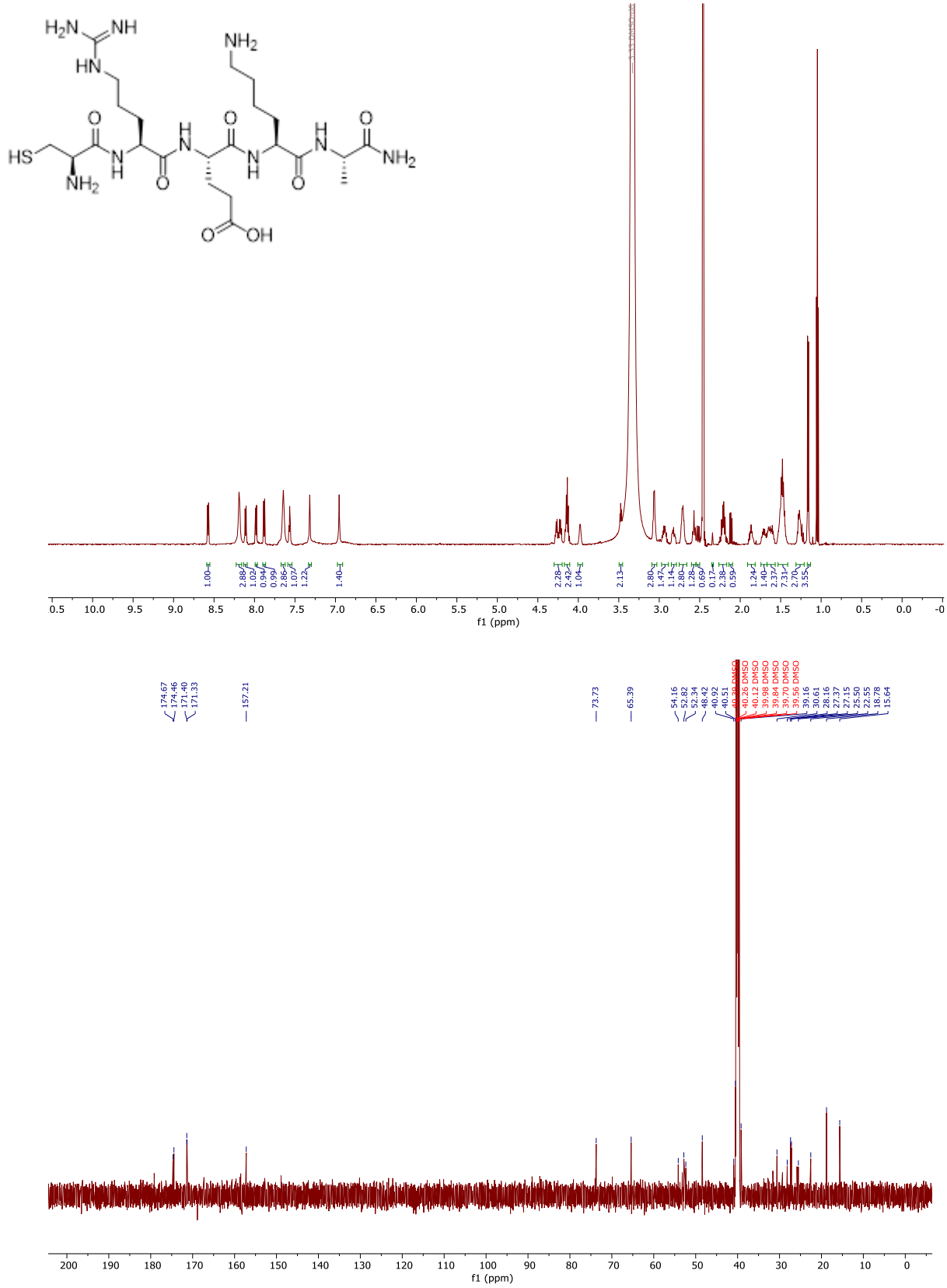

Figure S9.10: ^{1}H and ^{13}C NMR (600 MHz, DMSO) spectra of compound 77

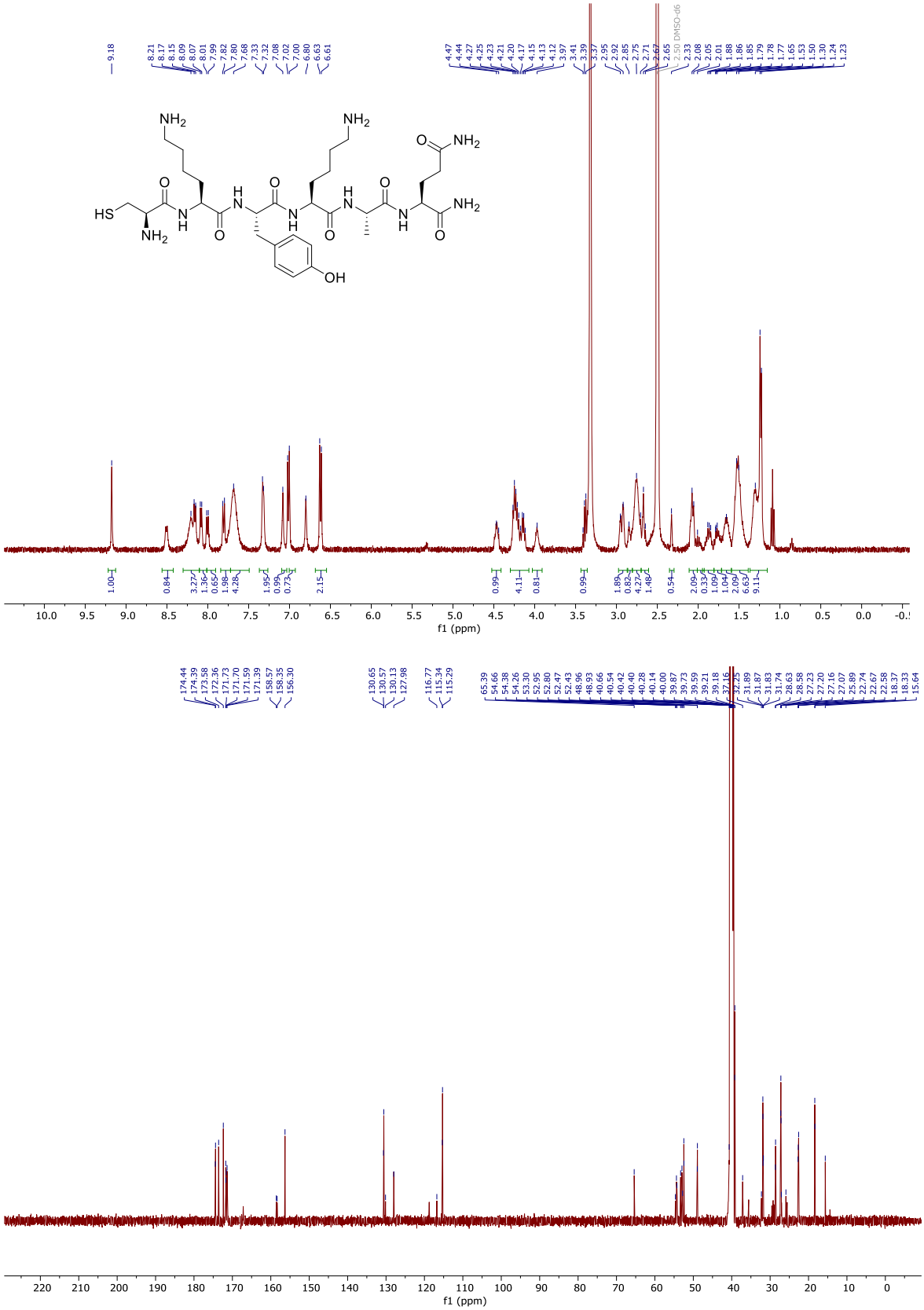

Figure S9.11: ^{1}H and ^{13}C NMR (600 MHz, DMSO) spectra of compound 79

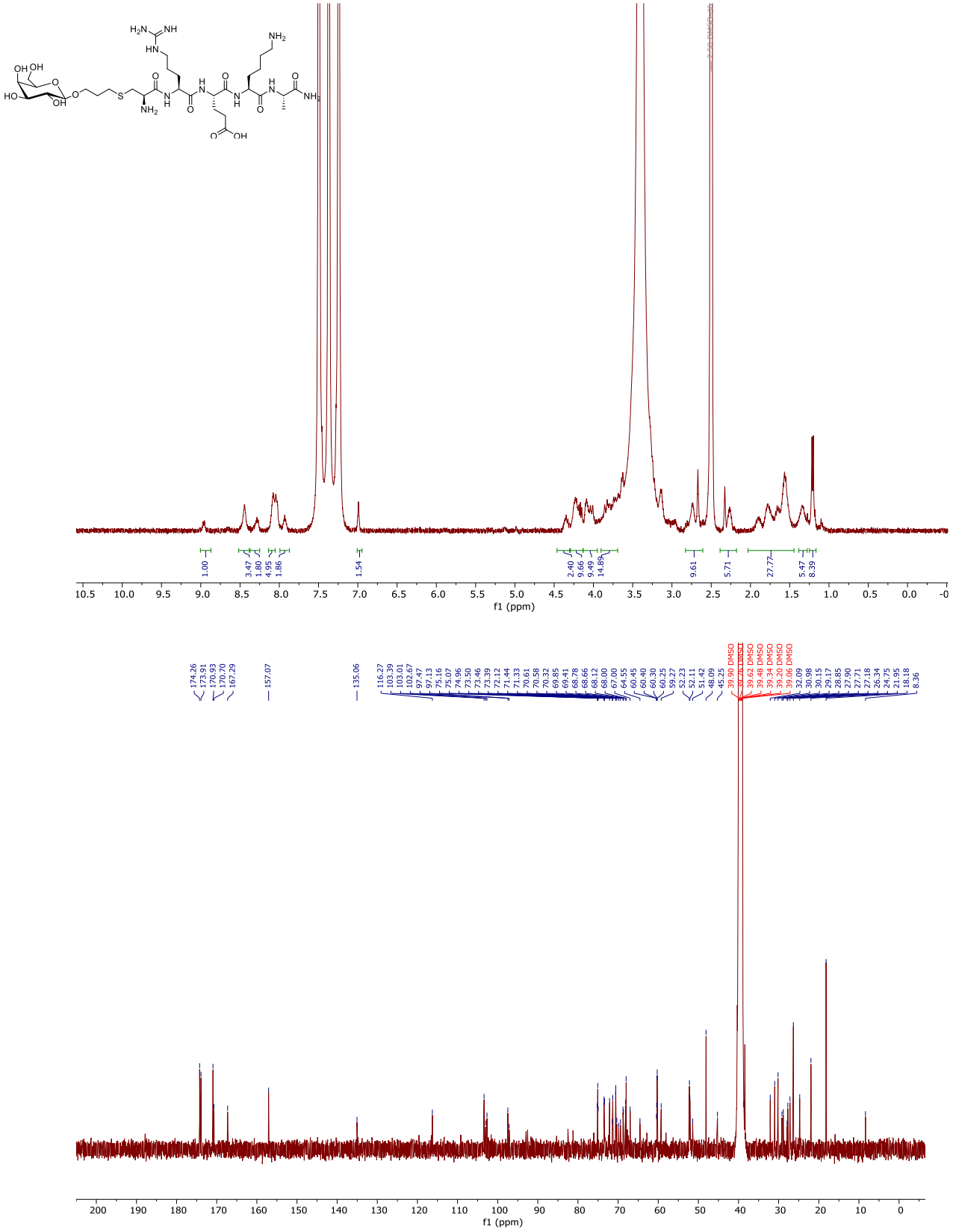

Figure S9.12: ^{1}H and ^{13}C NMR (600 MHz, DMSO) spectra of compound 78

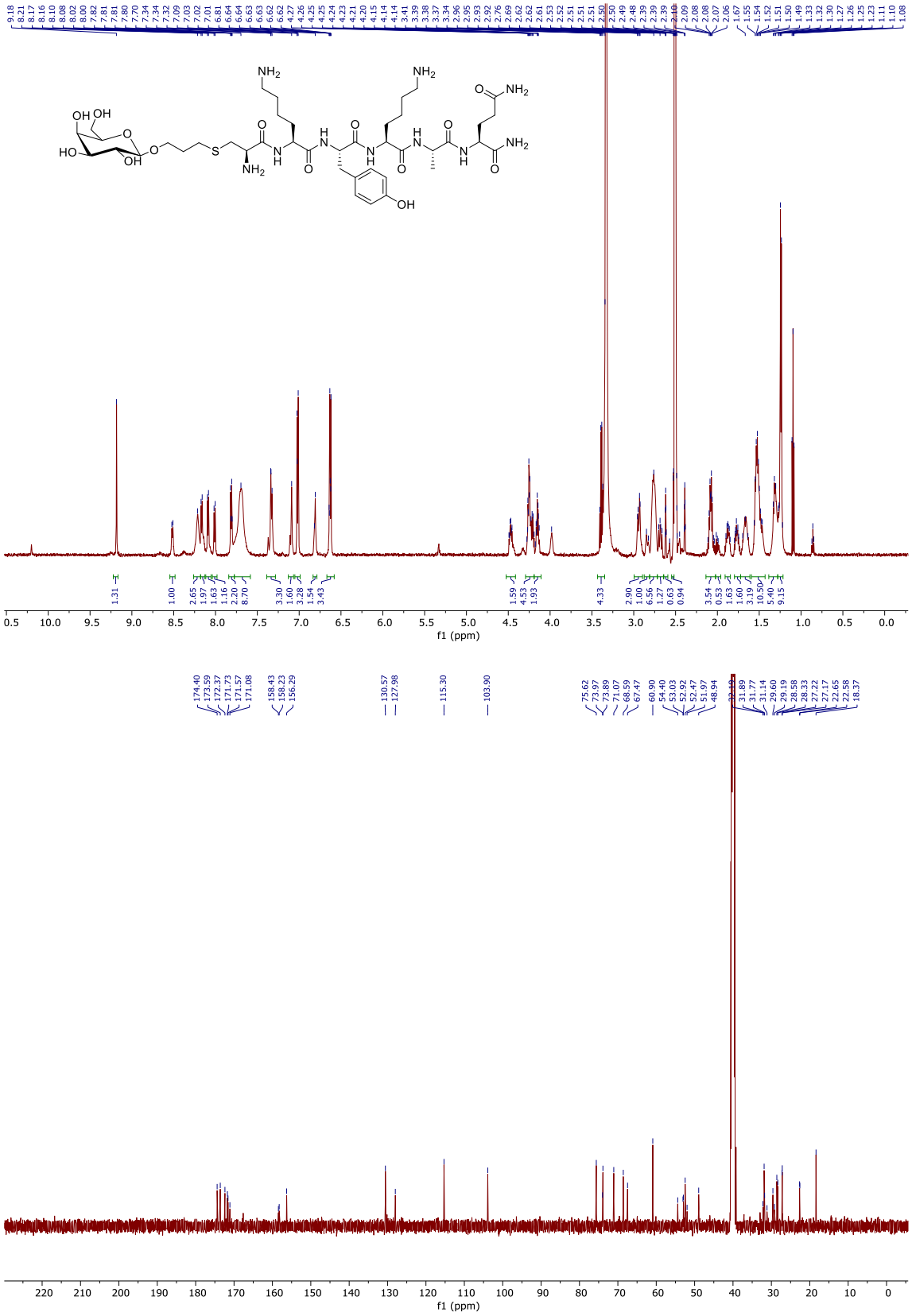

Figure S9.13: ^{1}H and ^{13}C NMR (600 MHz, DMSO) spectra of compound 80

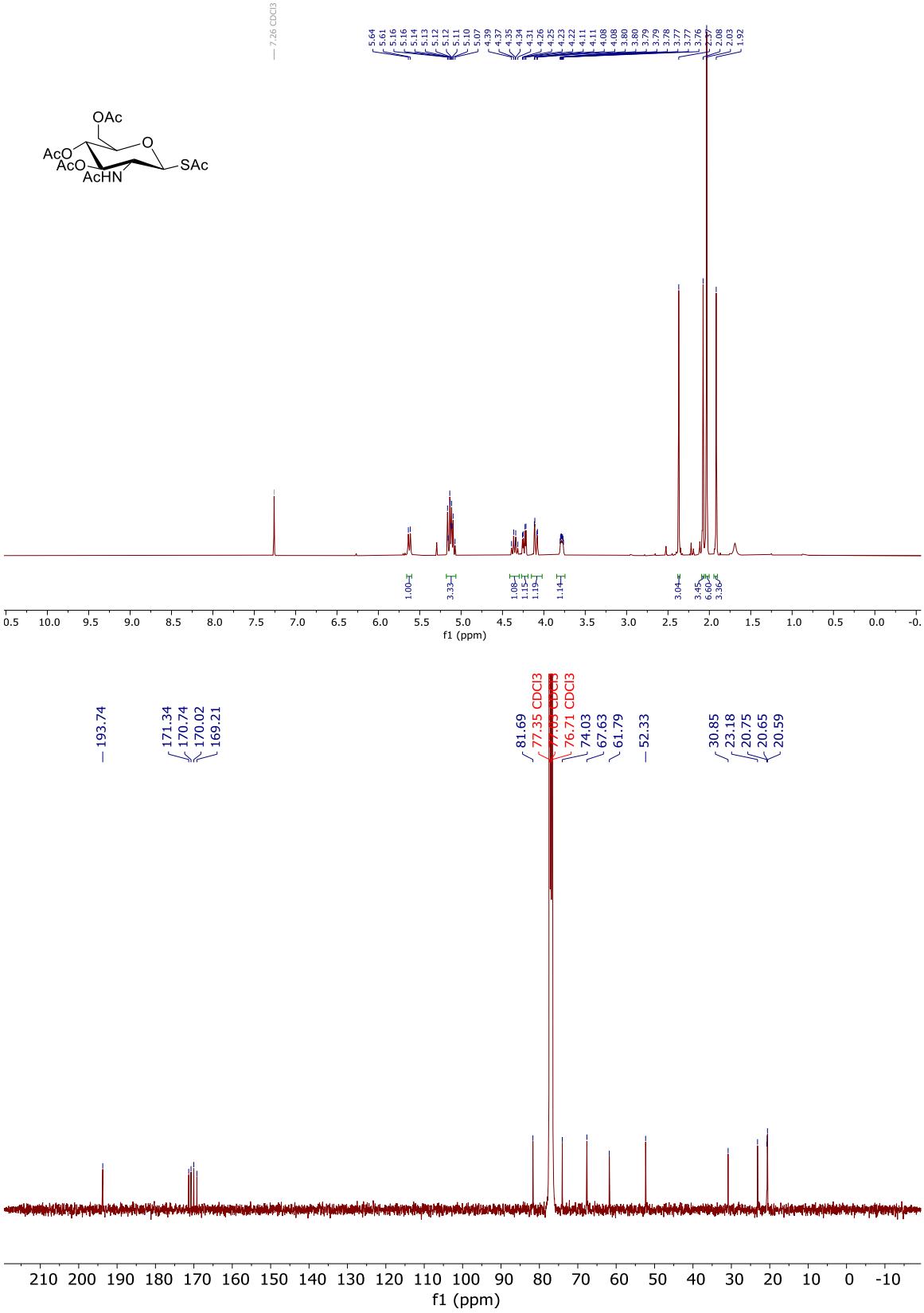

Figure S9.14: ^{1}H and ^{13}C NMR (600 MHz, $CDCl_3$) spectra of compound 83.

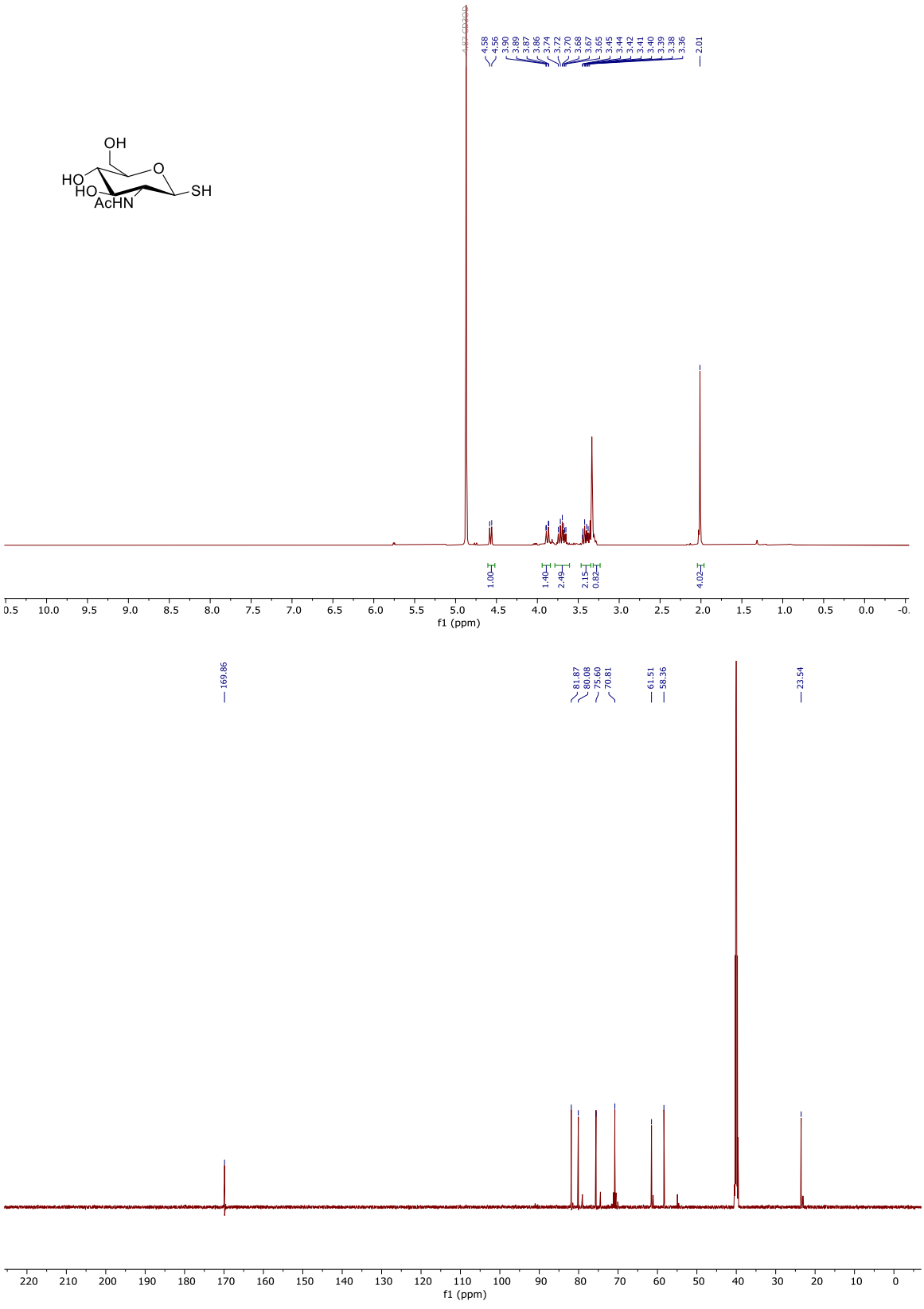

Figure S9.15: ^{1}H and ^{13}C NMR (400 MHz, $MeOD_4$) spectra of compound 84

9.1.2 Analytical Calibrations

Table S9.1: Measures of retention times for different concentrations of GSH, standard deviation (s) and coefficient of variation (RSD) and RP-HPLC data. (2 - 15% ACN, 20 min 0.1% TFA, λ = 214 nm).

C	Retention time			Average	s	RSD (%)
(mg·ml^{-1})	(min)					
1	1.911	1.916	1.903	1.91	0.00535	0.28
3.3	1.886	1.836	1.836	1.85	0.02357	1.27
4.8	1.873	1.879	1.875	1.88	0.00249	0.133
7.6	1.863	1.811	1.733	1.80	0.0534	2.96
9.7	1.853	1.754	1.789	1.80	0.0410	2.28

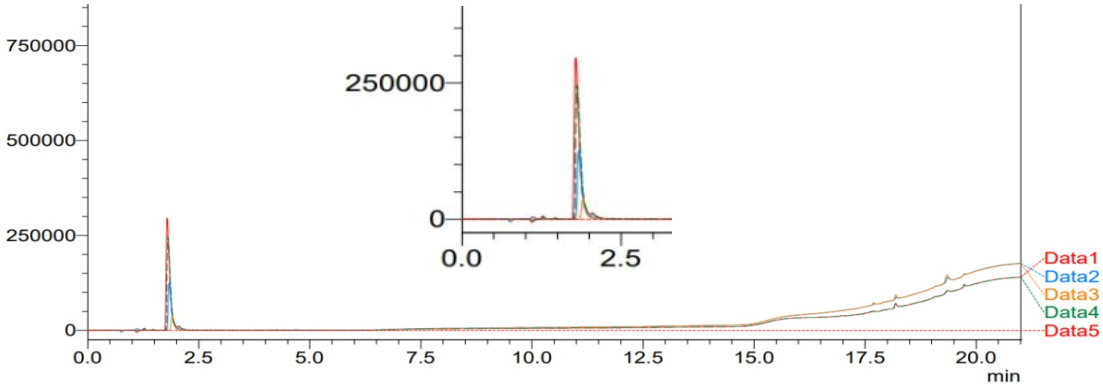

Figure S9.16: GSH **48** HPLC calibration data.

The suitability of the method was determined by quantifying the limit of detection (LOD) and limit of quantification (LOQ) of GSH calibration. LOD was evaluated by considering the analyte concentration that yield a signal-to-noise ratio (s/n) of 3. LOQ is the minimum concentration of the analyte that can be determined at an acceptable precision and accuracy under the analytical conditions used its calculated by determinate signal-to-noise ratio (s/n) of 10. LOD of this calibration was $5.08 \cdot 10^{-02}$ µmol mL^{-1} and LOQ 0.154 µmol mL^{-1}.

Table S9.2: Measures of different concentrations of GSH, peak area of GSH, and average between the 3 area measurements in RP-HPLC data. (2 - 15% ACN, 20 min 0.1% TFA, λ = 214 nm).

C ($mg \cdot ml^{-1}$)	Retention time (min)			Average	s	RSD (%)
1	1.911	1.916	1.903	1.91	0.00535	0.28
3.3	1.886	1.836	1.836	1.85	0.02357	1.27
4.8	1.873	1.879	1.875	1.88	0.00249	0.133
7.6	1.863	1.811	1.733	1.80	0.0534	2.96
9.7	1.853	1.754	1.789	1.80	0.0410	2.28

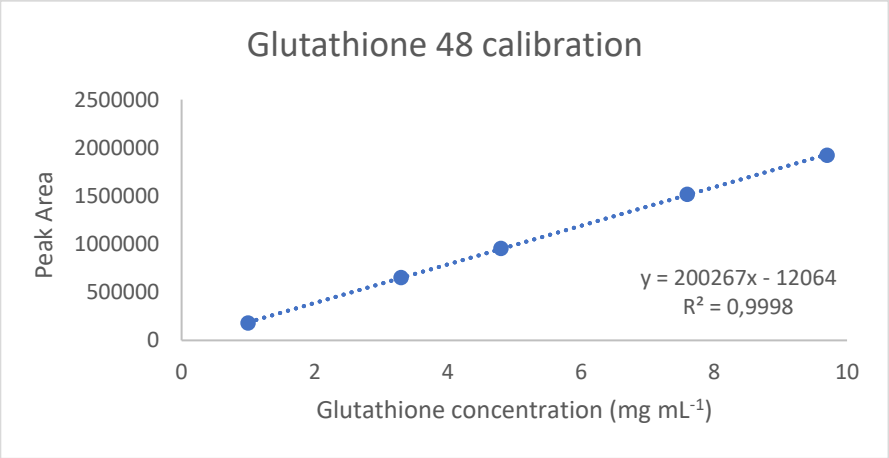

Figure S9.17: GSH **48** RP-HPLC calibration.

9.2 Chapter 3

9.2.1 NMR Spectra:

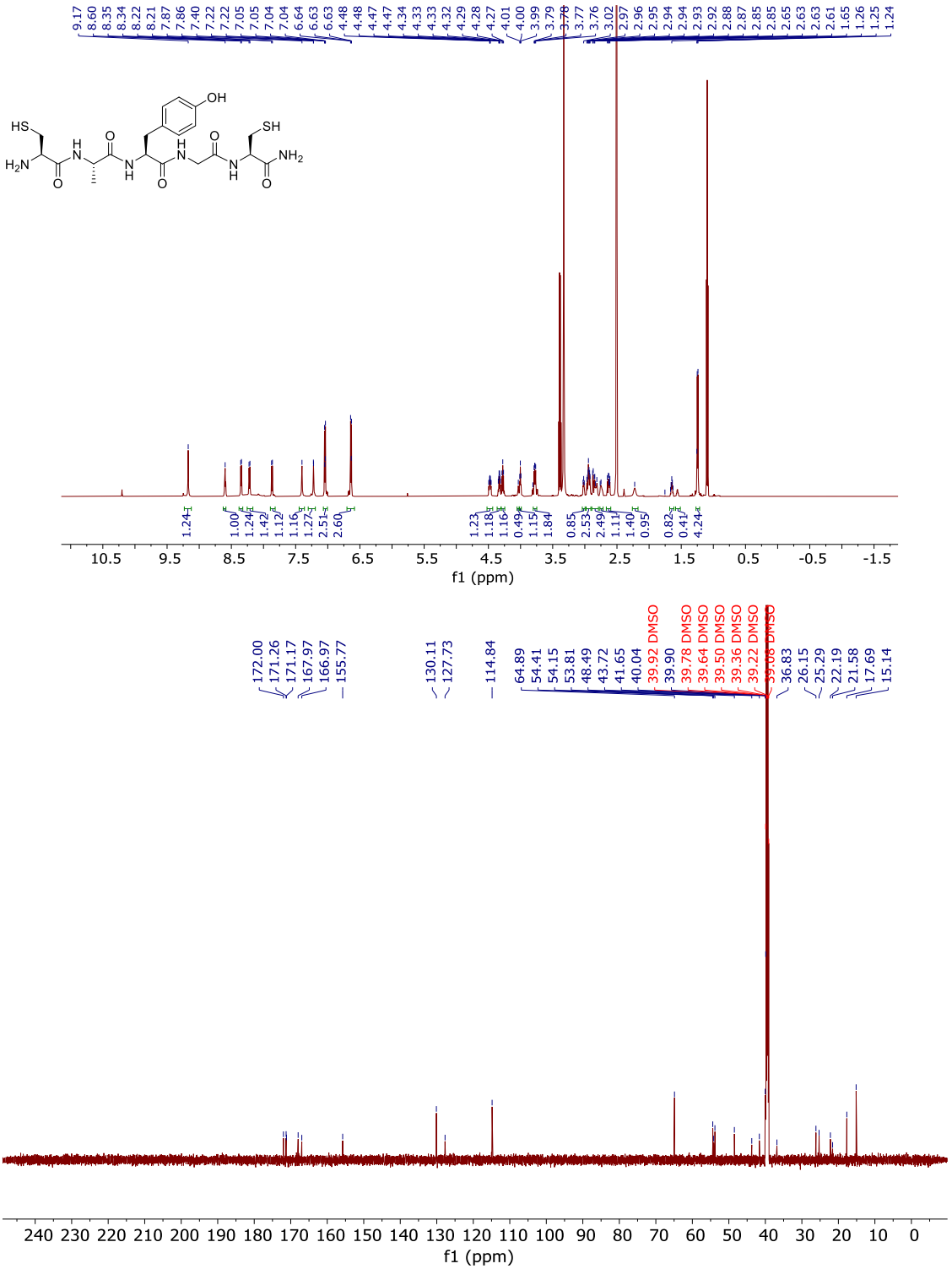

Figure S9.18: ^{1}H and ^{13}C NMR (600 MHz, DMSO) spectra of compound 88

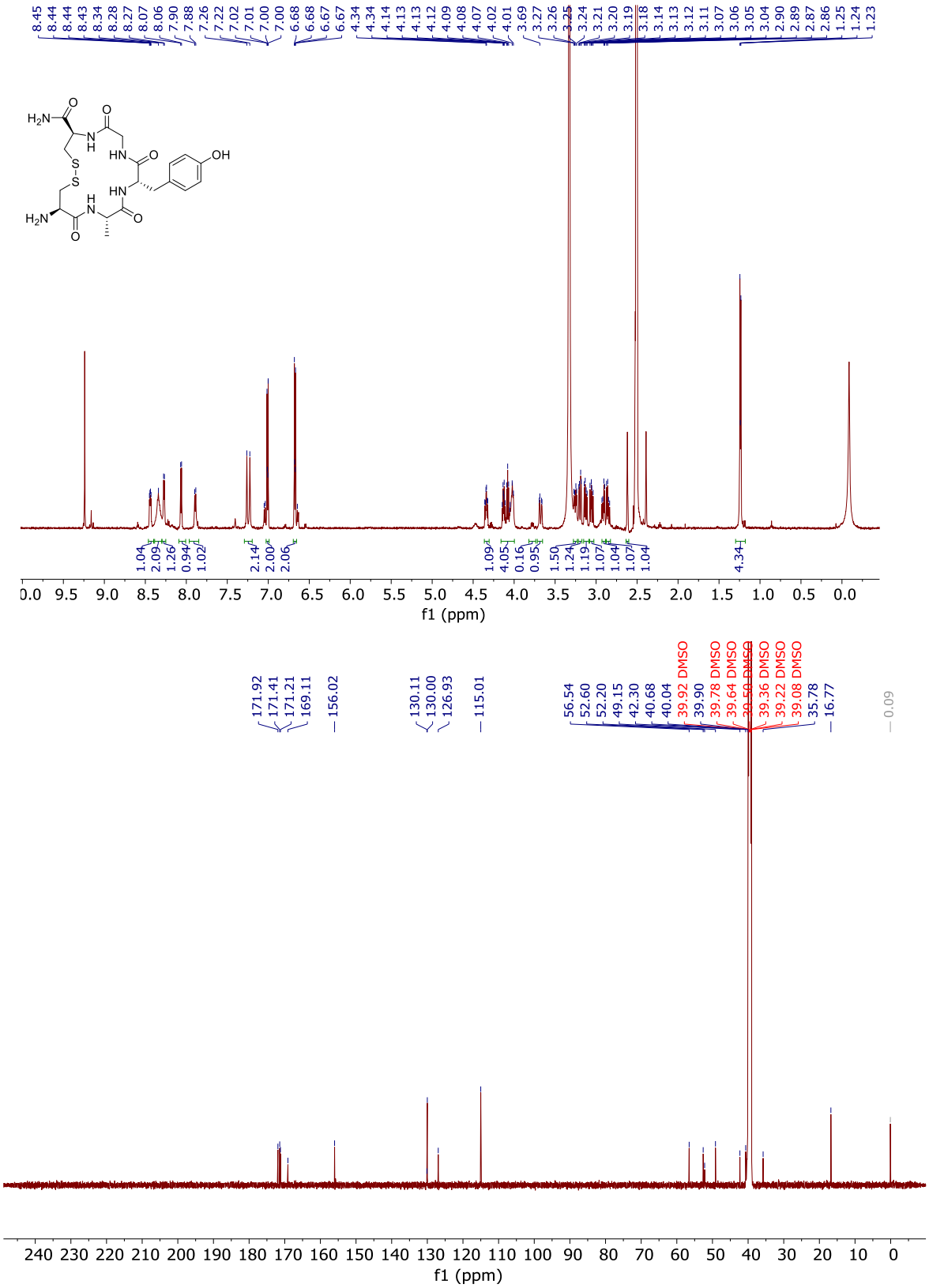

Figure S9.19: ^{1}H and ^{13}C NMR (600 MHz, DMSO) spectra of compound 89

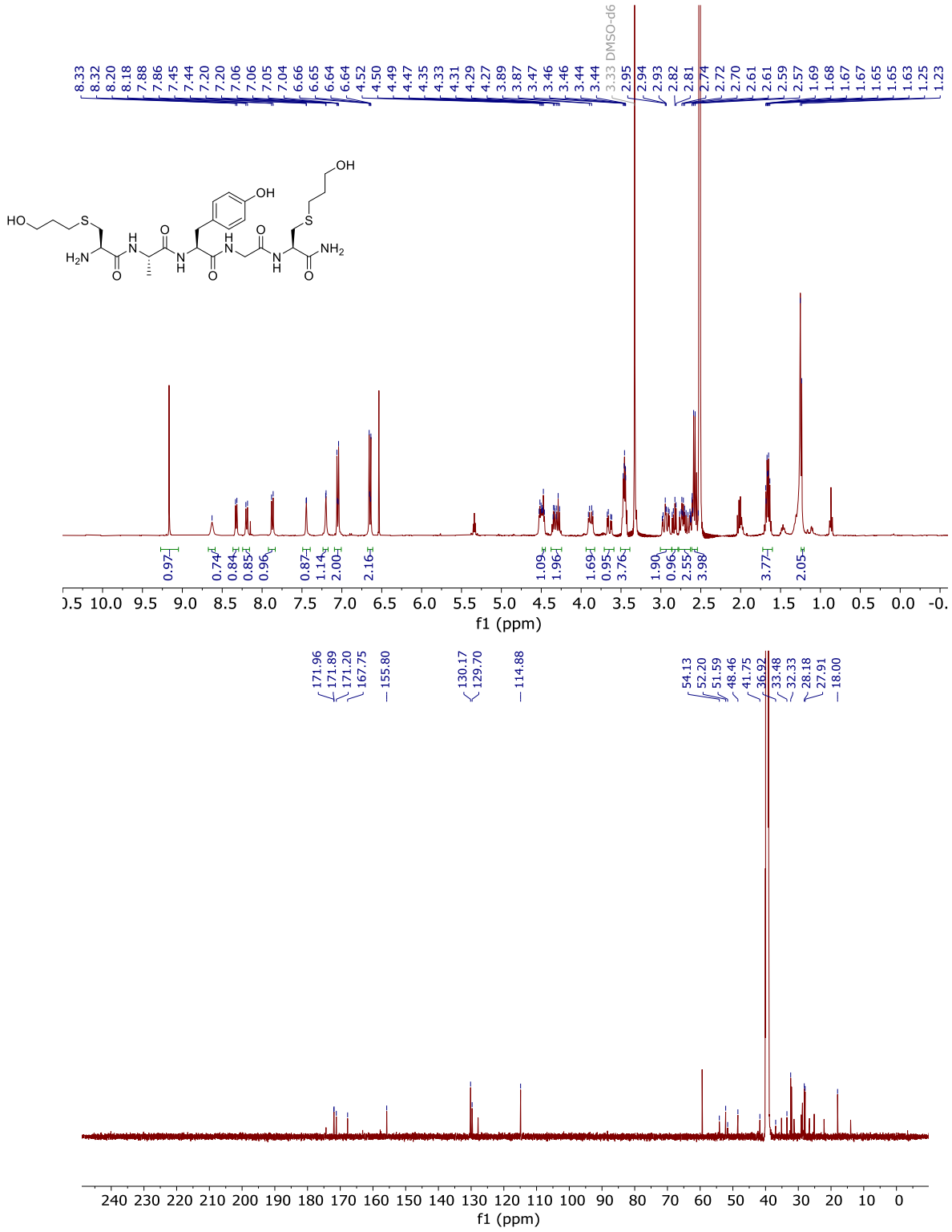

Figure S9.20: ^{1}H and ^{13}C NMR (600 MHz, DMSO) spectra of compound 90

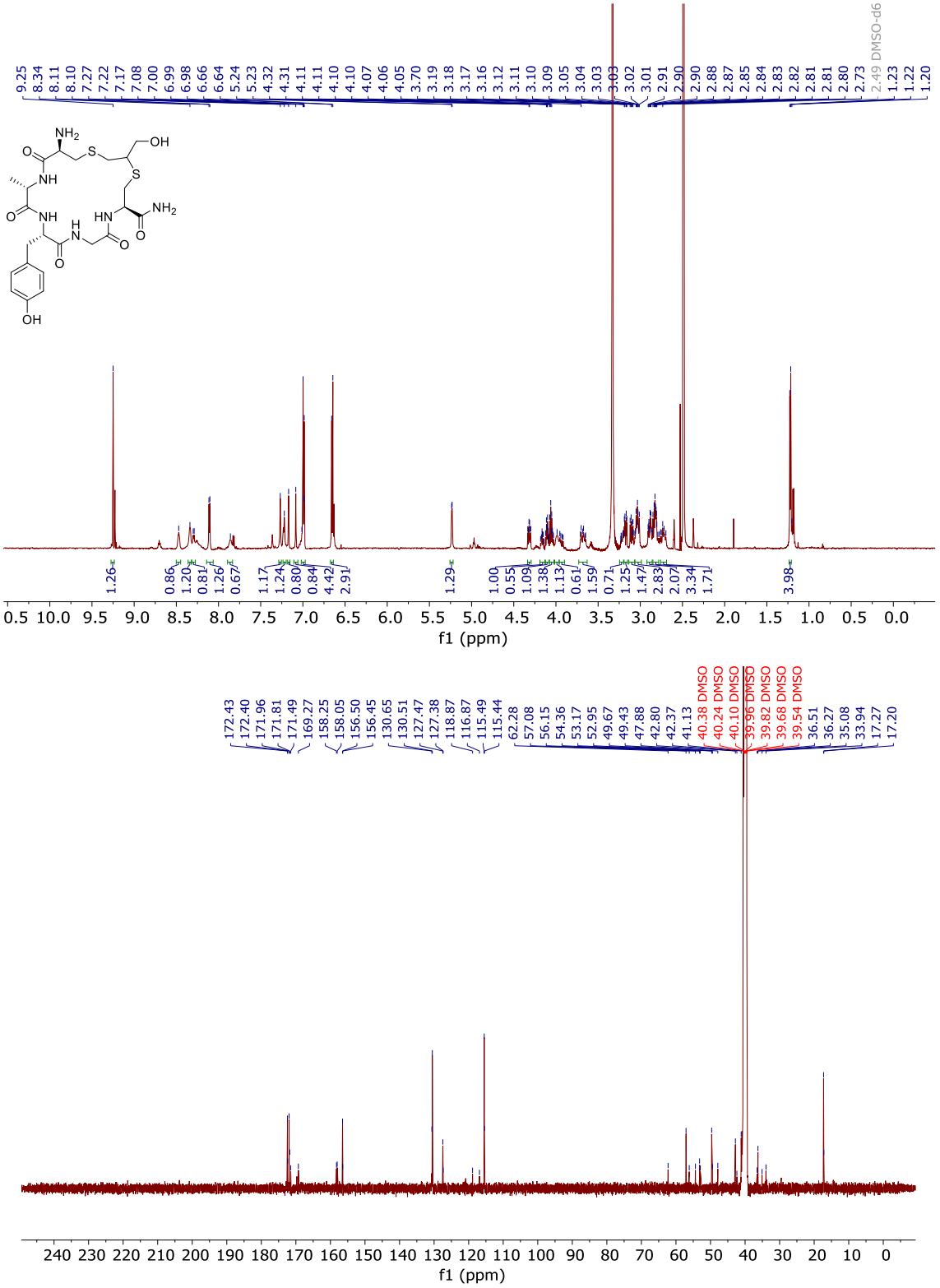

Figure S9.21: ^{1}H and ^{13}C NMR (600 MHz, DMSO) spectra of compound 92a/b

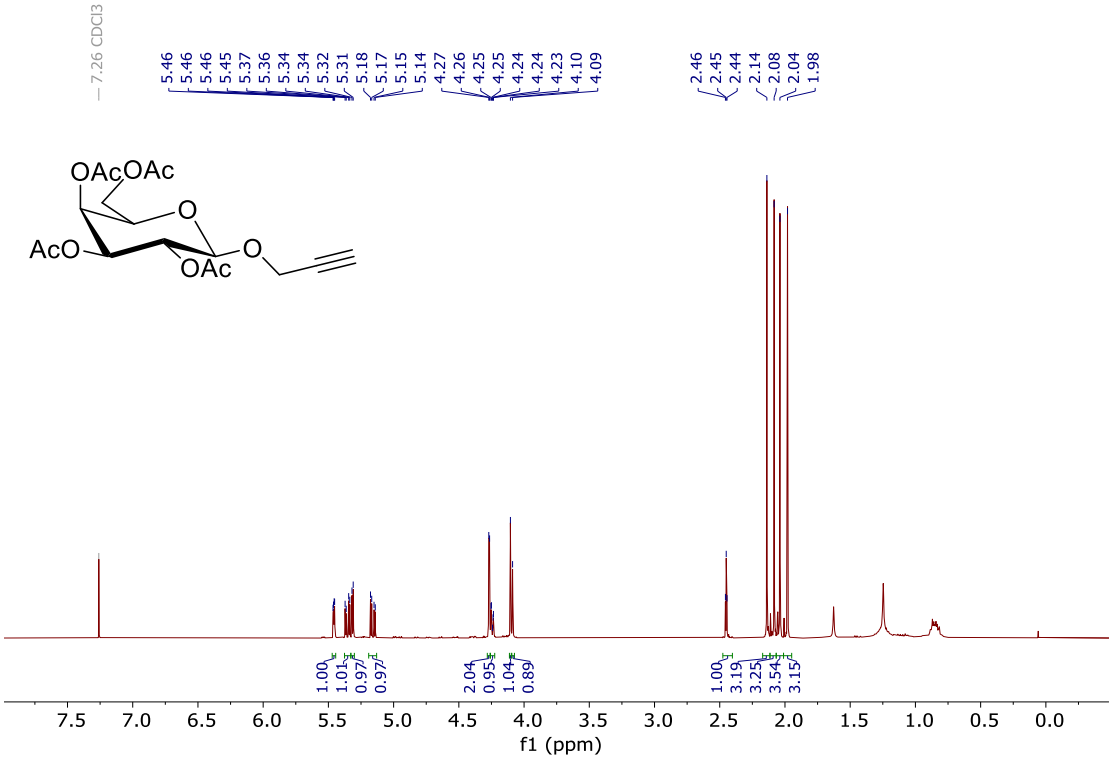

Figure S9.22: ^{1}H NMR (400 MHz, $CDCl_3$) spectrum of compound 101

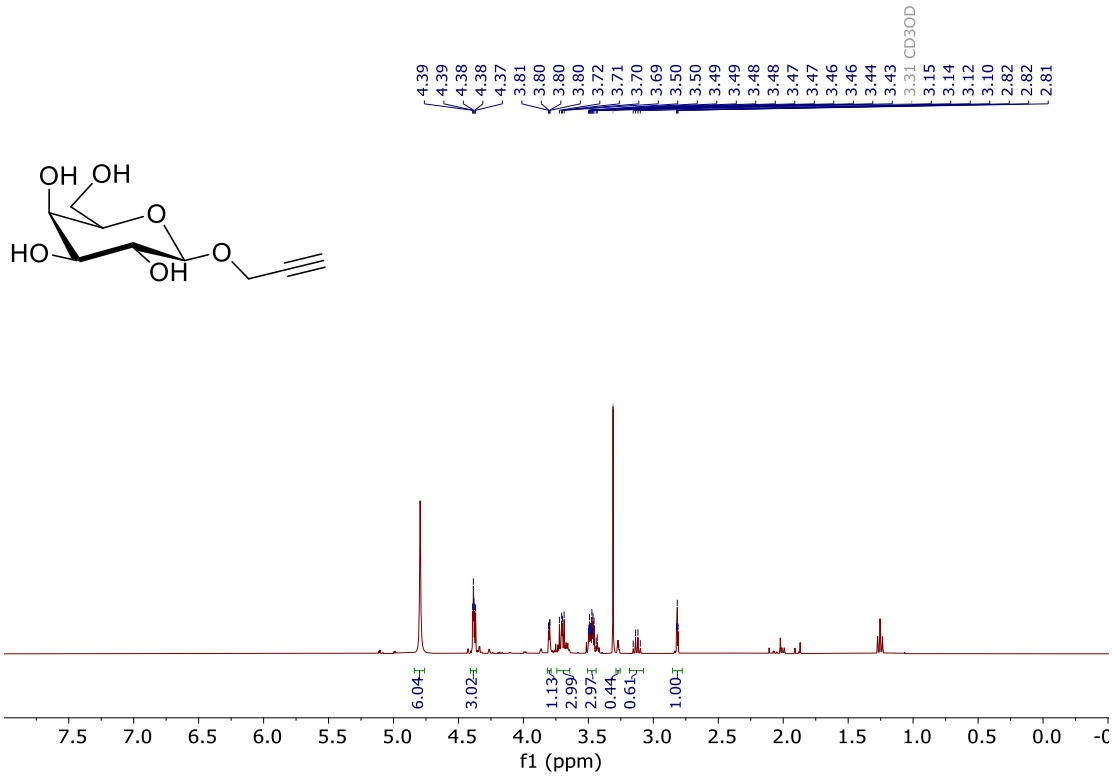

Figure S9.23: ^{1}H NMR (400 MHz, $MeOD_4$) spectrum of compound 96

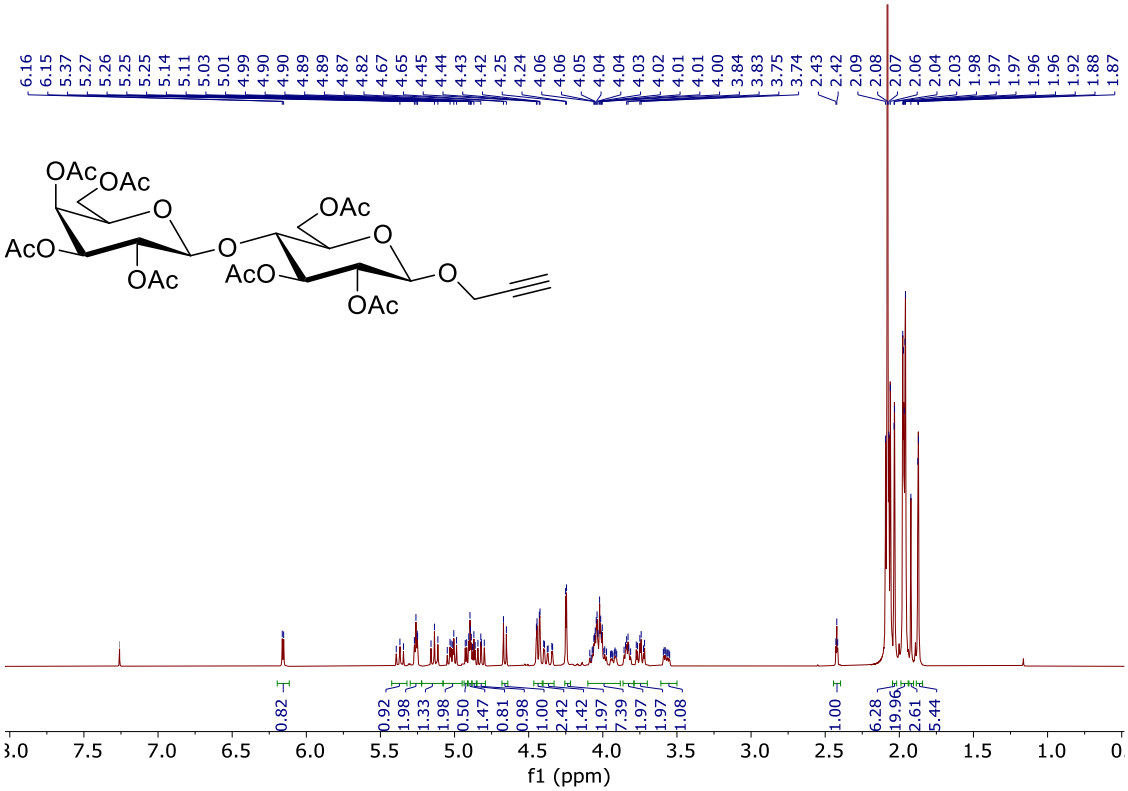

Figure S9.24: ^{1}H NMR (400 MHz, $CDCl_3$) spectrum of compound 102

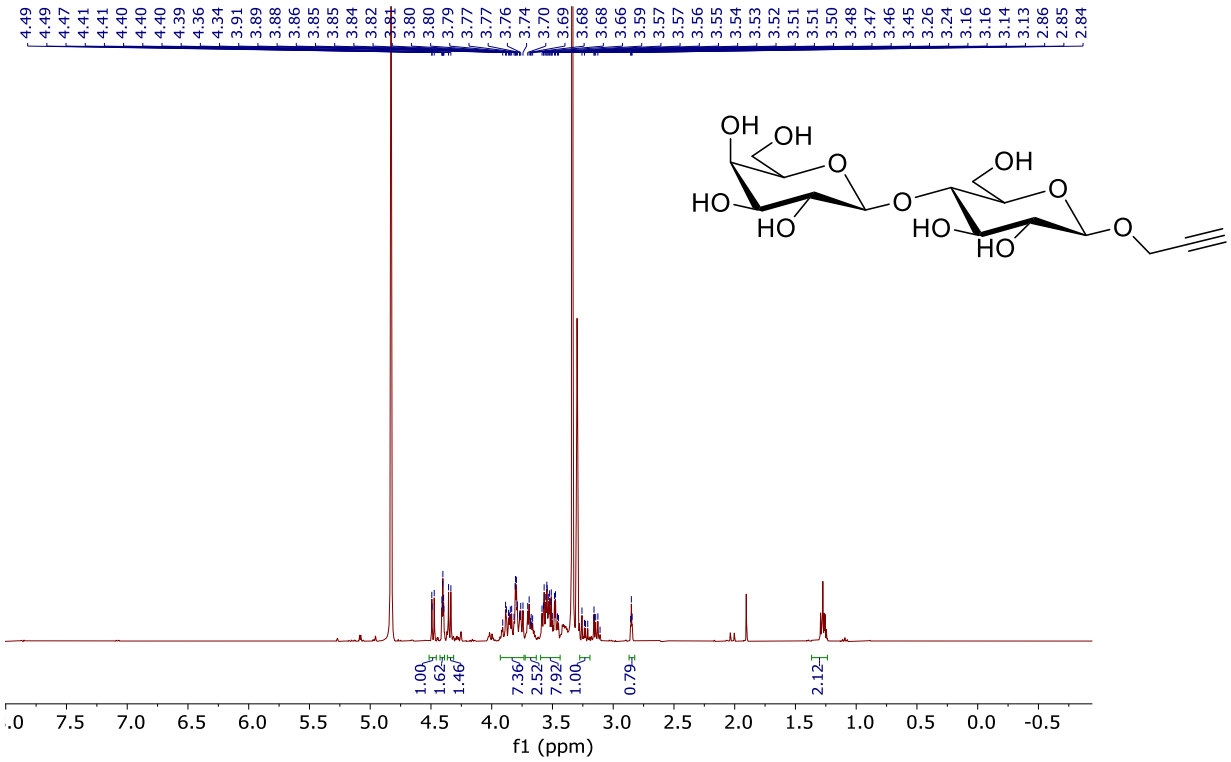

Figure S9.25: ^{1}H NMR (400 MHz, $MeOD_4$) spectrum of compound 97

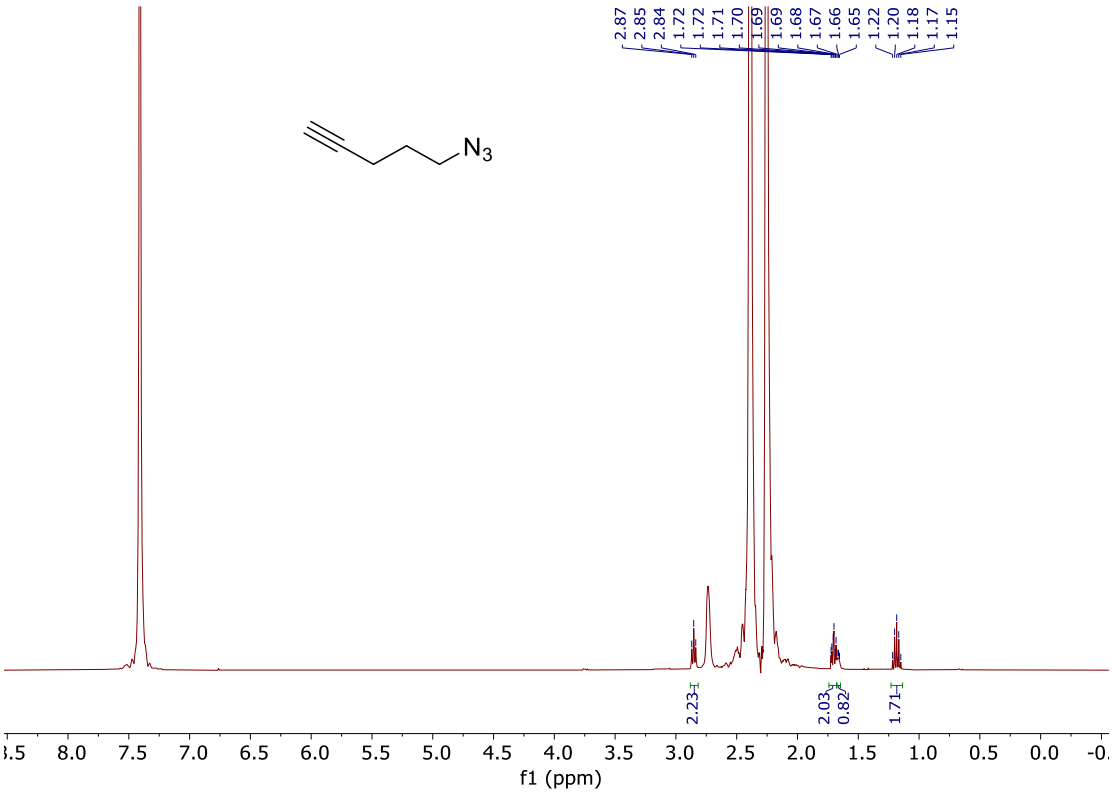

Figure S9.26: ^{1}H NMR (400 MHz, $CDCl_3$) spectrum of compound 98

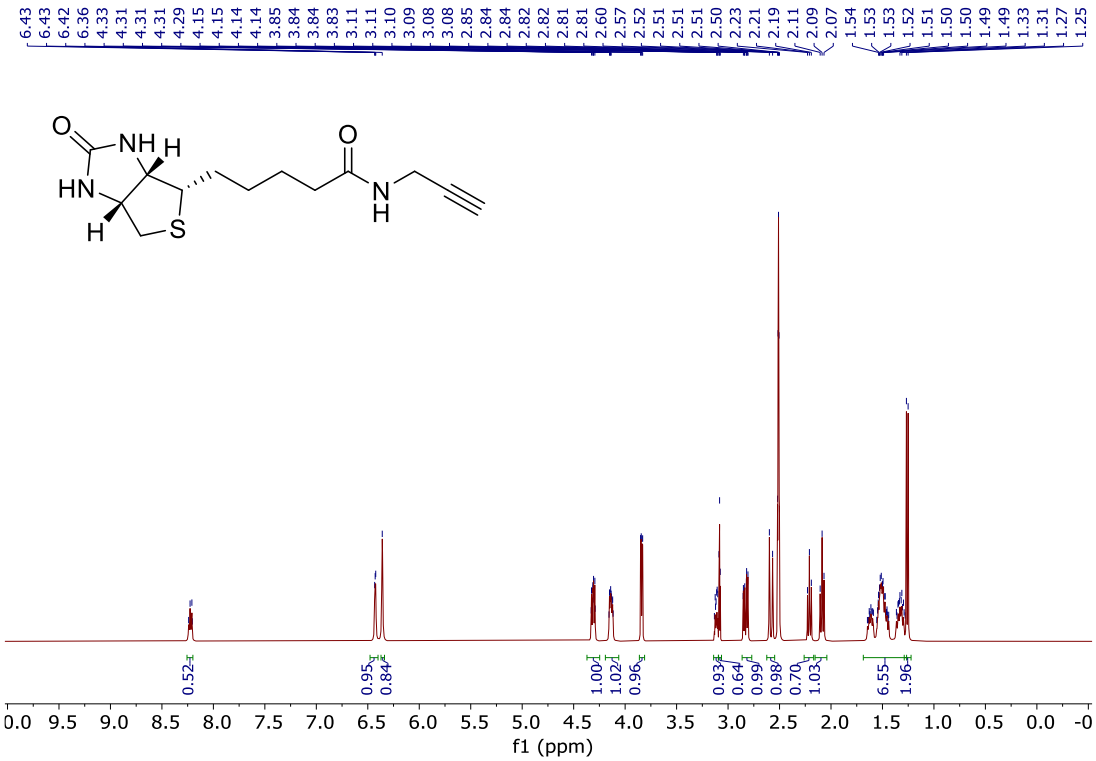

Figure S9.27: ^{1}H NMR (400 MHz, DMSO) spectrum of compound 99

9.2.2 Analytical Calibrations

Table S9.3: Calibration curve of peptide **88**

C (mg/mL)	**Area**	**Repeated Areas**		**Average**	**Average/1000**
1,1	865396	869910	844141	859815,7	859,8157
3,4	2543695	2534650	2582093	2553479	2553,479
5,0	3818996	3805620	3805041	3809886	3809,886
7,0	5393157	5453265	5387572	5411331	5411,331
10	7559610	7594535	7651840	7601995	7601,995

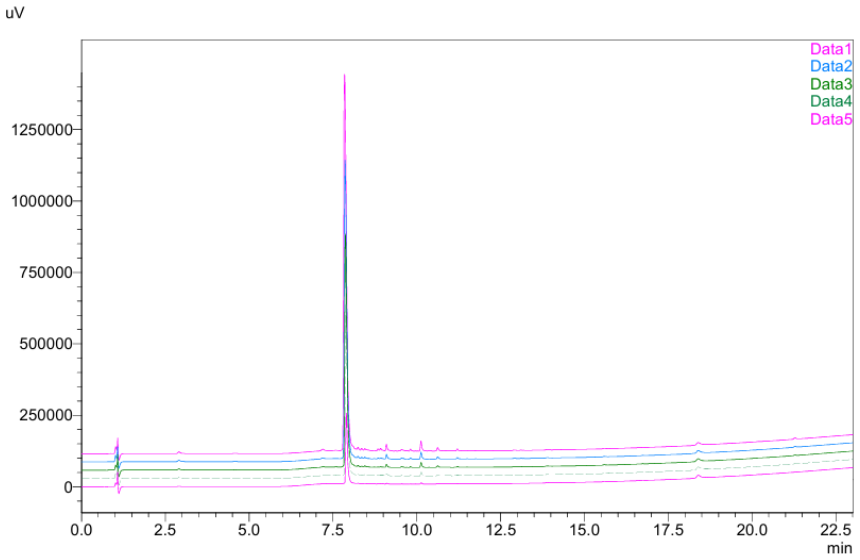

Figure S9.28: Peptide **88** HPLC calibration data.

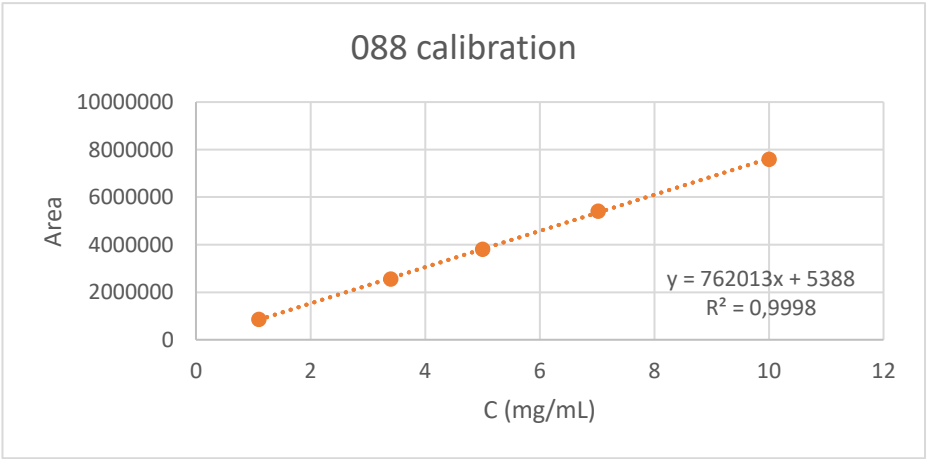

Figure S9.29: Peptide **88** RP-HPLC calibration curve.

9.3 Chapter 4

9.3.1 NMR Spectra

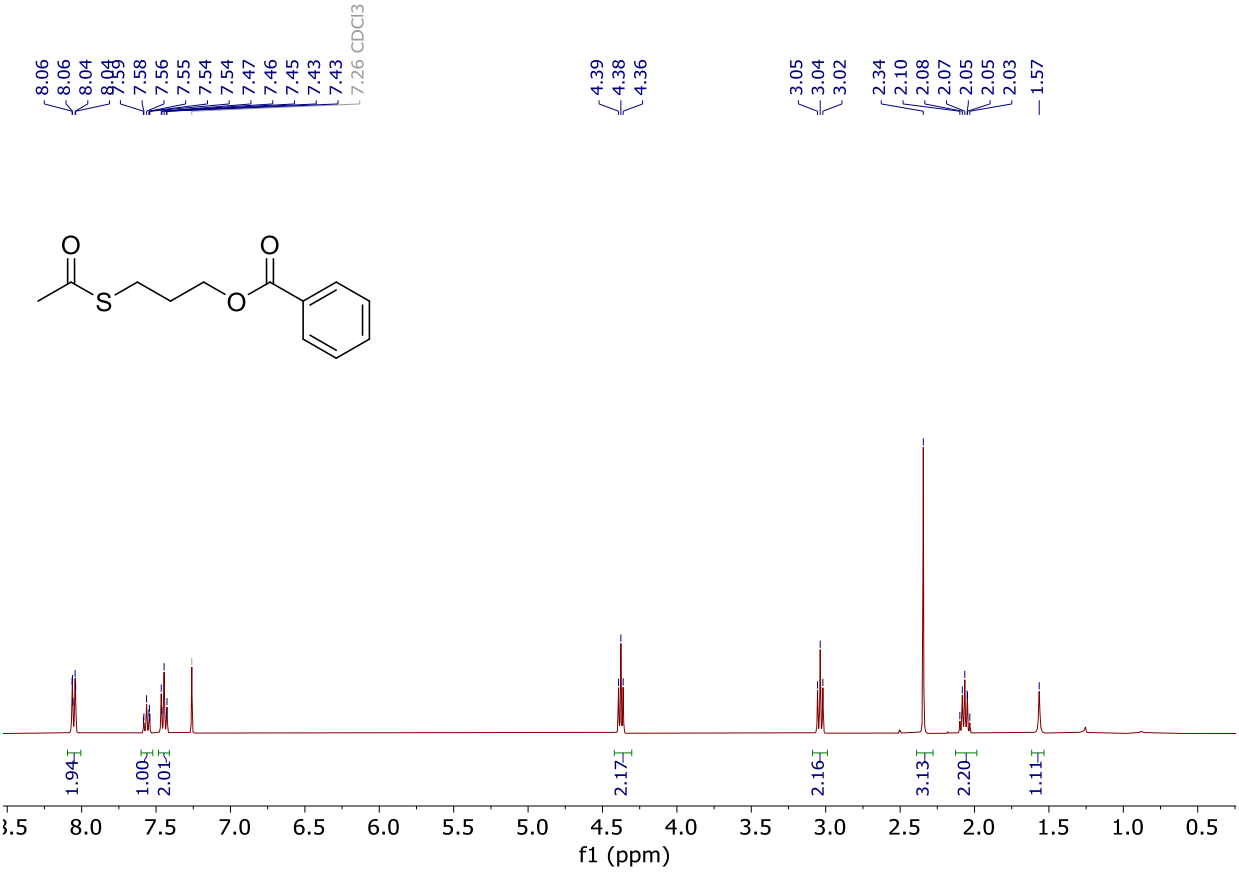

Figure S9.30: ^{1}H NMR (400 MHz, $CDCl_3$) spectrum of compound 116.

9.4 Chapter 5

9.4.1 Urea/SDS-PAGEs reported in Chapter 5.

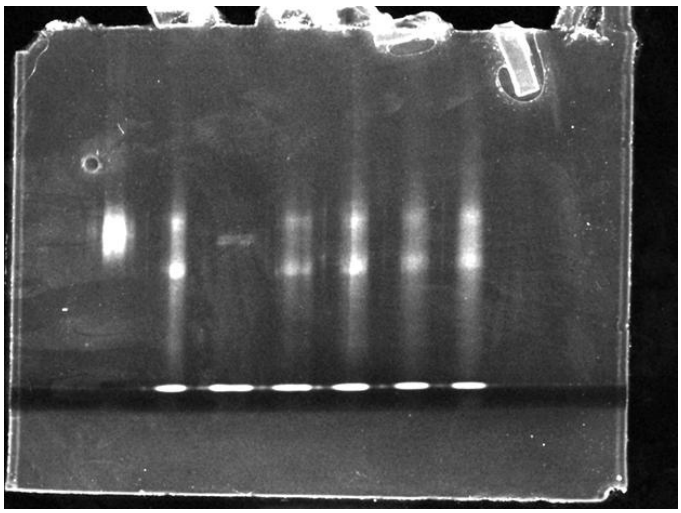

Figure S9.31: Full urea-SDS-PAGE stained by SYBRO Green II of the mRNA/cDNA complex.

Figure S9.32: full gel of 10% SDS-PAGE of TEC optimisation visualised by fluorescent.

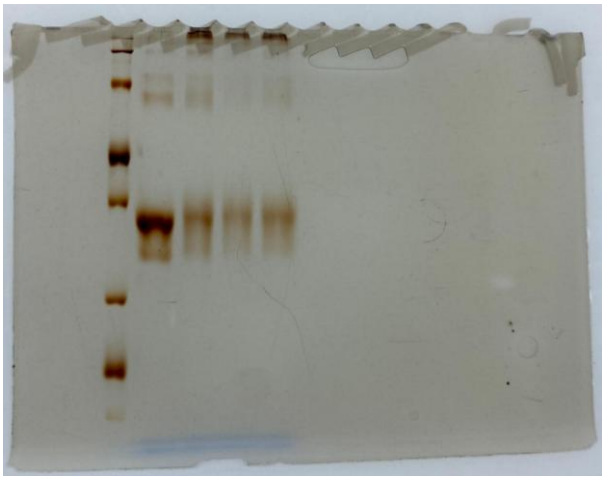

Figure S9.33: full gel of 10% SDS-PAGE of TEC optimisation visualised by silver stain.

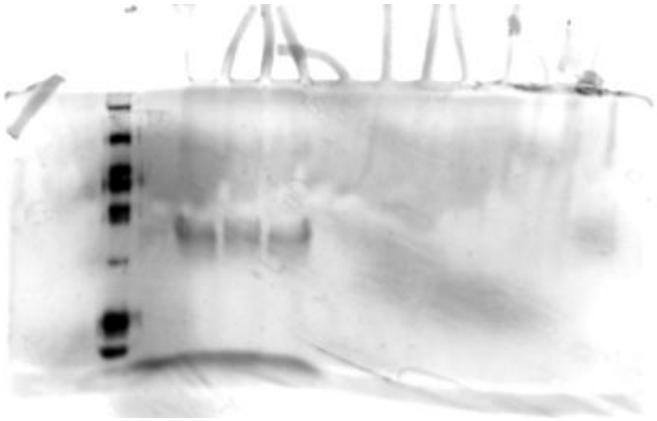

Figure S9.34: full gel of 10% SDS-PAGE of TEC optimisation visualised by silver stain.

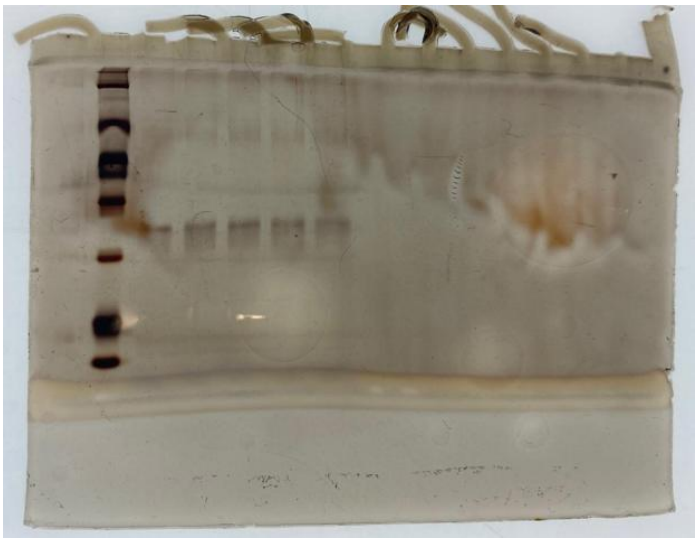

Figure S9.35: Full gel of 10% SDS-PAGE of TEC reaction under RaPID conditions visualised by silver stain.

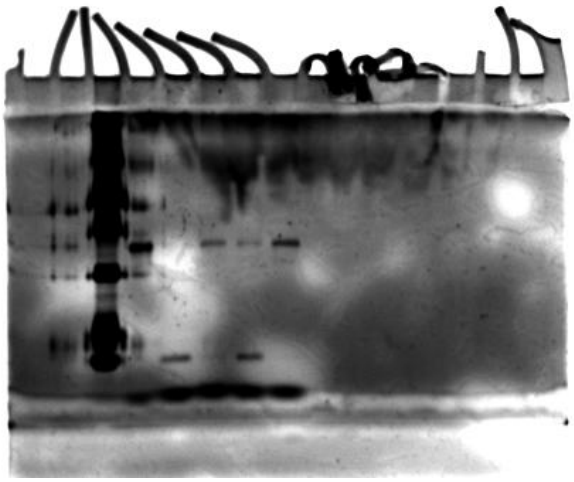

Figure S9.36: Full gel of 10% SDS-PAGE of TEC optimisation under RaPID conditions with streptavidin beads visualised by silver stain.